Advancing characterization techniques for structure-property determination of *in-situ* lignocelluloses

Sudip Chowdhury

Dissertation submitted to the faculty of the Virginia Polytechnic Institute and State University in partial fulfillment of the requirements for the degree of

Doctor of Philosophy
In
Macromolecular Science and Engineering

Charles E. Frazier, Chairman
Louis A. Madsen
Robert B. Moore
Scott H. Renneckar
Justin R. Barone
Garth L. Wilkes

July 21, 2011
Blacksburg, Virginia

Keywords: DMA, quadrupolar interaction, NMR, infrared spectroscopy, biomass fractionation, wood-adhesion promoter

Advancing characterization techniques for structure-property determination of *in-situ* lignocelluloses

Sudip Chowdhury

Abstract

The global progression towards sustainable energy, materials and chemicals requires novel and improved analytical tools to understand and optimize lignocellulosic biomass utilization. In an effort to advance lignocellulose characterization, gain insights into biomass processing, and obtain novel perspectives on cell wall ultrastructure, this study utilizes three principal polymer characterization techniques, namely compressive-torsion dynamic mechanical analysis (DMA), deuterium quadrupolar nuclear magnetic resonance (^{2}H NMR) and rheo-infrared spectroscopy.

A novel parallel-plate compressive-torsion DMA protocol is developed to analyze very small solvent-plasticized biomass specimens with or without mechanical integrity. The benefits and limitations of this technique are demonstrated by comparing it to a conventional tensile-torsion DMA while analyzing various solvent-plasticized lignocelluloses.

The rheology of wood in various organic solvents is studied through dynamic thermal scans, Time/temperature superposition (TTS) and fragility analysis. Plasticizing solvents and wood grain orientation significantly affected the lignin glass-transition temperature. Dynamic TTS reveals that while all storage modulus data shift smoothly, the thermorheological complexity of solvent-plasticized wood becomes evident in loss

component master curves. It is argued that the plasticized lignocellulose TTS is insightful and potentially useful, although it fails to satisfy the classic TTS validity criteria. Subsequently, it is justified that the fragility analysis is a better suited treatment than the WLF model to investigate cooperative segmental motions of plasticized wood.

Deuterium quadrupolar NMR reveals a new perspective on the orientation of amorphous wood polymers and two distinct amorphous polymer domains: a highly oriented phase in the S2 layer of the secondary cell wall and an isotropic phase postulated to occur in the compound middle lamella (CML). If the origin of the isotropic phase is confirmed to arise from the CML, then this technique provides a way to independently investigate the morphology and phase dynamics of CML and S2 in an intact tissue, and should bring novel insights into deconstructive strategies specific to the oriented and unoriented domains.

Finally the effects of a wood-adhesion promoter (hydroxymethyl resorcinol, HMR) on in-situ wood polymers are studied to elucidate the still unresolved HMR-lignocellulose interactions. DMA, creep-TTS and ^{2}H NMR reveal that HMR increases the crosslink density and restricts the mobility of wood amorphous phase. Rheo-IR spectroscopy shows that the molecular stress-transfer mechanism is altered within the wood cell wall.

Acknowledgement

This is the time to look back at the wonderful journey that has taken me to the end of my doctoral research. This has been the most enjoyable and enlightening stretch of my academic life and was possible only because of the people around me. Throughout my life I have received love and support/guidance from many people. I would like to pay my gratitude to some of them.

First of all, I wholeheartedly thank my major Ph.D. advisor, Prof. Charles E. Frazier. Whatever I have achieved during my Ph.D., I owe that to him. From the beginning to the end, he has kept faith in me, encouraged me in every step and helped me aim higher. It is not possible for me to thank him in words, but he will be my “guru” throughout my academic career.

I would like to thank my Ph.D. committee members, Professors Lou Madsen, Garth Wilkes, Robert Moore, Justin Barone and Scott Renneckar for their great support throughout my doctoral research. I would like to specially thank Prof. Louis Madsen for his great support and cooperation with my research. I have learned a lot from his class and from our discussions.

I would like to thank all the wonderful people in Department of Wood Science, especially, David Jones, Debbie Garnand, Rick Caudill, Linda Caudill and Prof. Audrey Zink-Sharp. Without their help this journey would have been very difficult. My sincere gratitude goes to my MS advisor Prof. Vikram Yadama, who gave me the first opportunity to US education and believed in my potential.

I enjoyed a wonderful research group, talented and funny. I thank Dakai Ren, Jesse Paris, Josh Hosen, James Fabiyi, and Xing Yang for their support. Thank you for your friendship.

It would not be possible for me to reach this feat without the selfless support of my parents. No word can express my gratefulness to them. Although they are half the world away from me, I felt their support and blessing each moment.

At the end I want to mention Susmita, my wife, who was with me at all my highs and lows, joys and pains, successes and failures, and made my life full of happiness. She is the keystone of my life and the reason of any success that I may have achieved.

Table of Content

List of Figures

List of Tables

Chapter 1 Introduction

1.1. Motivations and Research Outline

The ever-growing demand for renewable energy and materials requires development of new and advanced analytical tools to study lignocellulosic biomass. Over the last few years significant advancement has been made in the field of biomass processing. However, the optimum energy/cost efficient biomass deconstruction process is still not achieved. One significant limitation exists in the understanding of the ultrastructure of lignocellulosic cell wall as well as the effects of various technologically relevant treatments on interactions and morphology of in-situ cell wall polymers. This study is aimed to contribute towards advancing the in-situ lignocellulose characterization by developing and/or optimizing several polymer characterization techniques for lignocellulosic biomass. The research is outlined as follows:

1. In chapter 2, a parallel-plate compressive torsion DMA protocol is developed to analyze lignocellulosic biomass under solvent plasticized conditions. This method effectively analyzes very small biomass specimens with/without mechanical integrity. This method shows great promise in studying effects of various pre-treatments on fundamental lignocellulose relaxations. Chapter 3 demonstrates the scope of this technique by investigating fundamental viscoelasticity of wood plasticized in various organic media. An in-depth study of lignocellulose relaxation is conducted using various classic polymer physics approaches in chapter 4.

2. Chapter 5 details a novel application of deuterium quadrupolar nuclear magnetic resonance (^{2}H NMR) technique for in-situ lignocellulose analysis. This study demonstrates the power of ^{2}H NMR technique in gaining novel perspectives into the cell wall ultrastructure. ^{2}H NMR will open exciting new avenues for explaining effects of thermal, chemical or genetic modifications on sub-micron scale polymer domains within the xylem tissue.

3. Effects of a powerful wood-adhesion promoter (hydroxymethyl resorcinol, HMR) on intermolecular interactions and morphology of lignocelluloses are investigated using three different characterization techniques: compressive-torsion DMA, ^{2}H NMR and rheo-infrared spectroscopy, as detailed in chapters 6, 7 and 8. This study demonstrates the efficacy of these techniques in explaining effects of chemical treatments on in-situ polymers. They also facilitate a finer understanding of HMR-wood interaction mechanism.

1.2. Literature Review

1.2.1. Wood Cell wall Components

Wood is a natural polymer composite primarily composed of four different polymers: cellulose, lignin and hemicelluloses (xylan and glucomannan). Along with these main constituents different extractives such as terpinoids, fats and waxes are also present.(Lindblad and Albertsson, 2005) Cell wall formation consists of three primary stages. First, the middle lamella forms along with the primary cell wall, which mainly consists of pectic materials.(Timell, 1964) Subsequently, cellulose and hemicelluloses are deposited to form the secondary cell wall. Lastly, lignin is deposited in the middle lamella and in the secondary cell wall to act as the polymer matrix that holds cellulose fibers.(Timell, 1964; Sjöström, 1993)

<u>Cellulose</u>

Cellulose is a homopolysaccharide of β-D-glucopyranose monomers which are linked by (1→ 4)-glycosidic (acetal) bonds (Sjöström, 1993), as showed in Figure 1-1.

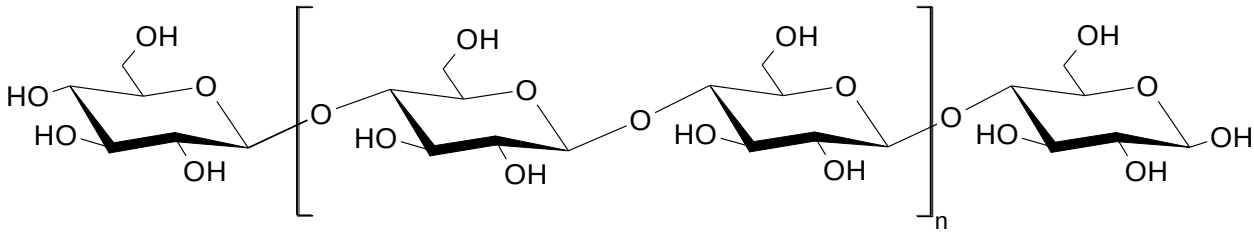

Figure 1-1 Schematic representation of cellulose.

Cellulose is the main component of wood (40 – 45% of wood dry mass). In comparison to other natural polymers, cellulose has a simple molecular structure. Because of its linear structure and abundance of polar hydroxyl groups, cellulose has

high affinity towards forming intermolecular and intramolecular hydrogen bonds (Fengel and Wegener, 1984; Sjöström, 1993). Cellulose is biosynthesized in living cell through the plasma membrane, more specifically by a sugar nucleaotide called UDP-D-glucose (Sjöström, 1993). Thirty six cellulose chains are simultaneously synthesized through the plasma membrane in a biosynthetic "extrusion" process. This process produces highly elongated cellulose elementary fibrils (cross sectional dimension: ~ 2 × 3 nm) (Kerr and Goring, 1975). Several of these elementary fibrils then aggregate to form a fibrillar structure, popularly known as microfibril. In native cellulose, microfibrils can be as long as 100 – 200 nm and are believed to have amorphous, or more appropriately non-crystalline regions in series(Fengel and Wegener, 1984; Sjöström, 1993) or in parallel(Salmén and Bergstrom, 2009) to the stiff crystalline structures.

Hemicelluloses

Hemicelluloses are groups of heteroglycans composed of D-xylose, D-mannose, L-arabinose, D-glucose, D-galactose and 4-O-methyl-D-glucuronic acid residues (Timell, 1964). Hemicelluloses constitute 20 to 35 percent of the total dry mass of the cell wall. The amount and chemical nature of hemicelluloses varies from species to species. In a most general way, two types of hemicelluloses are identified, popularly referred to as xylans and glucomannans.

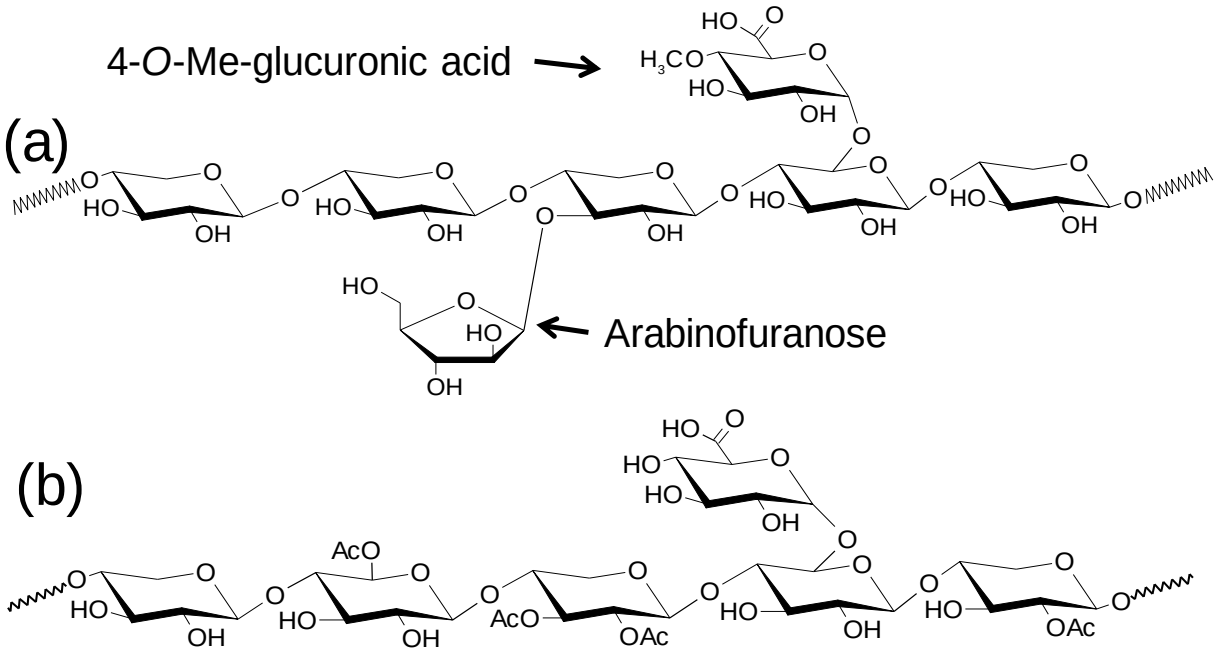

Figure 1-2 Schematic representation of xylan. (a) Fragment of softwood xylan. (b) Fragment of hardwood xylan.

Xylan is the major hemicellulose in hardwoods and is generally a minor component in softwoods. Schematic representations of hardwood and softwood xylans are shown in **Error! Reference source not found.**. The backbone of xylan is characterized by a comparatively short chain of β (1→4)-linked D-xylopyranosyl units with 4-O-methyl-D-glucuronopyranosyl branch units, attached by α (1→2) bonds(Thompson; Timell, 1964). In softwood xylan no acetylation is seen, whereas hardwood xylans are highly acetylated (**Error! Reference source not found.** a, b). The number average degree of polymerization of hardwood xylans vary from 100 to 200 depending on the species and the extent of decomposition during the isolation process (Thompson; Timell, 1964; Sjöström, 1993).

The other form of hemicelluloses is glucomannan. As the name indicates, these hemicelluloses are mainly composed of manopyranosyl and glucopyranosyl units

connected through β (1→4) linkages (Thompson; Timell, 1964; Fengel and Wegener, 1984; Sjöström, 1993). Figure 1-3 (a, b) show the representative structures for softwood and hardwood glucomannans.

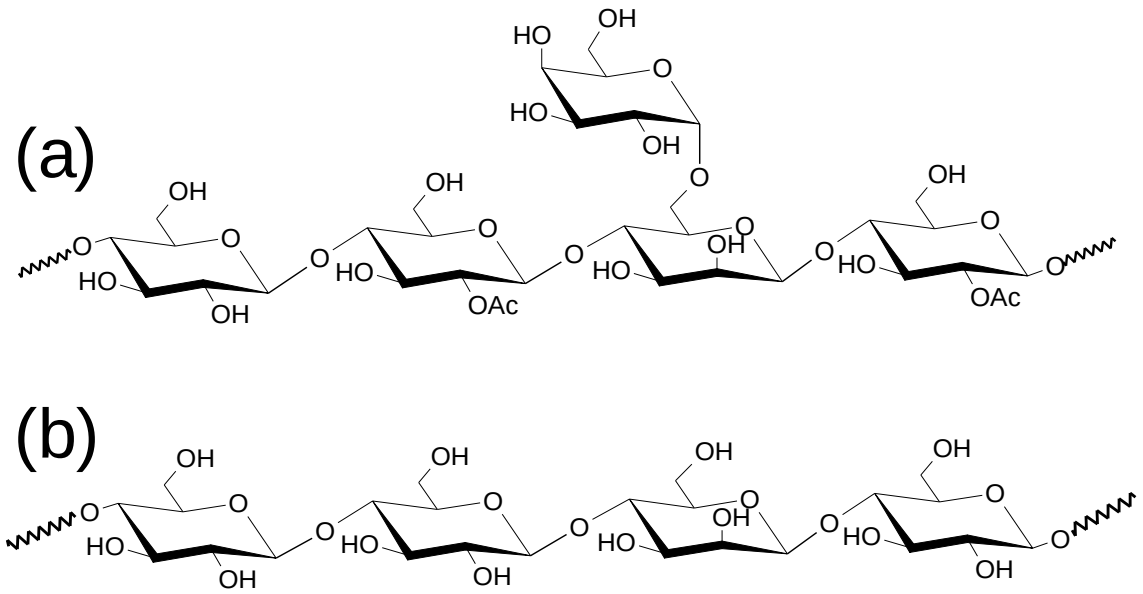

Figure 1-3 Schematic representation of glucomannan. (a) Fragment of softwood glucomannan. (b) Fragment of hardwood glucomannan.

Galactoglucomannan or more commonly known as glucomannan is a major softwood component, but found in a small quantity in hardwoods. In softwoods, a minor degree of acetylation is observed and it contains short galactose branches. In Hardwoods the glucomannan chains are generally considered linear and without detectable acetylation. Both hemicelluloses are non-crystalline/amorphous in nature.

Lignin

Lignin is the second most abundant biopolymer and the most important non-polysaccharide component of wood. Depending on species, lignin constitutes 10 to 30% of the mass of the mature cell wall (Hon and Shiraishi, 2001). Lignin is a three

dimensional cross linked macromolecule composed of phenylpropane units. The *in-situ* structure of lignin is not understood comprehensively, but it is accepted that the primary precursors of the lignin macromolecules are coniferyllic, coumaric and sinapyllic aromatic alcohols (Heredia *et al.*, 1993) as shown in Figure 1-4.

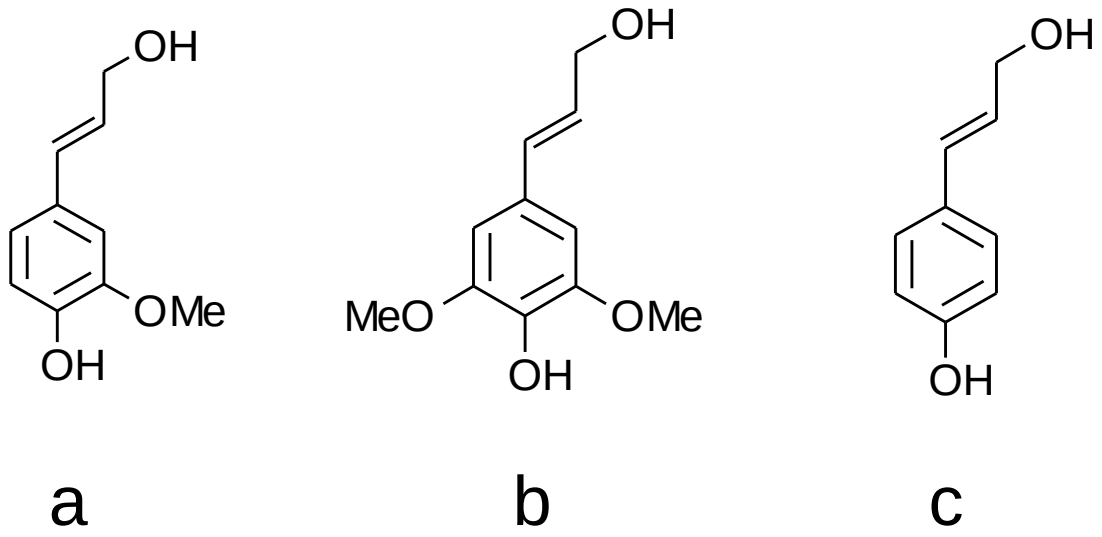

Figure 1-4 Precursors of lignin macromolecules. (a) *trans*-coniferyl alcohol. (b) *trans*-sinapyl alcohol. (c) *trans-p*-coumaryl alcohol.

The most common linkage between lignin monomers is β-O-4, where the β carbon atom on the side chain of one monomer is connected to the oxygen atom on the para-position of the second monomer (Faulon *et al.*, 1994). Softwoods primarily contain guaiacyl lignin units generated from *trans*-coniferyl alcohol. Hardwoods contain both guaiacyl and syringyl units originating from *trans*-coniferyl and *trans*-sinapyl alcohols. Lignin in grasses primarily contain *p*-hydroxyphenyl units, originating from *trans-p*-coumaryl alcohol (Hon and Shiraishi, 2001).

The organization of these polymers to form the supramolecular structure of wood and other lignocellulosic cell walls will be discussed in Section 0.

1.2.2. Hydroxymethyl resorcinol (HMR)

In 1995 Vick and coworkers introduced hydroxymethyl resorcinol (HMR) as a powerful wood-adhesion promoter (Vick *et al.*, 1995). In a very simple synthetic scheme, resorcinol and formaldehyde are mixed in 1:1.5 molar ratio under mildly alkaline aqueous condition. The reaction takes place at room temperature. Vick et al. (1995) showed that a simple wood surface treatment of the HMR solution dramatically improved the moisture durability of the wood-epoxy bond. They hypothesized that HMR was acting as a coupling agent in the wood-adhesive interphase, where it was making physical and chemical bonds between wood and epoxy adhesive (Vick *et al.*, 1995; Vick, 1996). The reaction time has significant effect on the HMR efficacy. Employing the ASTM D 2559 delamination test, HMR-treated, epoxy-bonded wood specimens were tested after a variety of HMR reaction times prior to bonding (Vick *et al.*, 1998). The optimum mix time was determined to be between 3 and 8 hours (percent delamination was less than 5% only within this timeframe). HMR effects have been studied using a variety of wood adhesives. For instance HMR wood pretreatment dramatically improved the moisture durability of polyurethanes (Vick and Okkonen, 2000), polymeric diphenylmethane diisocyanate (pMDI) (Vick, 1996), phenol-resorcinol-formaldehyde (Vick *et al.*, 1995; Vick, 1996) and also of wood-fiber-reinforced vinyl ester composites (Lopez-Anido *et al.*, 2000).

During the last decade, several studies were conducted to understand the fundamental mechanism behind the HMR durability enhancement. Vick et al. (1998) suggested that the efficacy of HMR depends strongly on its molecular weight distribution. An ensemble of methylolated monomers, dimers, and higher molecular

weight oligomers and polymers are required. This suggested that HMR monomer penetration into the cell wall and possible cross linking with wood-polymers might occur, but also that higher chains incapable of cell wall penetration are needed. Gardner et al. (2000) studied the HMR effect on the surface free energy of southern yellow pine wood (Gardner *et al.*, 2001). Using contact angle measurement it was shown that, with HMR treatment the dispersive (non-polar) free energy was reduced, whereas the polar free energy increased. This was attributed to the presence of free hydroxymethyl groups on treated surface. It was also speculated that this increased polar energy may cause enhanced hydrogen bonding and covalent bond formation between wood and adhesives (Gardner *et al.*, 2001). In a subsequent study, Son and Gardner (2004) showed that the HMR treated wood had significantly lower moisture affinity (Son and Gardner, 2004b). Improved dimensional stability due to HMR treatment was also reported, but curiously this finding was not correlated to cell wall modification (Son and Gardner, 2004a). This enhanced dimensional stability was believed to impart bondline stability. In 2005 Christiansen studied the effect of HMR cross-link density on its efficacy (Christiansen, 2005). In HMR synthesis the resorcinol was partially replaced by 2-methylresorcinol. Lower functionality in 2-methylresorcinol (functionality = 2) in comparison to resorcinol (functionality = 3) caused a reduction in the cross-link density. The de-lamination of wood-adhesive bonds significantly increased with lower cross-link density. In the same study, HMR treated wood was heat treated (70 °C for 3 months) before adhesive application, to consume residual HMR reactivity available for adhesive coupling. It was observed that heat treatment did not have any effect on the HMR efficacy. This finding indicated that proposed covalent bond between HMR and

adhesive might not be the cause for wood-adhesive bond durability enhancement (Christiansen, 2005).

Son and Gardner (2005) studied the thermomechanical behavior of HMR treated Maple wood veneers using dynamic mechanical analysis (DMA) (Son *et al.*, 2005). Authors reported no significant increase in the stiffness (storage modulus) due to HMR treatment. Additionally, reduction in lignin glass transition temperature was reported. With increasing HMR content, the reported lignin T_g varied from 56.9 to 42.2 °C. This trend was attributed to the plasticization of wood polymers by small HMR molecules. However, it is notable that during this DMA study the wood moisture content was ~ 7%. It is well established that for dry wood the lignin T_g is well beyond 180 °C (Back and Salmén, 1982). Even in the water saturated condition the lignin shows glass transition between 70 and 100 °C (Salmén, 1984). Therefore, it is very clear that the reported thermal transition by Son and Gardner is not the lignin glass transition temperature.

Sun and Frazier (2005) used static mechanical analysis in stress relaxation mode to determine the effect on HMR on amorphous wood polymers (Sun and Frazier, 2005). The stiffness of wood was reported to increase due to HMR treatment, which was in contradiction to the Son and Gardner (2005) finding. The coupling parameter (an indicator of polymer cooperativity), and relaxation time (the characteristic time required for a polymeric transition) was affected by HMR treatment. Both parameters were increased with HMR treatment, suggesting increased interaction between neighboring polymers in the amorphous region. This indicated that HMR effectively penetrated the cell wall and restricted the wood polymer mobility. It was however not very clear that which specific polymer was altered by HMR.

Based on the reviewed studies, a fundamental understanding of the interaction between wood and HMR is still not clear. Using different analytical tools, the studies described here are aimed to understand the fundamental mechanism underlying this durability enhancement.

1.2.3. Polymer viscoelasticity

Introduction

The mechanical response of a polymer as a response to an external force, almost without exception, is intermediate of an elastic solid and a viscous liquid. This type of behavior is known as viscoelasticity (Aklonis and MacKnight, 2005). An elastic solid, when deformed under an external stress, stores the energy and instantaneously returns to its original shape when the stress is removed. In contrast, when a viscous liquid is deformed it dissipates all the external energy and flows irreversibly to obtain a new shape. A polymeric material, however, demonstrates an intermediate behavior. When taken out of its equilibrium condition as a result of an external stress, a range of molecular motions take place to minimize this effect. These molecular motions are heavily dependent on temperature and time; and they provide information on the chemical and morphological nature of the polymeric system (Ward and Sweeney, 2004).

Time and temperature effect

Temperature and time have a profound effect on the mechanical properties of polymers. When an external stress/strain is applied to a polymeric material, molecules accommodate themselves such that the effect of stress/strain is minimized. These

molecular motions are dependent on the experimental temperature and time scale. At low temperatures polymer molecules have lower energy and restricted motion. Therefore, in response to an external excitation they react very slowly, thereby exhibiting a stiff behavior. This polymer state is called the glassy state. Similarly, at high temperatures, molecules are highly mobile and are able to dissipate the applied energy faster. This results in a softening; the polymer is considered to be in a rubbery state. Between these two states there is a characteristic temperature where stiff glassy polymers start to show long chain cooperative motions. This specific temperature is called the glass transition temperature (T_g) or glass/rubber transition temperature (Ngai and Rendell, 1991; Ward and Sweeney, 2004). Polymer mechanical properties are similarly affected by time, or rate of loading. If a short-term load is applied, the polymeric chains lack the time required to flow and dissipate energy, and thus behave in a stiff and glassy fashion. In contrast, if a load is applied over a long period of time, polymers have ample time to flow and dissipate energy and behave in a soft manner. Therefore, the effect of time and temperature is very similar on the polymeric motions and polymer mechanical properties. This wonderfully simple but powerful concept is widely used in polymer science to understand the physics of polymeric motions and consequently various polymer properties.

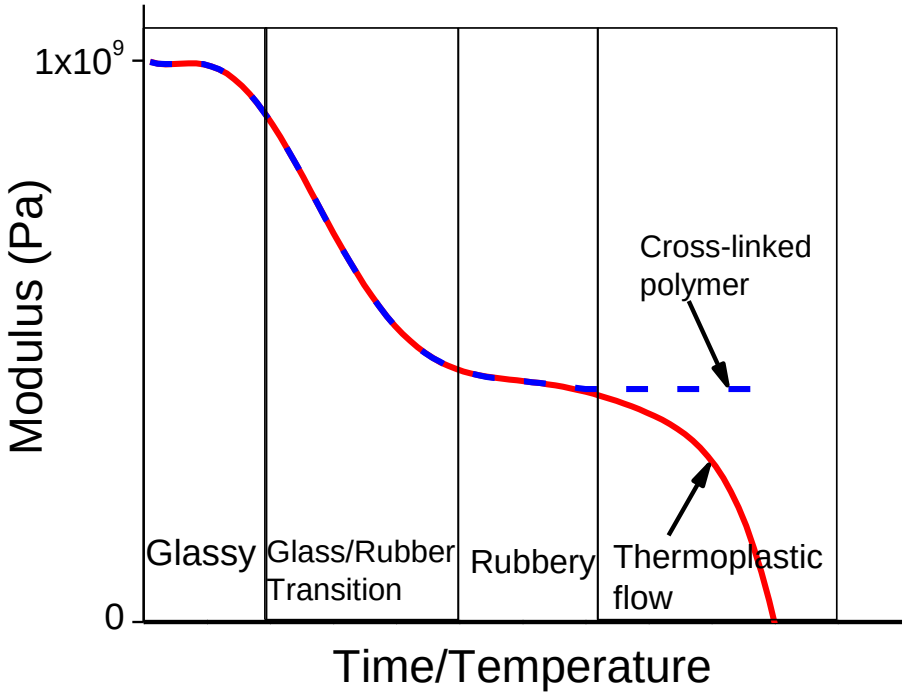

Figure 1-5 Generic representation of mechanical response zones for an amorphous polymer as a function of time or temperature.

Amorphous polymers show four distinct mechanical response zones as a function of time or temperature, Figure 1-5. At low temperatures or shorter experimental times the polymer acts as a glassy material (modulus ~ 10^9 Pa). This is often referred to as the glassy zone. As the temperature or time increases, the polymer goes through a zone where significant changes in the material response are seen. This is called the glass/rubber transition zone, or the viscoelastic transition zone (Ward and Sweeney, 2004). In this region, long chain segmental motions occur and polymer stiffness drops significantly (~ 10^3 Pa drop in stiffness). The temperature at which this occurs is called the glass transition temperature. Beyond this transition zone the

material property profile reaches a plateau region, called the rubbery plateau, which is due to chain entanglement. The magnitude of this region is an indication of the nature and extent of entanglement and/or cross-linking. For a cross-linked polymer this rubbery plateau holds flat to reach an equilibrium modulus with increasing time or temperature. However, for thermoplastic/uncross-linked polymers with increasing temperature or time, stiffness continues decreasing as the polymer chains disentangle and slide past one another. This last zone is called the flow region (Ward and Sweeney, 2004).

Glass transition temperature (T_g)

The glass transition temperature (T_g) is the characteristic temperature where within a narrow temperature range significant changes in the polymer mechanical properties are seen. At this temperature a discontinuity in the thermal expansion coefficient (α) of the polymer is observed (Ferry, 1980). Thermodynamically T_g is a second order transition because at this temperature the change in the heat capacity (C_P) and the thermal coefficient of expansion (α), as a function of temperature, show discontinuities. Since, these two quantities are obtained from the first order derivatives of the free energy, at T_g a second order change in the free energy is obtained, hence the name 2nd order thermodynamic transition.

Linear viscoelastic models

Most analytical techniques used for investigating polymer viscoelasticity are based on the assumption that within the range of applied stress/strain the behavior of the material is linearly viscoelastic. This means that the time-dependent relationship

between stress and strain can be described using a linear differential equation with constant coefficients (Ferry, 1980). In this scenario, the ratio of stress to strain is a only a function of time (or frequency) and not of the stress magnitude (Ferry, 1980; Rubinstein and Colby, 2003). The time-dependent stress/strain relationships are called constitutive relations or rheological equations of state. Simple mechanical analogs are used to deduce the constitutive equations and subsequently explain the material behavior.

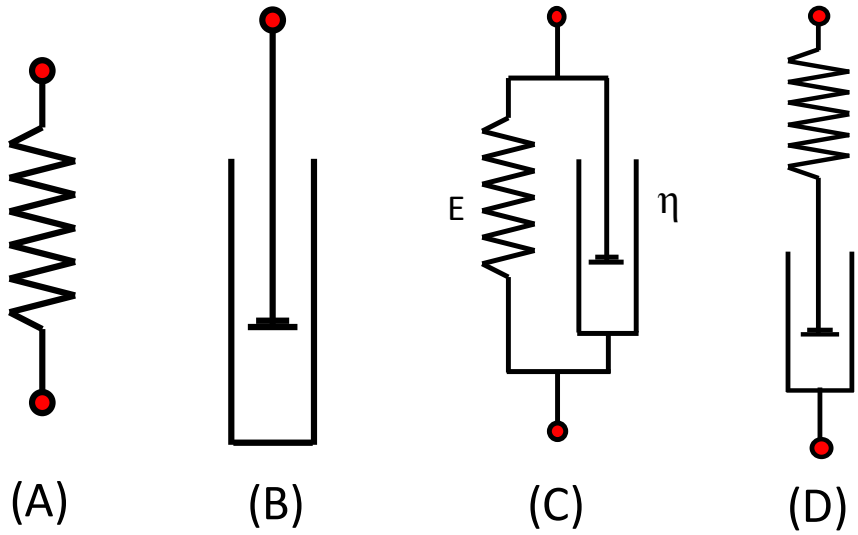

Figure 1-6 Mechanical analogs for (A) elastic solid, (B) viscous fluid, (C) Kelvin solid viscoelastic material, and (D) Maxwell fluid viscoelastic materials.

Linear elastic solids are represented as a Hookean spring Figure 1-6(A). The name came from English mathematician Robert Hook, who for the first time established the linear relationship between force and displacement. Hook's law relates axial stress to axial strain for an elastic body as,

$$\sigma = E\varepsilon. \qquad \text{Equation 1.1}$$

The idealized spring can store energy. When the load is removed stored energy causes the spring to regain its original shape (Ferry, 1980). A linearly viscous fluid is ideally represented as a Newtonian dashpot Figure 1-6 (B). For a linearly viscous fluid, the strain rate $\left(\frac{d\varepsilon}{dt}\right)$ is proportional to the applied stress. For a normal stress and resulting strain the constitutive relationship of stress and strain for a Newtonian dashpot is,

$$\sigma = \eta \frac{d\varepsilon}{dt} = \eta \dot{\varepsilon} \qquad \text{Equation 1.2}$$

A Newtonian dashpot cannot store any energy and all the applied energy is dissipated, almost always as heat. Therefore upon unloading, the dashpot lacks the energy to regain its original shape.

Individually Hookean springs and Newtonian dashpots are often not sufficient for phenomenological modeling of the polymeric viscoelastic response. However, these responses can be accurately modeled using different spring and dashpot combinations. A Voigt or Kelvin solid is a widely used building block to model polymer viscoelastic behavior Figure 1-6 (C). In this model a spring and a dashpot are combined in parallel. This formation works like a viscoelastic solid, as it does not show an instantaneous deformation upon step loading, but creep deformation is observed. Additionally, this element has a finite relaxed modulus (at time = ∞, relaxed modulus = E). Upon relaxing this element regains its original shape. The viscoelastic behavior of a cross linked polymeric system can also be explained with this representative model. The constitutive equation for the Kelvin solid element is,

$$\sigma = E\varepsilon + \eta \dot{\varepsilon} \qquad \text{Equation 1.3}$$

The Maxwell fluid is another widely used building block to model polymer viscoelasticity. In this model a Hookean spring and a Newtonian dashpot are combined in series Figure 1-6 (D). This element has fluid characteristics, as it has instantaneous response upon loading and the stress diminishes/dissipated with time. Additionally, after the load is removed this element does not regain its original shape. The constitutive equation for a Maxwell element is,

$$\sigma + \frac{\eta}{E}\dot{\sigma} = \eta\dot{\varepsilon} \qquad \text{Equation 1.4}$$

The difference in molecular motions for solid and fluid materials is clearly recognized at long experimental time ($t \rightarrow \infty$) or at high temperature. Cross linked polymers cannot deform indefinitely and their softening stops when the glass/rubber transition is complete. Consequently, these materials have non-zero equilibrium/relaxed modulus and are called viscoelastic solids. On the other hand thermoplastic polymers (without any cross-links) keep flowing indefinitely at high time or temperature regions as polymers continue to untangle and slide past one another. Therefore, the rubbery moduli of these materials keep decreasing. These are called viscoelastic fluids (Ngai and Rendell, 1991).

Individual Kelvin or Maxwell elements cannot adequately model the viscoelastic behavior of a polymer for large time/temperature ranges. However, combinations of spring, dashpot, Kelvin and Maxwell elements can accurately explain polymeric behavior. A long term creep response can be adequately modeled using an array of Kelvin elements connected in series such that the ratio of the viscosity coefficient (η) for the dashpot to the elastic coefficient (E) for the spring for each Kelvin element are in

increasing order. This ratio (η/E) is also called the retardation time (τ). Similarly, an array of Maxwell elements in parallel simulates stress relaxation. In this case the η/E is called the relaxation time (τ) and is arrayed in an increasing order.

Thermo-mechanical Analysis

Dynamic Mechanical Analysis

Dynamic mechanical analysis (DMA) is a widely used technique in polymer science, where a sinusoidal load/stress (σ) is applied on a material with an angular frequency (ω), and the corresponding sinusoidal strain (ε) is recorded. Figure 1-7 shows sinusoidal profiles of stress and corresponding strain in a typical DMA experiment. The applied stress and strain is given by,

$$\sigma(t) = \sigma_0 \cos \omega t \qquad \text{Equation 1.5}$$

$$\varepsilon(t) = \varepsilon_0 \cos(\omega t + \delta) \qquad \text{Equation 1.6}$$

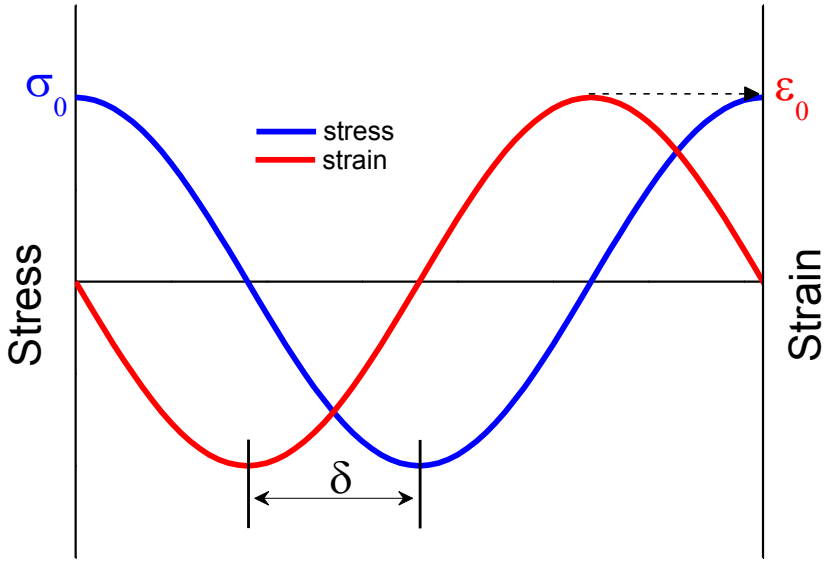

Figure 1-7. Response of a viscoelastic polymer to a sinusoidal stress in terms of sinusoidal strain. Sinusoidal stress leads the strain by a phase angle δ.

DMA experiments are generally performed within the linear viscoelastic region (LVR). Within the LVR, when a sinusoidal stress is applied on an elastic solid, the resulting sinusoidal strain perfectly follows the stress with a phase lag (δ) equal to zero, and is called in-phase. On the other hand, when a viscous liquid is loaded in a similar manner, the resulting sinusoidal strain follows the stress with a phase lag (δ) of 90° and is termed as out-of-phase(Ferry, 1980; Aklonis and MacKnight, 2005). During a DMA experiment, load applied by a load cell and corresponding displacement are recorded (Figure 1-7). These data are then processed in two different steps. First, the phase lag between the stress and strain is determined. This phase lag is recorded as an angle (δ). In the second step, the amplitudes of these two signals are compared. The stress

amplitude (σ_0) is calculated from applied load and specimen geometry. The strain amplitude (ε_0) is also calculated from the measured deformation. Using these two quantities and the phase lag (δ) two moduli are calculated as follows,

$$Storage\ Modulus = G' = \left(\frac{\sigma_0}{\varepsilon_0}\right)\cos\delta \qquad \text{Equation 1.7}$$

$$Loss\ Modulus = G'' = \left(\frac{\sigma_0}{\varepsilon_0}\right)\sin\delta \qquad \text{Equation 1.8}$$

Storage modulus, G′, is the energy stored in a material and recovered per cycle (Ferry, 1980; Ngai and Rendell, 1991; Ward and Sweeney, 2004). From Figure 1-7, the storage modulus, G′, is the stress at the maximum strain. In a physical sense of the material property, when strain is at its maximum, the strain rate is zero. Therefore, at that point the material is only acting as a response of the strain, thus acting as an elastic body (Ngai and Rendell, 1991). The loss modulus (G″), on the other hand, is the energy dissipated as heat through molecular friction (Ferry, 1980). From Figure 1-7, the loss modulus is the stress at zero strain. At zero strain for a sinusoidal strain profile, the strain rate is the maximum. Thus, at that point the material is acting in a response of strain rate as would a viscous material (Aklonis and MacKnight, 2005). Another highly useful quantity that can be obtained from this experiment is the loss tangent, defined as,

$$\tan\delta = \frac{Loss\ Modulus}{Storage\ Modulus} \qquad \text{Equation 1.9}$$

The loss tangent, tanδ, is a dimensionless quantity and is a ratio of the energy lost to the energy stored during a sinusoidal oscillation. tanδ is a measure of the macroscopic dampening effect of a free vibration, attenuation of a propagating wave and the frequency width of a resonance response (Ferry, 1980).

Effects of time and temperature on properties of a polymer reveal enormous information regarding the structure, morphology and processing conditions. DMA is the most sensitive tool to measure the polymer glass transition. Due to the large mechanical property change across the glass transition, DMA can document the T_g far more accurately than other thermal analysis methods like differential scanning calorimetry (DSC) or thermomechanical analysis (TMA) (Menard, 1999) where changes in the heat flow or sample dimension are recorded, respectively.

Static Mechanical Analysis

Static mechanical analysis is another convenient and powerful technique to investigate thermomechanical behavior of polymers. Instead of sinusoidal/dynamic stress/strain, a static stress or strain is applied on the specimen and the corresponding strain or stress is recorded. Two commonly employed static mechanical analysis modes are creep and stress relaxation. Creep is the measurement of time dependent strain following a step change in stress. Whereas, in a stress relaxation, a step change in the strain is applied and the time dependent stress is recorded (Ward and Sweeney, 2004). Phenomenologically a Kelvin element (or generalized Kelvin chain) and a Maxwell element (or generalized Maxwell ladder) adequately simulate the polymer creep and stress relaxation behaviors, respectively.

In case of a creep experiment, when the constitutive equation for the Kelvin element (Eq. 1.3) is solved between the experimental time scale ($0 < t < t_1$), the relation for the creep deformation as can be obtained as,

$$\varepsilon(t) = J\sigma\left[1 - \exp(-{}^{t}/_{\tau})\right] \qquad \text{Equation 1.10}$$

Where, J is the compliance and τ is the retardation time, the rate at which the relaxation is taking place (Ward and Sweeney, 2004). In a similar fashion for a stress relaxation experiment a Maxwell element gives the relation for time dependent stress as,

$$\sigma(t) = E\varepsilon \exp(-{}^{t}/_{\tau}) \qquad \text{Equation 1.11}$$

Where, E is the modulus and τ is the relaxation time with similar implication as the retardation time.

Time Temperature Superposition (TTS)

Effects of time and temperature on polymeric viscoelasticity are equivalent. This concept is briefly described in section 1.3.2. In its simplest form time-temperature equivalence suggests that viscoelastic behavior at one temperature can be related to the same property at another temperature by changing only the time scale (Ward and Sweeney, 2004). Depending on this principle, the time temperature superposition (TTS) concept has developed which states that the viscoelastic properties obtained at one temperature can be superimposed to the similar properties obtained at a different temperature only by shifting the curve along the log time axis (Williams *et al.*, 1955; Sperling, 2006). TTS is valid for amorphous polymeric transitions where the relaxation time distribution shows uniform temperature dependence. These polymers are termed as thermorheologically simple materials (Ferry, 1980; Laborie, 2002a; Ward and Sweeney, 2004). TTS experiments are performed for thermorheologically simple

polymers by conducting isothermal viscoelastic property measurements as a function of time/frequency. Similar measurements are conducted at different temperatures. Then, these isotherms are shifted along the time/frequency scale to form a smooth curve, popularly known as the master curve (Ward and Sweeney, 2004; Aklonis and MacKnight, 2005). The amount of shifting to make the master curve is known as the shift factor, $\log(a_T)$. The shift factor (a_T) is theorized as the ratio of mechanical relaxation time at temperature T to the relaxation time at the reference temperature (T_r). These times can be acquired from static or dynamic measurements of any viscoelastic properties or steady state viscosity measurements (Williams *et al.*, 1955). The shift factor in its physical sense reflects the temperature dependence of the segmental friction coefficient or molecular/segmental mobility; this is an important controlling factor for the rate of configurational rearrangement near the glass transition (Williams *et al.*, 1955).

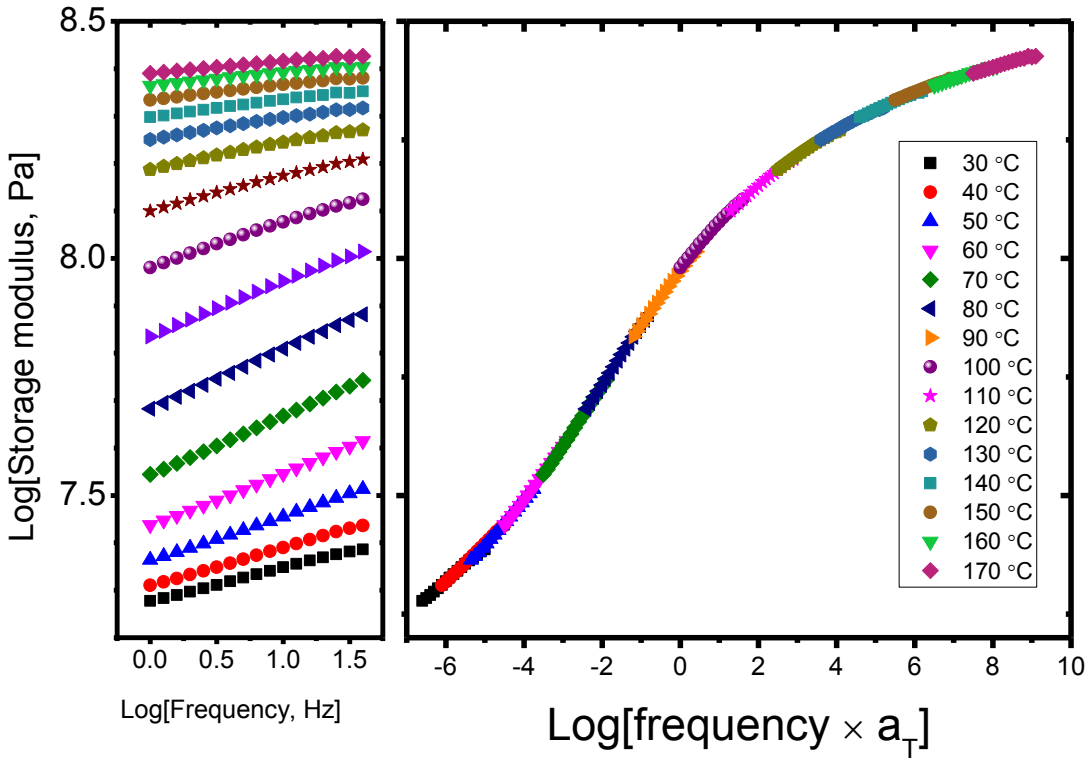

Figure 1-8 Construction of a master curve, illustrated with storage modulus data of glycerol-plasticized yellow-poplar (*Liriodendron tulipifera*) wood. The left hand section of the figure shows the isothermal frequency sweeps at different temperatures; the right hand section shows the shifted storage modulus master curve.

Figure 1-8 shows the formation of a master curve. Isothermal frequency sweep data of glycerol plasticized yellow-poplar (YP) wood were obtained at different temperatures. Isotherms were shifted along the frequency axis to form a smooth master curve. Figure 1-9 shows the shift factor plot as a function of temperature.

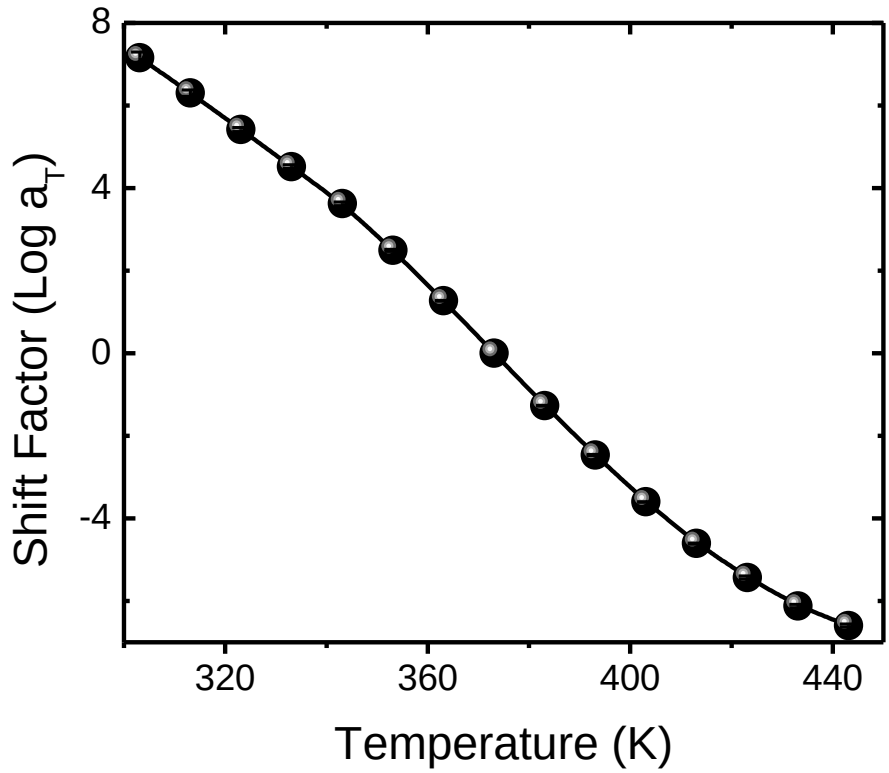

Figure 1-9 Shift factor plot for the master curve shown in Figure 1-8.

Williams, Lendel and Ferry (Williams *et al.*, 1955; Ferry, 1980; Ward and Sweeney, 2004) found that for thermorheologically simple amorphous polymers, the temperature dependence of the shift factor can be expressed with a unique empirical function (Eq. 1.12).

$$\log a_T = \log \frac{\tau_T}{\tau_r} = \log \frac{\eta_T}{\eta_r} = \frac{-C_1(T-T_r)}{C_2+(T-T_r)} \qquad \text{Equation 1.12}$$

Eq. 1.12 is known as the Williams-Lendel-Ferry (WLF) equation and is typically valid within a temperature window of [T_g ± 50] °C (Ward and Sweeney, 2004). In the WLF equation, the term C_1 and C_2 are constants and T_r is the reference temperature. When the reference temperature is set to the polymer's T_g, the constants C_1 and C_2 have been calculated to be 17.44 and 51.6K for many amorphous polymers. At first

thought to be universal constants, C_1 and C_2 are now recognized to vary from polymer to polymer (Ward and Sweeney, 2004; Aklonis and MacKnight, 2005). Introduced as an empirical relation, the WLF equation has strong physical interpretations in terms of molecular motions near the glass transition temperature. The equation can be derived from Doolittle's free volume theory or free space equation for viscosity (Doolittle, 1951; Williams *et al.*, 1955).

$$\eta = A \exp\left(B \times \frac{total\ volume}{free\ volume}\right) \qquad \text{Equation 1.13}$$

Where A and B are constants. According to Fox and Flory (Fox and Flory, 1950), as polymers are cooled near the glass transition the free volume sharply diminishes, a probable reason for sudden viscosity increase. This behavior is seen for all amorphous polymers, where the thermal expansion coefficient of polymers shows a discontinuity as it translates from rubber to glass, or vice versa (Figure 1-10) (Ward and Sweeney, 2004).

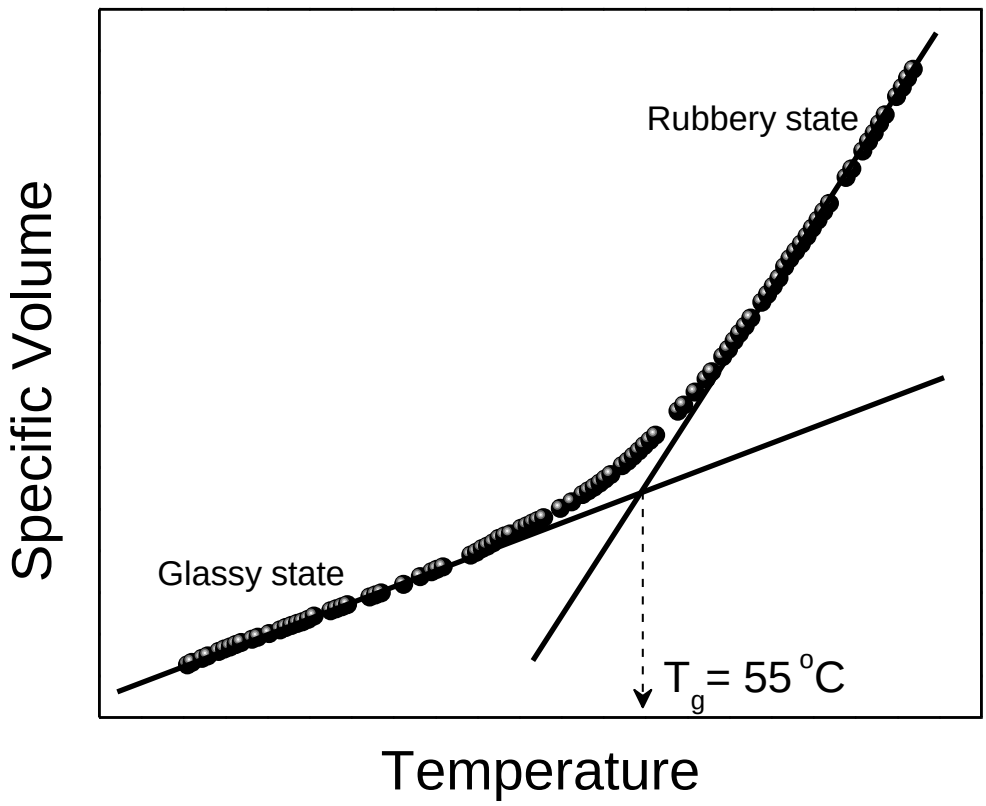

Figure 1-10 Volume-temperature relationship for amorphous polymers. Illustrated using swelling-temperature data for ethylene glycol plasticized yellow-poplar wood.

This discontinuity in the thermal expansion coefficient along with the change in the free volume indicates that at the transition temperature certain molecular rearrangements initiate which controls polymer viscoelastic properties Additionally, the presence of a universally applicable function such as the WLF equation implies that, independent of polymer molecular structures, the mechanism of this volume change and associated molecular/segmental rearrangements are essentially the same for all amorphous materials(Williams *et al.*, 1955; Ward and Sweeney, 2004).

As observed by many authors, the free volume (f_g) of glassy amorphous polymers changes very slightly until the T_g, and then increases linearly with increasing temperature (Fox and Flory, 1950; Williams *et al.*, 1955; Ward and Sweeney, 2004).

Therefore the fractional free volume $\left(f = \frac{free\ volume}{total\ volume}\right)$ can be expressed in terms of temperature and thermal coefficient of free volume expansion (α_f) as,

$$f = f_g + \alpha_f\left(T - T_g\right) \qquad \text{Equation 1.14}$$

Where f_g is the fractional free volume at the T_g. As mentioned previously, the shift factor is the ratio of relaxation time (τ) at temperature T to that at the T_g. Also, from the linear viscoelastic models (Section 141519.0.1073790980.) the relaxation time is the ratio of the viscosity of the dashpot (η) to the modulus of the spring (E). As the change in the viscosity is much larger in comparison to the change in the modulus, the modulus at both temperatures can be considered to be the same, and we have,

$$a_T = \frac{\tau_T}{\tau_{T_g}} = \frac{\eta_T}{\eta_{T_g}} \qquad \text{Equation 1.15}$$

Now combining Eq. 1.13 and Eq 1.15 we can have,

$$\ln a_T = B\left[\frac{1}{f} - \frac{1}{f_g}\right] \qquad \text{Equation 1.16}$$

In Eq. 1.16, substituting $f = f_g + \alpha_f\left(T - T_g\right)$ we have,

$$\log a_T = \frac{\left({}^{B}/_{2.303 f_g}\right)\left(T - T_g\right)}{\left({}^{f_g}/_{\alpha_f}\right) + T - T_g} \qquad \text{Equation 1.17}$$

This is the Williams-Lendel-Ferry equation derived from the free volume theory. Equating the constants of WLF equation with those of the obtained Eq. 1.17, we get the fractional free volume at T_g, f_g, as 0.025±0.0003 (Williams *et al.*, 1955; Ward and Sweeney, 2004) and thermal expansion coefficient of free volume, α_f, as 4.8×10^{-4} K.

These two quantities are applicable to most amorphous polymers (Williams *et al.*, 1955; Ward and Sweeney, 2004).

Cooperativity in glass forming polymers

The concept of molecular cooperativity was first introduced by Adams and Gibbs (Adam and Gibbs, 1965). They used the existing transition state theory, where the molecular change during relaxation was pictured as a change in energy state across an energy barrier (Ferry, 1980; Ward and Sweeney, 2004). The population for each state follows the Boltzmann distribution (Ferry, 1980). Adams and Gibbs modified the transition state theory by considering molecular relaxation taking place in a number of cooperatively rearranging molecular units (Adam and Gibbs, 1965). This number of units, namely z*(T), is a function of temperature (Adam and Gibbs, 1965). At a certain temperature these cooperatively rearranging units relax simultaneously, giving an expression for the relaxation time $\tau(T)$,

$$\tau(T) = \tau_0(T) \exp\left[z^*(T)\frac{\Delta\mu}{kT}\right] \qquad \text{Equation 1.18}$$

In the above equation, $\tau_0(T)$ is the independent relaxation time for molecules well above T_g, k is the Boltzmann constant and $\Delta\mu$ is the activation energy from transition state theory. In this theory, the slowing of molecular relaxation as glass-forming liquids are cooled from well above its T_g, is related to the increasing number of cooperatively rearranging molecular entities (Adam and Gibbs, 1965).

Ngai advanced the Adams-Gibbs theory to explain the cooperativity of amorphous polymers near the glass transition temperature. According to the Adams-Gibbs theory a unique molecular relaxation was considered for all temperature regions.

However, a deviation from the Arrhenius behavior is commonly observed for polymers near the glass transition. This suggests that the relaxation time is different near the glass transition temperature than when the temperature is far above the T_g. Ngai proposed two distinct relaxation zones for glass forming polymers (Ngai and Rendell, 1991). First, the temperature region far above the T_g ($T>T_g+80$ K). In this region the polymer molecules have enough energy to relax independent of non-bonded segments with the primitive relaxation time (τ_0), as defined by the Adams-Gibbs theory (see Eq 1.18) (Adam and Gibbs, 1965). The second zone was at the temperature below T_g+80K. In this region the molecular motions are cooperatively restricted by neighboring non-bonded segments. This restriction, or the extent of cooperativity, increases as the temperature approaches the T_g. This causes longer relaxation times due to larger cooperatively rearranging molecular entities. Consequently, the relaxation function deviates from its linear exponential form (as obtained from the Adams-Gibbs theory) to a non-linear profile. This non-linear relaxation profile near the glass transition temperature is well described by the Kohlrausch-Williams-Watt (KWW) stretched exponential model (Eq. 1.19) (Kohlrausch, 1847; Williams and Watts, 1970b).

$$\phi(t) = \exp\left[-\left({}^{t}/_{\tau}\right)^{\beta}\right] \qquad \text{Equation 1.19}$$

In Eq. 1.19 the two parameters are τ, the mean relaxation time and β, the non-exponentiality parameter, which describes the breadth of the relaxation time distribution (Williams and Watts, 1970b). The value of β ranges between 0 and 1. For a non-cooperative system, molecules have a unique relaxation time and the value of β

becomes 1 and the relaxation function becomes similar to the Adams-Gibbs theory (Ngai, 1999). In a system with high cooperativity between non-bonded segments, a distribution of relaxation time is obtained and the value of β decreases. At this region the relaxation time follows a stretched exponential function as suggested by Ngai (Eq. 1.20) (Ngai, 1999).

$$\phi(t) = \exp\left[-\left({}^{t}/_{\tau^*}\right)^{1-n}\right] \qquad \text{Equation 1.20}$$

Here, τ^* is the characteristic relaxation time for the cooperatively restricted polymer chains and 'n' is called the coupling constant. The coupling constant ($0 < n < 1$) is a quantitative measure of the extent of coupling between non-bonded segments in a polymer. When compared Eq. 1.19 and 1.20, the KWW non-exponentiality parameter β can easily be related to the coupling constant as $n=1-\beta$. The transition between the regions of independent relaxation and the regions of cooperative relaxation takes place at a temperature independent characteristic time, termed as the crossover time (t_c) (Ngai, 1999). For any time scale, a generalized expression for the relaxation time is provided by Ngai as a function of crossover frequency (ω_c), coupling constant (n) and primitive relaxation time (τ_0) as in Eq. 1.21.

$$\tau^*(T) = \left[(1-n)\omega_c^n \tau_0(T)\right]^{1/(1-n)} \qquad \text{Equation 1.21}$$

In Eq. 1.21, when n becomes 0, the relaxation time becomes identical to the primitive relaxation time (τ_0) as would be for an independent and non-cooparative relaxation. With increasing n the relaxation time distribution becomes wider and the model shows a non-exponential pattern, exhibiting a higher degree of cooperativity.

1.2.4. Viscoelasticity of Wood

Wood is viscoelastic in nature, i.e., when deformed it behaves as both elastic (that stores energy) and viscous (that dissipates energy) material (Olsson and Salmén, 1993). Viscoelastic properties of wood have been studied for last half a century because of its high importance in the construction, composite, and paper industries. Wood is one of the primary raw materials in construction industries and the primary source of paper pulp. Thermal softening and short and long term viscoelastic responses of wood are thus very important, and are often studied. Hoglund et al. was the first to show the effect of the thermal softening of lignin and its impact on energy consumption of pulping process (Höglund *et al.*, 1976). The recent need for sustainable bio-energy has enhanced the impetus to understand wood for its optimum utilization.

As discussed before, wood is composed of four primary bio-polymers, namely, semicrystalline cellulose, amorphous hemicelluloses (xylan and glucomannan) and amorphous lignin. These four polymers are combined in a complex fashion within the wood cell wall structure. Dynamic mechanical analysis (DMA) is extensively used to understand the behavior of these polymers, in both isolated and *in-situ* conditions. DMA was first used to investigate the viscoelasticity of wood in the 1960s, using a torsional pendulum mode on rectangular specimens (Norimoto and Yamada, 1966; Becker and Noack, 1968). Since then extensive studies on wood have been conducted in torsion, bending and tension modes (Becker and Noack, 1968; Sadoh, 1981; Salmén, 1984; Kelley *et al.*, 1987; Olsson and Salmén, 1992; Kojiro *et al.*, 2003b, a; Das and Frazier, 2004; Kojiro *et al.*, 2006; Sun *et al.*, 2007).

In dry wood, glass transitions temperatures (T_gs) for *in-situ* amorphous cellulose, hemicellulose and lignin take place between 200-250 °C, 150-220 °C and ~205 °C, respectively (Back and Salmén, 1982), typically in a thermodegradative fashion. However, plasticizing solvents can effectively reduce the wood T_g to much lower temperatures. Studies have been shown the effects of water (Höglund *et al.*, 1976; Salmén, 1984; Kelley *et al.*, 1987; Salmén and Olsson, 1998; Laborie *et al.*, 2004; Laborie *et al.*, 2006) and non-aqueous (Sadoh, 1981; Kelley *et al.*, 1987; Laborie *et al.*, 2004) solvents on the major wood-polymer relaxations. Water saturated wood shows a major relaxation between 60 and 95 °C. Among the non-aqueous solvents, ethylene glycol causes plasticization similar to water, and formamide is a much stronger plasticizer, reducing the lignin T_g close to 40 °C (Sadoh, 1981). In 1984 Salmén documented the viscoelastic properties of *in-situ* lignin in water-soaked spruce wood (Salmén, 1984). In this paper, the applicability of DMA and, for the first time, time temperature superposition (TTS) on wood-polymers was shown. The major transition around 100 °C was attributed to the lignin T_g and was found to follow the WLF model, although in a limited fashion. Salmén also calculated the activation energy for this transition to be 450 KJ/mol, which is within the standard glass transition activation energy range (Salmén, 1984). In a later study, Olsson and Salmén showed that this transition correlates with lignin polymers having different monomer compositions, proving that it is indeed the lignin T_g (Olsson and Salmén, 1997). It has also been reported that in solvent saturated conditions, the hemicellulose T_g is moved to sub ambient temperatures (Kelley *et al.*, 1987). Using moisture controlled DMA, Salmén and Olsson showed the morphological difference between *in-situ* xylan and

glucomannan (Salmén and Olsson, 1998). A humidity scan between 40 and 100% was performed at 80 °C. No hemicelluloses transition was observed in wood. However when lignin is extracted from the wood, the xylan softening was seen, which disappeared upon xylan removal. This led the authors conclude that xylan motion in wood is restricted by lignin and these two polymers are closely associated. Whereas, glucomannan was reported to be associated with cellulose microfibrils (Salmén and Olsson, 1998). Relaxation of *in-situ* hemicelluloses in water plasticized condition was studied by several researchers (Kelley *et al.*, 1987; Furuta *et al.*, 2001). Furuta et al. performed DMA on Japanese hinoki wood equilibrated at different moisture contents, and on isolated lignin and amorphous polysaccharides. They observed a relaxation at around -40 °C. This relaxation was frequency and solvent content dependent, with increasing solvent content and frequency the relaxation temperature decreased and increased, respectively. This relaxation in hinoki wood was consistent with a similar thermal relaxation for isolated polysaccharide solutions (Furuta *et al.*, 2001).

Viscoelastic measurements are also conducted to investigate the polymeric nature and mobility as it is affected by structure. Comparative studies of hardwood and softwood showed that the subtle structural differences in the wood cell wall composition can be identified using DMA. Olsson and Salmén conducted a comparative study of hardwoods and softwoods and found that hardwood lignins have lower T_g's in comparison to softwood lignins (Olsson and Salmén, 1992, 1993). This is attributed to the lower cross-link density in hardwood lignins than in softwood lignins, as dictated by differences in lignin monomer composition. In hardwood lignins, the lower occurrence of free phenolic hydroxyl groups and the higher occurrence of methoxyl groups causes

less cross-linking, thus higher polymer mobility is observed (Olsson and Salmén, 1992, 1993). When hardwood lignin is treated with acid and heat, the cross link density increases, causing an increase in the transition temperature (Olsson and Salmén, 1992). Applicability of the TTS principle is further established in this study for solvent plasticized wood (Olsson and Salmén, 1992). Laborie et al., for the first time, demonstrated the applicability of the Ngai coupling model on the lignin T_g (Laborie *et al.*, 2004). In this study the Plazek and Ngai intermolecular coupling model was applied on the *in-situ* lignin T_g of ethylene glycol plasticized yellow-poplar and spruce wood (Plazek and Ngai, 1991; Laborie *et al.*, 2004). Using dynamic TTS experiments and cooperativity analysis they showed that at a higher temperature, above the main softening of wood, the segmental relaxation could be described by the empirical Plazek and Ngai coupling model. This suggested that this subtle technique can be efficiently used to probe molecular motions in wood (Laborie *et al.*, 2004).

As described in section 162024.0.1073790980. , DMA is commonly performed within the linear viscoelastic response (LVR) region, where the viscoelastic response (e.g., strain) is proportional to the input (stress). Within this very low stress region the polymer packing is not affected by the applied stress and the response manifests the fundamental polymer properties (Rubinstein and Colby, 2003; Ward and Sweeney, 2004; Sun *et al.*, 2007). Using single cantilever bending mode Sun et al. found that the LVR strain limit for dry wood was very low (0.03 – 0.16%) (Sun *et al.*, 2007). The LVR was also found to be a function of grain direction and species. Similarly, investigating the grain direction effects on wood viscoelasticity, Backman and Lindberg (2001)

showed that dynamic tensile properties differ in the tangential and radial directions in *Pinus sylvestris* (Backman and Lindberg, 2001).

Viscoelastic measurement of wood is widely used to probe the effects of different chemical treatments on the wood polymer mobility. As an example, Obataya et al. (2003) showed that acetylation of spruce wood reduced the dry wood thermal softening temperature (Obataya *et al.*, 2003). This was a clear indication of increasing mobility in the amorphous domain of wood. Investigation of wood-adhesive interaction is another important field where dynamic/static mechanical analysis is extensively used. The presence of wood alters the adhesive curing at the same time mobility of wood polymers are also significantly influenced by adhesives. Using DMA and solid state NMR, Marcinko et al. (1998) showed that the major transition temperature of wood was significantly reduced in the presence of polymeric methylenebis(phenylisocyanate) (pMDI) adhesives; whereas urea formaldehyde (UF) did not influence the wood thermal softening (Marcinko *et al.*, 1998). Morphology of wood and phenol formaldehyde (PF) adhesive interphase was studied by Laborie et al. using DMA (Laborie, 2002a; Laborie *et al.*, 2006). In this study, yellow-poplar (*Liriodendron tulipifera*) was treated with low and high molecular weight PF resins. The low molecular weight PF did not influence the wood T_g. However, using the Ngai coupling model they showed that the intermolecular cooperativity/coupling was significantly increased due to curing of PF in wood. This phenomenon was attributed to the nanometer scale mixing of low molecular weight PF with the amorphous domain of wood and an interpenetrating network formation (Laborie, 2002a; Laborie *et al.*, 2006).

Static mechanical analyses in both creep and stress relaxation modes are used to study wood-polymeric motions and how these are affected by different chemical treatments (Das, 2005; Lopez-Suevos and Frazier, 2005; Sun and Frazier, 2005; Lopez- Suevos and Frazier, 2006; Lopez-Suevos and Frazier, 2006; Sun and Frazier, 2006). Long term creep behavior is conveniently studied using isothermal creep experiments at different temperatures, and subsequently applying the TTS principle to form a master curve. This method provides a wealth of wood molecular level information (Das, 2005; Sun and Frazier, 2006). Studies have shown that the static mechanical analysis is very sensitive to moisture content, temperature and physical aging (Bodig and Jayne, 1993; Das, 2005). Das (Das, 2005), for the first time, applied the empirical Kohlrausch-Williams-Watt (KWW) model to describe the creep behavior of wood and its interaction with pMDI adhesives. Creep behavior of two species (yellow-poplar and southern yellow pine) were shown to be different at the molecular level, as the coupling parameters for these two species were significantly different.

1.2.5. Nuclear Magnetic Resonance (NMR)

Nuclear magnetic resonance (NMR) is a phenomenon which depends on the magnetic property of atomic nuclei. Certain atomic nuclei, when placed in a strong magnetic field, resonate at a characteristic frequency in the radio frequency range of electromagnetic spectrum. Small variation in this characteristic frequency reveals wealth of information regarding the chemical and morphological environment of the nucleus(Jacobsen, 2007). Spin is an especially important nuclear property; it is a form of angular momentum, though not associated to rotational momentum(Levitt, 2008). The spin property of a particle is designated by the spin quantum number (S). Depending on the specific particle (proton, neutron, electron, photon etc.), the value of S can either be integers (S=0, 1, 2,…) or half integers (S= 1/2, 3/2, 5/2,…..). Particles with half integer S are categorized as the “fermions,” while particles with integer S are called the “bosons” (Levitt, 2008). The spin quantum number for any nucleus is conventionally denoted as “I”, and is the combination of the spin quantum numbers of its constituent elementary particles. Nuclei with spin I have (2I+1) energy sublevels, which are degenerate in the absence of any external field. However, when placed in an external magnetic/electric field this degeneracy is disrupted. The splitting between the spin sublevels is called the Zeeman splitting (Figure 1-11) This splitting is proportional to the external magnetic/electric field and in most scenarios NMR is the spectroscopy of this splitting (Levitt, 2008).

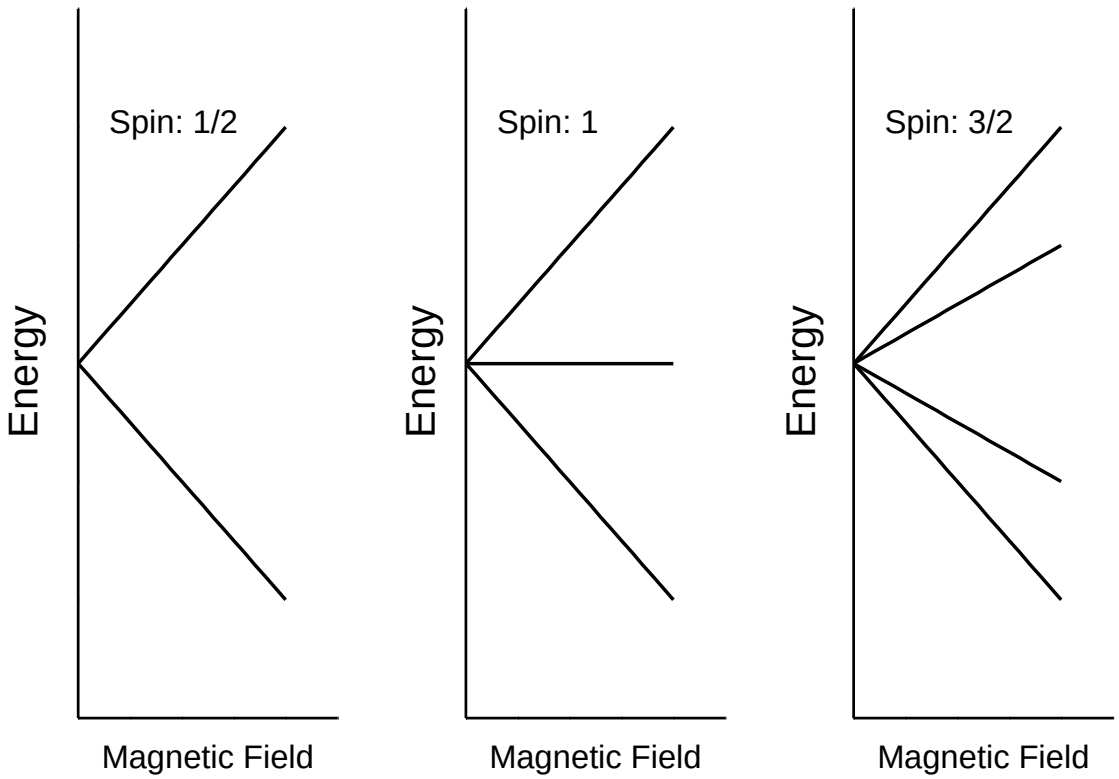

Figure 1-11. Nuclear Zeeman splitting for nuclei with different spins.

Quadrupolar Coupling

Nuclei with spin greater than ½ possess a non-spherical nuclear charge and are called quadrupolar nuclei. In a system, these nuclei interact with the surrounding electron cloud; this phenomenon is called quadrupolar coupling (Levitt, 2008). In this review quadrupolar coupling of spin (I) = 1 nuclei, specifically ^{2}H will be discussed. Quadrupolar interaction depends heavily on both nuclear and molecular properties,

such as the electric field gradient created around the nucleus. A very simple example of quadrupolar interaction can be explained using a C – D bond as shown in Figure 1-12.

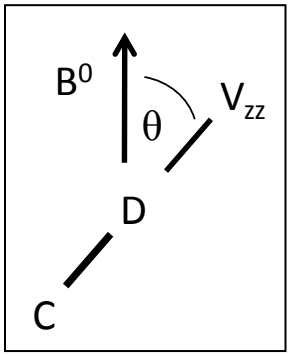

Figure 1-12 Electric field gradient for a C - D bond. B^0 is the spectrometer magnetic field and V_{zz} is the electric field gradient of C – D bond.

The Zeeman splitting for spin = 1 ^{2}H produces three energy levels (see Figure 1-11). Without the quadrupolar interaction these energy levels are equally spaced by the Larmor frequency (ω_0). However, when the environment around the nucleus is anisotropic these energy levels lose their degeneracy (see Figure 1-13).

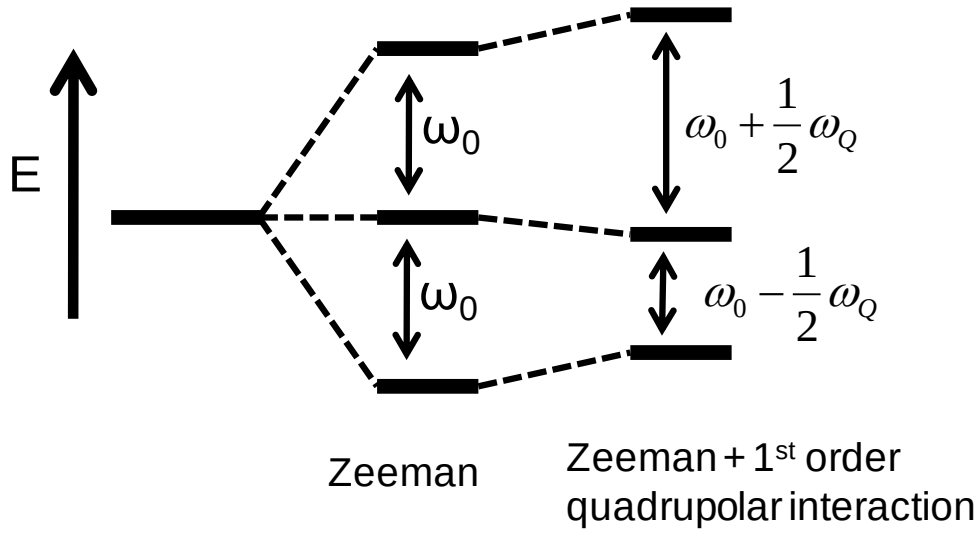

Figure 1-13 Energy levels for a ^{2}H nucleus under quadrupolar interaction. ω_0 is the Larmor frequency and ω_Q is the first order quadrupolar coupling.

In the case of ^{2}H, the quadrupolar shift is very small when compared to the large Zeeman splitting, ω_0. In that case the quadrupolar interaction can be conveniently assumed to be a first order perturbation along the z-magnetization axis (Deloche and Samulski, 1981; Kilfoil and Callaghan, 2000; Levitt, 2008). In the case of an axially symmetric bond axis (e.g., C – D bond, see Figure 1-12), the quadrupolar interaction Hamiltonian takes the form of Eq. 1.22.

$$\mathcal{H}_Q = \frac{3eV_{zz}Q}{4I(2I-1)} P_2(\cos\theta)(3I_z^2 - I^2) \qquad \text{Equation 1.22}$$

Where, θ is the angle between the field gradient axis and the B^0, V_{zz} is electric field gradient strength, I is the nuclear spin quantum number, Q is nuclear quadrupole moment, and $P_2(\cos\theta)$ is the 2nd Legendre polynomial representing the dependence of H_Q on θ. The quadrupolar coupling splits the resonance of ^{2}H into a doublet by the amount of $\left(\frac{3}{2}\frac{eV_{zz}Q}{\mathrm{h}}\right) P_2(\cos\theta)$ in the frequency scale (Deloche and Samulski, 1981; Kilfoil and Callaghan, 2000; Li *et al.*, 2009). In an isotropic liquid system, rapid molecular motions causes θ to rapidly fluctuate in all possible values, making the average $\mathcal{H}_Q$ to be zero, thus we get a singlet of ^{2}H resonance. Conversely, for a partially averaged $\mathcal{H}_Q$, the degeneracy of two of the three Zeeman levels is broken (Deloche and Samulski, 1981). This is manifested as a doublet in the ^{2}H spectrum. Eq. 1.23 explains the quadrupolar splitting in the frequency scale (Li *et al.*, 2009).

$$\Delta\nu = Q_P S P_2(\cos\theta) \qquad \text{Equation 1.23}$$

Here Q_P is the quadrupolar coupling constant, and $S = \langle P_2(\cos\chi)\rangle$ is the orientational order parameter (also known as Hermann's orientation function) which is equal to the ensemble average over the 2nd Legendre polynomial with χ as the angle

between a particular C – D bond and the alignment axis of the matrix. θ is the angle between the matrix alignment axis and B^0.

Now, let us consider that a small deuterated molecule is diffused in an oriented polymer matrix. The rapidly moving small molecule will sample the aligned polymer segment and will acquire a "scaled down" orientation (lower but comparable degree of orientation as that of the polymer segment). The ^2H spectrum of the probe molecule will consequently show a scaled down quadrupolar splitting due to so-called "pseudo-nematic interactions" (Deloche and Samulski, 1981; Kilfoil and Callaghan, 2000). Eq. 1.23 can be rewritten for the matrix where the probe molecules reside as: Eq. 1.24.

$$\Delta\nu = Q_P \rho S_{matrix} P_2(\cos\theta) \qquad \text{Equation 1.24}$$

Here, $S_{matrix} = \langle P_2(\cos\alpha)\rangle$ is the ensemble average over the 2nd Legendre polynomial, with α being the angle between the alignment axis of the matrix and B^0, and ρ representing a scaling factor depending on the interaction between a specific probe molecule and matrix (Li *et al.*, 2009). Therefore, for a specific probe-matrix system the quadrupolar splitting can be used as an indicator of orientational order and the angle of alignment.

1.2.6. Application of ^2H NMR in understanding polymer anisotropy

Polymer-orientations are extensively studied using ^2H NMR quadrupolar coupling (Deloche *et al.*, 1982; Gronski *et al.*, 1984; Deloche *et al.*, 1986; Dubault *et al.*, 1987; McLoughlin *et al.*, 1997). Deloche and Samulski studied the effect of uniaxial strain on the orientational order of polyisoprene using ^2H NMR (Deloche and Samulski, 1981). Small deuterated probe molecules were doped in the polymer network. The change in

the short range segmental orientation as a function of uniaxial strain was studied using quadrupolar splitting. In another work Gronski et al. (1984) studied the effect of extensional strain on the orientation of 1-4-polybutadiene (Gronski *et al.*, 1984). Instead of using a deuterated probe, the segmental orientation was studied using a homogeneously and selectively deuterated network. The quadrupolar splitting was adequately used to explain the increased orientation of the network with increasing elongation. Using ^{2}H NMR, the authors also showed that the degree of orientation was higher for short segments near a cross-link point rather than for a long segment. Dubault et al. (1987) investigated the effect of cross-link density on the effective orientation of poly(dimethylsiloxane) (Dubault *et al.*, 1987). The network was either swollen by deuterated benzene or labeled with ^{2}H. The cross-link density was found to increase the effective orientation in the network. Additionally it was shown that increasing swelling-solvent content reduced the quadrupolar splitting (Dubault *et al.*, 1987). Sotta et al. (1987) took another approach where they introduced deuterated linear chains of PDMS or polyurethanes (PU) in the cross-link network of PDMS and PU, respectively (Sotta *et al.*, 1987). The effect of strain on the orientation of the network was determined using the induced alignment of the doped linear chains. This work showed the applicability of the ^{2}H NMR technique to investigate polymer segmental motions. The stress-induced orientation in a rubber network was found to be strongly influenced by short range segmental couplings. In 1990 Sotta et al. showed that the local anisotropy of polymeric network could be studied using ^{2}H NMR (Sotta and Deloche, 1990). It was demonstrated that the shape of a deuterium spectrum could provide information regarding the local variation in the orientational order parameters

(S). The authors suggested that the distribution in the local S caused the spectra to deviate from a Lorentzian shape. These varying localized S were reported to be different than the mean orientational director of the sample. This inhomogeneity in the local S parameters was attributed to polydispersity of PDMS and inhomogeneous cross-link density.

McLoughlin et al. (1997) studied the change in the orientational ordering of a selectively deuterated PDMS network as a function of uniaxial compressive strain (McLoughlin *et al.*, 1997). The results indicated that the quadrupolar splitting was strongly related to the excluded volume interaction of all polymer segments under deformation. In another very significant study Zeghal et al. (1999) studied the effects of different solvents on the orientational order of PDMS having a swollen brush morphology (Zeghal *et al.*, 1999). The preferential orientation was reported to be solvent dependent (good solvent vs. poor solvent). In a poor solvent the polymer chains showed a negative orientational order parameter (S). This suggested that the chains were parallel to the grafting substrate, or in other words perpendicular to the static magnetic field. However, when grafted polymers were swollen with good solvents, the S parameter was positive. This suggested that the polymer chains were preferentially oriented perpendicular to the substrate, or in other words parallel to the magnetic field. Additionally, it was shown that for a set of poor solvents, with increasing solvent quality the anisotropy was decreased. On the contrary, for good solvents, with increasing solvent quality, the average anisotropy increased. This was rationalized by the relative swelling capacity of different solvents. In a poor solvent the grafted polymer chains were squeezed, whereas in a good solvent the polymer chains were swelled and

reached an extended conformation due to excluded volume interaction of solvent and the polymer. Unlike polymers in poor solvents, a broader distribution of the S parameter was also reported for polymer in good solvents. This suggested that when swollen with a good solvent, unoriented segments coexisted with highly oriented segments. In poor solvent however, a narrower distribution of S indicated a more uniform anisotropic organization in the network (Zeghal *et al.*, 1999).

Orientational properties of polymers under confined conditions are investigated using the ^{2}H quadrupolar interaction (Deloche, 2003; Lorthioir *et al.*, 2003). Segmental dynamics of polymers, while confined between two rigid phases (e.g., block copolymers, crystalline phases, rigid surfaces etc.), differ significantly from unconfined polymer melts. The S parameter and the distribution of S parameter P(S) were shown to be strongly dependent on the nature of confinement (Deloche, 2003; Lorthioir *et al.*, 2003). Polymer chains which are end grafted to a rigid surface showed a broader P(S) distribution than a free (yet confined) chain. It was also identified that in the vicinity of a rigid surface polymer segments acquire a surface-induced alignment along the surface direction. However, when grafted to the surface, the alignment was preferentially perpendicular to the surface. This type of behavior should be very important for understanding the organization of cell wall structure where the amorphous polymeric matrix is confined between rigid crystalline fibrils.

Li and coworkers studied the orientational order and dynamics of hydrophilic phases in perfluorosulfonate ionomers (Nafion®) (Li *et al.*, 2008, 2009). Extruded and dispersion-cast polymer films were doped using various levels of D_2O, and residual quadrupolar interaction was observed. Extruded films showed a biaxial orientation of

the hydrophilic channels along the extrusion direction, while dispersion cast films showed uniaxial orientation through-plane alignment (Li *et al.*, 2008, 2009). Self diffusion of D_2O was measured for various Nafion films using an isothermal pulse gradient stimulated echo (PGSTE) experiment (Li *et al.*, 2009). A direct correlation between the anisotropic water diffusion and orientational order parameter was reported.

Deuterium NMR is successfully employed to understand the morphology of various polymeric systems. This technique is chemically and orientationally very specific, and subtle changes in the molecular organization can be explained. As mentioned before, the supramolecular structure of the wood cell wall is very complex and not completely understood. Therefore, a wide scope of ^{2}H NMR lies in the analysis of cell wall structure of lignocellulosic biomass.

1.2.7. Fourier Transformed Infrared Spectroscopy (FT-IR)

Fourier transformed infrared spectroscopy has been a powerful tool to indentify the chemical nature of wood polymers as well as understanding the supramolecular cell wall structure. Historically, cellulose has been the main focus of the morphological research of the wood cell wall due to its major influence on the mechanical and physical properties of wood. However, these properties, especially along the transverse direction and in moist conditions, heavily depend on the morphology of the amorphous matrix (Salmén *et al.*, 2008). Table 1-1 lists some important IR bands for wood-polymers (Marchessault and Liang, 1962; Åkerholm and Salmén, 2004; Schwanninger *et al.*, 2004; Jungnikl *et al.*, 2008).

Table 1-1 Significant IR bands for wood-polymers in softwoods. (Jungnikl *et al.*, 2008))

Polymer	Wave-number (cm^{-1})	Band assignment	Reference
Cellulose	1107	Anti-symmetric ring stretching	Ref.(Liang and Marchessault, 1959; Marchessault and Liang, 1960)
	1160	Anti-symmetric C-O-C bridge stretching	Ref.(Liang and Marchessault, 1959)
Glucomannan	805	In-phase ring stretching, mannose residue	Ref. (Marchessault and Liang, 1962)
	870	Equatorial C(2)-H bond mannose residue deformation	Ref. (Marchessault and Liang, 1962)
Xylan	1245	C=O side groups	Ref. (Åkerholm and Salmén, 2004)
	1600	C=O stretch, side groups	Ref. (Åkerholm and Salmén, 2004)
	1730	C=O stretch, side groups	Ref. (Åkerholm and Salmén, 2004)
Lignin	1140	Aromatic in-plane C-H deformation, typical for Guiacyl units	Ref. (Schwanninger *et al.*, 2004)
	1221	C-C, C-O and C=O stretch, typical for Guiacyl units	Ref. (Schwanninger *et al.*, 2004)
	1423	Aromatic skeletal vibrations	Ref. (Schwanninger *et al.*, 2004)
	1510	Aromatic skeletal vibrations	Ref. (Schwanninger *et al.*, 2004)

Marchessault and Liang (1962) were among the first to employ polarized infrared spectroscopy to study the orientation of the amorphous wood polymers (Marchessault and Liang, 1962). The fiber direction of a red maple (*Acer rubrum*) section was aligned (0°) or made perpendicular (90°) with a polarizer. The orientation of xylan was demonstrated using the dichroism of the C = O stretching at 1725 cm^{-1} and $–CH_2$ symmetric bending at 1465 cm^{-1}, two characteristic peaks for xylan. It was concluded that xylan was oriented in that species, and likely others as well.

In another important work, Hinterstoisser and Salmén (1999) introduced 2D step-scan FT-IR coupled with DMA in the study of cellulose (Hinterstoisser and Salmén, 1999). With these techniques they showed that the broad hydroxyl infrared absorption between 3700 and 3000 cm^{-1} could be separated into distinct bands. This enabled the authors to identify different –OH groups in cellulose and the inter- and intra-molecular interactions between cellulose chains (Hinterstoisser and Salmén, 1999). In 2001, Akerholm and Salmén studied the mechanical interactions between cellulose, xylan and glucomannan using dynamic FT-IR (Åkerholm and Salmén, 2001). In this technique de-lignified Norway spruce fibers were formed into a sheet and tested under transmission mode. Sheets were dynamically stretched while a step-scan interferometry was employed to get in-phase (elastic), out-of-phase (viscous) and 2D correlation spectra. The authors showed that this technique could be used to separate the absorption spectra for cellulose and hemicelluloses. More importantly this work showed that glucomannan and xylan had different mechanical responses. It was claimed that the glucomannan was closely associated with cellulose than the xylan (Åkerholm and Salmén, 2001).

Cellulose and hemicelluloses showed strong an indication of being oriented (Liang and Marchessault, 1959; Åkerholm and Salmén, 2001). The degree and type of orientation in lignin are not very clear. Using Raman spectroscopy Atalla and Agarwal (1985) showed that the aromatic rings of lignin had an orientation parallel to the tangential wood surface (Atalla and Agarwal, 1985a). Using static and dynamic FT-IR Akerholm and Salmén (2003) further studied lignin orientation (Åkerholm and Salmén, 2003). In this work thermomechanical pulp containing 24% lignin was used to make thin sheets for testing under transmission. The static IR spectra revealed that the lignin phenyl propane unit had a preferred orientation parallel to the cellulose microfibrils (Åkerholm and Salmén, 2003). Dynamic FT-IR revealed that lignin had higher damping than wood-carbohydrates. Additionally it was claimed that along the transverse direction, the mechanical response of the cell wall was dominated by lignin (Åkerholm and Salmén, 2003). The softening characteristics of wood polymers, under moist conditions, were studied by Akerholm and Salmén (2004) using dynamic FT-IR spectroscopy (Åkerholm and Salmén, 2004); thin films of spruce wood pulp were used. The study showed that for specific moisture content at room temperature lignin dissipates more energy than hemicelluloses. This was rationalized by hypothesizing a β transition in lignin. The softening behavior of xylan and glucomannan were found to be different. Xylan softened more than glucomannan. This was an indication of rigid cellulose being more closely associated with glucomannan than with xylan (Åkerholm and Salmén, 2004). Imaging FT-IR was employed by Stevanic and Salmén (2009) to study the orientation of amorphous wood polymers (Stevanic and Salmén, 2009). It was shown that both xylan and glucomannan were strongly oriented parallel to cellulose

microfibrils. However, the authors did not find conclusive evidence of lignin being oriented (Stevanic and Salmén, 2009).

The effect of thermal treatments on the molecular mobility of beech wood was investigated using dynamic FT-IR (Salmén *et al.*, 2008). Wood was treated at 160 °C for varying times. With increasing time of heat treatment a significant change in the viscoelastic response of cellulose, xylan and lignin was seen. It was shown prior to this work that cellulose bears most of the load when wood was loaded along the fiber direction. With thermal treatment, the load bearing capabilities of xylan and lignin was found to be very close to that for cellulose. This was rationalized as probable cross-linking between xylan and cellulose by hemiacetal bond formation causing better load distribution between xylan, lignin and cellulose, as well as reduced moisture affinity (Salmén *et al.*, 2008).

Almgren and co-workers applied dynamic FT-IR to study wood-fiber reinforced polylactide composites under moist conditions (Almgren *et al.*, 2008). Results indicated that with increasing moisture content, the stress transfer to the rigid fiber (cellulose) becomes less effective. The authors inferred that in a qualitative sense, with increasing moisture content the applied stress was transferred from the fiber to the matrix (Almgren *et al.*, 2008).

Salmén and Bergstrom studied effects of static stress/strain on the micromechanical responses of *in-situ* wood polymers (Salmén and Bergstrom, 2009). Thin spruce wood sections were loaded along the fiber direction, under static stress/strain, while IR measurements were taken to monitor changes in bond vibrations. The 1160 cm^{-1}(C-O-C glycoside bond and glucose ring) and 3348 cm^{-1} (3OH$^{\cdots}$O5

intramolecular hydrogen bond) bands were studied as a function of stress/strain. A linear shift towards lower wavenumber was demonstrated with increasing stress and strain for the 1160 cm^{-1} band. This showed that along the fiber direction the load was carried primarily by cellulose, which caused an elongation of the C-O-C and glucose rings' bonds. The 3OH$^{\cdots}$O5 hydrogen bonds became weaker with increasing stress/strain causing an increasing shift of the 3348 cm^{-1} band. No observable effect was seen for the lignin and hemicelluloses bands. The authors tested the effect of stress/strain under dry and moist (90% RH) conditions. Results showed that the rate of shift for the 1160 cm^{-1} band as a function of stress was moisture dependent. However, the shifts were similar when plotted as a function of strain. This interesting finding led the authors to hypothesize that the moisture accessible regions of cellulose (the non-crystalline phase) could be arranged along the surface of the crystalline region (in a parallel organization) rather than having a discrete phase (in series organization) (Salmén and Bergstrom, 2009) as shown in Figure 1-14.

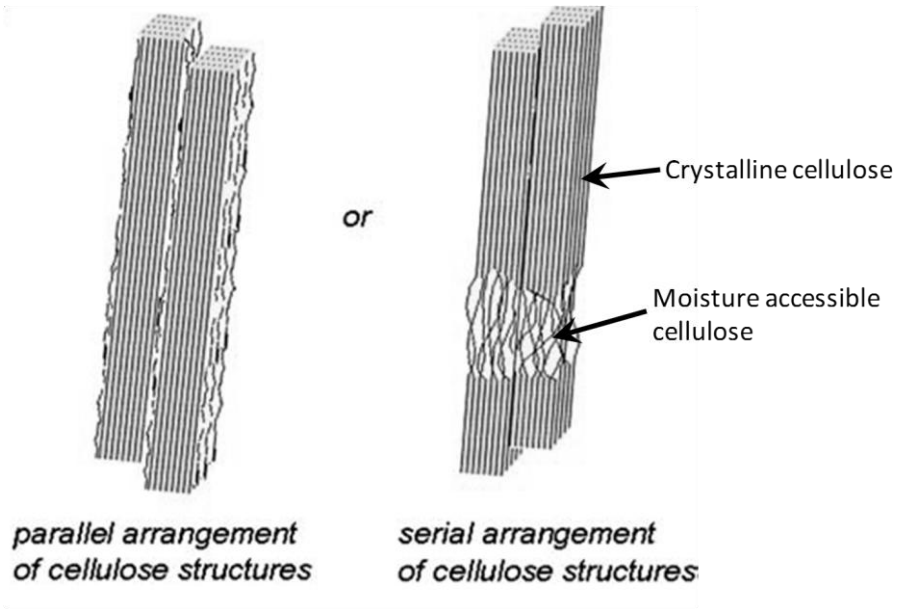

Figure 1-14 Cellulose microfibril structure with crystalline and moisture accessible regions. The parallel arrangement is logically supported by Salmén and Bergstrom. [Adapted from Ref (Salmén and Bergstrom, 2009)].

1.2.8. Organization of Wood Cell Wall

In a mature wood cell the secondary cell wall is composed of cellulose microfibrils embedded in a matrix of hemicellulose and lignin (Kerr and Goring, 1975; Hon and Shiraishi, 2001). However, the complete understanding of the organization of cellulose, lignin and hemicelluloses is not yet clear. Wood is orthotropic in nature, suggesting that properties of wood differ with the probing direction. A mature, normal secondary cell wall has three layers, namely S_1, S_2 and S_3. These three layers are arranged such that the microfibril angle with the cell axis of S_1 and S_3 are high, and are considered as a flat helix; whereas, the S_2 layer has a low microfibril angle and is considered as a steep helix (Hon and Shiraishi, 2001). During the formation of secondary cell wall, cellulose microfibrils are first formed and deposited in a regular

fashion to form a twisted honeycomb structure with intermittent hemicellulose chains (Terashima *et al.*, 1991). Later in cell wall formation, thickening by lignin-deposition occurs. This is a very important part of the process, as lignin deposition enhances the physical properties, and protects the more moisture susceptible polysaccharides from hydrolysis related degradation. Advancement in analytical techniques, specifically in the field of microscopy has allowed us to look more closely in the secondary cell wall structure. Cellulose microfibrils are intimately packed to form an extremely rigid and chemical and biological hydrolysis resistant structure. In cellulose chains, the chair conformation of glucose units restricts the hydroxyl groups to the equatorial/radial direction, whereas the aliphatic hydrogen atoms are directed toward the axial direction(Himmel, 2007). This generates a highly favorable condition for interchain hydrogen bonding. Cellulose microfibrils have a cross-section of 3-5 nm which subsequently form 16-20 nm aggregates (Fahlen and Salmén, 2003; Salmén, 2004). These aggregates show dimensional changes with moisture variation, which is an indication of the presence of the amorphous domains (Salmén, 2004; Abe and Yamamoto, 2005; Salmén and Burgert, 2009). These domains are either para-crystalline cellulose or hemicelluloses, primarily glucomannan; a close interaction between cellulose microfibrils and glucomannan was demonstrated using dynamic FT-IR(Åkerholm and Salmén, 2001; Salmén, 2004; Salmén and Burgert, 2009) and XRD (Jungnikl *et al.*, 2008). In the space between these cellulose aggregates and glucomannan, an amorphous phase of xylan and lignin exists, which acts as a matrix material to hold the crystalline domain. Attala and Agarwal (1985) showed for the first time with Raman spectroscopy that the lignin matrix has some degree of orientation, as

the planes of the lignin aromatic rings showed an orientation along the cell wall tangential direction (Atalla and Agarwal, 1985b). Spectroscopic studies also indicated that the phenylpropane units of lignin are oriented along the cellulose microfibrils (Åkerholm and Salmén, 2003). Xylan also showed an oriented morphology along the microfibril direction (Salmén, 1984). Molecular mechanics and dynamic modeling of lignocelluloses indicated that the lignin has a preferred helical structure (Faulon *et al.*, 1994). With knowledge of the helical organization of cellulose microfibrils in the secondary cell wall, it is a viable hypothesis that lignin is also to some extent helically oriented with the microfibrils.

Fengel (1971) proposed the first comprehensive model for the wood cell wall ultrastructure (Fengel, 1971). Using electron micrographs it was shown that 16 elementary fibrils (3 nm each) were arranged in a 4×4 organization to form aggregates of 12 nm wide fibers. Again, four of 12 nm wide aggregates associated to form 25 × 25 nm microfibrils (Fengel, 1971). Fengel suggested that hemicelluloses were arranged around the cellulose microfibrils and this assembly was embedded in a matrix of lignin.

Kerr and Goring (1975) proposed the most accepted concentric lamellar model for the wood cell wall (Kerr and Goring, 1975) as shown in Figure 1-15.

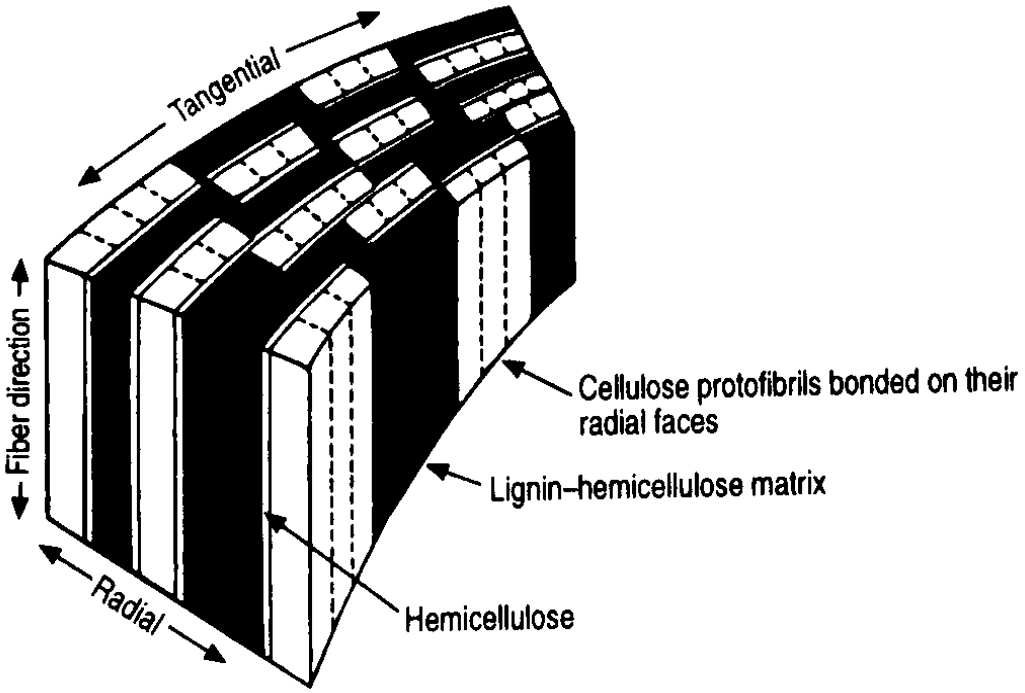

Figure 1-15 Kerr and Goring's model of cell wall. Concentric interrupted lamellar arrangement of wood-polymers in the cell wall. [ref. (Kerr and Goring, 1975)]

The cellulose microfibrils were considered as ribbon like structures, formed by the combination of 2 – 4 elementary fibrils, attached at their radial faces. The tangential surface of the ribbon was parallel to the middle lamella. Kerr and Goring suggested that hemicelluloses were partially associated with cellulose (~ 1/3 volume fraction) and partially distributed in the lignin matrix (~ 2/3 volume fraction). The authors also postulated that xylans might be associated with cellulose, which was proved otherwise in a later study using dynamic FT-IR (Åkerholm and Salmén, 2001). Akerholm and Salmen (2001) showed that glucomannan was in close association with cellulose microfibrils, whereas xylans were associated with lignin and cellulose.

Terashima et al. (1991) depicted the lignified cell wall model from a biosynthesis point of view (Terashima *et al.*, 1991). The cell wall starts to form with the formation of

cell plates made of cross linked pectin gel. On either side of these structures, cellulose and hemicelluloses are deposited to form the carbohydrate structures of the primary and secondary cell walls. Cellulose and hemicellulose form at the same time, with hemicellulose acting as a 'spacer' between the celluloses. This structure leads to secondary cell wall formation. Lignin is synthesized in the swollen gel of carbohydrates, causing a reduction of the system's moisture affinity. Also at this stage, the loss of moisture causes anisotropic shrinkage resulting in an orientation of lignin phenolic rings along the cell wall plane (Terashima *et al.*, 1991).

In 2006, Ding and Himmel used atomic force microscopy to characterize the cell wall structure (Ding and Himmel, 2006). They proposed a new model for maize (corn) primary cell wall. In their model, 36 glucan chains are synthesized from a cellulose synthesase complex (also referred to as rosettes). These are the elementary fibrils. The 36 cellulose chains in one elementary fibril showed varying morphology (Figure 1-16).

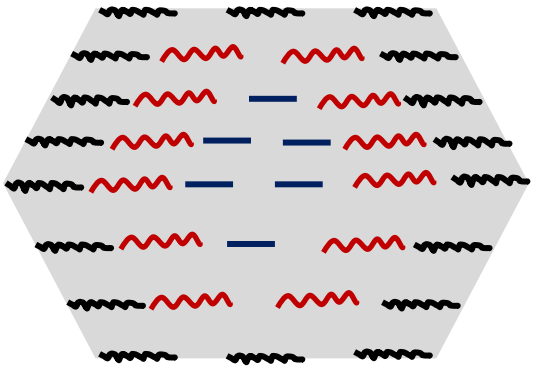

Figure 1-16 A schematic representation of an elementary fibril cross section containing 36 glucan chains. Blue lines at the center represents the true crystal core. Red lines represent sub-crystalline chains and black lines at the surface represent non-crystalline chains.

After biosynthesis, adjacent elementary fibrils combine to form a larger entity called ‘macrofibril’. This structure is comprised of large, uncoated elementary fibril-bundles. Macrofibrils break down during further fibril growth to form a thinner entity, popularly known as ‘microfibrils’. During microfibril formation, hemicelluloses coat the microfibril surfaces (Ding and Himmel, 2006).

In a recent study (2009), Terashima and coworkers studied the supramolecular organization of wood polymers in the secondary (S2) cell wall of Ginkgo (*Ginkgo biloba*) tracheids (Terashima *et al.*, 2009). Using field emission scanning electron microscopy (FE-SEM) authors showed that the nanostructure of the wood cell wall was a composite assembly of cellulose microfibrils (CMF) and a hemicellulose-lignin complex/module (HLM). The cross section of [CMF+HLM] structures was almost square (width 18 ± 1 nm). However, the cross-section of CMF bundles alone was not clear. The space between the CMF bundles is very important for the amount of lignin and its morphology. An almost linear relationship between [CMF+HLM] diameter and lignin content was reported (Jacobsen, 2007; Terashima *et al.*, 2009). Therefore, Terashima et al. suggested a more detailed investigation to find out the exact size and shape of CMF bundles for a better understanding of the lignification process (Terashima *et al.*, 2009).

A model experiment on the association of cellulose and hemicelluloses (galactoglucomannan and arabino-4-*O*-methylglucuronoxylan) showed that the aggregation of CMF to form CMF bundles could be influenced by galactoglucomannan; the spacing between the CMF bundles were controlled by arabino-4-*O*-methylglucuronoxylan (Terashima *et al.*, 2009). However, the mechanism of the

hemicellulose deposition was not well understood. The most recent wood cell wall model proposed by Terashima et al. is shown in Figure 1-17.

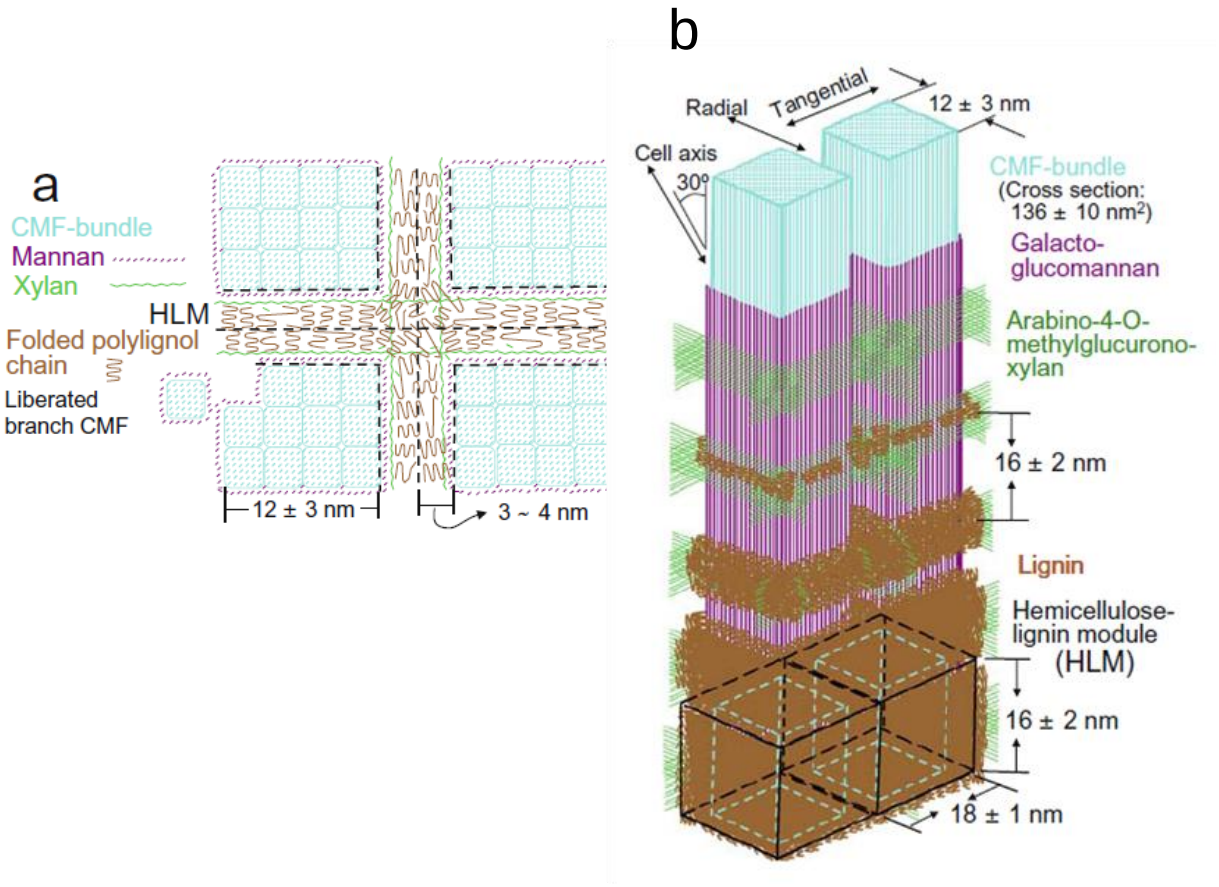

Figure 1-17 Cell wall model proposed by Terashima et al. (a) Cross-sectional view of the assembly of cellulose, hemicelluloses and lignin in S2 layer. (b) A simplified model showing assembly process (top to bottom) of cellulose, hemicelluloses and lignin with their approximate sizes in S2 layer.

In the proposed model (Figure 1-17 a) the cellulose microfibrils were coated with galactoglucomannan. Galactoglucomannan was also reported to interconnect two CMF assemblies. The arabino-4-*O*-methylglucuronoxylan (or simply xylan) chains penetrate into the HLM modules, which surrounds the CMF bundles on all four sides. It was also speculated that xylan chains act as lignification nucleation sites (Terashima *et al.*, 2009).

The proposed process of cell wall formation was presented in Figure 1-17 b. First, cellulose microfibrils are produced. These nascent CMFs are readily coated with galactoclucomannans. In the next stage CMFs form aggregates (sometime called ‘macrofibrils’) with xylan chains between them as ‘spacers’. Next, lignin is formed and deposited in close proximity to xylan chains, forming hemicellulose-lignin modules (Terashima *et al.*, 2009). The lignification process advances to form a fully matured cell wall.

The cell wall properties are dependent on the supramolecular organization of wood-polymers. The present review attempted to show relevant works conducted to elucidate the wood cell wall structure. Due to the highly complex nature and great natural variability of the wood cell wall, many questions about this natural composite are yet to be answered. Various advanced polymer characterization approaches are taken during this research to enhance the understanding of the lignocellulosic cell wall.

1.2.9. References

Abe, K. and H. Yamamoto, 2005. Mechanical interaction between cellulose microfibril and matrix substance in wood cell wall determined by X-ray diffraction., *Journal of Wood Science*, 51334-338.

Adam, G. and J. H. Gibbs, 1965. On the Temperature Dependence of Cooperative Relaxation Properties in Glass-Forming Liquids, *The Journal of Chemical Physics*, 43(1), 139-146.

Åkerholm, M. and L. Salmén, 2001. Interactions between wood polymers studied by dynamic FT-IR spectroscopy, *Polymer*, 42(3), 963-969.

Åkerholm, M. and L. Salmén, 2003. The oriented structure of lignin and its viscoelastic properties studied by static and dynamic FT-IR spectroscopy, *Holzforschung*, 57(5), 459-465.

Åkerholm, M. and L. Salmén, 2004. Softening of wood polymers induced by moisture studied by dynamic FTIR spectroscopy, *Journal of Applied Polymer Science*, 94(5), 2032-2040.

Aklonis, J. J. and W. J. MacKnight, 2005: Introduction to polymer viscoelasticity. Wiley,New York

Almgren, K. M., M. Åkerholm, E. K. Gamstedt, L. Salmén and M. Lindstrom, 2008. Effects of Moisture on Dynamic Mechanical Properties of Wood Fiber Composites Studied by Dynamic FT-IR Spectroscopy, *Journal of Reinforced Plastics and Composites*, 27(16-17), 1709-1721.

Atalla, R. H. and U. P. Agarwal, 1985a. Raman microprobe evidence for lignin orientation in the cell-walls of native woody tissue, *Science*, 227(4687), 636-638.

Atalla, R. H. and U. P. Agarwal, 1985b. Raman microprobe evidence for lignin orientation in the cell-walls of native woody tissue., *Science*, 227(4687), 636-638.

Back, E. L. and L. Salmén, 1982. Glass transitions of wood components hold implications for molding and pulping processes, *Tappi*, 65(7), 107-110.

Backman, A. C. and K. A. H. Lindberg, 2001. Differences in wood material responses for radial and tangential direction as measured by dynamic mechanical thermal analysis, *Journal of Materials Science*, 36(15), 3777-3783.

Becker, H. and D. Noack, 1968. Studies on dynamic torsional viscoelasticity of wood, *Wood Science and Technology*, 2213-230.

Bodig, J. and B. A. Jayne, 1993: Mechanics of wood and wood composities. Krieger Pub.,Malabar, Fla.

Christiansen, A. W., 2005. Chemical and mechanical aspects of HMR primer in relationship to wood bonding, *Forest Products Journal*, 55(11), 73-78.

Das, S., 2005. Wood/polymeric isocyanate resin interactions: Species dependence,

Das, S. and C. E. Frazier, 2004. Dynamic mechanical analysis of wood-polymeric isocyanate adhesive interactions., *Abstracts of Papers of the American Chemical Society*, 228U243-U243.

Deloche, B., 2003. Some remarks on the chain segment dynamics in confined polymers, *European Physical Journal E*, 12S117-S119.

Deloche, B., M. Beltzung and J. Herz, 1982. Segmental order in a uniaxially constrained polydimethylsiloxane network - a deuterium magnetic-resonance study, *Journal De Physique Lettres*, 43(22), L763-L769.

Deloche, B., A. Dubault, J. Herz and A. Lapp, 1986. Orientation of free polymer-chains dissolved in a strained elastomer - a deuterium magnetic-resonance study, *Europhysics Letters*, 1(12), 629-635.

Deloche, B. and E. T. Samulski, 1981. Short-range nematic-like orientational order in strained elastomers - a deuterium magnetic-resonance study, *Macromolecules*, 14(3), 575-581.

Ding, S. Y. and M. E. Himmel, 2006. The maize primary cell wall microfibril: A new model derived from direct visualization, *Journal of Agricultural and Food Chemistry*, 54(3), 597-606.

Doolittle, A. K., 1951. Studies in Newtonian Flow. II. The Dependence of the Viscosity of Liquids on Free-Space, *Journal of Applied Physics*, 22(12), 1471-1475.

Dubault, A., B. Deloche and J. Herz, 1987. Effects of trapped entanglements on the chain ordering in strained rubbers - a deuterium magnetic-resonance investigation, *Macromolecules*, 20(9), 2096-2099.

Fahlen, J. and L. Salmén, 2003. Cross-sectional structure of the secondary wall of wood fibers as affected by processing, *Journal of Materials Science*, 38(1), 119-126.

Faulon, J. L., G. A. Carlson and P. G. Hatcher, 1994. A 3-Dimensional Model for Lignocellulose from Gymnospermous Wood, *Organic Geochemistry*, 21(12), 1169-1179.

Fengel, D., 1971. Ideas on the ultrastructural organization of the cell wall components, *Journal of Polymer Science Part C*, 36383-392.

Fengel, D. and G. Wegener, 1984: Wood : chemistry, ultrastructure, reactions. W. de Gruyter,Berlin ; New York

Ferry, J. D., 1980: Viscoelastic properties of polymers. Wiley,New York

Fox, T. G. and P. J. Flory, 1950. Viscosity—Molecular Weight and Viscosity—Temperature Relationships for Polystyrene and Polyisobutylene1,2, *Journal of the American Chemical Society*, 70(7), 2384-2395.

Furuta, Y., Y. Obata and K. Kanayama, 2001. Thermal-softening properties of water-swollen wood: The relaxation process due to water soluble polysaccharides, *Journal of Materials Science*, 36(4), 887-890.

Gardner, D. J., W. T. Tze and S. Q. Shi, 2001. Adhesive wettability of hydroxymethyl resorcinol (HMR) treated wood, *Wood Adhesives 2000, [International Symposium], 7th, S. Lake Tahoe, NV, United States, June 22-23, 2000*321-327.

Gronski, W., R. Stadler and M. M. Jacobi, 1984. Evidence of nonaffine and inhomogeneous deformation of network chains in strained rubber-elastic networks by deuterium magnetic-resonance., *Macromolecules*, 17(4), 741-748.

Heredia, A., R. Guillen, A. Jimenez and J. Fernandezbolanos, 1993. Plant-Cell Wall Structure, *Revista Espanola De Ciencia Y Tecnologia De Alimentos*, 33(2), 113-131.

Himmel, M. E., 2007. Biomass recalcitrance: engineering plants and enzymes for biofuels production (vol 315, pg 804, 2007), *Science*, 316(5827), 982-982.

Hinterstoisser, B. and L. Salmén, 1999. Two-dimensional step-scan FTIR: a tool to unravel the OH-valency-range of the spectrum of Cellulose I, *Cellulose*, 6(3), 251-263.

Höglund, H., U. Sohlin and G. Tistad, 1976. Physical-Properties of Wood in Relation to Chip Refining, *Tappi*, 59(6), 144-147.

Hon, D. N. S. and N. Shiraishi, 2001: Wood and cellulosic chemistry. Marcel Dekker,New York

Jacobsen, N. E., 2007: NMR spectroscopy explained : simplified theory, applications and examples for organic chemistry and structural biology. Wiley-Interscience,Hoboken, N.J.

Jungnikl, K., O. Paris, P. Fratzl and I. Burgert, 2008. The implication of chemical extraction treatments on the cell wall nanostructure of softwood, *Cellulose*, 15(3), 407-418.

Kelley, S. S., T. G. Rials and W. G. Glasser, 1987. Relaxation Behavior of the Amorphous Components of Wood, *Journal of Materials Science*, 22(2), 617-624.

Kerr, A. J. and D. A. I. Goring, 1975. The ultrastructure arrangement of the wood cell wall, *Cellulose Chemistry and Technology*, 9563-573.

Kilfoil, M. L. and P. T. Callaghan, 2000. NMR measurement of the alignment tensor for a polymer melt under strong shearing flow, *Macromolecules*, 33(18), 6828-6833.

Kohlrausch, R., 1847. Ueber das Dellmann'sche Elektrometer, *Annalen der Physik und Chemie*, 148(11), 353-405.

Kojiro, K., Y. Furuta and Y. Ishimaru, 2003a. Influence of heating history on dynamic viscoelastic properties and dimensions of dry wood, Okayama, JAPAN, 196-201,

Kojiro, K., Y. Furuta and Y. Ishimaru, 2003b. Influence of histories on dynamic viscoelastic properties and dimensions of water-swollen wood, Fukuoka, JAPAN, 95-99,

Kojiro, K., Y. Furuta and Y. Ishimaru, 2006. Influence of heating and drying history on micropores in dry wood, Akita, JAPAN, 202-207,

Laborie, M.-P. G. 2002a: Investigation of the wood/phenol-formaldehyde adhesive interphase morphology. *VPI & SU. Wood Science and Forest Products. Ph. D. 2002.*, [Blacksburg, Va.: University Libraries, Virginia Polytechnic Institute and State University.

Laborie, M.-P. G., L. Salmén and C. E. Frazier, 2004. Cooperativity analysis of the in situ lignin glass transition, *Holzforschung*, 58(2), 129-133.

Laborie, M.-P. G., L. Salmén and C. E. Frazier, 2006. A morphological study of the wood/phenol-formaldehyde adhesive interphase, *Journal of Adhesion Science and Technology*, 20(8), 729-741.

Levitt, M. H., 2008: Spin dynamics : basics of nuclear magnetic resonance. John Wiley & Sons,Chichester, England ; Hoboken, NJ

Li, J., K. G. Wilmsmeyer and L. A. Madsen, 2008. Hydrophilic channel alignment modes in perfluorosulfonate ionomers: Implications for proton transport, *Macromolecules*, 41(13), 4555-4557.

Li, J., K. G. Wilmsmeyer and L. A. Madsen, 2009. Anisotropic Diffusion and Morphology in Perfluorosulfonate Ionomers Investigated by NMR, *Macromolecules*, 42(1), 255-262.

Liang, C. Y. and R. H. Marchessault, 1959. Infrared spectra of crystalline polysaccharides.2. Native celluloses in the region from 640 to 1700 cm-1, *Journal of Polymer Science*, 39(269-278), 269.

Lindblad, M. S. and A.-C. Albertsson. 2005: Chemical Modification of Hemicelluloses and Gums. In Dumitriu, S., editor, *Polysaccharides : structural diversity and functional versatility*, New York: Marcel Dekker, 491-508.

Lopez- Suevos, F. and C. E. Frazier, 2006. Rheology of latex films bonded to wood: influence of cross-linking, *Holzforschung*, 60(1), 47-52.

Lopez-Anido, R., D. J. Gardner and J. L. Hensley, 2000. Adhesive bonding of eastern hemlock glulam panels with E-glass/vinyl ester reinforcement, *Forest Products Journal*, 50(11/12), 43-47.

Lopez-Suevos, F. and C. E. Frazier, 2005. Parallel-plate rheology of latex films bonded to wood, *Holzforschung*, 59(4), 435-440.

Lopez-Suevos, F. and C. E. Frazier, 2006. The role of resol fortifiers in latex wood adhesives, *Holzforschung*, 60(5), 561-566.

Lorthioir, C., B. Deloche, A. Alegria, J. Colmenero, P. Auroy and Y. Gallot, 2003. Segmental order and dynamics of polymer chains confined in block copolymer lamellar mesophases: NMR and dielectric relaxation studies, *European Physical Journal E*, 12S121-S125.

Marchessault, R. H. and C. Y. Liang, 1960. Infrared spectra of crystalline polysaccharides.3. Mercerized cellulose., *Journal of Polymer Science*, 4371-84.

Marchessault, R. H. and C. Y. Liang, 1962. The infrared spectra of crystalline polysaccharides. ςIII. Xylans, *Journal of Polymer Science*, 59357-378.

Marcinko, J. J., S. Devathala, P. L. Rinaldi and S. Bao, 1998. Investigating the molecular and bulk dynamics of pMDI/wood and UF/wood composites, *Forest Products Journal*, 48(6), 81-84.

McLoughlin, K., J. K. Waldbieser, C. Cohen and T. M. Duncan, 1997. End-linked poly(dimethylsiloxane) elastomers: H-2-nuclear magnetic resonance investigations of compression-induced segment anisotropy, *Macromolecules*, 30(4), 1044-1052.

Menard, K. P. 1999: Dynamic mechanical analysis a practical introduction. Boca Raton, Fla.: CRC Press, 208 p.

Ngai, K. L., 1999. Modification of the Adam-Gibbs model of glass transition for consistency with experimental data, *Journal of Physical Chemistry B*, 103(28), 5895-5902.

Ngai, K. L. and R. W. Rendell, 1991. From conformational transitions in a polymer-chain to segmental relaxation in a bulk polymer, *Journal of Non-Crystalline Solids*, 131942-948.

Norimoto, M. and T. Yamada, 1966. Dynamic torsional viscoelasticity of wood, *Wood Res*, 3832-39.

Obataya, E., Y. Furuta and J. Gril, 2003. Dynamic viscoelastic properties of wood acetylated with acetic anhydride solution of glucose pentaacetate, *Journal of Wood Science*, 49(2), 152-157.

Olsson, A.-M. and L. Salmén, 1997. The effect of lignin composition on the viscoelastic properties of wood, *Nord. Pulp Pap. Res. J.*, 12(3), 140-144.

Olsson, A. M. and L. Salmén, 1992. Viscoelasticity of Insitu Lignin as Affected by Structure - Softwood Vs Hardwood, *ACS Symposium Series*, 489133-143.

Olsson, A. M. and L. Salmén. 1993: Mechanical spectroscopy - a tool for lignin structure studies. In Kennedy, J. F., Philipps, G. O. and Williams, P. A., editors, *Cellulosics: Chemical, Biochemical & Material Aspect*, Chichester: Ellis Horwood, 257-262.

Plazek, D. J. and K. L. Ngai, 1991. Correlation of Polymer Segmental Chain Dynamics with Temperature-Dependent Time-Scale Shifts, *Macromolecules*, 24(5), 1222-1224.

Rubinstein, M. and R. H. Colby, 2003: Polymer physics. Oxford University Press,Oxford ; New York

Sadoh, T., 1981. Viscoelastic Properties of Wood in Swelling Systems, *Wood Science and Technology*, 15(1), 57-66.

Salmén, L., 1984. Viscoelastic properties of in situ lignin under water-saturated conditions, *Journal of Materials Science*, 19(9), 3090-3096.

Salmén, L., 2004. Micromechanical understanding of the cell-wall structure, *Comptes Rendus Biologies*, 327(9-10), 873-880.

Salmén, L. and E. Bergstrom, 2009. Cellulose structural arrangement in relation to spectral changes in tensile loading FTIR, *Cellulose*, 16(6), 975-982.

Salmén, L. and I. Burgert, 2009. Cell wall features with regard to mechanical performance. A review: COST action E35 2004-2008: wood machining - micromechanics and fracture, *Holzforschung*, 63(2), 121-129.

Salmén, L. and A. M. Olsson, 1998. Interaction Between Hemicellulose, Lignin and Cellulose: Structure-Property Relationship, *Journal of Pulp and Paper Science*, 24(3), 99-103.

Salmén, L., H. Possler, J. S. Stevanic and S. E. Stanzl-Tschegg, 2008. Analysis of thermally treated wood samples using dynamic FT-IR-spectroscopy, *Holzforschung*, 62(6), 676-678.

Schwanninger, M., J. C. Rodrigues, H. Pereira and B. Hinterstoisser, 2004. Effects of short-time vibratory ball milling on the shape of FT-IR spectra of wood and cellulose, *Vibrational Spectroscopy*, 36(1), 23-40.

Sjöström, E., 1993: Wood chemistry : fundamentals and applications. Academic Press,San Diego,51.

Son, J. and D. J. Gardner, 2004a. Dimensional stability measurements of thin wood veneers using the Wilhelmy plate technique, *Wood and Fiber Science*, 36(1), 98-106.

Son, J. and D. J. Gardner, 2004b. Dimensional stability measurements of thin wood veneers using the Wilhelmy plate technique, *Wood and Fiber Science*, 36(1), 98-106.

Son, J., W. T. Y. Tze and D. J. Gardner, 2005. Thermal behavior of hydroxymethylated resorcinol (HMR)-treated maple veneer, *Wood and Fiber Science*, 37(2), 220-231.

Sotta, P. and B. Deloche, 1990. Uniaxiality induced in a strained poly(dimethylsiloxane) network, *Macromolecules*, 23(7), 1999-2007.

Sotta, P., B. Deloche, J. Herz, A. Lapp, D. Durand and J. C. Rabadeux, 1987. Evidence for short-range orientational couplings between chain segments in strained rubbers - a deuterium magnetic-resonance investigation, *Macromolecules*, 20(11), 2769-2774.

Sperling, L. H., 2006: Introduction to physical polymer science. Wiley,Hoboken, N.J.

Stevanic, J. S. and L. Salmén, 2009. Orientation of the wood polymers in the cell wall of spruce wood fibres, *Holzforschung*, 63(5), 497-503.

Sun, N., S. Das and C. E. Frazier, 2007. Dynamic mechanical analysis of dry wood: Linear viscoelastic response region and effects of minor moisture changes, *Holzforschung*, 61(1), 28-33.

Sun, N. and C. E. Frazier, 2005. Probing the hydroxymethylated resorcinol coupling mechanism with stress relaxation, *Wood and Fiber Science*, 37(4), 673-681.

Sun, N. and C. E. Frazier, 2006. Hydroxymethylated resorcinol coupling agent: stress relaxation analysis, *Wood Adhesives 2005, [Proceedings Symposium], San Diego, CA, United States, Nov. 2-4, 2005*65-71.

Terashima, N., K. Fukushima, L. F. He and K. Takabe, 1991. Comprehensive model of the lignified plant-cell wall, Madison, Wi, 247-270,

Terashima, N., K. Kitano, M. Kojima, M. Yoshida, H. Yamamoto and U. Westermark, 2009. Nanostructural assembly of cellulose, hemicellulose, and lignin in the middle layer of secondary wall of ginkgo tracheid, *Journal of Wood Science*, 55(6), 409-416.

Thompson, N. S. Hemicellulose. Kirk-Othmer Encyclopedia of Chemical Technology.

Timell, T. E. 1964: Wood hemicelluloses: Part I. In Wolfrom, M. L., editor, *Advances in Carbohydrate Chemistry*: Academic, 247-302.

Vick, C. B., 1996. Hydroxymethylated resorcinol coupling agent for enhanced adhesion of epoxy and other thermosetting adhesives to wood, Wood Adhesives 1995, Portland, OR, 47-55, Forest Products Society, Madison, WI.

Vick, C. B., A. W. Christiansen and E. A. Okkonen, 1998. Reactivity of hydroxymethylated resorcinol coupling agent as it affects durability of epoxy bonds to Douglas-fir, *Wood and Fiber Science*, 30(3), 312-322.

Vick, C. B. and E. A. Okkonen, 2000. Durability of one-part polyurethane bonds to wood improved by HMR coupling agent, *Forest Products Journal*, 50(10), 69-75.

Vick, C. B., K. Richter, B. H. River and A. R. Fried, Jr., 1995. Hydroxymethylated resorcinol coupling agent for enhanced durability of bisphenol-A epoxy bonds to Sitka spruce, *Wood and Fiber Science*, 27(1), 2-12.

Ward, I. M. and J. Sweeney, 2004: An introduction to the mechanical properties of solid polymers. Wiley,Chichester, West Sussex, England

Williams, G. and D. C. Watts, 1970b. Non-symmetrical dielectric relaxation behaviour arising from a simple empirical decay function, *Transactions of the Faraday Society*, 66(1), 80-85.

Williams, M. L., R. F. Landel and J. D. Ferry, 1955. The Temperature Dependence of Relaxation Mechanisms in Amorphous Polymers and Other Glass-forming Liquids, *Journal of the American Chemical Society*, 77(14), 3701-3707.

Zeghal, M., B. Deloche and P. Auroy, 1999. Chain segment ordering in swollen polymer brushes: Deuterium NMR investigations, *Macromolecules*, 32(15), 4947-4955.

Chapter 2 Advancing the dynamic mechanical analysis of biomass: comparison of tensile-torsion and compressive-torsion wood DMA

Sudip Chowdhury, James Fabiyi, Charles E. Frazier
Macromolecular Science & Engineering, Wood Science & Forest Products
Virginia Tech, Blacksburg VA 24061, U.S.A.
Published: Holzforschung (2010) v.64, p747-756

Attribution

In this paper the studies conducted in ethylene glycol were performed by the dissertation author; the studies in water were conducted by Dr. James Fabiyi. Experimental protocol setup, research strategy determination, data analysis and interpretations were conducted by all three contributing authors.

2.1. Abstract

In an effort to advance the dynamic mechanical analysis (DMA) of very small biomass specimens, and/or specimens having poor mechanical integrity, the functional equivalent of pendulum-torsion (tensile-torsion) DMA was compared to parallel-plate compressive-torsion DMA. The solvent-saturated lignin glass transition in yellow-poplar (*Liriodendron tulipifera*) was generally similar determined by both modes; however direct data comparisons should be avoided or carefully considered. First-heat glass transition temperatures (Tg's) were quite similar; however specimen densification elevated subsequent cooling-mode Tg's by 5-8˚C in compressive-torsion. Both modes

revealed a first-heat tan δ shoulder; it was more prominent and had grain dependency in compressive-torsion. Below fiber saturation, subambient tensile-torsion DMA was superior; compressive-torsion resulted in an anomalous response, obscuring subambient secondary relaxations. With these differences and limitations in mind, compressive-torsion offers specific advantages. Solvent-submersion studies are simplified because solvent cups are easily devised for torsional rheometers. Specimens lacking mechanical integrity are more easily analyzed. Heavily biodegraded spruce (*Picea* sp.) was analyzed in the solvent-submersion mode as fibrous mats and the different actions of *G. trabeum* and *P. placenta* were revealed. Very small specimens are easily analyzed in compressive-torsion; tissue maturity effects were revealed in minute sections of switchgrass (*Panicum virgatum*) stems. Applied appropriately, parallel-plate compressive-torsion DMA will provide new research opportunities.

2.2. Introduction

Global needs for renewable materials, chemicals, and energy require the development of new and improved analytical methods for understanding and optimizing biomass utilization. Thermomechanical analysis is still evolving, even though the discipline is well established. For example, the dynamic mechanical analysis (DMA) of wood has been a productive endeavor since the 1960's (Norimoto and Yamada, 1666; Becker and Noack, 1968). Nevertheless, novel wood DMA techniques remain available and will provide new opportunities for discovery. Intrinsically convenient is that wood is shapeable into practically any analytical form. Traditional specimen geometries are typically rectangular, as originally employed for pendulum-torsion and now commonly

for three-point and cantilever bending. However, many analytical scenarios are not amenable to traditional rectangular specimens and bending-mode analyses, for example: genetically transformed wood is often available as only minor sections from very small sapling stems; tree increment cores hold potential for tissue maturity studies, but 1-3 year sections are quite small; and specimens less convenient than solid wood include grass stems and fibrous mats derived from biomass deconstruction. Many researchers worked with specimens not easily applied to pendulum torsion and bending-mode DMA. Additional complication arises from the need to control specimen moisture content. The simplest and most effective moisture (or organic plasticizer) control is perhaps found with solvent-submersion, where the specimen is immersed in a suitable plasticizer during analysis.

The work described here is a new look at an old method: solvent-submersion torsional DMA where a cylindrical specimen is compressed between parallel-plates (compressive-torsion) while immersed in a plasticizer. The earliest wood DMA was also conducted in torsion, but with a minor tensile force acting through the specimen and supporting the torsional pendulum (Norimoto and Yamada, 1666; Becker and Noack, 1968; Höglund *et al.*, 1976; Sadoh, 1981). Obviously, pendulum torsion (classified here as “tensile-torsion”) requires a certain specimen geometry and integrity. In contrast, parallel-plate compressive-torsion makes available a far greater variety of specimen types and geometries since clamping requires simple compression. Additional satisfaction is found from the ease with which solvent-submersion is applied using the parallel-plate geometry. A cylindrical solvent-submersion cup is easily fashioned for rheometers designed for parallel-plate DMA.

Of course, the stress modes in tensile-torsion and compressive-torsion DMA are quite different. Consequently, the utility of parallel-plate compressive-torsion DMA should be demonstrated by thorough comparison with tensile-torsion DMA. Such a comparison reveals differences, advantages, and limitations for compressive-torsion, as will be demonstrated.

2.3. Experimental

2.3.1. Materials

All specimens were machined from a single piece of commercial yellow-poplar (*Liriodendron tulipifera*) sapwood lumber; density was not measured but on average the diffuse-porous cross-section exhibited two growth rings per centimeter. Specimens were machined with precise grain orientation (described below), however, the positioning of the growth rings within the specimen geometry was random. For compressive-torsion, cylindrical discs (8 mm diameter, 4 mm thickness) were machined with a commercially available “plug-cutter” (Note that the discs were machined in the dry state; during solvent-submersion differential swelling slightly distorts the cylinder shape; the minor error in measured moduli was ignored). For tensile-torsion, rectangular specimens (thickness × width × length: 4 × 10 × 40 mm^3) were prepared. All experiments were conducted with a TA Instruments ARG2 rheometer. Compressive-torsion disc specimens were tested in parallel-plate torsion such that the cylinder axis (thickness direction) was parallel to the torsional axis and the cylinder ends were in contact with the parallel plates. In tensile-torsion, rectangular specimens were secured by the tension clamps (across the thickness dimension) while the specimen length was parallel

to the torsional axis. With respect to compressive-torsion, three grain orientations were defined as RT, TR, and XL; the first letter indicates the wood surface contacting the parallel plates, perpendicular to the torsional axis (T-tangential, R-radial and X-cross sectional); the second letter indicates the grain direction parallel to the torsional axis (T-tangential, R-radial and L-longitudinal). The same grain designations are applicable to the tensile-torsion specimens.

2.3.2. Methods

Specimens were vacuum-dried (0.04-0.1 mm Hg) at ambient temperature for 24 h over anhydrous P_2O_5 and stored in a desiccator at ambient temperature over anhydrous P_2O_5 and under N_2 gas for a minimum of 48 h prior to solvent impregnation. Specimens were saturated with either ethylene glycol (99.8% grade) or aqueous buffer (pH = 7, potassium phosphate monobasic - sodium hydroxide) using vacuum/pressure treatment: 40 min vacuum (5-6 mm Hg), followed by atmospheric pressure for 40 min (aqueous buffer) or 24 h (ethylene glycol), all at room temperature.

For compressive-torsion, solvent-submersion analysis was conducted with modified 8 mm diameter parallel-plates such that the bottom plate was surrounded by a stainless steel cup that maintained specimen immersion. An aluminum solvent-cup cover reduced evaporative losses. Water evaporation was further reduced by applying a thin silicon oil layer over the buffer surface. During analysis, compressive-torsion specimens were maintained under a 15 N compressive force; required to prevent plate slippage, this represents a stress of about 1.6% and 16% of yellow-poplar green compression strength parallel and perpendicular to grain, respectively (Green *et al.*,

1999). Safety note: when organic solvents are used as specimen plasticizers, caution is required since the solvent bath is enclosed within an oven having exposed heating elements; consequently, anhydrous N_2 gas is directed through the heating chamber to prevent ignition; and the oven must never be opened to the oxygenated atmosphere while the oven temperature is near the solvent flash point. Attention to these details results in safe and reliable analysis.

Tensile-torsion was also conducted under solvent-submersion using a TA Instruments concentric cylinder attachment containing a fluid-cooled jacket that is conveniently configured for solvent-submersion tensile-torsion. The solvent bath was surrounded by the fluid-cooled jacket that was maintained isothermally with a fluid circulator; specimen (bath) heating and cooling occurred through the underlying peltier-plate that heats or cools in opposition to the fluid-cooled jacket surrounding the specimen bath (Greater range and thermal response is achieved by devising a temperature-ramping circulator working in concert with the peltier-plate, not the case in this work). Tensile-torsion rectangular specimens were secured in tension clamps using 15 cN.m torque; during analysis rectangular specimens were maintained under a 2 N tensile force (approximately 0.05% and 1.4% of the green tensile strength parallel and perpendicular to grain, respectively; Green et al. 1999). No heating elements are exposed to flammable vapors in the experimental design of “solvent-submersion tensile-torsion fixture” described above; while the specimen bath is covered, it is essentially open to the atmosphere and intrinsically safer than the solvent-submersion described for compressive-torsion.

All analyses were rigorously conducted within the linear viscoelastic response (LVR) region. This was determined from stress sweep experiments at the temperature extremes with specimens that were dedicated for that purpose, and obtained from the same sample. Linear stress/strain plots were created, and the LVR limit was defined as the highest stress level that maintained the plot's correlation coefficient (r^2, for the least squares fit) above or equal to 0.9995. Regardless of the stress mode (compressive-torsion or tensile-torsion), the static tensile or compressive load caused no interference in the LVR determination; the associated stress/strain plots were all highly linear.

In ethylene glycol, sequential heating and cooling was applied as follows: 1) thermal equilibration (0°C, 10 min), 2) 0 to 120°C (1°C min^{-1}, 5 Hz), 3) 120°C, 40 min, and 4) 120 to 0°C (1°C min^{-1}, 5 Hz). However, in water the acquisition parameters were slightly different as follows: 1) thermal equilibration (5°C, 10 min), 2) 5 to 95°C (3°C min^{-1}, 10 Hz), 3) 95°C, 10 min, 4) 95 to 5°C (3°C min^{-1}, 10 Hz). Ideally, the acquisition parameters for the two different plasticizers, ethylene glycol and water, should be identical; however the respective data sets were taken from separate and independent studies for the purpose of this communication. Three specimens were analyzed within each subsample. Average storage modulus, loss modulus, and tan δ traces were created using OriginPro software version 8.0.63 (OriginLab, Northampton, MA, U.S.A.); raw data files were input into the "Average" method function based on a 0.5°C tolerance.

Thermal reversibility

A demonstration of thermal reversibility was conducted in compressive-torsion with a single TR specimen analyzed in ethylene glycol. The specimen was subjected to two sequential rounds of cyclic heating and cooling; after the first round the specimen was extracted to remove ethylene glycol, dried, and then re-saturated in ethylene glycol and subjected to the second round of heating/cooling. First round (15 N normal force, 5 Hz, heating/cooling rates = 3°C min^{-1}): 1) thermal equilibration (0°C, 10 min), 2) 0 to 120°C, 3) 120°C, 40 min, 4) 120 to 0°C, 5) 0°C, 10 min, 6) 0 to 120°C, 7) 120°C, 10 min, 8) 120 to 0°C. After the first round, specimen extraction and drying occurred as follows: 1) specimen soaked in 500 ml distilled water, 2 h room temperature rapid stirring, 2) water exchanged with 500 ml fresh distilled water, 2 h room temperature rapid stirring, 3) water exchanged with 500 ml fresh distilled water, room temperature stirring resumed over night, 4) specimen vacuum dried at room temperature in the presence of P_2O_5 for 36 h (based upon the dry mass prior to the first round, extraction caused a 3% mass reduction). The specimen was re-saturated in ethylene glycol and subjected to the second round of heating/cooling. Second round (15 N normal force, 5 Hz, heating/cooling rates = 3°C min^{-1}): same as first round except after the first heat, the 120°C isothermal hold period was reduced to 10 min.

<u>Fungal treatments</u>

Specimens subjected to fungal biodegradation were supplied from colleagues at the University of Maine, Orono, U.S.A. Spruce (*Picea* sp.) specimens were subjected to a modified soil block jar procedure for a period of 12 weeks with the brown rot fungi

Postia placenta and separately *Gloeophyllum trabeum*. Weight loss for specimens treated with *G. trabeum* and *P. placenta* were about 56% and 50%, respectively. The specimens were heavily degraded, crumbly and lacking mechanical integrity. Consequently, about 0.9 - 1.0 g of degraded wood was ground with mortar and pestle under liquid nitrogen. The resulting fiber was dispersed and saturated in ethylene glycol, then filtered into a 10 mm diameter mat; this was crudely tamped into an 8 mm diameter circular mold and the resulting mat (~ 5 mm in thickness) was analyzed in compressive-torsion while immersed in ethylene glycol (normal force = 10 N, equilibrated at 120˚C for 10 min; cooled to 0˚C at 3˚C min^{-1}, 5 Hz).

Switchgrass analysis

Switchgrass (*Panicum virgatum*) stem tissue was excised from the basal (first internode) and terminal (sixth) internodes, dried and then saturated in ethylene glycol as describe above. The cylindrical sections were cut longitudinally such that the hollow stem could be opened and flattened into a sheet. An 8 mm diameter disk (thickness = 0.6 mm, single layer) was removed with a razor and then analyzed in ethylene glycol by means of compressive-torsion under a 10 N normal force: 1) thermal equilibration (0°C, 10 min), 2) 0 to 120°C (2°C min^{-1}, 1 Hz), 3) 120°C, 10 min, 4) 120 to 0°C (2°C min^{-1}, 1 Hz).

2.4. Results and discussion

The following comparison of compressive-torsion and tensile-torsion DMA will employ either heating or cooling scans. Consequently, a discussion of thermal reversibility in wood DMA is first required. To that end, a single specimen was subjected

to two sequential rounds of cyclic heating/cooling under compressive-torsion in ethylene glycol. After round-1, the specimen was extracted, dried, and then re-saturated in ethylene glycol for cyclic heating/cooling in round-2 (Figure 2-1).

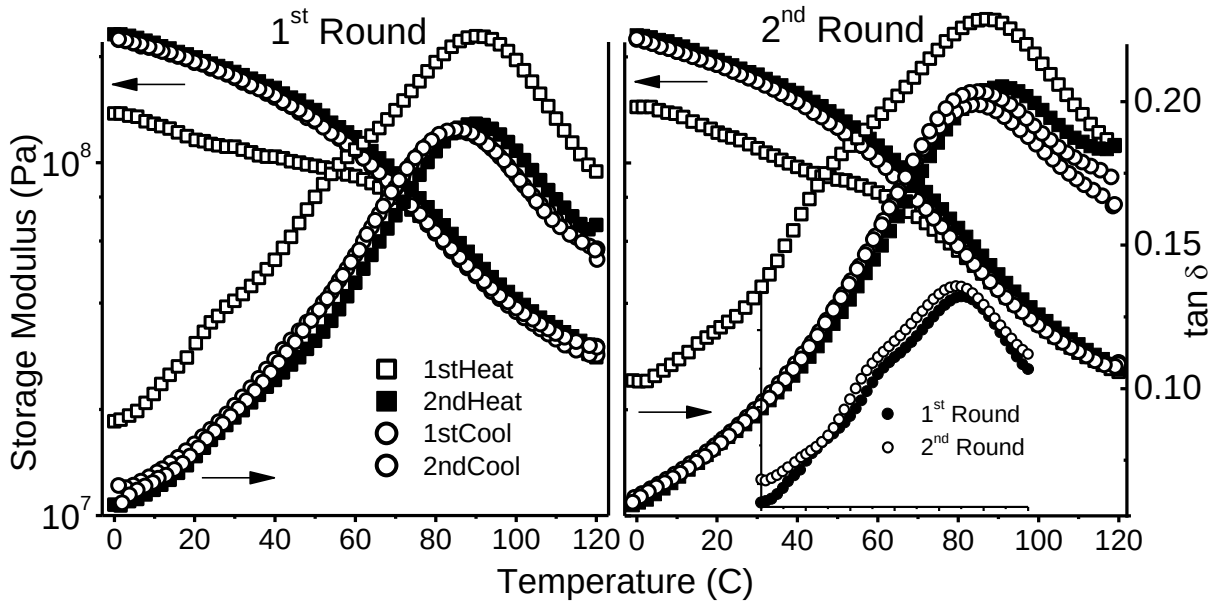

Figure 2-1 Compressive-torsion sequential analysis. Left: First round of sequential DMA heating/cooling curves of a TR specimen in ethylene glycol. Right: Second round of DMA sequential heating/cooling on the same specimen shown at left. Between rounds, the specimen was water-extracted, dried, and re-saturated in ethylene glycol. Right insert: Comparison of first heat curves resulting from the first and second rounds of cyclic heating/cooling (3°C min–1, 5 Hz).

Both the storage modulus and the tan δ responses exhibit reversibility after the first heat. Regarding the storage modulus, after the first heat the specimen stiffens upon cooling because of densification caused by the compressive clamping force. Densification effects will be discussed later, and so the discussion at first will focus on the tan δ response. Considering this parameter, the round-1 first heat is clearly different from the subsequent round-1 cooling/heating scans: the first heat tan δ displays two

minor shoulders, one near 20˚C and another at 40˚C, and across the temperature range the tan δ intensity (damping) is significantly greater. Our experience shows that the shoulder near 20˚C is variable in occurrence and intensity, whereas the shoulder near 40˚C is much less variable. After the first heat, the cooling/heating scans exhibit reduced damping and also excellent thermal reversibility (the heating and cooling tan δ maximum temperatures are slightly different, again due to densification, as explained later). The round-1 first heat tan δ shoulder (~40˚C) is nonreversible only within round-1 heating/cooling. Once the specimen is extracted, dried, re-saturated and subjected to round-2, the peculiar first heat response is again observed (however, only the 40˚C shoulder is clearly seen). In round-2, thermal reversibility is slightly compromised, as indicated by the minor divergence of the round-2 cooling scans. Consequently, some degree of thermal decomposition likely occurred, which is consistent with the Figure 2-1 inset, where comparison of the first heat scans demonstrates slight change. The peculiar first heat behavior (tan δ) is a manifestation of the specimen's solvo-thermal history, and is not related to irreversible chemical change. Salmén (1984) has mentioned an irreversible change that occurs above 100˚C; and this has been associated with boiling water or steam treatments that reduce storage modulus and increase damping (Höglund *et al.*, 1976; Salmen and Fellers, 1982). In contrast, Figure 2-1 clearly shows that after the first heat the damping is reduced, not increased; and the first heat storage moduli in rounds 1 and 2 are quite similar. Consequently, the first heat response shown here appears to be unrelated to the irreversible softening previously associated with boiling water or steaming (Höglund *et al.*, 1976; Salmen and Fellers, 1982). Specimens analyzed in ethylene glycol were conditioned at 120˚C for 40 min

after the first heat. This would seem to be a damaging solvolytic treatment; however, Figure 2-1 demonstrates that relatively minor changes occurred. Since the first heat response can be recreated within a single specimen, this response represents an as yet unknown structural feature in wood. Furthermore, since the unusual first heat behavior is clearly reversible, it should be the subject of further study. This topic will be revisited after the comparison of compressive-torsion and tensile-torsion DMA.

Figure 2-2 permits a comparison of compressive-torsion and tensile-torsion DMA scans of yellow-poplar immersed in ethylene glycol; first heats and first cools are shown.

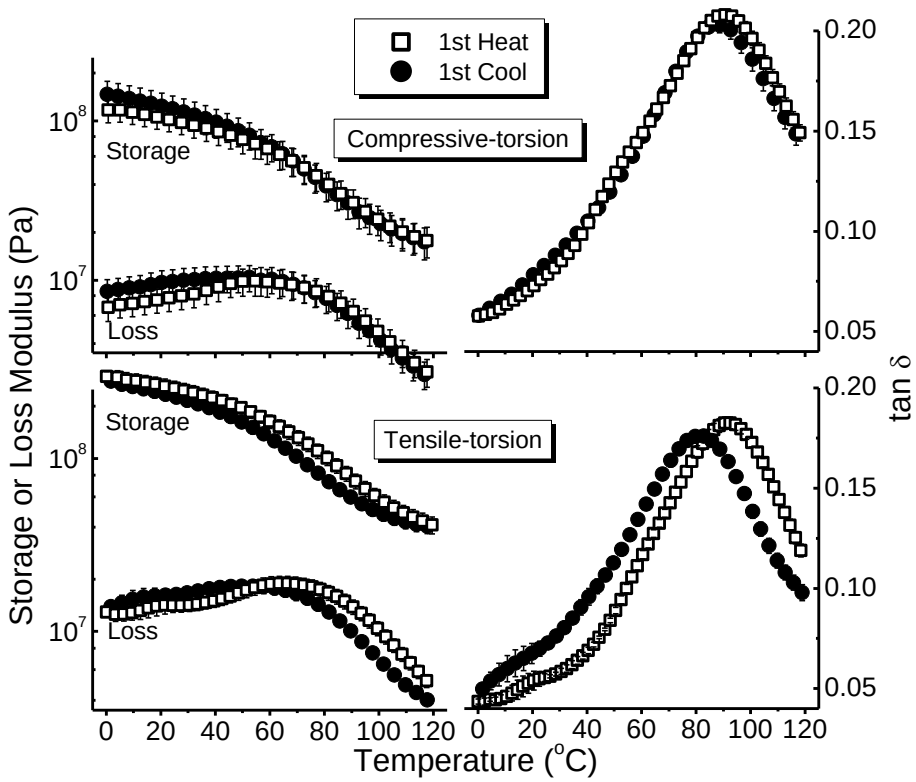

Figure 2-2 Comparison of compressive-torsion (top) and tensile-torsion (bottom) DMA heating and cooling scans (1˚C min^{-1}, 5 Hz) performed on yellow-poplar specimens (RT) immersed in ethylene glycol. Average curves are presented; error bars represent ±1 standard deviation, n = 3; non-visible error bars are smaller than symbols.

The two different stress modes produce generally similar responses. As mentioned above however, compressive-torsion specimens experience significant densification. For example in compressive-torsion the cooling and heating-mode storage moduli are quite similar at higher temperatures (Figure 2-2); but in the low temperature region, densification causes the cooling-mode storage modulus to exceed that for the heating-mode (The expanded scaling in Figure 2-1 reveals the storage modulus densification effect more dramatically). This is not the case in tensile-torsion where across the temperature scale it is seen that the cooling-mode storage modulus is slightly lower than for the heating-mode, with the greatest difference seen from 60˚C - 90˚C. The impact of specimen densification is most evident when inspecting the temperature of the tan δ maximum (glass transition temperature, Tg). In tensile-torsion, the heating and cooling-mode Tg's differ by approximately 10°C. This difference is not due to thermal lag (effect studied; data not shown). Rather in tensile-torsion, the cooling-mode Tg is naturally and significantly lower because the specimen experiences additional swelling during the glass/rubber transition (Eriksson *et al.*, 1991; Mantanis *et al.*, 1994). This additional swelling expands free volume and alters the nature and rate of polymer "repacking" during cooling. In contrast, under compressive-torsion the heating and cooling-mode Tg's differ by only about 3°C because the compressive clamping force densifies the rubbery specimen and restricts chain flexibility during cooling. Between methods, the heating-mode Tg's compare as essentially identical or quite similar, while the cooling-mode Tg's differ by 6-8°C (In ethylene glycol, Table 2-1).

Table 2-1 Summary of yellow-poplar wood glass transition temperatures as a function of stress mode, plasticizer, frequency, and grain orientation.

			Average Tg,˚C (standard deviation)			
	Freq.		Tensile-torsion		Compresive-torsion	
Solvent	(Hz)	Grain	Heating	Cooling	Heating	Cooling
Et-glycol	5	RT	92 (0.5)	81.7 (0.8)	90.5 (0.9)	87.7 (1.2)
		TR	91.7 (0.3)	81.5 (0.5)	93.0 (0.8)	90.0 (0.3)
		XL	93.8 (1.1)	83.3 (0.6)	93.1 (1.5)	89.5 (1.4)
Water (pH=7)	10	RT	87.7 (0.6)	81.0 (0.0)	91.0 (0.5)	88.3 (0.8)
		TR	86.7 (0.6)	80.3 (0.6)	86.8 (0.3)	87.6 (1.1)
		XL	95.0 (0.0)	86.1 (0.0)	92.0 (0.9)	91.4 (0.7)

Other differences between the two stress modes are more subtle. For instance, across the temperature scale, Figure 2-2 shows that tensile-torsion loss and storage moduli are greater than for compressive-torsion, and the overall damping intensity is generally greater in compressive-torsion. Also, the shapes of the respective tan δ traces differ slightly; notice that the first heat shoulder (near 40°C as discussed above) is absent in tensile-torsion, and it appears only very weakly in compressive-torsion (Figure 2-2). In fact, it was found that the intensity of the first heat tan δ shoulder is a function of the stress setting. As described in the experimental section, all experiments were

conducted within the limits of linear viscoelastic response (LVR); but higher stress settings within the LVR increase the intensity of the first heat shoulder. Regarding the relative weakness of the first heat tan δ shoulders in Figure 2-2, this data was obtained with a relatively low stress setting. While operating within the LVR, this shoulder can be enhanced by operating at the highest linear stress settings (data not shown; in this regard comparisons of Figure 2-1 and Figure 2-2 are invalid because of differing grain orientations).

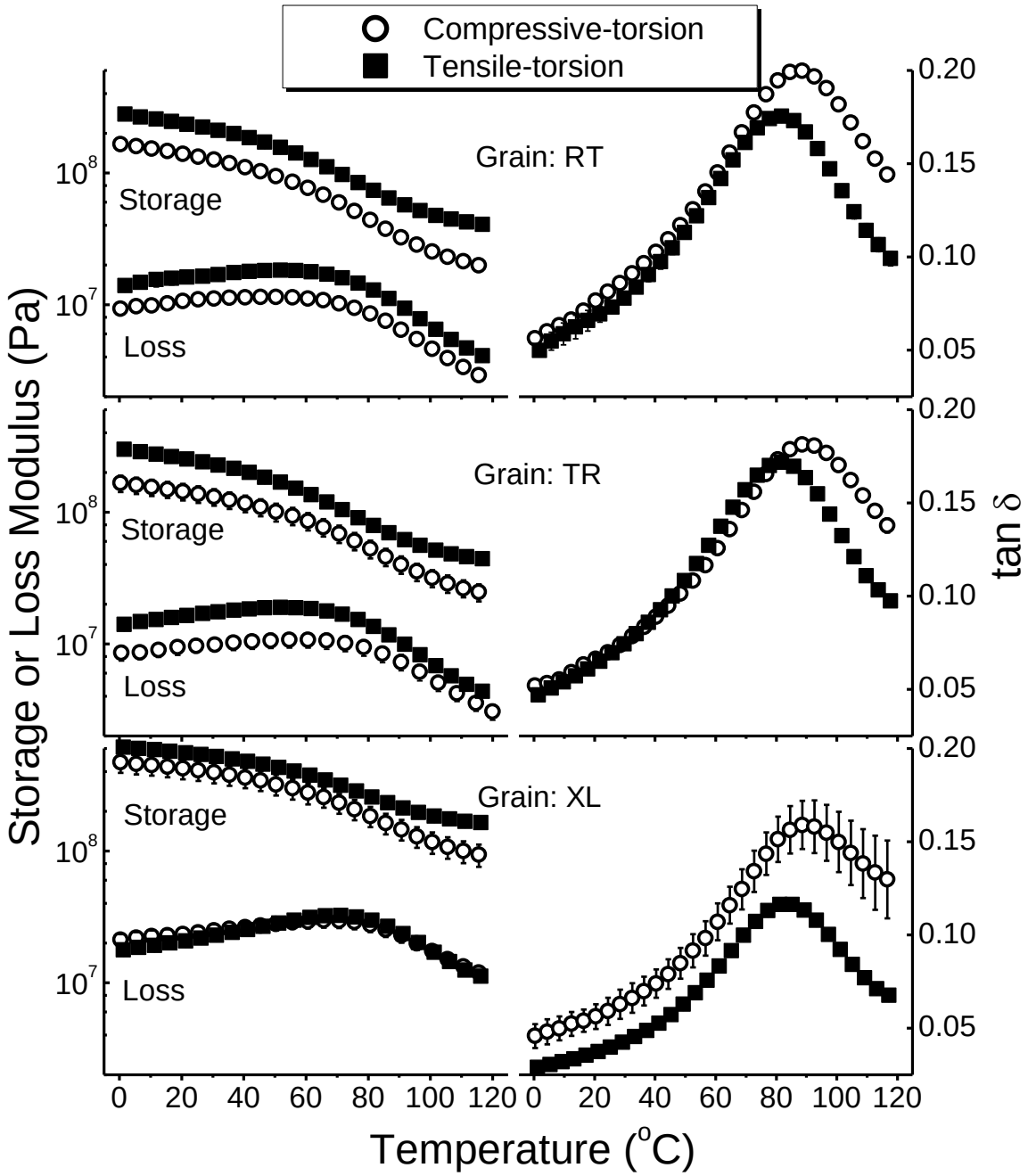

Figure 2-3 Comparison of compressive-torsion and tensile-torsion DMA cooling scans (1˚C min^{-1}, 5 Hz) for yellow-poplar in ethylene glycol as a function of grain orientation as indicated. Average curves are presented; error bars represent ± 1 standard deviation, n = 3; nonvisible error bars are smaller than symbols.

Figure 2-3 is a comparison of cooling scans obtained by tensile-torsion and compressive-torsion DMA as a function of grain orientation. Note that the scatter seen with compressive-torsion XL specimens is quite typical, and thus inferior to tensile-torsion which provides equally good data quality in all grain orientations. In this study, the Tg grain dependency was varied; it was minor in ethylene glycol but significant in water. Figure 2-3 and Table 2-1 show that in ethylene glycol the grain dependence of the Tg was minor; and this was true in either stress mode (grain effects in water are discussed below). As found in this study, literature reports on the Tg grain dependency in solvent saturated wood are highly varied. A recent review by Havimo (2009) suggests that the grain dependency of the Tg is minor. For instance, Höglund et al. (1976), Salmén (1984; 1988), and Olsson and Salmén (1992) reported that grain orientation had a minor or no effect on the temperature of the tan δ maximum (grain dependent differences in damping intensity are commonly observed). However, the Tg grain dependency was reported to be slightly more significant at higher frequencies, ~ 400 to 900 Hz (Becker *et al.*, 1977); and Furuta et al. (1997) demonstrate that the Tg grain dependency can exceed 10˚C. More recently Placet et al. (2007) reported grain dependent Tg differences on the order of 5-10˚C (water saturation). The explanation for this apparent discrepancy is unknown. In this context, it should be pointed out that the interpretation of published wood-DMA data in reviews (such as Havimo 2009) is challenging because various researchers have employed differing hygrothermal pretreatments that might impact transition temperature measurements.

As mentioned, in this work the grain dependency of the measured Tg was more significant in water (buffer pH = 7), as shown in the first heat curves of Figure 2-4 (and

also Table 2-1). For instance, XL specimens in tensile-torsion exhibit Tg's about 8˚C greater than for RT and TL specimens. Curiously, compression-torsion reveals a Tg grain dependency on the order of 3-5˚C; but in heating TR specimens are lower, and in cooling XL specimens are slightly higher. Between methods, the heating-mode Tg's are very nearly equivalent, while the cooling-mode Tg's differ by 5-7°C (in water, Table 2-1). Clearly, while individually consistent, tensile-torsion and compressive-torsion DMA produce slightly different results owing to the different stress modes and densification effects mentioned above. Consequently, data comparisons between stress modes should be avoided, or very carefully scrutinized.

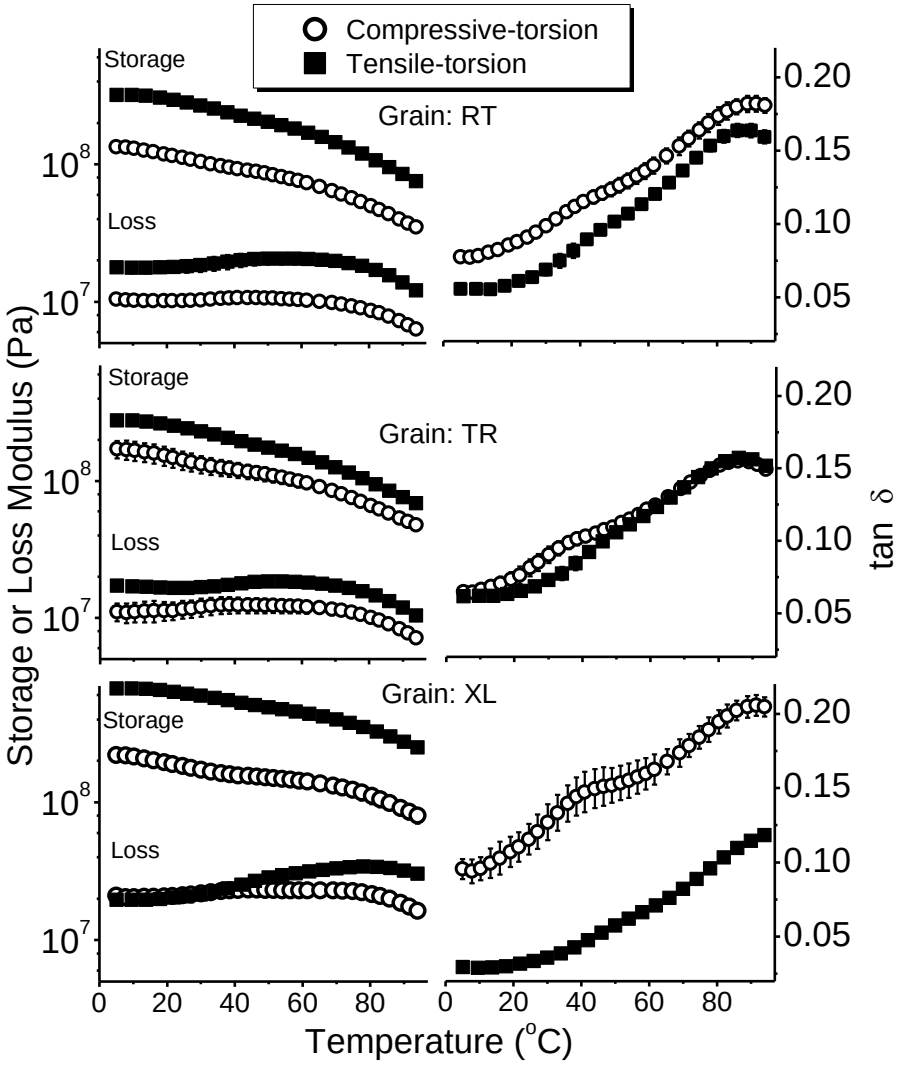

Figure 2-4 Comparison of compressive-torsion and tensile-torsion DMA 1st heating scans (3˚C min^{-1}, 10 Hz) for yellow-poplar in pH = 7 buffer as a function of grain orientation as indicated. Average curves are presented; error bars represent ± 1 standard deviation, n = 3; nonvisible error bars are smaller than symbols.

Notable in Figure 2-4 is again the tan δ shoulder (near 40°C) that was previously discussed for first heats in ethylene glycol (Figure 2-1 and Figure 2-2). This first heat response is consistent with the observations on *Chamaecyparis obtusa* made by Furuta et al. (1998) and Ishimaru et al. (2001). Furuta et al. (1998) found with water as

plasticizer that this peculiar response was related to drying history, that never-dried specimens did not exhibit the transition; and this is consistent with the data published by Heitner and Atack (1984), with *Populus tremuloides*, and by Placet et al. (2007), with Quercus sessiliflora, *Fagus sylvatica*, and *Populus* sp. In this study, the drying history effect was confirmed with ethylene glycol. Increment bores were obtained from the perimeter (outer 20 mm) of a living yellow-poplar tree and immediately immersed in ethylene glycol; the subsequent first heat in ethylene glycol showed no evidence of the tan δ shoulder (data not shown). Using a variety of organic plasticizers, Ishimaru et al. (2001) hypothesized that the first heat tan δ shoulder was related to the “redistribution” of the swelling liquid towards an equilibrium state. While this characterization is perhaps correct, it does not address the lignocellulosic molecular features from which the relaxation is borne. To our knowledge, none besides Furuta et al. (1997; 1998) and Ishimaru et al. (2001) have specifically mentioned this curious relaxation. Carefully reviewing the wealth of wood DMA publications, one will notice that a similar tan δ shoulder appears occasionally, as in Becker and Noack (1968), with *Fagus sylvatica*, and in Olsson and Salmén (1997), with *Ulmus americana*. Whatever the molecular basis, the feature is disrupted at low temperatures (40-60°C), whereafter only the underlying broad and rapidly reversible relaxation is observed. However as demonstrated above, the first heat tan δ shoulder is reversible, but over much longer time scales which include specimen drying. Even though special efforts were required to demonstrate reversibility, the first heat tan δ shoulder must reflect a preferred chain configuration and/or state of wood polymer association. While the appearance of this first heat tan δ shoulder appears to be related to drying history, it reflects an as yet

unknown molecular or supramolecular feature in wood. Perhaps this weak tan δ shoulder could be used to gain morphological insight, or just practical correlation to biomass treatment. Should that be the case, then it can be suggested based on Figure 4 that compressive-torsion might be a preferred analytical stress mode since the relaxation is much less prominent in tensile-torsion. Furthermore, the grain dependency of the tan δ shoulder is unnoticeable in tensile-torsion, but it is pronounced in compressive-torsion where XL specimens show it most clearly.

When considering grain effects in wood DMA, it is tempting to postulate when stresses are borne more or less by cellulose fibrils, or more or less by the middle lamella. In tension parallel to grain or bending along the grain, cellulose fibrils bear the greatest stress, resulting in the highest storage moduli and the lowest tan δ intensities; stresses transverse to the fibrils provide lower storage moduli and greater damping (Salmén, 1984; 1988; Furuta *et al.*, 1997; Jiang and Lu, 2009a). When comparing the glass transition along or across the fiber direction (as in tension or bending), it has been argued that the relaxation reflects a homogeneous lignin response, not favoring localized morphologies (i.e. S2 layer versus middle lamella); this was supported by the shape-similarity of the respective tan δ curves and the similarity of the measured transition temperatures and activation energies (Salmén, 1984; 1988). However, Furuta et al. (1997) found a significant grain dependence of the transition temperatures, and suggested that this was from the varied response of localized structures. The conflict here is further complicated by the fact that S2 lignin is itself oriented (Atalla and Agarwal, 1985a; Åkerholm and Salmén, 2003).

We suggest that the anatomical and molecular complexity of xylem tissue exceeds current abilities to simply explain the grain dependency of wood DMA data. A similar opinion was expressed by Placet et al. (2007), however these authors did cite shear stresses local to the middle lamella when explaining bending differences along the radial and tangential directions. As described in this work, XL specimens experience torsion in the cross-sectional plane, where both microfibrillar and also cellular twist is imposed as if threads are wound around a common axis. In contrast, torsion in either the radial or tangential planes (respectively RT and TR specimens) imposes a lengthwise (end-over-end) cellular rotation; this might seem to focus on the middle lamella, but adjacent microfibrils will also experience lengthwise displacement. Considering tensile-torsion as the purest form of torsional stress, Figure 2-3 and Figure 2-4 demonstrate that XL specimens exhibit the highest storage modulus and the lowest tan δ intensity. This can be interpreted that torsion in the cross-sectional plane (XL specimens) imposes the greatest microfibrillar stress. Likewise, Figure 2-3 and Figure 2-4 also show that tensile-torsion storage moduli and tan δ intensities are quite similar for RT and TR specimens. Furthermore, again notice that tensile-torsion Tg's in ethylene glycol show little or no grain dependence (Table 2-1); but in water, XL specimens exhibit Tg's that are 6-8°C higher than for RT and TR. In other words, the grain dependency is further complicated by plasticizer effects, again suggesting that wood DMA data cannot be simply related to localized xylem structure. When considering compressive-torsion, stress fields become much more complex and are very different from tensile-torsion. For instance note that relative to tensile-torsion, compressive-torsion in the cross-sectional plane (XL specimens) shows a much greater

tan δ intensity. Furthermore, while tensile-torsion Tg's in the radial and tangential planes are quite similar, compressive-torsion Tg's slightly diverge in these planes, particularly in the first heat; but again this effect is also plasticizer dependent (Table 2-1). Relative to bending and tension, both torsional modes are much less sensitive to grain effects (Salmén, 1984; Furuta *et al.*, 1997; Backman and Lindberg, 2001; Placet *et al.*, 2007; Jiang and Lu, 2009a).

As discussed previously, compressive-torsion and tensile-torsion DMA both provide reliable but different views of the lignin glass/rubber transition in solvent saturated wood; and direct comparisons should be avoided or conducted very carefully. When considering subambient relaxations in dry wood or wood equilibrated below fiber saturation, the methodologies diverge dramatically. Figure 2-5 demonstrates that tensile-torsion reveals the familiar secondary relaxations that have been attributed to methylol rotation (Obataya *et al.*, 1996) and the effects of very low moisture content (~0.7%) (Obataya *et al.*, 1996; Sun *et al.*, 2007).

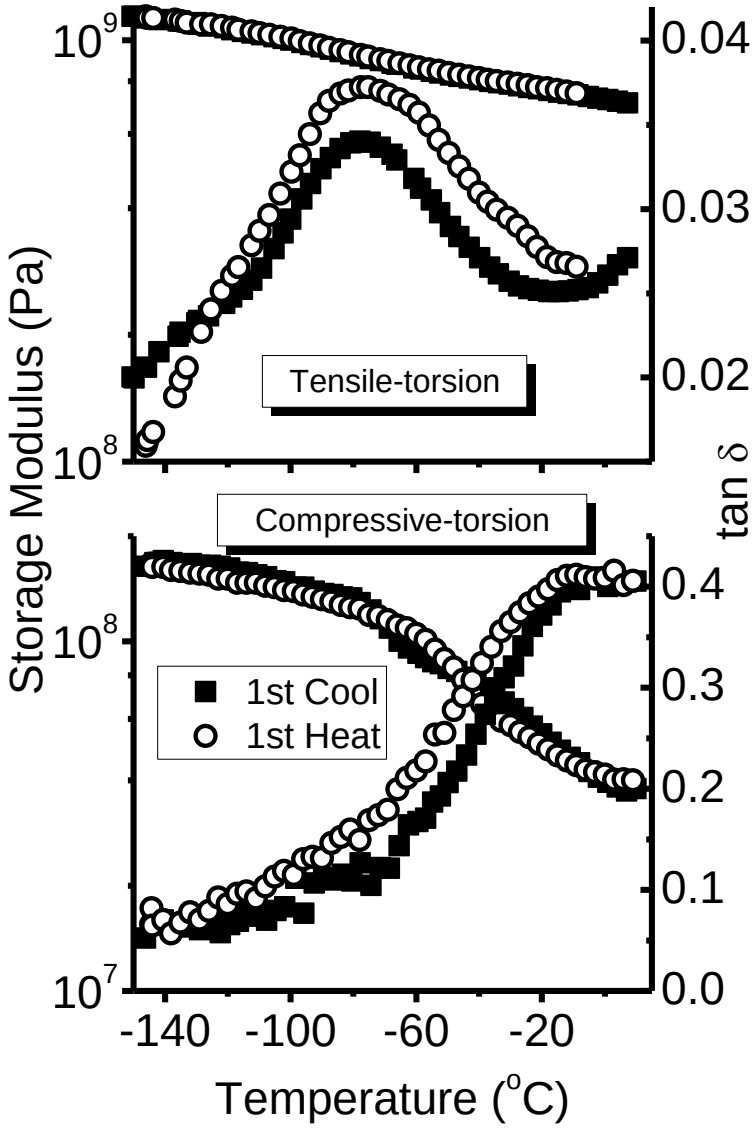

Figure 2-5 Comparison of tensile-torsion (top) and compressive-torsion (bottom) subambient relaxations in dry yellow-poplar specimens (TR) during first cool and subsequent heating as indicated (2˚C min–1, 1 Hz). Note differences in storage modulus and tan δ scales.

As demonstrated in the literature, these secondary relaxations correspond to a minor stiffness change and to a very weak tan δ signal (< 0.04) when studied in cantilever bending (Sun *et al.*, 2007), tension (Backman and Lindberg, 2001), and also

tensile-torsion as demonstrated here. In contrast, the compressive-torsion subambient response is entirely different; the stiffening/softening transition occurs over nearly one decade of storage modulus, and the tan δ intensity is quite significant, much greater even than the lignin glass transition (compare to Figure 2-1 to Figure 2-4). Furthermore, the effects of increasing moisture and also of stress frequency are anomalous in compressive-torsion, while tensile-torsion provides a very satisfying response in this regard (data not shown). It is clear that compressive-torsion is not suitable for a simple analysis of the low temperature secondary relaxations in wood. While compressive-torsion DMA has its limitations, the method excels with very small and difficult-to-clamp specimens. For instance, Figure 2.6 shows average compressive-torsion DMA scans for spruce wood that was severely biodegraded by *G. trabeum* and *P. placenta*.

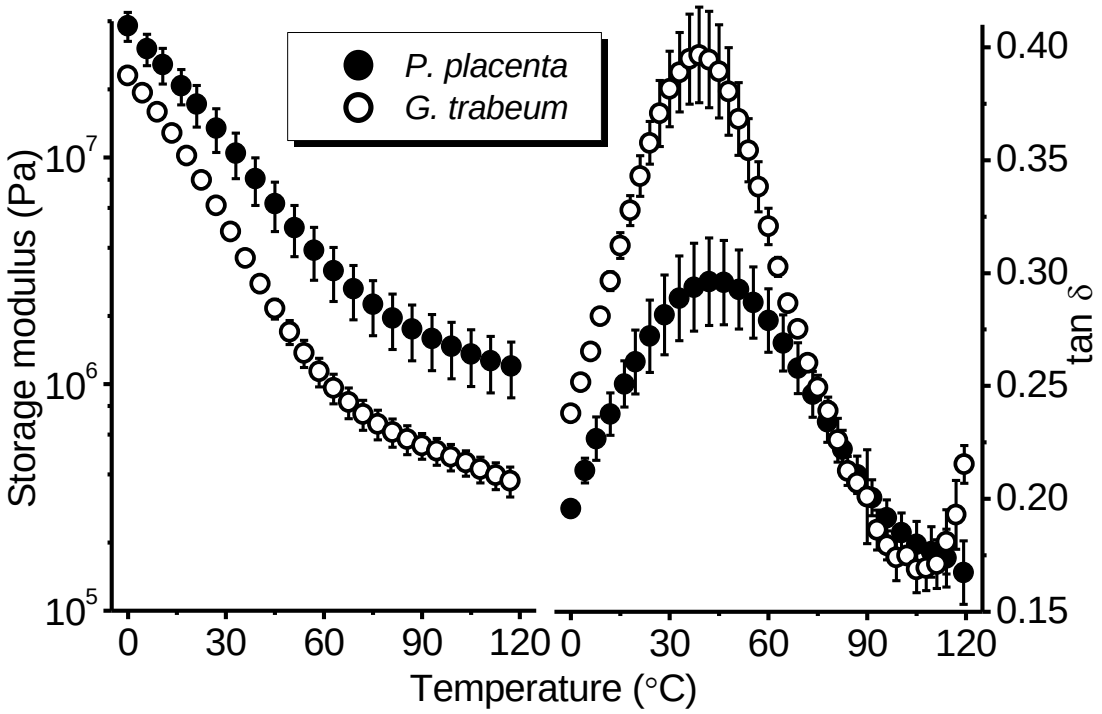

Figure 2-6 Average compressive-torsion cooling scans of spruce fiber mats resulting from fungal biodegradation as indicated (in ethylene glycol, 3°C min^{-1}, 5 Hz); error bars = ± 1 standard deviation, n = 3; nonvisible error bars are smaller than symbols.

In this case advanced fungal degradation destroyed the mechanical integrity required for normal analysis. Instead, the crumbly specimens were ground under liquid N_2 using mortar and pestle, dispersed and saturated in ethylene glycol, and then filtered into a fibrous mat that was analyzed while immersed in ethylene glycol. Here it is seen that both fungi caused a dramatic Tg reduction, but the effects of *G. trabeum* were more severe. Regarding extremely small specimens, Figure 2-7 demonstrates tissue maturity effects in minute sections taken from the stem of switchgrass (*Panicum virgatum*).

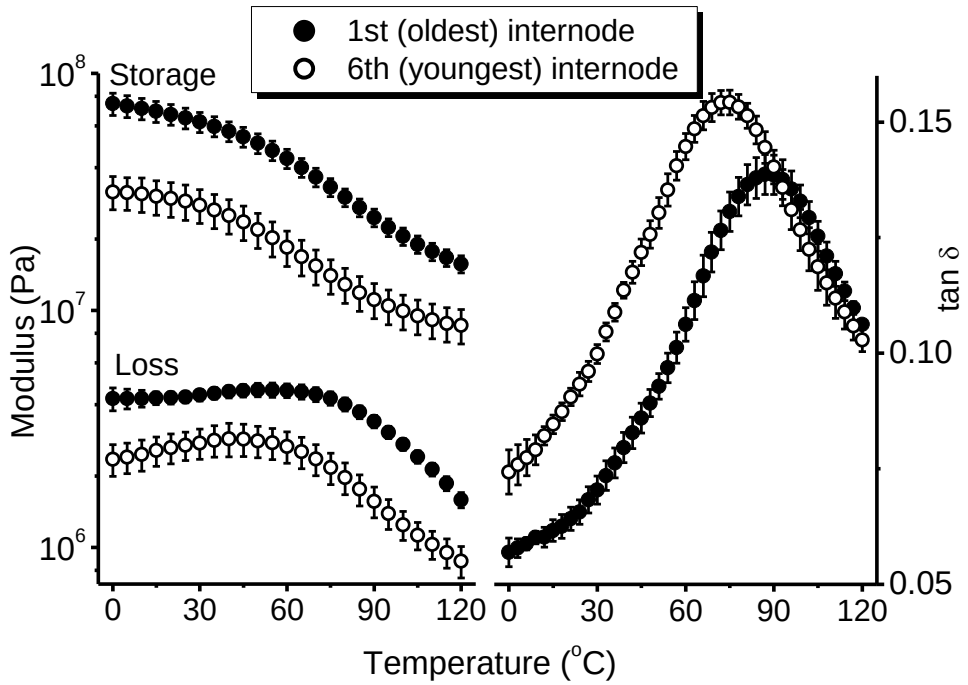

Figure 2-7 Average compressive-torsion cooling scans of switchgrass stem as a function of tissue maturity as indicated (in ethylene glycol, 2°C min^{-1}, 1 Hz); error bars = ± 1 standard deviation, n = 3; nonvisible error bars are smaller than symbols.

The stem section taken from within the first internode exhibits a significantly higher Tg than for the younger specimen taken from within the sixth, terminal internode. (Not shown here is that switch grass specimens also exhibited the first heat tan δ shoulder, but with a far greater intensity). The examples in Figure 2-6 and Figure 2-7 demonstrate that compressive-torsion DMA is effective for studies that are constrained by specimen integrity and/or size.

2.5. Summary

Parallel-plate compressive-torsion DMA combined with solvent-submersion is effective for probing the lignin glass/rubber transition in lignocellulosic materials. The solvent-saturated lignin response is generally similar in compressive-torsion and

traditional tensile-torsion DMA, but direct data comparisons should be avoided or carefully considered. In tensile-torsion, the tensile force required for specimen clamping is minor and results in a more nearly pure torsional stress. To prevent specimen slippage, compressive-torsion imposes a significant compression force, and densification occurs such that cooling-mode lignin Tg's are elevated by 5-8°C. Furthermore, compressive-torsion seems poorly suited for the subambient analysis of secondary relaxations in specimens below fiber saturation. Keeping these limitations in mind, compressive-torsion DMA also offers distinct advantages. Solvent-submersion DMA is simple because solvent cups are easily fashioned for torsional rheometers designed for parallel-plate DMA. Also, compressive-torsion DMA is better suited to probe an as yet unidentified tan δ shoulder (~40°C) that appears in the first heat. Most notable is that extremely small and/or difficult-to-clamp specimens are easily studied because of the simplified specimen clamping. Applied appropriately, parallel-plate compressive-torsion DMA provides a facile and effective means for solvent-submersion DMA of lignocellulosic materials.

2.6. Acknowledgements

This project was supported by the National Research Initiative of the USDA Cooperative State Research, Education and Extension Service, grant number 2006-35504-17424. Support from the Wood-Based Composites Center and also from the Sustainable Engineered Materials Institute at Virginia Tech is gratefully acknowledged. Switchgrass was kindly provided by Dr. Bingyu Zhao, Department of Horticulture, Virginia Tech. Fungal biodeterioration specimens were graciously provided by

Professors Barry Goodell and Jody Jellison, both at the University of Maine, Orono, U.S.A.

2.7. References

Åkerholm, M. and L. Salmén, 2003. The oriented structure of lignin and its viscoelastic properties studied by static and dynamic FT-IR spectroscopy, *Holzforschung*, 57(5), 459-465.

Atalla, R. H. and U. P. Agarwal, 1985a. Raman microprobe evidence for lignin orientation in the cell-walls of native woody tissue, *Science*, 227(4687), 636-638.

Backman, A. C. and K. A. H. Lindberg, 2001. Differences in wood material responses for radial and tangential direction as measured by dynamic mechanical thermal analysis, *Journal of Materials Science*, 36(15), 3777-3783.

Becker, H., H. Hoglund and G. Tistad, 1977. Frequency and temperature in chip refining, *Paperi Ja Puu-Paper and Timber*, 59(3), 123-&.

Becker, H. and D. Noack, 1968. Studies on dynamic torsional viscoelasticity of wood, *Wood Science and Technology*, 2213-230.

Eriksson, I., I. Haglind, O. Lidbrandt and L. Salmen, 1991. Fiber swelling favoured by lignin softening, *Wood Science and Technology*, 25(2), 135-144.

Furuta, Y., M. Makinaga, H. Yano and H. Kajita, 1997. Thermal-softening properties of water-swollen wood .2. Anisotropic characteristics of thermal-softening properties, *Mokuzai Gakkaishi*, 43(1), 16-23.

Furuta, Y., M. Norimoto and H. Yano, 1998. Thermal-softening properties of water-swollen wood V. The effects of drying and heating histories, *Mokuzai Gakkaishi*, 44(2), 82-88.

Green, D. W., J. E. Winandy and D. E. Kretschmann. 1999: Mechanical properties of wood. *Wood handbook, wood as an engineering material.*, Madison, WI, USA: Forest Products Society, 1-45.

Havimo, M., 2009. A literature-based study on the loss tangent of wood in connection with mechanical pulping, *Wood Science and Technology*, 43(7-8), 627-642.

Heitner, C. and D. Atack, 1984. Dynamic mechanical-properties of sulfite treated aspen, *Paperi Ja Puu-Paper and Timber*, 66(2), 84-89.

Höglund, H., U. Sohlin and G. Tistad, 1976. Physical-Properties of Wood in Relation to Chip Refining, *Tappi*, 59(6), 144-147.

Ishimaru, Y., S. Narimoto and I. Iida, 2001. Mechanical properties of wood swollen in organic liquids with two or more functional groups for hydrogen bonding in a molecule, *Journal of Wood Science*, 47(3), 171-177.

Jiang, J. L. and J. Lu, 2009a. Anisotropic characteristics of wood dynamic viscoelastic properties, *Forest Products Journal*, 59(7-8), 59-64.

Mantanis, G. I., R. A. Young and R. M. Rowell, 1994. Swelling of wood, *Wood Science and Technology*, 28(2), 119-134.

Norimoto, M. and T. Yamada, 1666. Dynamic torsional viscoelasticity of wood, *Wood Res*, 3832-39.

Obataya, E., M. Yokoyama and M. Norimoto, 1996. Mechanical and dielectric relaxations of wood in a low temperature range .1. Relaxations due to methylol groups and adsorbed water, *Mokuzai Gakkaishi*, 42(3), 243-249.

Olsson, A.-M. and L. Salmén, 1997. The effect of lignin composition on the viscoelastic properties of wood, *Nord. Pulp Pap. Res. J.*, 12(3), 140-144.

Olsson, A. M. and L. Salmén, 1992. Viscoelasticity of Insitu Lignin as Affected by Structure - Softwood Vs Hardwood, *ACS Symposium Series*, 489133-143.

Placet, V., J. Passard and P. Perre, 2007. Viscoelastic properties of green wood across the grain measured by harmonic tests in the range 0-95 degrees C: Hardwood vs. softwood and normal wood vs. reaction wood, *Holzforschung*, 61(5), 548-557.

Sadoh, T., 1981. Viscoelastic Properties of Wood in Swelling Systems, *Wood Science and Technology*, 15(1), 57-66.

Salmén, L., 1984. Viscoelastic properties of in situ lignin under water-saturated conditions, *Journal of Materials Science*, 19(9), 3090-3096.

Salmén, L., 1988. Directional viscoelastic properties of wood, Progress and trends in rheology II: Proceedings of the 2nd conference of european rheologists, Prague, 234-235, Steinkopff.

Salmen, N. L. and C. Fellers, 1982. The fundamentals of energy consumption during viscoelastic and plastic deformation of wood, *Pulp & Paper-Canada*, 83(12), TR93-TR99.

Sun, N., S. Das and C. E. Frazier, 2007. Dynamic mechanical analysis of dry wood: Linear viscoelastic response region and effects of minor moisture changes, *Holzforschung*, 61(1), 28-33.

Chapter 3 Compressive-torsion DMA of wood in organic media

Sudip Chowdhury and Charles E. Frazier
Macromolecular Science & Engineering, Wood Science & Forest Products
Virginia Tech, Blacksburg VA 24061, U.S.A.
(Submitted to Holzforschung, August 2011)

3.1. Abstract

Novel biorefinery approaches for renewable materials and energy have generated new interest in the application of organic solvents in lignocellulose processing. This requires further advances in the rheology of lignocellulose in various organic solvents. Using compressive-torsion dynamic mechanical analysis (DMA), this study investigates the viscoelasticity of yellow-poplar (*Liriodendron tulipifera*) wood swollen in various organic solvents, specifically, aprotic tertiary amides: N,N-dimethylformamide (DMF) and N-methylpyrrolidone (NMP) and protic alcohols: ethylene glycol and glycerol. A systematic documentation of the linear viscoelastic response (LVR) revealed a complex relationship of LVR with grain orientation, temperature and solvent. Glass/rubber transition temperatures (Tg) of swollen wood showed inverse relationship with solvent induced volumetric swelling. DMF and NMP swelled wood similarly and revealed similar Tgs, which were lower than Tgs in ethylene glycol and glycerol. Glycerol showed significantly higher solvolytic power than ethylene glycol. Glycerol plasticized wood underwent extreme swelling when heated beyond Tg; this swelling was associated with solvolysis, causing a reduction in the effective crosslink

density and Tg . Consistent with the literature, the observed Tg grain dependency was highly varied. The weakest plasticizer, glycerol, produced a prominent Tg grain dependency, whereas grain dependency was variable in the stronger swelling agents. This study demonstrates the importance of researching lignocellulose rheology in a greater variety of organic liquids to achieve new perspectives into lignocellulose structure and processing.

3.2. Introduction

Wood viscoelasticity has been widely studied over the past half century to help optimize wood utilization in paper and pulp and also in composite material applications. The global progression towards biorefineries and renewable fuels provides additional motivation to advance research in lignocellulose viscoelasticity. The earliest reports of wood dynamic mechanical analysis (DMA) are found in the works of Norimoto and Yamada (1666) and Becker and Noack (1968) using torsion pendulum DMA. A vast body of static and dynamic mechanical analysis work followed to study wood in dry and solvent plasticized conditions. In dry wood, glass/rubber transitions occur near 200 °C in a thermo-degradative fashion(Back and Salmén, 1982). However, plasticizing solvents can effectively reduce the transition to non-damaging or less damaging temperatures. Therefore wood is often processed under plasticized conditions for higher processing and energy efficiencies (Havimo, 2009). For its widest applicability, water swollen wood has been extensively studied using various DMA modes such as torsion (Becker and Noack, 1968; Höglund *et al.*, 1976; Furuta *et al.*, 1997; Obataya *et al.*, 2003; Chowdhury *et al.*, 2010), bending (Olsson and Salmén, 1997; Placet *et al.*, 2007,

2008) and tension (Salmén, 1984). Although water swollen wood is extensively studied, relatively few reports exist on DMA of non-aqueous solvent swollen wood (Sadoh, 1972; Sadoh, 1981; Kelley *et al.*, 1987; Laborie *et al.*, 2004; Chowdhury *et al.*, 2010). Takeshi Sadoh and co-workers conducted a series of torsional DMA studies of Japanese birch swollen in different glycols, amines and formamide. Formamide was reported to be a powerful swelling agent (1.2 times greater swelling than water) whereas, ethylene glycol swelled wood to a degree similar to water (Sadoh, 1981). Sadoh also found that at an identical swelling level formamide plasticized wood exhibited a significantly lower glass/rubber transition temperature (Tg) than water-saturated wood. This difference was attributed to formamide's ability to interact and mobilize wood components to a degree that water and ethylene glycol could not achieve (Sadoh, 1981). This was the earliest indication that lignocellulose swelling is highly varied in different organic media and that insights to lignocellulose structure and processing vary similarly.

The vision towards biorefineries is generating novel perspectives on lignocellulose processing that include organic media, as in organosolv pulping and fractionation using ionic liquids for example. Therefore, it is becoming increasingly important to systematically document lignocellulose rheology in a greater variety of organic liquids.

Besides a greater variety of organic plasticizers, the continued advance of lignocellulose rheology must also include greater emphasis on fine experimental details. Perhaps the most fundamental is characterization of the linear to nonlinear viscoelastic transition. The linear viscoelastic response (LVR) region is typically preferred for structure/property insights because the mathematical descriptions are the simplest.

Whereas the nonlinear or high stress/strain response is most relevant to industrial processing. A wealth of wood DMA literature exists, however mention of the topic is uncommon and detailed studies are rare (Laborie *et al.*, 2004; Sun *et al.*, 2007; Jiang and Lu, 2009b; Chowdhury *et al.*, 2010). Within the LVR, the applied sinusoidal stress/strain provides a reproducible response independent of the stress/strain level, and polymer packing is not irreversibly distorted within the time frame of the observation (Menard, 1999); this allows accurate calculation of the component plastic and elastic responses (Rubinstein and Colby, 2003) and the simplest understanding of structure/property relationships.

This paper continues an introduction to parallel-plate compressive-torsion DMA, which for lignocellulose research has certain advantages and limitations (Chowdhury *et al.*, 2010). Here emphasis was placed upon the use of organic plasticizers, specifically aprotic tertiary amides and also protic alcohols. Furthermore, the LVR strain limits were carefully measured as a function of plasticizer, temperature, and grain orientation, both to document this property and to determine if structural insight could be revealed from this fundamental response.

3.3. Experimental

3.3.1. Materials

A single piece of yellow-poplar (*Liriodendron tulipifera*) sapwood lumber (80×80×450 mm) was used to make specimens for volumetric swelling measurements (Radial × Tangential × Longitudinal: 25×25×5 mm) and for DMA. In the latter case, cylindrical discs (8 mm dia., 3 mm thick) were machined using a “plug-cutter.” (discs

were machined in the dry state; during solvent-submersion differential swelling slightly distorts the cylinder shape; the minor error in measured moduli was ignored). Specimens averaged 2 growth rings per centimeter and ring positioning within specimens was random. Cylindrical specimens were tested in parallel-plate compressive-torsion using a TA Instruments AR 2000 rheometer such that the cylinder axis (thickness direction) was parallel to the torsional axis and the cylinder ends were in contact with the parallel-plates; torsional slippage was prevented with a compressive clamping force exerted by the parallel-plates. Three different grain orientations were tested, denoted as RT, TR and XL; the first letter indicates the wood surfaces in contact with the parallel-plates (R-radial, T-tangential and X-cross-sectional) and the secondindicates the grain direction parallel to the torsional axis (T-tangential, R-radial and L-longitudinal). Four different plasticizing solvents were used: N,N-dimethylformamide (DMF, >99.8%), N-methyl-2-pyrrolidone (NMP, 99.5%), ethylene glycol (99.8%) and glycerol (99.8%).

3.3.2. Methods

All specimens were vacuum-dried (0.04-0.1 mm Hg, 24 h, ambient temperature) and stored in a desiccator (anhydrous P_2O_5 and N_2) for at least 48 h prior to analysis. Thereafter specimens were saturated with plasticizer using a vacuum-pressure treatment (5 mm Hg for 1 h, followed by atmospheric pressure for at least 24 h). Solvent submersion was conducted such that the bottom plate was surrounded by a stainless steel cup that maintained specimen immersion during analysis. All tests were performed under anhydrous N_2 gas; liquid N_2 was used to control temperature.

Compressive clamping was achieved with a 40 N static normal force, representing approximately 4.2% and 42% of the wet compression strength respectively parallel and perpendicular to grain (Green *et al.*, 1999). Safety note: when organic solvents are used as specimen plasticizers caution is required because the solvent bath is enclosed within an oven having exposed heating elements; consequently, anhydrous N_2 gas is directed through the heating chamber to prevent ignition; and the oven must never be opened to the atmosphere while the oven temperature is near the solvent flash point. Attention to these details results in safe and reliable analysis.

The linear viscoelastic response (LVR) region was determined using a stress sweep (2-200 KPa, frequency: 5 Hz), three observations for each sample type. Measurements were conducted at temperature extremes and also near the glass/rubber transition (at or near tan δ max, Tg) in heating and then cooling as follows: 1) equilibrate at initial temperature for 5 min; run stress sweep, 2) heat to intermediate temperature (3°C/min); equilibrate ~ 10 sec; run stress sweep, 3) heat to max temperature (3°C/min); equilibrate ~ 10 sec; run stress sweep, 4) equilibrate at max temperature for 40 min; run stress sweep, 5) rapid cool (~ 6-13°C/min) to intermediate temperature; equilibrate 5 min; run stress sweep, 6) rapid cool (~ 6-13°C/min) to low temperature; equilibrate 5 min; run stress sweep. The LVR strain limit was identified by the corresponding stress that caused a 5% reduction in the initial storage modulus.

A separate collection of specimens were subjected to a sequential heat/cool/heat treatment as follows: 1) heat to maximum temperature (3°C/min, 5 Hz); hold 40 min, 2) isothermal frequency sweep (1-100 Hz, 25 - 130 KPa depending upon the LVR limit), 3) rapid cool (~ 6-13°C/min) to next lowest temperature (10 °C step), equilibrate 10 min, 4)

Repeat steps 2 & 3 over experimental temperature range, 5) heat to maximum temperature, (3 °C/min, 5 Hz). Note that steps 2-4 describe frequency sweep acquisitions used for time/temperature superposition; that data will not be discussed here and only the first and second heating scans will be presented. All tests were conducted in stress-control with stress settings very near but not greater than the LVR limits. Temperature ranges were chosen to avoid plasticizer freezing and to minimize excessive evaporation (DMF: -10 to 80°C, NMP: -30 to 130°C, ethylene glycol: 0 to 120°C and glycerol: 30 to 170°C).

Thermal reversibility in glycerol was investigated using a single glycerol-plasticized TR specimen. The specimen was subjected to two sequential rounds of cyclic heating and cooling. After the 1st round the specimen was extracted in water to remove glycerol, dried, resaturated with glycerol and then the 2nd round was conducted. First round (15 N normal force, 5 Hz, 3 °C/min, 0.05% strain): 1) 5min, 30 °C, 2) 1st heat: 30 – 170 °C, 3) 170 °C ,40 min, 4) 1st cool: 170-30 °C, 5) 2nd heat: 30-170 °C, 6) 170 °C, 1 min, 7) 2nd cool: 170-30 °C. Specimen extraction: 1) Soaked in 200 ml distilled water, 2 h at room temperature, rapid stirring, 2) Water exchanged with 200 ml fresh distilled water, 48 h, rapid stirring. After extraction the specimen was dried under vacuum (1-5 mm Hg) for 48 h in the presence of fresh P_2O_5 and resaturated and subjected to the 2nd round of cyclic heating and cooling with same experimental parameters.

Dry and saturated dimensions of the swelling measurement specimens were used to calculate the volumetric swelling before heating (pre-heat swelling). Saturated specimens were then heated for 40 min (above Tg) in their respective solvents under

dry N_2. Bath temperatures were: DMF: 60 °C, NMP: 75 °C, ethylene glycol: 100 °C and glycerol: 130 °C. Dry and heat treated swollen dimensions were used to calculate swelling after heating (post-heat swelling).

3.4. Results and Discussion

Table 3-1 and Figure 3-1 present average LVR strain limits for specimens as a function of plasticizer, grain orientation, and temperature; measurements were taken in heating and subsequently in cooling with an intervening 40-min isothermal conditioning at the maximum temperature employed for the respective solvents.

Table 3-1 LVR strain limits (5 Hz) for yellow-poplar sapwood specimens by grain orientation, plasticizer, and temperature during heating/cooling modes separated by a maximum-temperature isothermal conditioning period; percent change between heating and cooling modes (entries in parenthesis significantly different with 95% confidence).

Solvent	Grain	*Temp (°C)*	*Heating Mode*		*Cooling Mode*		*% change (Significant)*
			Strain (%)	St. Dev.	Strain (%)	St. Dev.	
Glycerol	RT	30	0.026	0.005	0.093	0.007	(255)
		100	0.085	0.011	0.189	0.009	(122)
		170	0.220	0.013	0.279	0.045	27
	TR	30	0.025	0.010	0.064	0.006	(152)
		100	0.037	0.012	0.133	0.015	(265)
		170	0.065	0.023	0.215	0.022	(228)
	XL	30	0.007	0.004	0.015	0.006	114
		100	0.010	0	0.030	0	(200)
		170	0.043	0.015	0.058	0.010	35
Ethylene glycol	RT	0	0.039	0.023	0.072	0.011	86
		90	0.067	0.017	0.122	0.017	84
		120	0.185	0.091	0.181	0.016	-2
	TR	0	0.022	0.003	0.021	0.009	-8
		90	0.038	0.002	0.057	0.023	52
		120	0.065	0.013	0.048	0.009	-25
	XL	0	0.011	0.001	0.014	0.005	19
		90	0.015	0.001	0.024	0.006	61
		120	0.026	0.002	0.028	0.008	6
NMP	RT	-20	0.052	0.008	0.091	0.007	76
		50	0.087	0.012	0.186	0.047	114
		130	0.224	0.022	0.244	0.029	9
	TR	-20	0.033	0.019	0.043	0.014	29
		50	0.050	0.010	0.076	0.029	53
		130	0.097	0.014	0.069	0.015	-29
	XL	-20	0.018	0.002	0.031	0.002	(78)
		50	0.025	0.005	0.073	0.020	191
		130	0.073	0.043	0.076	0.041	4
DMF	RT	-10	0.047	0.009	0.072	0.037	52
		45	0.052	0.018	0.121	0.058	132
		80	0.100	0.015	0.134	0.031	33
	TR	-10	0.015	0.007	0.028	0.006	79
		45	0.027	0.009	0.031	0.006	14
		80	0.026	0.013	0.034	0.011	(32)
	XL	-10	0.018	0.005	0.028	0.009	57
		45	0.024	0.003	0.025	0.009	5
		80	0.023	0.013	0.027	0.008	15

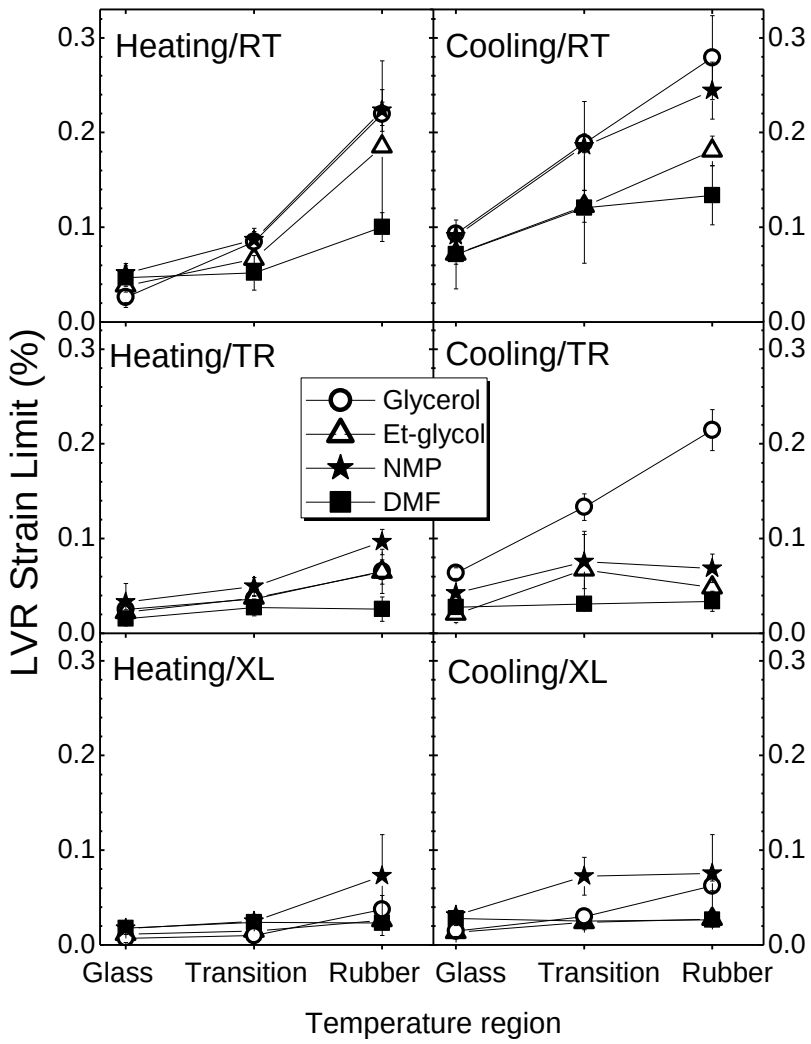

Figure 3-1. Average LVR strain limits (5 Hz) as a function of solvent, grain orientation, and temperature, where heating and cooling measurements were separated by a 40-min heating at the maximum temperature specific to the respective solvents. Error bars represent ± 1 standard deviation; n = 3.

Specimen swelling and Tg was solvent dependent as will be discussed later. For each plasticizer, LVR analysis was conducted within three regions, the low temperature glassy region, the glass transition region at or near the tan δ maximum (Tg), and the high temperature rubbery region. A multivariate analysis was conducted, considering

plasticizer, grain orientation and temperature as three independent categorical variables. LVR strain limits before and after thermal conditioning were the responses. Analysis of variance revealed that all three independent variables and interaction terms between them were significant ($P < 0.0001$). Consequently the LVR response was complex and simple generalizations were precluded. Nevertheless, various highlights are discussed below.

Grain direction had a significant effect on LVR strain limits in both heating and cooling. Generally, the RT grain orientation stood out as having the highest LVR strain limits in all 4 plasticizers (Figure 3-1); TR was somewhat lower and XL was substantially lower. Practically speaking this implies that RT specimens will provide the highest quality DMA data, because a common strategy is to operate at the upper limits of the LVR where instrument sensitivity and signal quality are optimal. Likewise XL specimens will provide the noisiest data because the LVR is so low and perhaps near the sensitivity limits of the instrument (assuming that one restricts operation to within the linear response). The remarkably low LVR limit for XL specimens must reflect the unique stress state of torsion in the cross-sectional plane where microfibrillar and cellular twist predominate. In contrast the two other grain orientations primarily promote a lengthwise (end-over-end) cellular rotation with some degree of lengthwise displacement between adjacent microfibrils. Recalling that the nonlinear response indicates a significant disruption in polymer packing, one might speculate that the low XL LVR limit reflects some unique behavior of the middle lamella. However the anatomical and molecular complexities of xylem tissue might preclude such a simple conclusion (Chowdhury *et al.*, 2010). For instance it was previously demonstrated that among the three grain

orientations studied, torsion in the cross-sectional plane provides the greatest storage modulus and therefore the greatest cellulose fibrillar stress state (Chowdhury *et al.*, 2010); that observation is again demonstrated below. Since the XL orientation induces the greatest fibrillar stress, perhaps extreme shear forces are localized at fibrillar surfaces thereby promoting lignin and/or hemicellulose chain dislocations at very low strains. Until rigorous modeling is applied, the anatomical and molecular complexity of xylem perhaps renders this discussion as pedantic speculation.

With increasing temperature, RT always showed an increase in LVR strain limits whereas this was not always true for TR and XL specimens. The plasticizers are all polar solvents with molar volumes less than 100 cm^3/mol. They can be classified either as protic (ethylene glycol and glycerol) or as aprotic tertiary amides (DMF and NMP). Later it will be shown that the plasticizing capacity was a function of this classification, but the solvent class had no discernible impact on the LVR limit. Generally speaking, plasticizer effects were not noticeable in the glassy response, but they became more noticeable with increasing temperatures, particularly in the rubbery response where different solvents could be expected to stimulate varied degrees of polymer motion (Figure 3-1). With regard to temperature effects, the LVR response was highly variable, but in many cases the rubbery LVR limit was significantly greater than that for the lower temperature responses.

Paired-t-tests were performed to determine the significance of the thermal conditioning imposed between heating and cooling (Table 3-1). Though in most cases the numerical value of the LVR strain limit was increased by thermal conditioning, statistical significance was observed only a few times. Notice that the significant

changes mostly occurred with glycerol, corresponding to the highest temperature exposure (170 °C), and suggesting that an irreversible change occurred (thermal degradation and/or solvolysis). On the other hand, the relatively mild 80 °C conditioning in DMF caused one significant LVR increase. At only 80 °C it seems unlikely that DMF would cause thermal degradation; perhaps this alteration reflects changes in polymer association that are driven by extreme swelling. Consequently, the combined effects of thermal degradation/solvolysis and extreme swelling must be considered. Nevertheless the relative thermal stability is remarkable. For instance a 40 minute conditioning at 120°C in ethylene glycol and at 130°C in NMP appears not terribly damaging. In summation the wood LVR response appears to be extremely complex and not amenable to simple generalization. In other words these results demonstrate that DMA stress/strain settings require careful and constant attention if operation within the LVR is critical.

The primary transitions in dry wood take place at or beyond 180 °C (Back and Salmén, 1982), and these are accompanied by thermal degradation. Plasticizers reduce the transition temperature to non-damaging or less damaging temperatures. Figure 3-2 compares 1st and 2nd heating scans of yellow-poplar RT specimens in different solvents. The 1st and 2nd heats were separated by a 40 min thermal conditioning at the maximum temperature (and also isothermal frequency sweeps for time/temperature superposition experiments that are not discussed here). Lignin transition temperatures (temperature at tan δ maximum, Tg) are tabulated in Table 3-2 along with the volumetric-swelling in each solvent before and after thermal conditioning at a temperature beyond the respective Tgs.

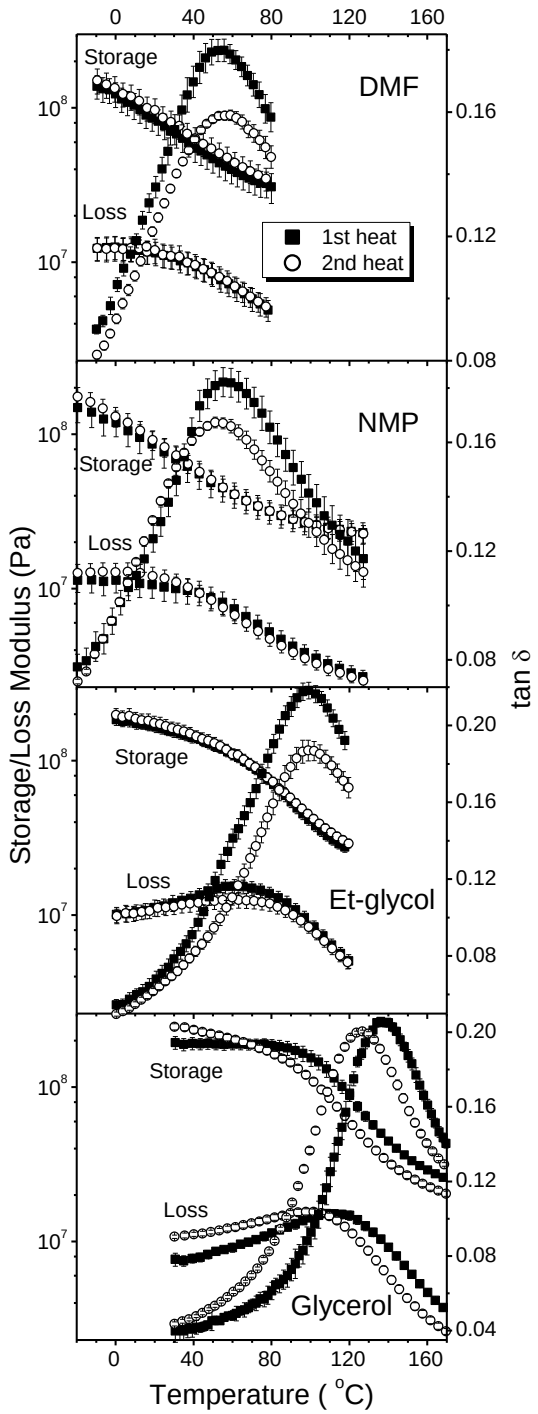

Figure 3-2. Average 1st and 2nd heating scans (3°C/min, 5 Hz) for yellow-poplar RT specimens in different plasticizers. A 40 min thermal conditioning at the maximum temperature separated the 1st and 2nd heats. Note the variable tan δ scales for different solvents; modulus scales are uniform. Error bars represent ±1 standard deviation (n=3).

Table 3-2. Average volumetric swelling and Tg (grain: RT) of solvent-plasticized yellow-poplar. Pre- and post-heat swelling and also 1st and 2nd heat Tg measurements were separated by a 40 min heating at the swelling and DMA maximum temperatures indicated. Standard deviations in parentheses (n = 3).

Solvent	Volumetric swelling,%			Average Tg, °C (5 Hz)		Max. Temp.(˚C)	
	Before heat	After heat	Increase	1st heat	2nd heat	Swelling	DMA
DMF	26 (0.2)	27 (0.7)	1	53 (2.4)	56 (2.2)	60	80
NMP	25 (0.4)	26 (0.4)	1	56 (0.2)	52 (0.5)	75	130
Et-glycol	21 (0.8)	25 (0.4)	4	98 (0.9)	100 (0.9)	100	120
Glycerol	0.7 (1)	23 (2)	22	136 (1.2)	126 (2)	130	170

The 1st heat Tgs displayed an inverse linear relationship with volumetric swelling measured before heating; but the correlation coefficient (r^2) was only 0.80. The tertiary amides DMF and NMP caused the greatest volumetric swelling which resulted in the lowest 1st heat Tgs. Likewise, glycerol was a poor swelling agent and the associated 1st heat Tg was the highest of those measured. The changes in swelling and in Tg caused by a 40 min thermal treatment are summarized in Table 3-2. Most changes in swelling occurred as minor incremental increases of 1 – 4 units. The notable exception was with glycerol where heating caused a dramatic swelling increase (22 units). When they were significant, the thermally induced changes in Tg (ΔTg) appeared as reductions (4˚C in NMP and 10˚C in glycerol). Correlations between swelling changes and ΔTg must be

considered carefully because the swelling specimens were heated at lower temperatures (within the glass transition) while DMA specimens were heated at higher temperatures sometimes well above the Tg. Note that there was a direct linear relationship (r^2=0.82) between the swelling temperature and the resulting incremental swelling increase. This might suggest that 40 min heating at temperatures near and above 100˚C promotes irreversible change. This is proven in the case of glycerol, below. It was not investigated in NMP where the swelling temperature was low but the maximum DMA temperature was high. The ΔTg observed in NMP might be attributed to thermal degradation; but degradation is expected to result in a reduced rubbery modulus and the 1st and 2nd heat rubbery moduli in NMP are identical. With respect to ethylene glycol, heating significantly increased swelling, but the rubbery modulus was essentially unchanged, and ΔTg was insignificant. Previous work (Chowdhury *et al.*, 2010) demonstrated that yellow-poplar wood exhibits surprisingly little change when heated in ethylene glycol (120˚C, 40 min). Consequently many changes noted in Table 3-2 are not clearly attributable to thermal degradation and solvolysis; reversible effects caused by swelling might also contribute to the observations shown here. Figure 3-2 reveals other details. For instance the 1st heat in ethylene glycol presents a minor tan δ shoulder (~50˚C) that is related to drying history and that was proven to be reversible (Chowdhury *et al.*, 2010). This 1st heat feature is absent in the other solvents. Finally, note that the Tgs in ethylene glycol deviate from a prior report (Chowdhury *et al.*, 2010); here the Tg's in ethylene glycol are 8 to 10 °C higher because of the higher compressive clamping force (normal force in experimental section). Other effects of the

compressive force are discussed in (Chowdhury *et al.*, 2010), and generally this normal force should be the minimum required to prevent plate slippage.

As alluded to above, changes between 1st and 2nd heat wood DMA scans are not easily attributable to degradation and solvolysis, and special efforts are required to prove irreversibility (Chowdhury *et al.*, 2010). Here irreversibility was proven in the case of glycerol where a single specimen was subjected to two rounds of sequential heating and cooling; between rounds the specimen was water extracted, thoroughly dried, and then resaturated in glycerol. Figure 3-3 compares the 1st heats and 1st cools from rounds 1 and 2.

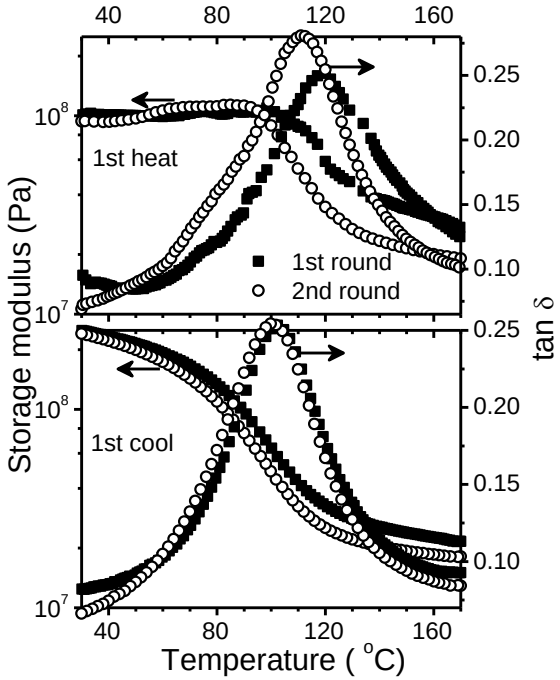

Figure 3-3. Thermal reversibility analysis: (Top) Comparison of 1st heats from two rounds of heat-cools in glycerol (Bottom) Comparison of the associated 1st cools. Between rounds, the yellow-poplar TR specimen was water extracted, dried and resaturated in glycerol; within rounds heating and cooling was intervened by a 40 min equilibration at 170 °C.

Comparison of the respective 1st heats proves the occurrence of substantial and irreversible change in round 1, probably due to solvolysis. For instance the 1st heat Tg's differ by 10°C, and the rubbery moduli differ by about 20%, respectively indicating an increase in chain flexibility and a reduction in the effective crosslink density. Comparison of the respective 1st cools reveals that changes caused by the second round were less significant; the Tgs differ by about 2˚C and the rubbery moduli differ by about 4%. The 1st cool glassy moduli are not affected by thermal treatment. Therefore it can be speculated that the irreversible changes cited here impact rubbery motions as modulated by entanglements and effective crosslinking, but the highly localized glassy motions were not significantly affected by the thermal treatments.

Figure 3-4 shows the effects of different grain orientation on the storage modulus, loss modulus and tan δ.

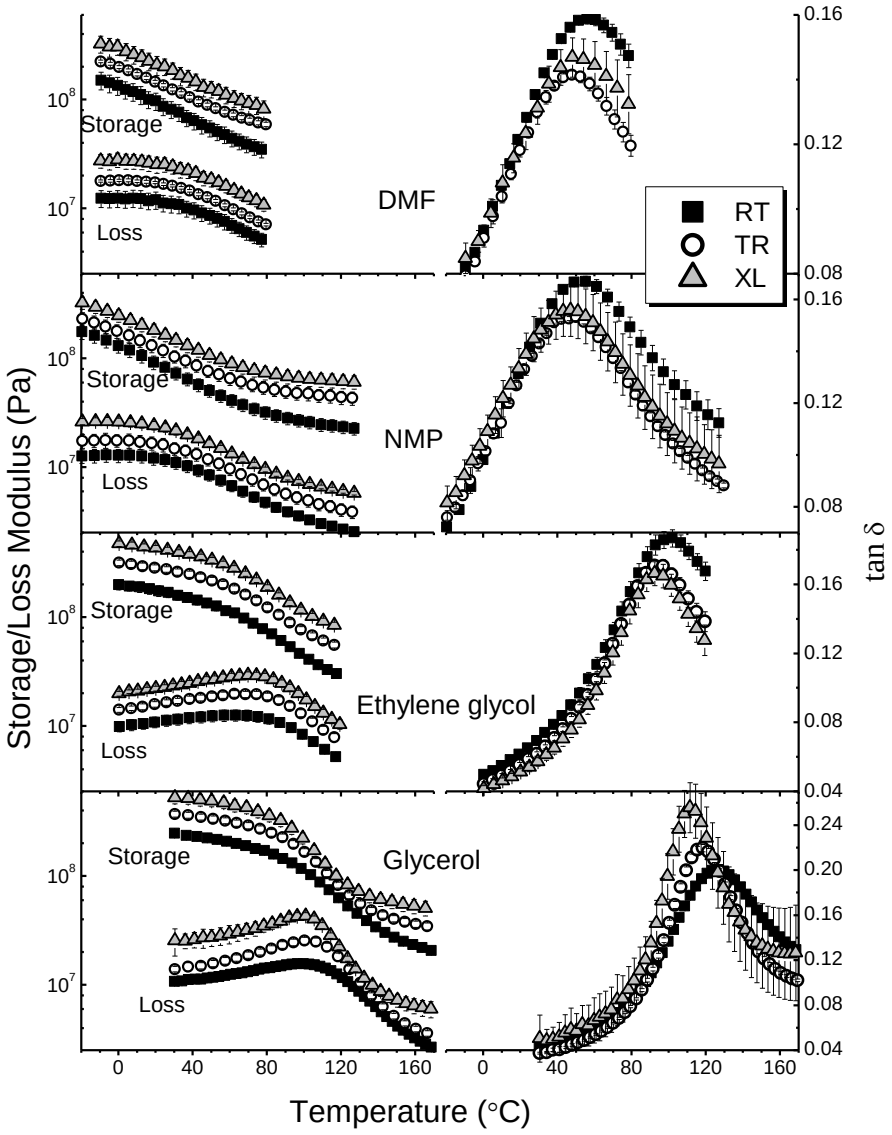

Figure 3-4. Average 2nd heat storage, loss and tan δ curves for yellow-poplar in different plasticizers. Thermal profiles of three different grain orientations are demonstrated. Error bars represents ±1 standard deviations (n=3). Note that tan δ axes vary; modulus axes are uniform.

Specimens with XL orientation showed the highest storage and loss moduli across the temperature ranges for all solvents, followed by TR and RT specimens,

which is in agreement with the findings of Höglund et al.(1976) using water as the plasticizer.

Table 3-3 Average 2nd heat lignin Tg for yellow-poplar of different grain direction in different plasticizing solvents as indicated. Standard deviations are in the parenthesis.

Solvent→ ↓Grain	DMF	NMP	Ethylene glycol	Glycerol
RT	56 °C (4)	52 °C (0.6)	100 °C (0.9)	126 °C (2)
TR	46.5 °C (2)	48 °C (1.8)	94.4 °C (1)	118 °C (0.3)
XL	52 °C (2)	46 °C (1.8)	93 °C (0.8)	112 °C (0.8)

Using 2nd heat data, Figure 3-4 and Table 3-3 demonstrate that the DMA grain dependency varied by solvent. Grain dependency should be considered in two ways, by the shape of the tan δ curve (temperature of tan δ max. or Tg, and tan δ breadth/intensity) and also in the absolute values of the storage and loss moduli (Figure 3-4). First regarding the shape of the tan δ curve, the weakest swelling agent, glycerol, caused the greatest grain dependency where each orientation was distinct with respect to Tg, and tan δ breadth/intensity. In all other solvents the XL and TR responses were generally similar while RT curves exhibited distinctly greater Tgs and tan δ breadth/intensities. This similarity of XL and TR tan δ responses (ethylene glycol, DMF, NMP) was surprising since the torsional stress state in XL specimens is so distinct from that envisioned for TR and RT specimens (For instance recall the prior discussion of LVR strain limits above). Regarding the absolute values of storage and loss moduli, all

solvents exhibited a very similar grain dependency; regardless of solvent all moduli appeared in order of decreasing magnitude XL, TR, and RT. The literature reports on the grain dependency of wood Tgs are highly variable; negligible to significant grain effects are reported. A previous report (Chowdhury *et al.*, 2010) showed minor grain dependency of 1st-heat and 1st-cool Tgs in ethylene glycol. In contrast to that report, Figure 3-4 and Table 3-3 reveal Tgs with a greater grain dependency and this is likely explained by the considerably higher normal force applied in the present study (40 N in the present study vs. 15 N in Chowdhury et al. 2010). This reemphasizes the impact of the compressive clamping force discussed previously (Chowdhury *et al.*, 2010), and that compressive-torsion is not simply comparable to other stress modes.

3.5. Summary

Parallel plate compressive-torsion DMA was used to analyze the effects of various organic solvents on the dynamic viscoelasticity of yellow-poplar. Detailed LVR measurement revealed significant and statistically interactive dependency on grain direction, temperature and plasticizers.

As tertiary amides, DMF and NMP swelled wood to a similar degree, and provided very similar DMA scans. However, less toxic and higher boiling point solvent NMP provides for a more complete relaxation measurement; and while the relaxation in the two appear similar a subsequent publication will demonstrate that lignocellulose motions in NMP and DMF are very different. Furthermore, the DMA responses in two protic alcohols, ethylene glycol and glycerol are perhaps surprisingly different. Although both are small and polar, they demonstrated clear differences in swelling and

plasticization capacity. For instance, ethylene glycol induced about 20% swelling at room temperature; very little incremental swelling took place upon heating beyond the Tg. Conversely, glycerol swelled wood less than 1% at room temperature; when heated beyond Tg, extreme irreversible swelling took place (22% incremental swelling). This effect was reflected in the 10 °C drop in wood-Tg, in subsequent heats and cools. Therefore, although the respective temperature ranges are not perfectly comparable, glycerol demonstrates a greater solvolytic capacity than ethylene glycol. Furthermore, thermal treatment in glycerol significantly reduced the effective crosslink density, which was evident from reduction in the rubbery plateau modulus; however, unchanged the glassy modulus indicated that the short-range localized motions were not significantly altered.

Grain orientation impacted wood viscoelasticity; however this effect was most prominent in glycerol, the weakest plasticizer, where each grain orientation differed with respect to Tg and storage modulus. In more powerful plasticizers (DMF, NMP and ethylene glycol) varied grain dependency was observed. This suggests different solvents mobilized lignocellulose in different fashions. Altogether, this work demonstrates the need for the expansion of lignocellulose rheology to a larger array of solvents to gain new insights in the structure and processing of biomass.

3.6. References

Back, E. L. and L. Salmén, 1982. Glass transitions of wood components hold implications for molding and pulping processes, *Tappi*, 65(7), 107-110.

Becker, H. and D. Noack, 1968. Studies on dynamic torsional viscoelasticity of wood, *Wood Science and Technology*, 2213-230.

Chowdhury, S., J. Fabiyi and C. E. Frazier, 2010. Advancing the dynamic mechanical analysis of biomass: comparison of tensile-torsion and compressive-torsion wood DMA, *Holzforschung*, 64(6), 747-756.

Furuta, Y., M. Makinaga, H. Yano and H. Kajita, 1997. Thermal-softening properties of water-swollen wood .2. Anisotropic characteristics of thermal-softening properties, *Mokuzai Gakkaishi*, 43(1), 16-23.

Green, D. W., J. E. Winandy and D. E. Kretschmann. 1999: Mechanical properties of wood. *Wood handbook, wood as an engineering material.*, Madison, WI, USA: Forest Products Society, 1-45.

Havimo, M., 2009. A literature-based study on the loss tangent of wood in connection with mechanical pulping, *Wood Science and Technology*, 43(7-8), 627-642.

Höglund, H., U. Sohlin and G. Tistad, 1976. Physical-Properties of Wood in Relation to Chip Refining, *Tappi*, 59(6), 144-147.

Jiang, J. L. and J. X. Lu, 2009b. Impact of temperature on the linear viscoelastic region of wood, *Canadian Journal of Forest Research-Revue Canadienne De Recherche Forestiere*, 39(11), 2092-2099.

Kelley, S. S., T. G. Rials and W. G. Glasser, 1987. Relaxation Behavior of the Amorphous Components of Wood, *Journal of Materials Science*, 22(2), 617-624.

Laborie, M.-P. G., L. Salmén and C. E. Frazier, 2004. Cooperativity analysis of the in situ lignin glass transition, *Holzforschung*, 58(2), 129-133.

Menard, K. P. 1999: Dynamic mechanical analysis a practical introduction. Boca Raton, Fla.: CRC Press, 208 p.

Norimoto, M. and T. Yamada, 1666. Dynamic torsional viscoelasticity of wood, *Wood Res*, 3832-39.

Obataya, E., Y. Furuta and J. Gril, 2003. Dynamic viscoelastic properties of wood acetylated with acetic anhydride solution of glucose pentaacetate, *Journal of Wood Science*, 49(2), 152-157.

Olsson, A.-M. and L. Salmén, 1997. The effect of lignin composition on the viscoelastic properties of wood, *Nord. Pulp Pap. Res. J.*, 12(3), 140-144.

Placet, V., J. Passard and P. Perre, 2007. Viscoelastic properties of green wood across the grain measured by harmonic tests in the range 0-95 degrees C: Hardwood vs. softwood and normal wood vs. reaction wood, *Holzforschung*, 61(5), 548-557.

Placet, V., J. Passard and P. Perre, 2008. Viscoelastic properties of wood across the grain measured under water-saturated conditions up to 135 degrees C: evidence of thermal degradation, *Journal of Materials Science*, 43(9), 3210-3217.

Rubinstein, M. and R. H. Colby, 2003: Polymer physics. Oxford University Press,Oxford ; New York

Sadoh, T., 1972. Studies on the Plasticization of Wood. III. Temperature Dependence of the Rheological Properties of Wood Plasticized with Tetraethylene Pentamine *Mokuzai Gakkaishi*, 18(11), 543-548.

Sadoh, T., 1981. Viscoelastic Properties of Wood in Swelling Systems, *Wood Science and Technology*, 15(1), 57-66.

Salmén, L., 1984. Viscoelastic properties of in situ lignin under water-saturated conditions, *Journal of Materials Science*, 19(9), 3090-3096.

Sun, N., S. Das and C. E. Frazier, 2007. Dynamic mechanical analysis of dry wood: Linear viscoelastic response region and effects of minor moisture changes, *Holzforschung*, 61(1), 28-33.

Chapter 4 Time/temperature equivalence and fragility of organic solvent plasticized wood

Sudip Chowdhury and Charles E. Frazier
Macromolecular Science & Engineering, Wood Science & Forest Products
Virginia Tech, Blacksburg VA 24061, U.S.A.

4.1. Abstract

The rheology of wood in four different organic liquids was investigated through time/temperature superposition (TTS) using parallel plate compressive-torsion DMA. While all storage modulus data shifted smoothly, the thermorheological complexity of plasticized wood was detected in the form of shift failures in the loss component master curves. The severity of the shift failures varied and was solvent and grain direction dependent. It is argued that the classic criteria for TTS validity are somewhat arbitrary, and that efforts to judge TTS validity in plasticized lignocellulose are perhaps misplaced. Even when severe shift failures occur in the loss modulus, the storage modulus shift factors clearly reflect a broad range of lignocellulose relaxation behavior. In other words plasticized lignocellulose fails to satisfy TTS validity criteria, but the TTS analysis is nevertheless insightful and potentially useful. This approach should be further developed to facilitate biomass conversion technologies. It was found the Vogel-Fulcher-Tamman-Hess equation was effective for determining the Tg at relaxation time = 100s (Tg_0) in the four different solvents. The WLF model was applied to the

temperature range of Tg_0 + 40 to 120 K. However it was argued that the WLF model is not well suited to plasticized lignocellulose because the breadth of the relaxation window can vary so dramatically in different solvents. Instead the fragility analysis of cooperative segmental motions emphasizes a narrower temperature window that seems better suited for plasticized lignocellulose. This treatment should offer practical utility in developing useful correlations for biomass processing and for probing the effects of chemical, thermomechanical, or genetic manipulations. Fragility analysis demonstrated that lignocellulose relaxations were distinctly different in all four solvents, ethylene glycol, glycerol, N, N-dimethylformamide, and N-methylpyrrolidone; and fragility was greater for the protic alcohols which are less powerful wood swelling agents.

4.2. Introduction

Lignocellulose rheology in the form of dynamic mechanical analysis (DMA) provides valuable insight on structure, supramolecular order, and changes thereof resulting from biomass pretreatment and fractionation. The most useful form of lignocellulose DMA requires specimen plasticization so that segmental motions are stimulated at lower, non-damaging or less damaging temperatures. Regarding wood DMA, most studies have employed water plasticization because of the prevalence of water-based processing technologies. However, the global progression towards biorefineries and renewable fuels from biomass potentially also includes the application of organic media for fractionation, as with ionic liquids (Maki-Arvela *et al.*, 2010) and organosolv pulping (Rodriguez and Jimenez, 2008; Zhu *et al.*, 2010). Relatively little effort has been devoted to the detailed study of wood viscoelasticity in organic media.

Wood viscoelasticity is affected by the organization of its components, cellulose, hemicelluloses, lignin, and water (Olsson and Salmén, 1997); and wood-polymer relaxations are strongly coupled among neighboring chains as described by (Ngai and Plazek, 1995). A common means for evaluating chain coupling during the glass/rubber transition is through time/temperature superposition (TTS) where the master curve is generated by a series of shift factors that reflect the temperature dependence of relaxation. For many synthetic, amorphous polymers this temperature dependence is highly nonlinear, but much less so for plasticized lignocellulose. Ferry and coworkers established TTS in the early 1950s (Ferry, 1950; Ferry *et al.*, 1953), and thereafter the widely applied Williams Landel Ferry (WLF) model was introduced (Williams *et al.*, 1955). The applicability of TTS on wood was first demonstrated by Salmén (1984) using water saturated *Picea abies*; smooth storage modulus master curves were demonstrated and the resulting shift factors obeyed the WLF model within a limited temperature zone, limited probably by the low degree of nonlinear behavior. Multiple wood-TTS studies followed in time (static) and frequency (dynamic) domains to study interactions within the cell wall (Samarasinghe *et al.*, 1994; Lenth and Kamke, 2001; Laborie *et al.*, 2004; Placet *et al.*, 2007; Sun and Frazier, 2007; Dlouha *et al.*, 2009). Although most of the previous wood-TTS studies explicitly or implicitly claimed TTS validity, justifiable concern exists against such claims because wood must be considered as thermorheologically complex (Nakano, 1995). For instance the WLF model assumes a linear temperature dependence of free volume which does not occur in a thermorheologically complex material (Ferry, 1980; Ngai and Plazek, 1995).

Consequently some caution must be exercised when applying both TTS and the WLF models to wood.

Of course other treatments may be applied to TTS data such as the cooperativity model described by Ngai and Plazek (1991; 1995). As the glass/rubber transition zone is approached from the rubbery region polymeric motions involve increasing degrees of intermolecular coupling between non-bonded polymeric segments and increasing sizes of cooperatively rearranging units; at a characteristic temperature (so called glass transition temperature, Tg) the coupling reaches a high point where segmental motions stop and linear Arrhenius behavior becomes evident. (Ngai *et al.*, 1991; Boehmer *et al.*, 1993; Laborie, 2002b). Laborie et al. (2004) successfully employed this cooperativity model to probe the in-situ lignin glass/rubber transition; this method was used to quantify changes in cooperativity due to physical and chemical modifications (Laborie *et al.*, 2004; Laborie *et al.*, 2006). Angell proposed the concept of dynamic fragility to quantify the non-Arrhenius response often associated with the glass/rubber transition. (Angell, 1991). In this so called “fragile-strong” scheme, a fragile polymer undergoes extreme configurational change across the transition; conversely, a strong polymer hardly deviates from linear Arrhenius behavior. Effects of chemical and morphological changes on the relaxation and cooperativity are extensively studied using this concept (Ngai and Roland, 1993a, b; Saiter *et al.*, 2010), and much potential remains for such treatments of lignocellulose.

This work describes recent developments in wood DMA with specimens immersed in organic plasticizers and using parallel-plate geometry in compressive-torsion. This stress mode has certain limitations and advantages; one advantage is that

compressive clamping allows the analysis of specimens that lack mechanical integrity, as in fibrous filter cakes for example (Chowdhury *et al.*, 2010). Time/temperature superposition and dynamic fragility were studied in aprotic tertiary amides and protic alcohols to demonstrate how novel insights and strategies could be realized to help optimize biomass utilization.

4.3. Experimental

4.3.1. Materials

A single piece of yellow-poplar (*Liriodendron tulipifera*) sapwood lumber (80×80×450 mm) was used to make specimens for volumetric swelling measurements (Radial × Tangential × Longitudinal: 25×25×5 mm) and for DMA. In the latter case, cylindrical discs (8 mm dia., 3 mm thick) were machined using a “plug-cutter.” (discs were machined in the dry state; during solvent-submersion differential swelling slightly distorts the cylinder shape; the minor error in measured moduli was ignored). Specimens averaged 2 growth rings per centimeter and ring positioning within specimens was random. Cylindrical specimens were tested in parallel-plate compressive-torsion using a TA Instruments AR 2000 rheometer such that the cylinder axis (thickness direction) was parallel to the torsional axis and the cylinder ends were in contact with the parallel-plates; torsional slippage was prevented with a compressive clamping force exerted by the parallel-plates. Three different grain orientations were tested, denoted as RT, TR and XL; the first letter indicates the wood surfaces in contact with the parallel-plates (R-radial, T-tangential and X-cross-sectional) and the second indicates the grain direction parallel to the torsional axis (T-tangential, R-radial and L-

longitudinal). Four different plasticizing solvents were used: N,N-dimethylformamide (DMF, >99.8%), N-methyl-2-pyrrolidone (NMP, 99.5%), ethylene glycol (99.8%) and glycerol (99.8%).

4.3.2. Methods

All specimens were vacuum-dried (0.04-0.1 mm Hg, 24 h, ambient temperature) and stored in a desiccator (anhydrous P_2O_5 and N_2) for at least 48 h prior to analysis. Thereafter specimens were saturated with plasticizer using a vacuum-pressure treatment (5 mm Hg for 1 h, followed by atmospheric pressure for at least 24 h). Solvent submersion was conducted such that the bottom plate was surrounded by a stainless steel cup that maintained specimen immersion during analysis. All tests were performed under anhydrous N_2 gas; liquid N_2 was used to control temperature. Compressive clamping was achieved with a 40 N static normal force, representing approximately 4.2% and 42% of the wet compression strength respectively parallel and perpendicular to grain (Green *et al.*, 1999). Safety note: when organic solvents are used as specimen plasticizers caution is required because the solvent bath is enclosed within an oven having exposed heating elements; consequently, anhydrous N_2 gas is directed through the heating chamber to prevent ignition; and the oven must never be opened to the atmosphere while the oven temperature is near the solvent flash point. Attention to these details results in safe and reliable analysis.

All experiments were carried out within the linear viscoelastic response (LVR) limit of solvent plasticized wood. Specimens were subjected to a sequential heat/cool/heat treatment as follows: 1) heat to maximum temperature (3°C/min, 5 Hz);

hold 40 min, 2) isothermal frequency sweep (1-100 Hz, 25 - 130 KPa depending upon the LVR limit), 3) rapid cool (~ 6-13°C/min) to next lowest temperature (10 °C step), equilibrate 10 min, 4) Repeat steps 2 & 3 over experimental temperature range, 5) heat to maximum temperature, (3 °C/min, 5 Hz). All tests were conducted in stress-control with stress settings very near but not greater than the LVR limits. Temperature ranges were chosen to avoid plasticizer freezing and to minimize excessive evaporation (DMF: -10 to 80°C, NMP: -30 to 130°C, ethylene glycol: 0 to 120°C and glycerol: 30 to 170°C).

4.3.3. Data analysis

The glass transition with 100 s relaxation time was considered as the quasi-static glass transition temperature (Tg_0), calculated as follows (Appendix A shows detailed Tg_0 determination procedure.) (Plazek and Ngai, 1991; Saiter *et al.*, 2010). Isothermal frequency scans (1-100 Hz, 7-10 data points/decade) at different temperatures were used to construct tan δ vs. temperature profiles for each discrete frequency. The resulting tan δ curves had a temperature resolution of 10 °C. A 6th order polynomial was fitted to tan δ curves so as to clearly indentify the Tg (temperature at tan δ max) with 1 °C resolution. For all specimens high frequency responses (generally beyond 40 Hz) did not produce clear tan δ maxima, and were therefore not used for Tg detection. For each frequency (*f*) the relaxation time at Tg (τ_{Tg}) was calculated as, $\tau_{Tg} = 1/2\pi f$. Next, τ_{Tg} vs. Tg was plotted, and was fitted to the Vogel-Fulcher-Tamman-Hess (VFTH) equation (Eq. 4.1) to obtain VFTH parameters ($\tau_0, B\ and\ T_0$) (Vogel, 1921; Fulcher, 1925; Tammann, 1926).

$$\tau = \tau_0 \exp\left(\frac{B}{T - T_0}\right) \qquad \text{Equation 4.1}$$

The 100 s relaxation time glass transition temperature (Tg_0) was then estimated from the rearranged VTFH equation, as in Eq. 4.2.

$$T_{g_0}(\tau = 100s) = T_0 + \frac{B}{\ln(100) - \ln \tau_0} \qquad \text{Equation 4.2}$$

Arrhenius activation energy was calculated from the polynomial fitted thermal scans at different frequencies. Log-frequency vs. corresponding reciprocal Tg was plotted and fitted with a linear function; the slope of the line is equal to $[-Ea/(2.303 \times R)]$; where, Ea is the Arrhenius activation energy for the Tg and R is the universal gas constant. All such Arrhenius plots were highly linear with correlation coefficients (R^2) ≥ 0.99.

Time/temperature-superposition (TTS) master curves were constructed by shifting isothermal frequency scans (1 – 100 Hz) along the log-frequency scale to form a storage modulus (G′) master curve. The temperature of the isothermal step closest to the Tg_0 was chosen as the reference temperature. The amount of shifting along the log-frequency scale was plotted against the corresponding temperatures to form the shift factor plot. The Williams-Landel-Ferry (WLF) model (Eq. 4.3) was fitted to obtain the WLF constants (Williams *et al.*, 1955).

$$\log a_T = \frac{-C_1(T - T_{ref})}{C_2 + (T - T_{ref})} \qquad \text{Equation 4.3}$$

Dynamic fragility (m) was calculated from Angell's plot of log a_T vs. Tg/T using Eq. 4.4.(Plazek and Ngai, 1991; Qin and McKenna, 2006; Zuza *et al.*, 2008).

$$m = \left[\frac{d(\log a_T)}{d(T_g/T)}\right]_{T=T_g} \qquad \text{Equation 4.4}$$

4.4. Results and Discussion

Isothermal frequency scans were shifted to obtain storage modulus master curves, and the resulting shift factors were used to generate the corresponding loss modulus and tan δ master curves (Figure 4-1). No vertical shifting was employed. Note that the master curve data was collected after 40 min thermal equilibration at the respective maximum temperatures. A previous publication showed that varying degrees of degradation/solvolysis resulted from this 40 min heating period; it was minor in DMF and ethylene glycol, moderate in NMP, and significant in glycerol (Chowdhury and Frazier, 2011d). However, it was also shown that no further changes occurred after this 40 min thermal conditioning. Consequently the cooling mode TTS data presented here reflects a stable condition; no further specimen changes were detected after the initial heating. In ethylene glycol and glycerol plasticized specimens, frequencies between 50 – 100 Hz occasionally produced spurious loss values at all temperatures, perhaps due to system/specimen resonance. However, no data were excluded from the master curves (Figure 4-1).

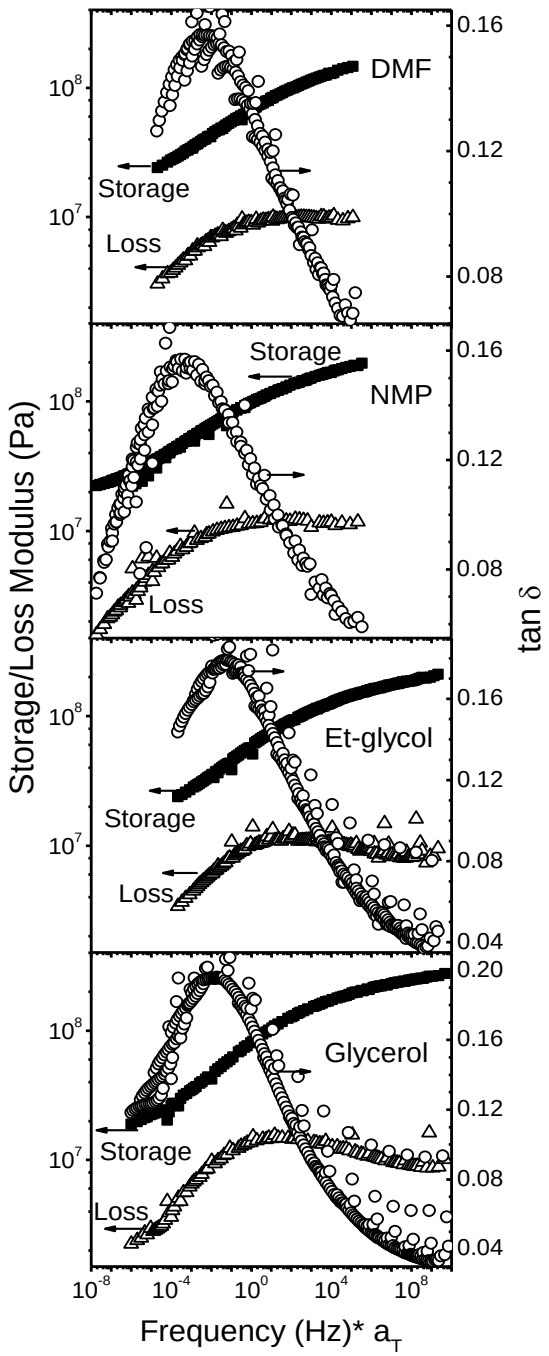

Figure 4-1 Storage modulus, loss modulus and tan δ master curves for yellow-poplar-RT specimens in different plasticizing solvents. Variable tan δ scale; uniform modulus scale.

By definition the time (or frequency) and temperature equivalence of a dynamic process requires that the ratio of relaxation time at a temperature (T) to the relaxation time at the reference temperature (T_r) is constant (a_T). This can only be achieved if all mechanisms occurring in the relaxation zone have the same temperature dependence (Fesko and Tschoegl, 1971; Ferry, 1980; Ngai and Plazek, 1995). Materials obeying this criterion are referred to as thermorheologically simple. Empirically, the criteria for TTS validity are the formation of smooth storage and loss master curves created with the same shift factors, and a continuous evolution of the Log a_T vs. temperature plot (Ferry, 1980). Ferry showed that during relaxation the storage and loss components are not weighted uniformly; at a specific frequency the storage modulus is more influenced by shorter relaxation time processes, whereas the loss components are more influenced by mechanisms with longer relaxation time (Ferry, 1980). Taking this into account, if in any material the temperature dependence of the short and long relaxation time processes differ, in other words if a_T is not the same for short and long relaxation times, a single set of shift factors fails to superpose all dynamic properties (Fesko and Tschoegl, 1971; Ferry, 1980). This defines a thermorheologically complex material.

Being a multiphase polymeric system, wood is predictably thermorheologically complex. However, multiple successful wood-TTS studies have been reported in static (Samarasinghe *et al.*, 1994; Wolcott *et al.*, 1994; Sun and Frazier, 2006; Sun and Frazier, 2007; Dlouha *et al.*, 2009) and dynamic experiments (Salmén, 1984; Kelley *et al.*, 1987; Lenth and Kamke, 2001; Laborie *et al.*, 2004; Placet *et al.*, 2007). Conversely, Nakano (1995) studied the validity of TTS in wood from a theoretical approach. He concluded that the TTS principle was invalid due to multi-component relaxations from

hemicelluloses and lignin. This claim although theoretically sound, requires qualification because of the large body of data showing the experimental success of wood-TTS. The criteria for valid TTS are also somewhat arbitrary and no quantitative definition of TTS invalidation exists. In other words, even thermorheologically complex materials can satisfy validity criteria if a sufficiently narrow relaxation window is defined. Moreover in a multiphase system thermorheological complexity itself speaks to the nature of molecular relaxation, and failure to meet TTS validity criteria is also informative. Therefore a careful application of this tool will provide valuable insights into the relaxations in wood-polymer networks, as will be demonstrated here.

Figure 4-1 shows that the storage modulus master curves for all solvent-plasticized specimens were smooth, consistent with most prior wood-TTS studies. However when using the same shift factors for superposition of the loss modulus, slight shift failures occurred. Note how the loss modulus master curves were actually quite smooth (but less perfect than for the storage modulus). As the ratio of loss to storage, the tan δ master curves magnify how the respective storage and loss shift factors deviate, most clearly in the rubbery regime. Vertical shifting would not improve the smoothness of tan δ master curves. Although a lack of smoothness in the tan δ master curves occurred in all solvent-plasticized specimens, the effect was most prominent in DMF-plasticized wood. This reflects how different solvents stimulate different relaxations and varying degrees of thermorheological complexity (shift failure).

In dynamic wood- TTS studies superposition validity is commonly claimed by producing smooth storage modulus master curves. However to our knowledge none except Salmén (1984) and Placet et al. (2007) have reported the loss components of

dynamic wood-TTS. Salmén (1984) reported that for water saturated *Picea abies* both storage and loss moduli produced smooth master curves. However unlike the storage modulus which shifted properly across the whole temperature range, the loss modulus did not shift properly below the Tg. Placet et al. (2007) studied dynamic TTS of water saturated *Quercus sessiliflora* and *Fagus sylvatica* in bending along the radial and tangential directions. Uniform storage modulus master curves were produced for both species in both grain directions. However, a lack of superposition in the loss modulus data was reported (Placet *et al.*, 2007). Consequently of the published reports on the loss component, both indicate a degree of superposition failure. Likewise the loss and tan δ master curves in Figure 4-1 exhibit varied degrees of shift failure that are solvent dependent and which mostly occur in the transition and rubbery zones (low frequency region).

A similar phenomenon was previously reported and explained for poly(n-alkylmethacrylates) that are highly entangled (effectively crosslinked) (Berge *et al.*, 1959; Saunders *et al.*, 1959; Ferry, 1980). In the low frequency zone (rubbery zone), polymer mechanical properties are predominantly controlled by long range coupling through widely spaced entanglements (also considered as entanglement disruption with changing molecular weight between entanglements). The response depends heavily on the number, distribution and strength of these entanglements, and the associated temperature dependency could vary from that of the more localized segmental relaxation (Berge *et al.*, 1959). Consequently a superposition failure occurs (in the low frequency region of the loss component) if the localized segmental relaxations and the longer range entanglement couplings diverge in temperature dependency.

Since amorphous wood polymers are crosslinked through primary and secondary structures, it is possible that shift failures in the loss component are related to long range couplings among effective crosslinks. Secondary structures that effectively crosslink the amorphous matrix could exhibit long range couplings (disruptions and/or alterations), with a temperature dependence that diverges from the localized segmental relaxation. Conversely, these shift failures could also be caused by the onset of distinct segmental relaxation mechanisms that possess different temperature dependencies. For instance it appears that the bulk of secondary-wall lignin exhibits discreet zones of differing crosslink density (Lawoko *et al.*, 2005; Salmén, 2007; Li *et al.*, 2011a), and such discreet lignin zones might exhibit different relaxation mechanisms. Consequently the relative ability or inability to satisfy classic superposition criteria in different solvents might reflect fine structural details that are not currently understood, as with discreet zones of lignin structure or with effective crosslinks within the amorphous matrix. In spite of the various degrees of superposition failure, the corresponding shift factor plots exhibit relaxation temperature dependencies that are clearly different and that must reflect specific wood/solvent interactions.

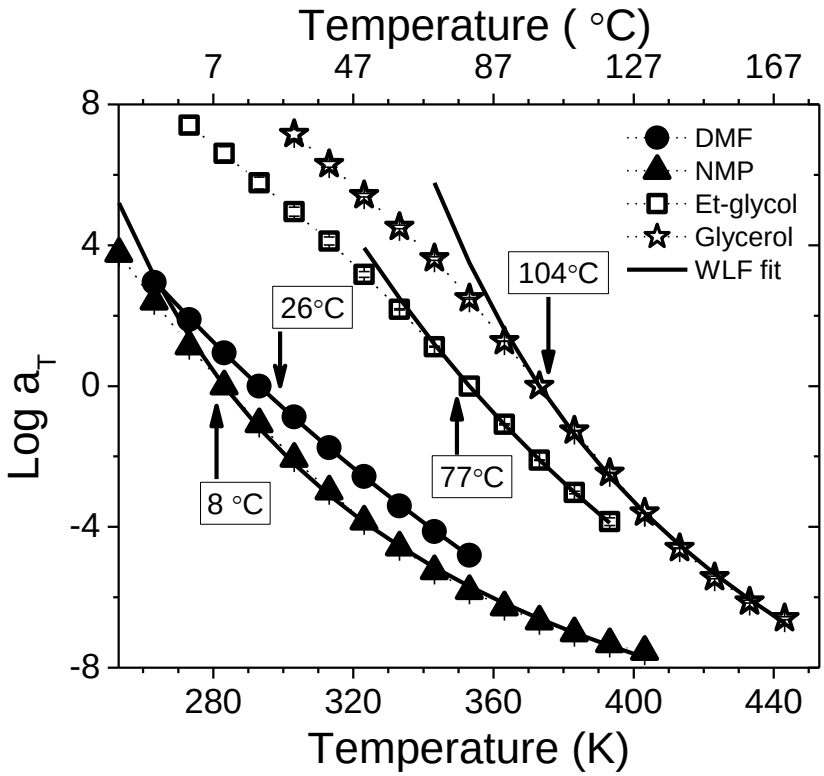

Figure 4-2 Average shift factor vs. temperature plots for yellow-poplar at RT grain orientation, plasticized with different solvents. Error bars indicate ±1 standard deviation (n = 3). WLF fits for the average shift factor plots are also included. Arrows indicate the 100 s Tg_0 in respective solvents.

For example Figure 4-2 shows the shift factor plots generated from storage modulus master curves. Ethylene glycol and glycerol plasticized specimens showed a simple Arrhenius (linear) response at lower temperatures (glassy region), and increasing nonlinearity in the transition region (more so for glycerol). Comparing the two alcohols employed here, Figure 4-1 and Figure 4-2 suggest that the responses in ethylene glycol and glycerol are quite similar but with variations in Tg and that glycerol allows for a broader frequency (temperature) range.

Compared to the alcohols the tertiary amides are much more powerful wood plasticizers; Tgs were 60 - 100˚C lower (Table 4-1) in the amides. Considering only the measured Tgs and the respective master curve shapes, NMP and DMF might appear to be similar plasticizers, but that NMP provides a much broader frequency (temperature) range. However Figure 4-2 demonstrates that the temperature dependency of relaxation is remarkably different in these two amides. In NMP, the Arrhenius region was not evident; the system showed a wide nonlinear response, Figure 4-2. Conversely, in DMF the shift factor plot was highly linear. This difference was also evident from the tan δ master curves, where the thermorheoogical complexity (shift failure) was most prominent in DMF-plasticized wood.

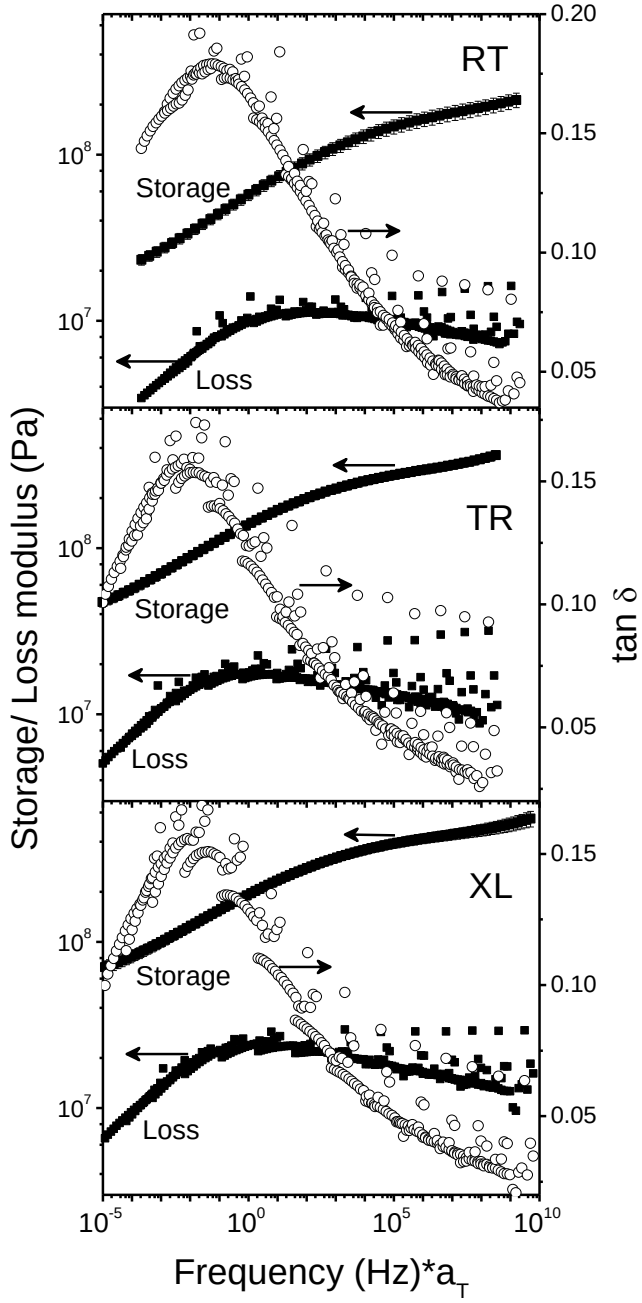

Figure 4-3 Average (n = 3) storage modulus and representative loss modulus and tan δ master curves for ethylene glycol plasticized wood at different grain directions, as indicated. Error bars indicate ±1 standard deviations. Note: uniform moduli scale; variable tan δ scale.

Grain effects on superposition were studied and they were essentially the same in all solvents. The storage modulus always shifted smoothly, independent from the grain. Whereas the quality of superposition in the loss component was strongly affected by grain orientation, where the RT specimens shifted most effectively and TR and XL specimens shifted poorly; but XL shifting was always the worst (Figure 4-3). Regarding the absolute storage modulus values, XL specimens showed the highest stiffness followed by TR, and RT was most compliant, consistent with prior reports (Höglund *et al.*, 1976; Chowdhury *et al.*, 2010). It is perhaps reasonable to expect the greatest shift failure for XL specimens where torsion occurs in the cross-sectional plane, and with fibrillar twist that provides the greatest stiffness and therefore the greatest shear forces near fibril surfaces. On the other hand it seems unlikely that one could predict that RT and TR specimens would exhibit differences in shift quality, and that the RT grain orientation would always produce smoother master curves regardless of the solvent.

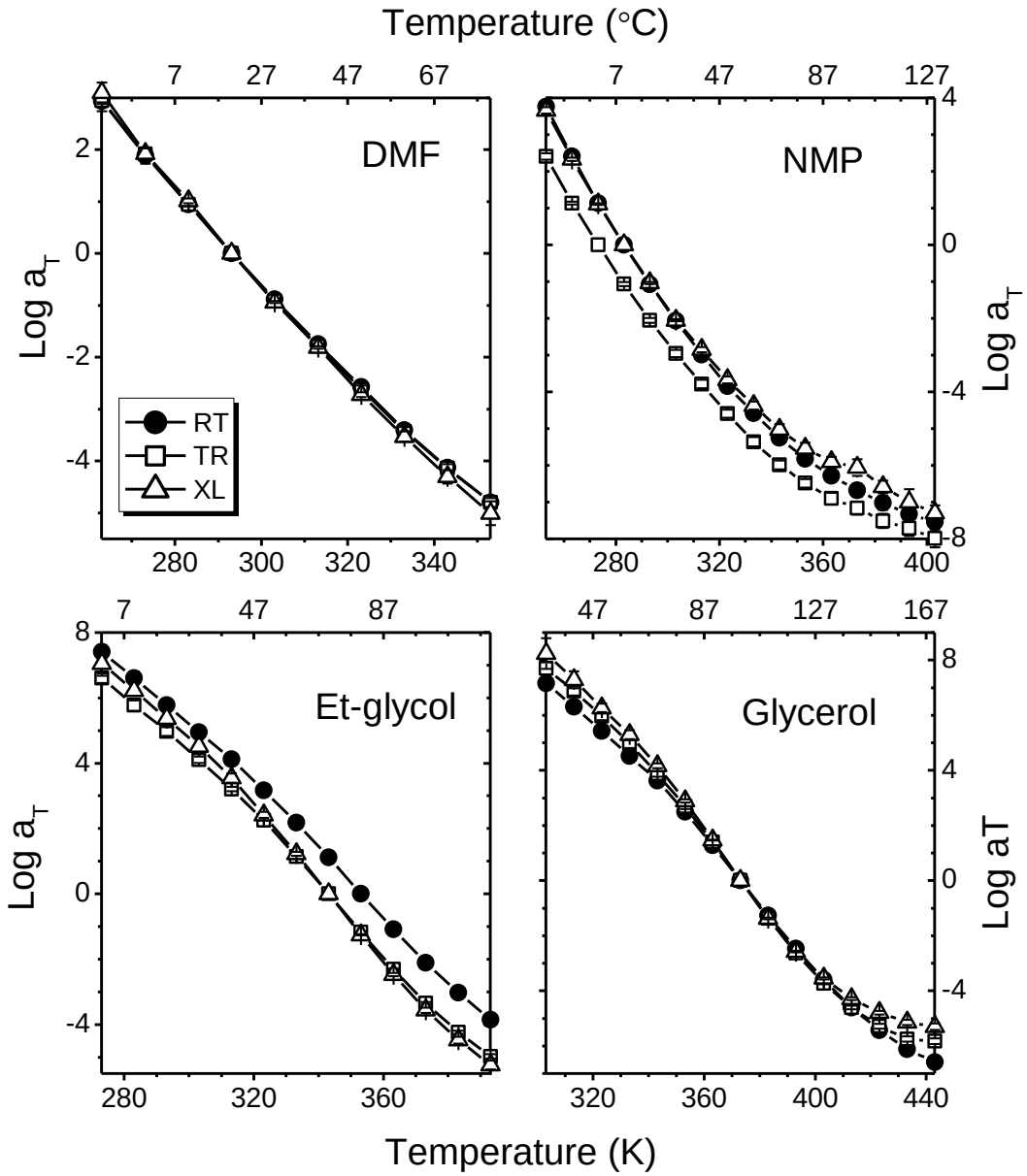

Figure 4-4 Effects of grain direction on the average (n=3) shift factor of solvent plasticized yellow-poplar. Error bars represents ± standard deviation. Note: variable temperature and shift factor scales.

While grain orientation clearly impacted the superposition quality of the loss component, grain effects were much less evident in the corresponding shift factor plots, Figure 4-4. Within solvent groupings the shift factor curves all exhibit quite similar

shapes, and with minor grain dependency in DMF and glycerol and slightly more grain dependency in NMP and ethylene glycol.

Summarizing to this point, the application of TTS to plasticized wood must be conducted with great care. Demonstrated here, and also by others, is that storage modulus master curves are almost always smooth and satisfying. However the corresponding loss components exhibit a broad range of superposition quality that is dependent upon the solvent and the grain orientation. In other words, it is quite clear that plasticized lignocellulose is thermorheologicaly complex, and that many of the classic criteria for TTS validity cannot be met. Nevertheless, the TTS of plasticized lignocellulose should not be labeled as invalid; doing so would preclude the practical application of this methodology. For instance even when significant shift failures occur, the corresponding shift factor plots clearly reflect the temperature dependence of relaxation, and relaxations in the respective solvents are clearly different. Instead of invalidating the TTS of lignocellulose, perhaps superposition failure should be considered more carefully for potential insight into the fractionation of biomass in different liquid media, organic or aqueous. The data presented here clearly demonstrate that lignocellulose relaxations are varied in different solvents, as expected. What remains unknown is if aspects of the TTS response could be correlated to the efficacy of biomass fractionation.

WLF parameters and dynamic fragility of solvent plasticized wood

The Williams-Landel-Ferry (WLF) model (Williams *et al.*, 1955) is commonly used to analyze the non-Arrhenius (glass-transition) region of the shift factor plot. In synthetic

polymers the WLF model is applicable to the Tg ± 50 K region. However, for solvent-plasticized wood the applicable region is reported as being considerably reduced (Salmén, 1984; Laborie *et al.*, 2004; Placet *et al.*, 2007). In this work the WLF model fitted best to the temperature region at and beyond the 100 s glass-transition temperature (Tg_0), a range of about 40 – 120 K, Figure 4-2. WLF parameters (C_1 and C_2) were estimated by least squares fit of the model to the shift factor plots for all solvent plasticized specimens (Table 4-1).

Table 4-1 Average (n=3) dynamic fragility, Tg (5 Hz), Tg_0, Arrhenius activation energy at Tg and WLF parameters for solvent plasticized yellow-poplar wood at different grain orientations. Volumetric swelling after thermal equilibration above Tg in each solvent is indicated. ±1 standard deviations are in parenthesis.

Solvent	Grain	Fragility	5 Hz Tg, °C	Tg_0 °C	Ea (KJ/mol)	C_1	C_2 (K)	Vol. Swelling,(%)
DMF	RT	26.68 (0.56)	56 (4)	26 (4)	181 (6)	37.8 (8)	409.1 (97)	27 (0.7)
	TR	27.19 (0.62)	47 (2)	16 (1)	173 (3)	29.3 (4)	304.7 (52)	
	XL	27.57 (0.84)	52 (2)	17 (4)	167 (7)	39.7 (16)	409.2 (171)	
NMP	RT	32.11 (0.91)	52 (1)	8 (3)	157 (9)	15.3 (0.4)	118.3 (4)	26 (0.4)
	TR	30.82 (1.15)	48 (2)	-6 (6)	123 (10)	15.9 (0.5)	121.8 (2)	
	XL	32.21 (0.82)	46 (2)	7 (4)	158 (12)	14.8 (0.9)	122.8 (10)	
Et-glycol	RT	37.80 (0.34)	100 (1)	77 (3)	345 (28)	26.3 (12)	231.1 (111)	25 (0.4)
	TR	39.54 (0.08)	94 (1)	71 (4)	322 (7)	22.0 (0.8)	168.9 (5)	
	XL	42.96 (1.05)	93 (1)	73 (1)	338 (30)	21.3 (2.0)	151.6 (15)	
Glycerol	RT	47.53 (0.21)	126 (2)	104 (1)	404 (24)	19.2 (0.6)	129.8 (4.9)	23 (2)
	TR	49.73 (1.21)	118 (0.3)	95 (3)	363 (58)	11.9 (0.6)	66.0 (4.6)	
	XL	50.65 (1.28)	112 (1)	91 (2)	367 (64)	9.54 (0.5)	51.9 (4.2)	

The WLF parameters reported here are in general higher than previously reported values (Salmén, 1984; Kelley *et al.*, 1987; Lenth and Kamke, 2001; Laborie *et al.*, 2004), but differences in stress modes and solvo-thermal history complicate direct comparisons. The WLF model is intended for a broad relaxation window and is best

suited for the strongly non-linear temperature dependence seen in synthetic amorphous thermoplastics. Of the shift factor plots in Figure 4-2 and Figure 4-4, only those in NMP resemble the classic WLF behavior of synthetic thermoplastics. In any wood/solvent combination a unique relaxation window is defined by the solvent physical constants (i.e. melting and boiling points) and also by the strength of wood/solvent interaction. Furthermore one rarely if ever observes a complete lignocellulose transition from the glass into the rubbery plateau, Figure 4-1. Consequently, the singular nature of a particular wood/solvent relaxation severely complicates any attempt to draw physical significance from the WLF parameters. Consequently it seems that some alternative to the WLF (free volume) treatment is desirable for solvent plasticized wood.

Since the relaxation window for a particular lignocellulose/solvent pair can vary so widely (as in Figure 4-2), one could argue in favor of an alternative treatment that favors a more narrow window within the glass/rubber transition. The treatment of segmental cooperativity and dynamic fragility is one such approach. Near the Tg, the viscoelastic response is predominantly governed by local segmental motions; with increasing temperature the relaxation is dominated by coordinated molecular motions with larger distances; in the rubbery region the response is dominated by long range cooperative motions with interaction distances larger than the radius of gyration (Ngai and Plazek, 1995). A quantitative comparison of polymer relaxation and cooperativity at the glass-transition region can be achieved by plotting the logarithm of relaxation time (τ) or shift factor (a_T), as a function of the Tg-normalized reciprocal temperature (Tg/T) (Angell, 1991; Ngai and Plazek, 1995). This is widely known as the “fragility plot”. This concept was popularized by Angell to quantify the deviation of relaxation times (τ) from

the thermally activated Arrhenius behavior at the glass transition in inorganic glasses (Angell, 1991). Angell used the term “fragility” to describe the extent of structural changes in a glass when the system is heated across the Tg. Conventionally, in this treatment the Tg is taken as the temperature at which τ becomes an arbitrary long time, 100 s (Ngai and Plazek, 1995). The fragility is obtained from the slope of the fragility plot at Tg.

Ngai and Plazek (1995) suggested that fragility originates from intermolecular cooperativity or coupling within polymeric materials. They used the term “cooperativity plot” interchangeably with “fragility plot”. A large number of studies have been published to successfully correlate polymer segmental motion and cooperativity with various chemical and morphological properties (Ngai and Roland, 1993a, b; Roland and Ngai, 1993; Roland *et al.*, 1993). In a significant study that is quite relevant to wood, Ngai and Roland (1993b) justified that fragility can reveal the cooperativity of the amorphous region in a semi-crystalline polymer, excluding the effects of crystallinity. The confounding effects of crystallinity are removed when temperatures are normalized by the Tg. In this work normalization was achieved using Tg_0 (Tg at τ = 100 s), which was determined using the Vogel-Fulcher-Tamman-Hess equation as described in the experimental. Shift factors (log a_T) were plotted versus Tg_0/T (Figure 4-5). The dynamic fragility is the slope of this plot at $T=Tg_0$, as in equation 4.4.

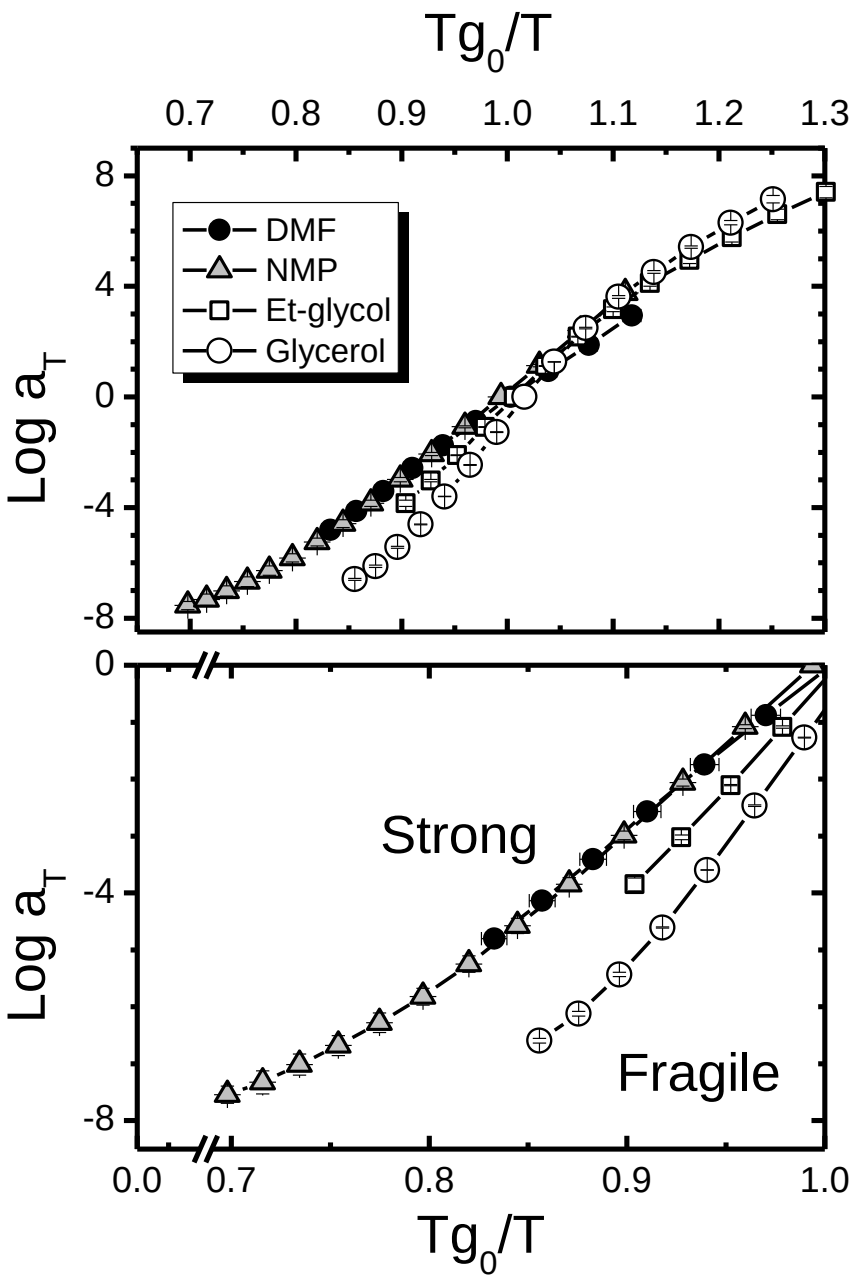

Figure 4-5 Average (n=3) fragility plot, log a_T vs Tg_0/T for solvent plasticized yellow-poplar. Grain direction: RT. Top: Fragility plot for full temperature range. Bottom: fragility plot for temperature range at $T \geq Tg_0$. Error bars represent ±1 standard deviations.

Table 4-1 summarizes the fragility (m) and glass transition Arrhenius activation energy (Ea) for specimens as a function of grain direction and solvent. Specimens in protic alcohols showed higher fragility than specimens in tertiary amides. Glycerol-

plasticized wood showed the highest fragility and DMF-plasticized wood showed the lowest. Fragility bears a proportional relationship with the intermolecular coupling (Plazek and Ngai, 1991; Ngai and Plazek, 1995). Therefore, the intermolecular cooperativity in the wood amorphous regime is highest in glycerol, followed by ethylene glycol, NMP and DMF.

The estimated Tg_0 for ethylene glycol and glycerol were approximately 20 °C lower than Tg (5 Hz). For DMF this difference was between 30 to 35 °C, and about 40 to 54°C in NMP. The Tg, activation energy and the fragility show a direct correlation in synthetic polymers and glasses (Ngai and Roland, 1993a, b; Qin and McKenna, 2006), where increasing molecular flexibility correspond to lower fragility and lower Ea. Indeed, we observed a linear proportionality between Tg_0 and Ea (R^2=0.98) and Tg (5 Hz) vs. Ea (R^2=0.96). However, a weaker linear proportionality existed between fragility and Tg_0 (R^2=0.81). When comparing DMF and NMP, which had similar 5 Hz Tg, the activation energies in NMP were significantly lower than in DMF. However, the fragility of NMP-plasticized specimens was higher than that in DMF.

Each of the plasticizers resulted in significant differences in fragility ($p<0.001$). Figure 4-6 compares the grain and solvent effect on fragility (m) and Arrhenius activation energy (Ea).

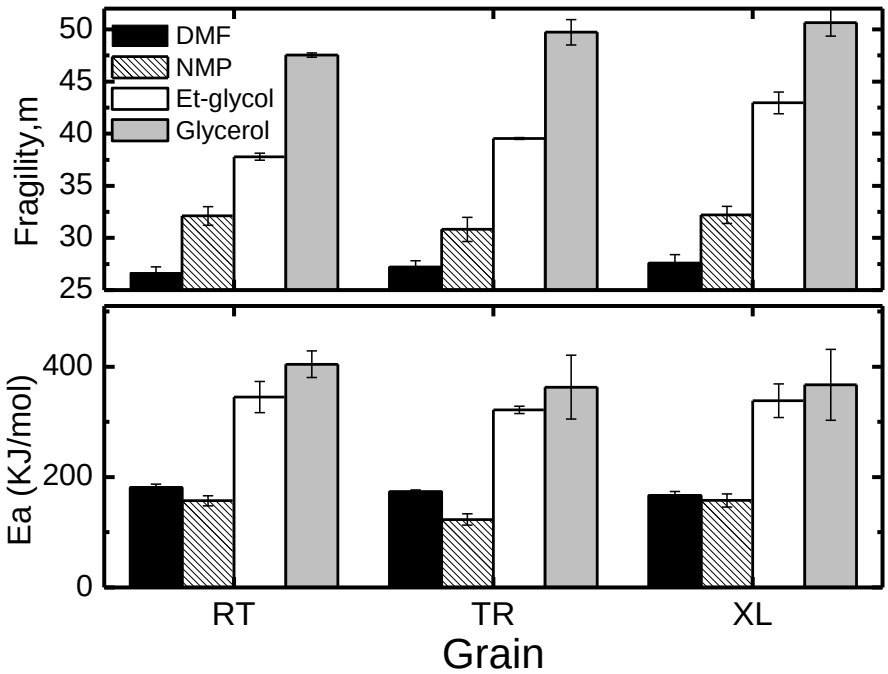

Figure 4-6 Fragility and Arrhenius activation energy for glass transition of solvent plasticized yellow-poplar at different grain directions. Error bars: ±1 standard deviations (n=3).

Grain direction showed varied effects on fragility. In DMF and NMP, the two more powerful plasticizers, grain direction did not have a significant effect. Grain direction effects were significant in glycerol and ethylene glycol, the two less powerful plasticizers. The lack of grain effects on fragilities in DMF and NMP could perhaps be explained by the extreme wood-swelling capacities of these two solvents causing significant alteration in the amorphous phase and the anisotropy of the segmental relaxations was reduced.

4.5. Summary

The rheology of wood in four different organic liquids was investigated through time/temperature superposition (TTS) using parallel plate compressive-torsion DMA.

While all storage modulus data shifted smoothly, the thermorheological complexity of plasticized wood was clearly detected in the form of shift failures in the loss component (loss modulus and tan δ) master curves. The severity of the shift failures varied and was solvent and grain direction dependent. It is argued here that the classic criteria for TTS validity are somewhat arbitrary, and that efforts to judge TTS validity in plasticized lignocellulose are perhaps misplaced. Even when severe shift failures occur in the loss modulus, the storage modulus shift factors clearly reflect a broad range of lignocellulose relaxation behavior. In other words plasticized lignocellulose fails to satisfy TTS validity criteria, but the TTS analysis is nevertheless insightful and potentially useful. This approach should be further developed to facilitate biomass conversion technologies. With further study, perhaps loss modulus shift failures will be useful to understand the complexities of lignocellulose structure and properties. It was found the Vogel-Fulcher-Tamman-Hess equation was effective for determining the Tg at relaxation time = 100s (Tg_0) in the four different solvents. The WLF model was applied to the temperature range of Tg_0 + 40 to 120 K. However it was argued that the WLF model is not well suited to plasticized lignocellulose because the breadth of the relaxation window can vary so dramatically in different solvents. Instead the fragility analysis of cooperative segmental motions emphasizes a narrower temperature window that seems better suited for plasticized lignocellulose. Fragility quantifies the segmental cooperativity at the glass-transition. This treatment should offer practical utility in developing useful correlations for biomass processing and for probing the effects of chemical, thermomechanical, or genetic manipulations. Fragility analysis demonsrated that lignocellulose relaxations were distinctly different in all four solvents, ethylene glycol,

glycerol, N, N-dimethylformamide, and N-methylpyrrolidone; and fragility was greater for the protic alcohols which are less powerful wood swelling agents.

4.6. References

Angell, C. A., 1991. Relaxation in Liquids, Polymers and Plastic Crystals - Strong Fragile Patterns and Problems, *Journal of Non-Crystalline Solids*, 13113-31.

Berge, J. W., P. R. Saunders and J. D. Ferry, 1959. Mechanical properties of poly-n-octyl methacrylate at low frequencies and in creep; entanglements in methacrylate polymers, *Journal of Colloid Science*, 14(2), 135-146.

Boehmer, R., K. L. Ngai, C. A. Angell and D. J. Plazek, 1993. Nonexponential relaxations in strong and fragile glass formers, *Journal of Chemical Physics*, 99(5), 4201-4209.

Chowdhury, S., J. Fabiyi and C. E. Frazier, 2010. Advancing the dynamic mechanical analysis of biomass: comparison of tensile-torsion and compressive-torsion wood DMA, *Holzforschung*, 64(6), 747-756.

Chowdhury, S. and C. E. Frazier, 2011d. Compressive-torsion DMA of wood in organic media *Unpublished work*

Dlouha, J., B. Clair, O. Arnould, P. Horacek and J. Gril, 2009. On the time-temperature equivalency in green wood: Characterisation of viscoelastic properties in longitudinal direction, *Holzforschung*, 63(3), 327-333.

Ferry, J. D., 1950. Mechanical properties of substances of high molecular weight. VI. Dispersion in concentrated polymer solutions and its dependence on temperature and concentration, *Journal of the American Chemical Society*, 72(8), 3746-3752.

Ferry, J. D., 1980: Viscoelastic properties of polymers. Wiley,New York

Ferry, J. D., L. D. Grandine, Jr. and E. R. Fitzgerald, 1953. The relaxation distribution function of polyisobutylene in the transition from rubberlike to glasslike behavior, *Journal of Applied Physics*, 24(7), 911-916.

Fesko, D. G. and N. W. Tschoegl, 1971. Time-temperature superposition in thermorheologically complex materials, *Journal of Polymer Science, Polymer Symposia*, No. 3551-69.

Fulcher, G. S., 1925. Analysis of recent measurements of the viscosity of glasses, *Journal of the American Ceramic Society*, 8339-355.

Green, D. W., J. E. Winandy and D. E. Kretschmann. 1999: Mechanical properties of wood. *Wood handbook, wood as an engineering material.*, Madison, WI, USA: Forest Products Society, 1-45.

Höglund, H., U. Sohlin and G. Tistad, 1976. Physical-Properties of Wood in Relation to Chip Refining, *Tappi*, 59(6), 144-147.

Kelley, S. S., T. G. Rials and W. G. Glasser, 1987. Relaxation Behavior of the Amorphous Components of Wood, *Journal of Materials Science*, 22(2), 617-624.

Laborie, M.-P. G., 2002b. Investigation of the wood/phenol-formaldehyde adhesive interphase morphology, Wood Science and Forest Products, University Libraries, Virginia Polytechnic Institute and State University, Blacksburg, Va., *http://scholar.lib.vt.edu/theses/available/etd-03112002-110430*

Laborie, M.-P. G., L. Salmén and C. E. Frazier, 2004. Cooperativity analysis of the in situ lignin glass transition, *Holzforschung*, 58(2), 129-133.

Laborie, M.-P. G., L. Salmén and C. E. Frazier, 2006. A morphological study of the wood/phenol-formaldehyde adhesive interphase, *Journal of Adhesion Science and Technology*, 20(8), 729-741.

Lawoko, M., G. Henriksson and G. Gellerstedt, 2005. Structural Differences between the Lignin-Carbohydrate Complexes Present in Wood and in Chemical Pulps, *Biomacromolecules*, 6(6), 3467-3473.

Lenth, C. A. and F. A. Kamke, 2001. Moisture dependent softening behavior of wood, *Wood and Fiber Science*, 33(3), 492-507.

Li, J., R. Martin-Sampedro, C. Pedrazzi and G. Gellerstedt, 2011a. Fractionation and characterization of lignin-carbohydrate complexes (LCCs) from eucalyptus fibers, *Holzforschung*, 65(1), 43-50.

Maki-Arvela, P., I. Anugwom, P. Virtanen, R. Sjoholm and J. P. Mikkola, 2010. Dissolution of lignocellulosic materials and its constituents using ionic liquids-A review, *Industrial Crops and Products*, 32(3), 175-201.

Nakano, T., 1995. Time-Temperature Superposition Principle on Relaxational Behavior of Wood as a Multiphase Material, *Holz Als Roh-Und Werkstoff*, 53(1), 39-42.

Ngai, K. L. and D. J. Plazek, 1995. Identification of different modes of molecular motion in polymers that cause thermorheological complexity, *Rubber Chemistry and Technology*, 68(3), 376-334.

Ngai, K. L., R. W. Rendell and D. J. Plazek, 1991. Couplings between the cooperatively rearranging regions of the adam-gibbs theory of relaxations in glass-forming liquids, *Journal of Chemical Physics*, 94(4), 3018-3029.

Ngai, K. L. and C. M. Roland, 1993a. Chemical structure and intermolecular cooperativity: dielectric relaxation results, *Macromolecules*, 26(25), 6824-6830.

Ngai, K. L. and C. M. Roland, 1993b. Intermolecular cooperativity and the temperature dependence of segmental relaxation in semicrystalline polymers, *Macromolecules*, 26(11), 2688-2690.

Olsson, A.-M. and L. Salmén, 1997. The effect of lignin composition on the viscoelastic properties of wood, *Nord. Pulp Pap. Res. J.*, 12(3), 140-144.

Placet, V., J. Passard and P. Perre, 2007. Viscoelastic properties of green wood across the grain measured by harmonic tests in the range 0-95 degrees C: Hardwood vs. softwood and normal wood vs. reaction wood, *Holzforschung*, 61(5), 548-557.

Plazek, D. J. and K. L. Ngai, 1991. Correlation of Polymer Segmental Chain Dynamics with Temperature-Dependent Time-Scale Shifts, *Macromolecules*, 24(5), 1222-1224.

Qin, Q. and G. B. McKenna, 2006. Correlation between dynamic fragility and glass transition temperature for different classes of glass forming liquids, *Journal of Non-Crystalline Solids*, 352(28-29), 2977-2985.

Rodriguez, A. and L. Jimenez, 2008. Pulping with Organic Solvents other than Alcohols, *Afinidad*, 65(535), 188-196.

Roland, C. M. and K. L. Ngai, 1993. Concentration fluctuations and segmental relaxation in miscible polymer blends, *Progress in Colloid and Polymer Science*, 9175-79.

Roland, C. M., P. G. Santangelo, K. L. Ngai and G. Meier, 1993. Relaxation dynamics in poly(methylphenylsiloxane), 1,1-bis(p-methoxyphenyl)cyclohexane, and their mixtures, *Macromolecules*, 26(23), 6164-6170.

Saiter, J. M., L. Dobircau, R. Saiah, P. A. Sreekumar, A. Galandon, R. Gattin, N. Leblanc and R. Adhikari, 2010. Relaxation map of a 100% green thermoplastic film. Glass transition and fragility, *Phys. B (Amsterdam, Neth.)*, 405(3), 900-905.

Salmén, L., 1984. Viscoelastic properties of in situ lignin under water-saturated conditions, *Journal of Materials Science*, 19(9), 3090-3096.

Salmén, L., 2007. The mechanical deformation of wood—relation to ultrastructure., The comprised wood workshop 2007. , University of Canterbury, Christchurch, 143-157,

Samarasinghe, S., J. R. Loferski and S. M. Holzer, 1994. Creep Modeling of Wood Using Time-Temperature Superposition, *Wood and Fiber Science*, 26(1), 122-130.

Saunders, P. R., D. M. Stern, S. F. Kurath, C. Sakoonkim and J. D. Ferry, 1959. Dynamic mechanical properties of concentrated solutions of poly(butyl methacrylate) in diethyl phthalate, *Journal of Colloid Science*, 14(2), 222-238.

Sun, N. and C. E. Frazier, 2006. Hydroxymethylated resorcinol coupling agent: stress relaxation analysis, *Wood Adhesives 2005, [Proceedings Symposium], San Diego, CA, United States, Nov. 2-4, 2005*65-71.

Sun, N. and C. E. Frazier, 2007. Time/temperature equivalence in the dry wood creep response, *Holzforschung*, 61(6), 702-706.

Tammann, G., 1926. Die abhangigkeit der viskositat von der temperature bei unterkuhlten flussigkeiten, *Zeitschrift für anorganische und allgemeine Chemie (1950)*, 156245-257.

Vogel, H., 1921. The law of relation between the viscosity of liquids and the temperature, *Physik Z*, 22645-646.

Williams, M. L., R. F. Landel and J. D. Ferry, 1955. The Temperature Dependence of Relaxation Mechanisms in Amorphous Polymers and Other Glass-forming Liquids, *Journal of the American Chemical Society*, 77(14), 3701-3707.

Wolcott, M. P., F. Kamke and D. Dillard, 1994. Fundamental-aspects of wood deformation pertaining to manufacture of wood-based composites, *Wood and Fiber Science*, 26(4), 496-511.

Zhu, J. Y., X. J. Pan and R. S. Zalesny, 2010. Pretreatment of woody biomass for biofuel production: energy efficiency, technologies, and recalcitrance, *Applied Microbiology and Biotechnology*, 87(3), 847-857.

Zuza, E., J. M. Ugartemendia, A. Lopez, E. Meaurio, A. Lejardi and J. R. Sarasua, 2008. Glass transition behavior and dynamic fragility in polylactides containing mobile and rigid amorphous fractions, *Polymer*, 49(20), 4427-4432.

Chapter 5 Probing alignment and phase behavior in intact wood cell walls using ^{2}H NMR spectroscopy

Sudip Chowdhury, Louis A. Madsen, and Charles E. Frazier
Departments of Wood Science and Chemistry, and
Macromolecules and Interfaces Institute
Virginia Tech, Blacksburg, VA 24061

5.1. Abstract

Oriented morphology of wood cell wall controls its unique mechanical properties and also its deconstruction for biorefinery applications. This study presents a new technique utilizing ^{2}H NMR spectroscopy to quantitatively investigate the lignocellulosic cell wall morphology and phase behavior. ^{2}H NMR spectroscopy of small deuterated probe molecules doped in yellow-poplar (*Liriodendron tulipifera*) showed two distinct amorphous polymer domains: a highly oriented phase in the S2 layer of the secondary cell wall and an isotropic phase postulated to occur in the compound middle lamella (CML). This technique demonstrates the ability to independently investigate the morphology and phase dynamics specific to the oriented and unoriented domains. Using ethylene glycol-d4 as the probe molecule this study showed that the highly oriented phase was uniaxialy aligned along the fiber axis, i.e., single symmetry axis exists along the fiber direction (transverse directions were indistinguishable). With increasing temperature, between 40 and 60 °C the oriented polymer domain exhibits

glass-transition, which was manifested in the non-linear increase in the T_2 relaxation time, indicating that ^{2}H NMR can provide a localized probe to investigate segmental relaxation in sub-micron scale domains. This study also revealed that the interactions of lignocellulose with ethylene glycol and DMF were significantly different. A probable temperature induced solvent redistribution between S2 and CML was suggested, which showed significantly different dynamics in these two solvents. ^{2}H NMR should be useful in understanding correlations between biomass processing and morphological changes, and also in providing novel perspectives on lignocellulose ultrastructure.

5.2. Introduction

Optimum biomass utilization to meet the global need for sustainable energy and materials requires a comprehensive understanding of the lignocellulosic cell wall. Detailed knowledge of the cell wall ultrastructure will enable energy efficient biomass deconstruction and mimicry of nature's finesse in fabricating superior bio-composites. The knowledge of cell wall ultrastructure is still growing and requires development of novel and improved tools to characterize lignocellulosic biomass. Here we present novel features of lignocellulosic phase behavior and morphological alignment using a new method for characterization of intact xylem tissue based on deuterium (^{2}H) NMR.

The wood cell wall is a hierarchical structure with multiple concentric layers. These layers respectively from outside to inside, consist of: the middle lamella, primary wall, outer layer of secondary wall (S1), middle layer of secondary wall (S2) and the inner layer of secondary wall (S3). The middle lamella and the primary wall are often referred together as the combined middle lamella (CML) (Sjöström, 1993). The primary

and secondary cell walls are composed of rigid, semi-crystalline cellulose fibrils embedded in the amorphous matrix of hemicelluloses (glucomannan and xylan) and lignin. Thirty six cellulose chains form elementary fibrils (3 – 4 nm wide) which are coated primarily with glucomannan; subsequently, the elementary fibrils aggregate to form microfibrils (15 – 50 nm) which are also coated with glucomannan and are embedded in an amorphous matrix of lignin and xylan (Page *et al.*, 1976; Fahlén and Salmén, 2005a; Salmén and Burgert, 2009). In the major cell wall layer (S2: ~ 80% of the total weight) the microfibrils run almost parallel to the fiber axis (5 – 20°) and form a template for the amorphous polymers (Salmén, 2007; Salmén and Burgert, 2009).

The narrow space between microfibrils (~ 10 – 20 nm, in softwood) requires a systematic deposition of amorphous polymers during cell maturation (Fahlén and Salmén, 2005b, a; Salmén and Burgert, 2009). Orientation of hemicelluloses along the microfibrils is well documented (Page *et al.*, 1976; Åkerholm and Salmén, 2001; Stevanic and Salmén, 2009; Olsson *et al.*, 2011). Using dynamic Fourier-transform infrared spectroscopy (dFTIR) Akerholm and Salmén (2001) reported that glucomannan, the major softwood hemicellulose, was highly oriented and closely associated with cellulose. Orientation of xylan along the fiber direction was also confirmed in softwoods by Stevanic and Salmén (2009) and in hardwoods by Olsson et al. (2011) using imaging FTIR.

Observations of lignin orientation have varied. Using Raman spectroscopy of the secondary cell wall of *Picea marinara* (black spruce), Attala and Agarwal (1985a) reported evidence for the preferential orientation of lignin aromatic rings along the tangential grain direction. Subsequent dynamic and imaging FTIR studies of *Picea*

abies reported that the lignin phenyl propane units were slightly orientated along the cellulose microfibrils (Åkerholm and Salmén, 2003; Stevanic and Salmén, 2009). Recently, Olsson et al. (2011) reported that the amorphous phase organization in hardwood is significantly different; lignin chains are highly oriented along the microfibrils in aspen (*Populus tremula* × *Populus tremuloides*). Moreover, it is becoming increasingly clear that the secondary wall lignin itself is heterogeneous; a more condensed lignin appears to exist close to fibrils, whereas a less condensed lignin phase occurs away from the fibril surfaces (Lawoko *et al.*, 2005; Ruel and Joseleau, 2005; Salmén, 2007; Li *et al.*, 2011a). In spite of significant advances, questions exist regarding the amorphous polymer morphologies within and outside the cellulose microfibrils and their dynamics in relation to thermal and chemical treatments. Is a novel analytical approach needed to address these issues?

Deuterium nuclear magnetic resonance (^{2}H NMR), more specifically the ^{2}H quadrupolar interaction of absorbed probe molecules, is employed to study the orientation and phase dynamics of liquid crystals and synthetic polymers (Deloche and Samulski, 1981; Burnell and De Lange, 2003; Callaghan and Samulski, 2003; Li *et al.*, 2009). Quadrupolar nuclei (spin > ½) having a non-spherical nuclear charge are highly sensitive to localized orientation (Levitt, 2008). When a deuterated probe is doped into an oriented polymeric matrix, probe motions are biased by the matrix, thus imparting a partial ordering due to nematic-like short-range coupling with the matrix (so called “pseudo-nematic interactions”) (Deloche and Samulski, 1981; Callaghan and Samulski, 2003; Li *et al.*, 2009). Figure 5-1 represents the resulting spectra arising from a

quadrupolar interaction experienced by a deuterated probe in an isotropic and an oriented polymer matrix.

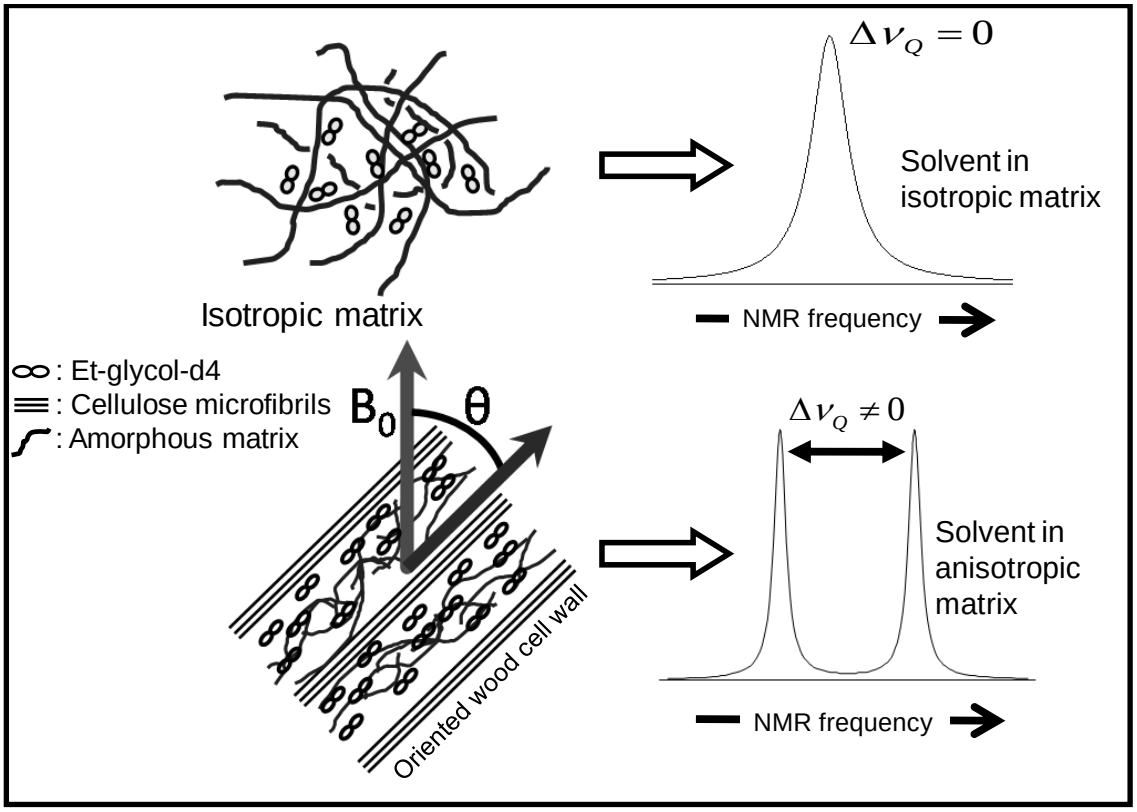

Figure 5-1. Schematic illustration of deuterium quadrupolar interaction in probing local orientational order in wood. (Top) Deuterated probe-solvent in an isotropic matrix produces a singlet spectrum. (Bottom) Deuterated probe-solvent in an oriented matrix produces a doublet.

In an isotropic matrix probe molecules rapidly sample all possible orientations, thereby the quadrupolar coupling averages to zero. Whereas in an oriented matrix the partial ordering causes the non-zero quadrupolar coupling, resulting a splitting in the ^{2}H spectrum of the probe molecule. The quadrupolar splitting $\Delta\nu_Q$ of probe deuterons is expressed in equation 5-1, which allows quantification of local orientational order information (Deloche and Samulski, 1981; Callaghan and Samulski, 2003; Li *et al.*, 2009).

$$\Delta\nu_Q = Q_P S P_2(\cos\theta) = Q_P \rho S_{matrix} P_2(\cos\theta) \qquad \text{Equation 5.1}$$

Here, Q_P is the quadrupolar coupling constant (~ 260 KHz); the orientational order parameter $S = \langle P_2(\cos\chi)\rangle$, where $\langle P_2(\cos\chi)\rangle$ is the ensemble average over the 2nd Legendre polynomial with χ = angle between a particular C-D bond and the matrix alignment axis, and θ being the angle between matrix alignment axis and the static magnetic field (B_0). From the probe orientational order (S) the orientational order parameter for the matrix (S_{matrix}) can be obtained as, $S = \rho S_{matrix}$, where $S_{matrix} = \langle P_2(\cos\alpha)\rangle$ with α being the angle between the channel where the probe is diffusing and the alignment axis of the matrix, and ρ represents a scaling factor that depends on the interaction between a specific probe molecule and its host matrix (Li *et al.*, 2009). Therefore, for a specific probe-matrix system the quadrupolar splitting can be used to measure the orientational order parameter(s) and alignment symmetries in the matrix.

In this study, we demonstrate the application of ^{2}H NMR as a quantitative tool to investigate the lignocellulosic cell wall morphology and phase behavior. Application of this highly developed NMR method provides novel perspectives on lignocellulosic ultrastructure. Additionally, treatment-induced changes in the phase dynamics can be observed and quantified at the sub-micron scale. This work provides a quantitative measure of the degree and type (uniaxial/multi-axial) of amorphous polymer orientation within an intact xylem tissue. Additionally, we investigate the effects of temperature and two organic solvents (a protic alcohol and a tertiary amide) on the oriented and isotropic polymer domain properties.

5.3. Experimental

5.3.1. Materials

All specimens were machined from a single piece of commercial yellow-poplar (*Liriodendron tulipifera*) sapwood lumber (30×5×5 cm); density was not measured but on average the diffuse-porous cross-section exhibited two growth rings per centimeter. 2 and 5 mm cubes were machined with precise grain orientation. The 2 mm cubes were sampled exclusively from within early wood; early and late wood proportions in 5 mm cubes were not controlled. Specimen dimensions for self-diffusion coefficient measurements were 2×2×16 mm, with the long axis along the fiber direction. Two partially deuterated solvents were used: ethylene glycol-d4 ($OH\text{-}(CD_2)_2\text{-}OH$) and N,N-dimethylformamide-d1 ($DCON(CH_3)_2$), obtained from Cambridge Isotopes Laboratories, Inc (Andover, MA) with minimum purity of 99%. The self-diffusion coefficient of ethylene glycol in wood was measured using anhydrous ethylene glycol ($C_2H_6O_2$), obtained from Sigma-Aldrich (99.8% purity).

5.3.2. Sample preparation

Specimens were vacuum dried (1 – 5 mm Hg, 48 h) at ambient temperature over anhydrous P_2O_5. After noting the dry weight, specimens were saturated with ethylene glycol-d4 or DMF-d1 using a room temperature vacuum/pressure treatment as follows: specimens were soaked in an excess of the deuterated solvent; vacuum was applied (10 – 12 mm Hg, 30 min) followed by atmospheric pressure (15 min). From this saturated condition, the solvent content of the specimens was reduced via controlled evaporation using a rotary evaporator (10 mm Hg). The final solvent content of the

specimens was targeted at 25% of dry wood weight (5 mm cube specimens for investigating the specimen size/heterogeneity effect had 30% solvent content). Within any sample group the solvent content variation was within 1%. After reaching the required solvent content and before NMR analyses, specimens were wrapped with Teflon tape and allowed to equilibrate for a minimum of 24 h at 4 °C in a 15 × 45 mm (OD × L) Teflon-capped glass vial.

5.3.3. Angular dependence of orientational order

Experiments were performed on Bruker Avance III widebore NMR spectrometer at 9.39 T static magnetic field (B_0), corresponding to ^{1}H and ^{2}H Larmor frequencies of 400 MHz and 61.4 MHz, respectively. A single-channel-detection static solids probe with a 10.7 mm ID horizontal solenoid coil was used. 2 mm cube specimens were placed in a Teflon vial (9.5×8.5×40 mm OD×ID×L) with a 2.3 mm diameter and 2.3 mm deep slot that accommodated the specimen. A cylindrical Teflon plug eliminated the free space above the specimen to prevent solvent evaporation. Grain directions (Longitudinal – *L*, radial – *R* and tangential – *T*) denoted for each specimen were fixed parallel to B_0. The sample cell was rotated in the horizontal NMR coil using a goniometer to control the angle between the grain orientation and B_0 to within ± 2°.

The spin-lattice relaxation time (T_1) of the ^{2}H of ethylene glycol-d4 in wood varied from 0.01 s at 0 °C to 0.2 s at 120 °C, as measured using inversion-recovery. The ^{2}H NMR experimental parameters were: acquisition time = 0.05 s, relaxation delay = 0.1 s, pulse time = 11.5 ($\pi/2$ pulse = 12 ms), spectral width = 25 KHz, number of scans per spectrum = 1000. No sample spinning was performed. Spectra were collected at 30 °C.

The temperature probe was calibrated to within ±1 °C using a pure dry ethylene glycol standard. The specimens were rotated in the radial plane from 0° (*L* direction parallel to B_0) to 90° (*R* direction parallel to B_0) in 10° steps, with spectra collected at each step. Spectra were then collected with the specimen's tangential (*T*) direction parallel to B_0. The experiment was repeated with three specimens to obtain three observations per data point.

Deuterium spectra were processed using MestReNova® (v. 6.1.1-6384). A 10 Hz exponential apodization was applied to the spectra. After phasing and baseline correction, a doublet and a singlet (all of Lorentzian lineshape) were fitted to the spectra to obtain quadrupolar splitting, area and width.

5.3.4. Temperature dependence of orientational order

Experiments were performed on a Varian INOVA spectrometer at 9.39 T magnetic field (B_0). A standard 5 mm axial-coil multinuclear liquids probe was used. Specimens were placed in a standard 5 mm NMR glass tube and the head space above the specimen was occupied using a 5 mm diameter Kel-F® plug (Wilmad-LabGlass, Vineland, NJ). Acquisition parameters were: acquisition time = 0.08 s, relaxation delay = 0.02 s, pulse time = 30 μs, spectral width = 25 KHz, number of scans = 1000 (except for DMF, where 6000 scans per experiment were averaged). Spectra were collected in isothermal conditions at different temperatures. The temperature probe was calibrated using pure and dry ethylene glycol to within ±1 °C. Temperatures were increased (Et-glycol: 0 to 100 °C and DMF: - 10 to 80 °C) in 10 °C increments, followed by a 10 °C stepwise cooling to the minimum temperature. At each temperature specimens were

equilibrated for 10 min before collecting spectra. Three specimens for each solvent were tested.

All spectra were exponentially apodized (10 – 20 Hz) and phase and baseline corrected. The high temperature spectrum, which showed best peak resolution, was used to establish the number of peaks to be fit across the temperature range. All spectra were fit with one Lorentzian doublet and a Lorentzian singlet. The distance between the doublet peaks (in Hz) was recorded as the quadrupolar splitting $\Delta\nu_Q$.

Self-diffusion coefficient of ethylene glycol ($C_2H_6O_2$) (25% on dry wood mass) along the longitudinal direction was measured using a pulse-gradient stimulated echo (PGSTE) pulse sequence (Tanner, 1970; Hou *et al.*, 2010) at 80 °C. Specimens were placed in a standard 5 mm NMR glass tube and the head space above the specimen was occupied using a 5 mm diameter Kel-F® plug (Wilmad-LabGlass, Vineland, NJ). Using a single axis diffusion probe the PGSTE sequence used a $\pi/2$ pulse of 4.5 μs, gradient pulse duration (δ) 1 ms, and diffusion times (Δ) ranging from 50 – 300 ms. Adequate signal-to-noise ratio was achieved with 56 scans.

5.4. Results and Discussion

Figure 5-2 shows the ^{2}H NMR spectra of ethylene glycol-d4 in yellow-poplar as a function of the angle θ between the fiber axis and the static magnetic field (B_0). Specimens were rotated in the radial plane so the 0° and 90° acquisitions represented the longitudinal (*L*) and the radial (*R*) directions parallel to B_0, respectively. Separate measurements were conducted with the *T* direction parallel to B_0.

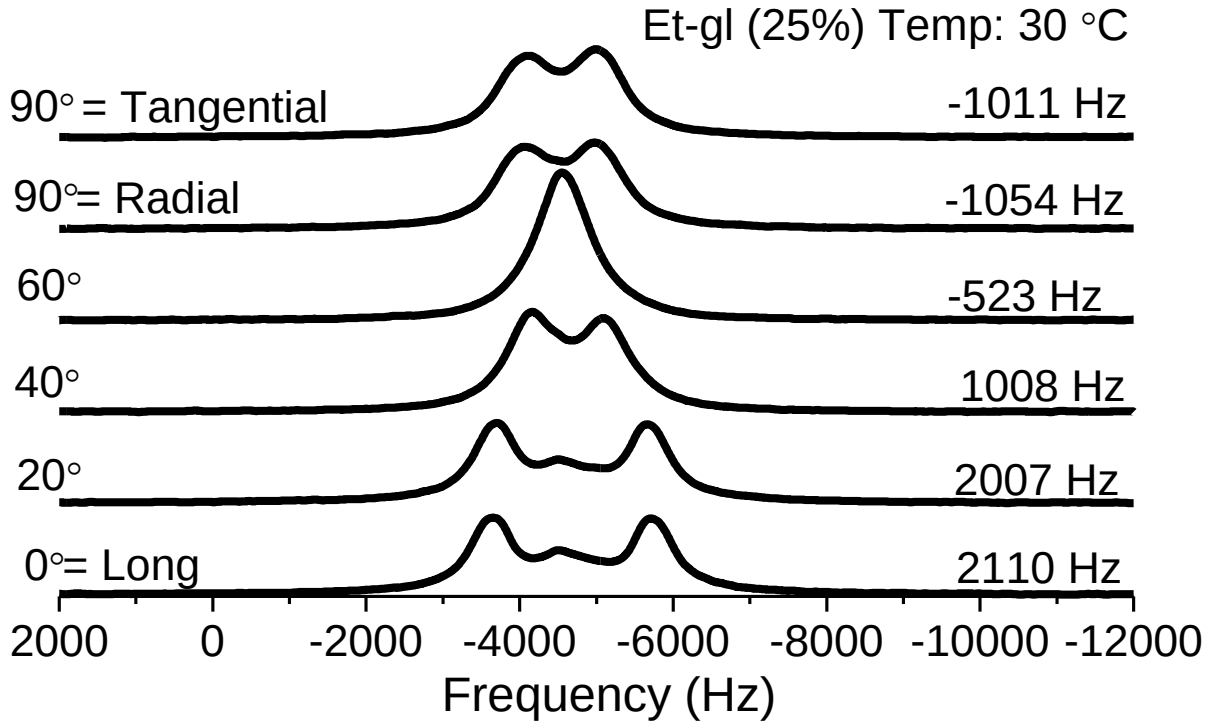

Figure 5-2 Deuterium NMR spectra for 25 wt % ethylene glycol-d4 in yellow-poplar at 30 °C. The quadrupolar splitting $\Delta\nu_Q$ changes as in eq. 1 as a function of the angle θ between the wood fiber axis and B_0.

At the *L*-orientation, a doublet signifying an oriented phase, and hint of a singlet representing an isotropic phase, were observed. Probes were chosen such that single chemically specific types of ^{2}H were present, resulting in only one doublet/singlet in the spectrum. The shapes and proportions of the singlet and doublet will be discussed later, but note that all spectra presented here indicate that the swollen specimens were below fiber saturation.

The quadrupolar splitting was measured in each spectrum using a least-square fit of a Lorentzian doublet and a singlet. Within the experimental uncertainties (coefficient of variation: 10%), the quadrupolar splitting for the *L* direction (defined as $\Delta\nu_L$) was double the splitting at the *R* ($\Delta\nu_R$) and the *T* ($\Delta\nu_T$) directions (Figure 5-2). By

definition, this is characteristic of a uniaxialy oriented material ($\Delta\nu_L = 2\Delta\nu_R = 2\Delta\nu_T$) (Burnell and De Lange, 2003; Li *et al.*, 2008, 2009). This signifies that at the length scale probed (sub-micron, discussed later) the two transverse directions of wood amorphous domains were indistinguishable. Figure 5-3 plots the quadrupolar splitting $\Delta\nu_Q$ as a function of the angle θ between B_0 and the grain/fiber direction along with a uniaxial fit according to equation 5.1.

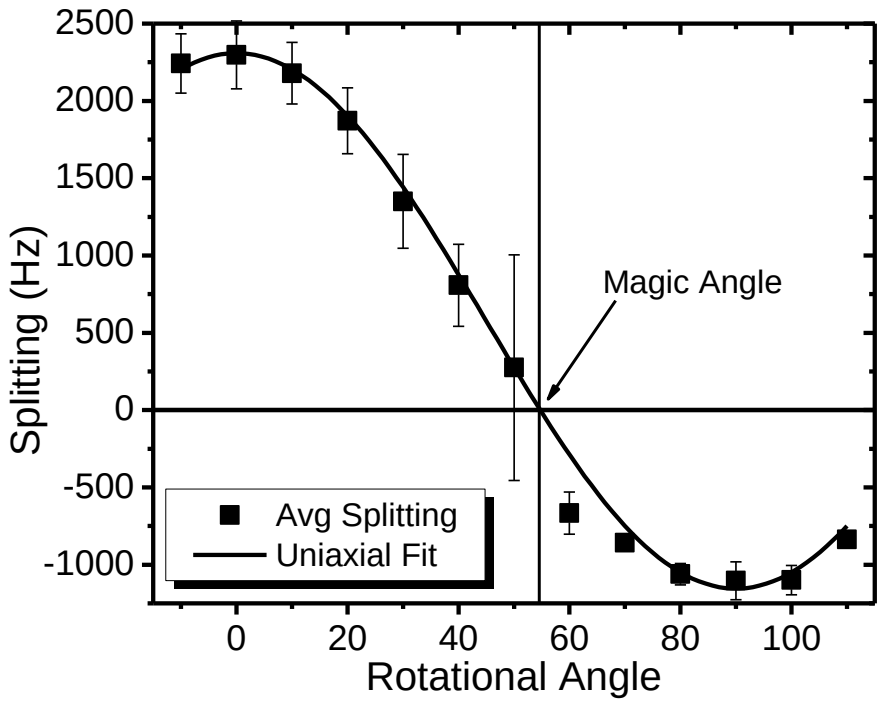

Figure 5-3. Average quadrupolar splitting vs. alignment angle for 25% ethylene glycol-d4 in yellow-poplar. Solid line represents uniaxial fit to the average splitting data. Error bar represents ±1 standard deviation (n = 3).

The uniaxial equation fit the experimental data very well (R^2: 0.97) with the zero-crossing angle for the quadrupolar spitting at the magic angle, 54.7°. The probe orientational order parameter (S_{probe}) was 0.009±0.002. This provides a relative measure

of the matrix orientational order (S_{matrix}), which is generally a few orders of magnitude higher than the S_{probe}, depending on the probe aspect ratio and probe-matrix interactions (Li *et al.*, 2009; Li *et al.*, 2011b). In a perfectly oriented system, S becomes 1 (for orientation axis/director parallel to B_0) or -0.5 (director perpendicular to B_0) (Deloche and Samulski, 1981); the value of S becomes 0 for systems with no orientation or when the orientation axis/director assumes 54.7° with B_0. S_{probe} = 0.009 is a relatively large value in comparison to other oriented polymers such as Nylon-6 and Nafion® (Loo *et al.*, 2000; Li *et al.*, 2009; Li *et al.*, 2011b; Park *et al.*, 2011). For instance, in a hydrated perfluoronated ionomer (Nafion®) S_{probe} ~ 10^{-3} was reported, where the respective S_{matrix} was ~0.5 (Park *et al.*, 2011). In hydrated Nylon-6, Loo et al. (2000) observed S_{Probe} ~10^{-3} with S_{matrix} = 0.78. Accurate measurement of S_{matrix} requires knowledge of the scaling factor ($\rho = S_{probe}/S_{matrix}$), which contains the probe geometry (aspect ratio) effects and probe-matrix interaction information. This scaling factor can be obtained using small angle X-ray scattering experiments (Li *et al.*, 2011b; Park *et al.*, 2011). However, it is reasonable to believe that the wood S_{matrix} should be fairly large (perhaps close to 1) signifying a highly oriented amorphous domain parallel to the fiber axis, this is consistent with the current knowledge of hardwood characteristics (Salmén and Burgert, 2009; Olsson *et al.*, 2011).

In wood the probe molecules rapidly diffuses throughout the amorphous phase and the observed ^{2}H NMR response is the average of the orientational order in the domain where the probe resides. Depending on the probe diffusion coefficient (D) and the ^{2}H NMR time scale (t_{NMR} ~ $1/\Delta\nu_Q \approx 0.5$ ms), the experimental length scale can be estimated (the root-mean-square distance travelled under a 1D random walk: $\langle r^2 \rangle^{1/2} =$

$\sqrt{2Dt}$). PGSTE diffusometry revealed that the ethylene glycol diffusion coefficients (*D*) along the longitudinal direction of wood range from 7×10^{12} m^2/s to 1×10^{12} m^2/s for the diffusion time (Δ) range of 50 to 300 ms, respectively. Using the 1D random walk expression (substituting t with Δ) the corresponding length scales were 30 to 80 nm. However with decreasing Δ the *D* increases, although not in a linear trend. Therefore for the ^2H NMR time scale, 0.5 ms, we estimate the 1D length scale to be between 100 to 300 nm. Detailed diffusometry studies should provide a more precise estimate of the experimental length scale probed. It was previously reported that the self-diffusion of water in saturated wood is anisotropic; NMR diffusometry of water saturated hardwood revealed about 3 times higher diffusion coefficients along the fiber direction as compared to the transverse directions (MacGregor *et al.*, 1983). For the present study, therefore, the domain probed by ethylene glycol-d4 is also hypothesized to be non-spherical (cylindrical or ellipsoidal), with the transverse length scale being roughly one-third of the longitudinal length scale.

Figure 5-3 reports that the maximum splitting occurred near 0°, i.e., when the fibers were parallel to B_0, suggesting that the cellulose fibrils were on average aligned with the fiber axis (and B_0) as occurs in the S2 layer (Fengel and Wegener, 1984). Consequently this demonstrates that the doublet signal originated from the S2 layer which comprises ≈ 70% of the hardwood tissue (Fergus and Goring, 1970). Moreover, it is known that cellulose rarely allows solvent penetration into its crystalline core (Hofstetter *et al.*, 2006; Salmén, 2007). Although a variety of exotic solvents including ionic liquids have been identified as cellulose solvents (Klemm *et al.*, 1998; Maki-Arvela *et al.*, 2010), the cellulose crystalline structure is impervious to the solvents used in this

study (ethylene glycol and DMF) (Sadoh and Yamaguchi, 1968; Sadoh, 1981). Therefore it is assumed that the probes in this study could only reside in the solvent accessible amorphous domains.

In the secondary cell wall of hardwoods, all amorphous polymers are thought to be oriented parallel to the cellulose microfibrils (Page *et al.*, 1976; Åkerholm and Salmén, 2003; Olsson *et al.*, 2011). Considering that S_{probe} = 0.009 in a highly oriented uniaxial matrix with roughly cylindrical domains of at least 100 - 300 nm in length, it is reasonable to consider that the doublet reflects the average over the oriented matrix of lignin and hemicellulose within and between cellulose microfibrils in the S2 layer, which is consistent with contemporary wood cell wall models (Salmén and Burgert, 2009).

The effects of temperature on the ^{2}H NMR spectra are demonstrated in Figure 5-4, where over this temperature range ethylene glycol-saturated yellow-poplar exhibits a glass/rubber transition around 70 °C (Chowdhury and Frazier, 2011a, b). At low temperatures (between 0° and 40 °C) a broad doublet was observed, signifying slowly moving deuterated probe molecules in an oriented phase. With increasing temperature the doublet width decreased, especially beyond 40 °C, where also a broad singlet emerged between the doublet peaks.

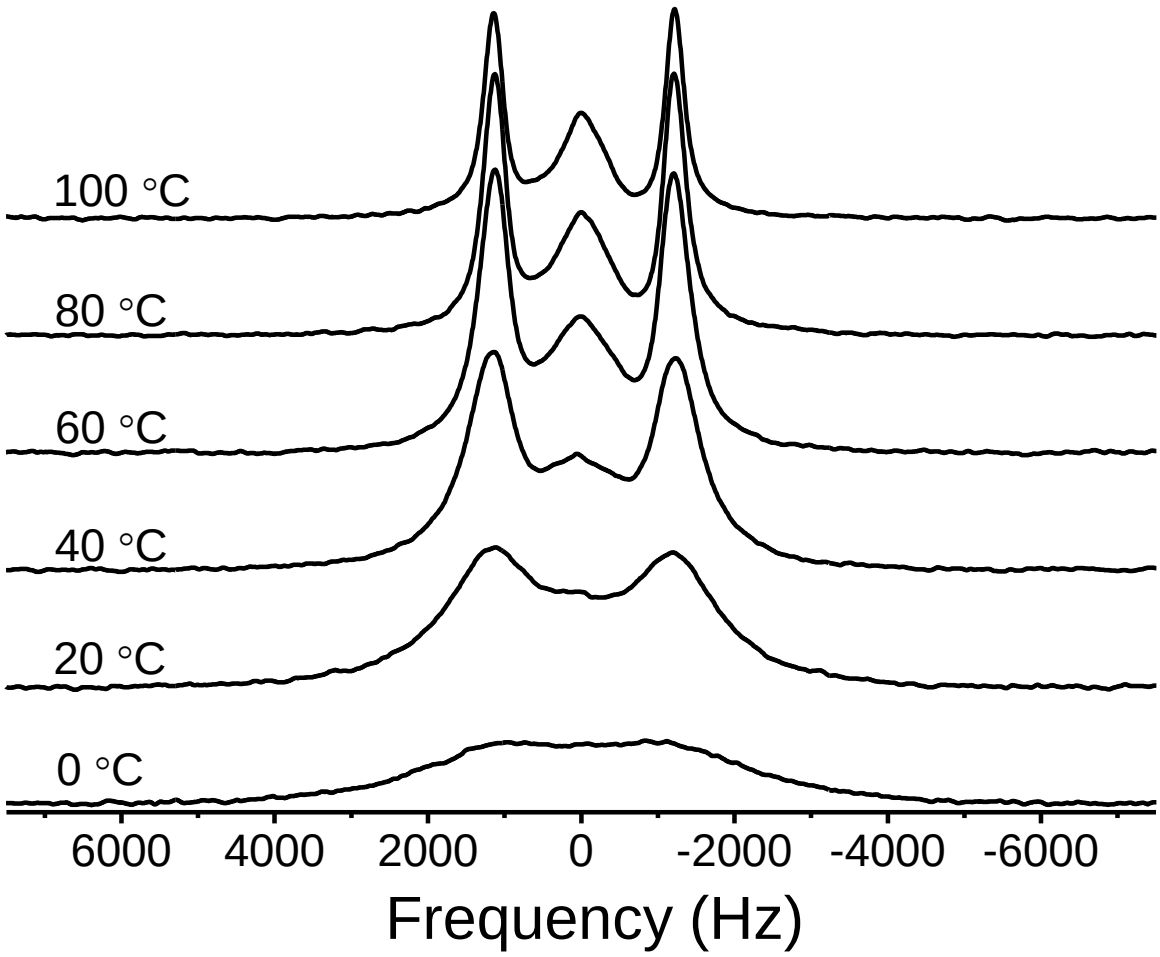

Figure 5-4 Isothermal ^{2}H Spectra for 25% ethylene glycol-d4 equilibrated in yellow-poplar, collected at different temperatures. Specimen longitudinal grain is parallel to B_0.

As mentioned, the specimens existed below fiber saturation; this was indicated by the high singlet linewidth (~ 700 Hz) and that a free liquid probe molecule phase would exhibit a linewidth of ~ 1 – 10 Hz. The broad singlet reflects an isotropic polymer domain of no smaller than 100 – 300 nm, and physically separated from the oriented phase on this same experimental length scale. These features suggest that the singlet represents the unoriented tissue found in the primary cell wall and the middle lamella (together termed as the compound middle lamella, CML). The CML accounts for 8 –

15% of the hardwood xylem tissue mass, with little cellulose (< 4%) and high lignin concentration (~55 – 85%) (Fergus and Goring, 1970; Fengel and Wegener, 1984; Sjöström and Alén, 1999). Cellulose fibrils within the CML are randomly oriented and so little or no matrix orientation is expected. Summarizing, the angular dependence of the doublet suggests that its origin is from the S2 layer, and the size of the singlet is consistent with it arising from the isotropic amorphous matrix within the CML. Additional experiments are required to confirm this hypothesis, but this method should hold promise for bulk lignocellulose studies, where distinction of the CML and S2 layers would be very useful. For instance the push towards bioenergy is stimulating efforts towards lignocellulose fractionation in a variety of liquid media. It would be very useful to distinguish the S2 layer (where most chemical energy is stored) from the CML which must be efficiently degraded and/or cleaved for mechanical or chemi-mechanical reduction of tissue particle size. Currently there are no other methods capable of distinguishing the S2 layer from the CML in bulk intact tissue. Using deuterium quadrupolar NMR, we anticipate novel insights into deconstructive strategies specific to the oriented and unoriented matrices probed with this technique.

Quadrupolar splitting, peak width and area as a function of temperature were determined by fitting a doublet and a singlet to the spectra. Although each least square fit adequately simulated the observed spectra, a high degree of peak overlap at lower temperatures is expected to cause greater error in the measured spectral parameters, particularly those determined below 40˚C. Measurement quality dramatically improved above 40 ˚C because of the increased matrix mobility associated with the glass/rubber transition depicted in Figure 5-4. The wood amorphous domain was in the glassy region

at low temperature, and with increasing temperature the quadrupolar splitting decreased (Figure 5-5).

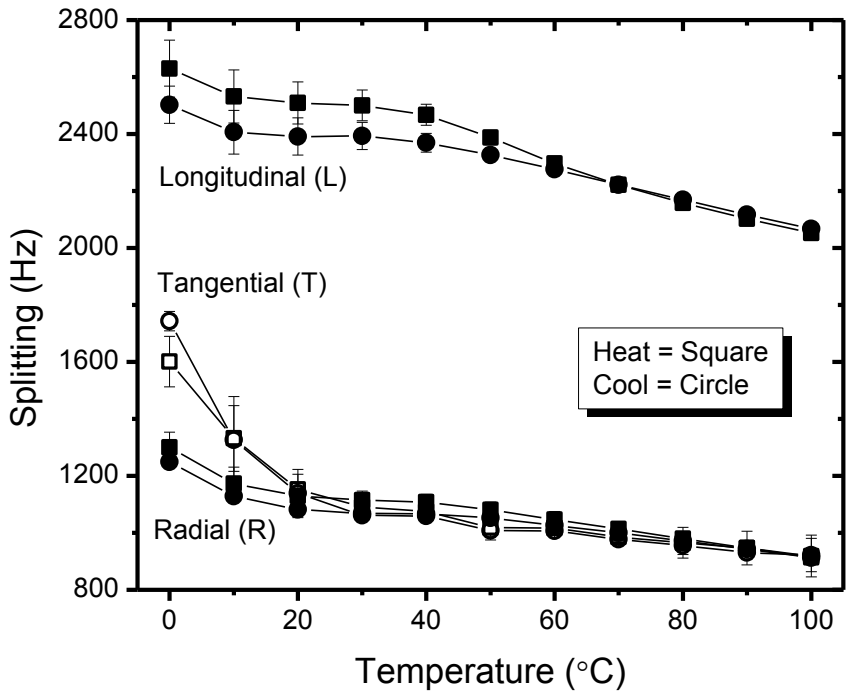

Figure 5-5 Average (n=3) quadrupolar splitting as a function of sequential heat and cool for 25% ethylene glycol-d4 in yellow poplar. Grain direction parallel to B_0 as indicated. Error bars indicate ±1 standard deviation.

In addition to the increased randomized probe motions, the higher thermal energy stimulates greater configurational change among the matrix polymers such that the average degree of matrix orientation reduced, and probe alignment was less biased (Callaghan and Samulski, 2003). Therefore, the ensemble average orientational order (S) was reduced, resulting in smaller splittings with increasing temperature (Li *et al.*, 2009). Similarly in cooling the splitting increased due to lowered probe and polymer mobility. Heating and cooling produced highly reversible quadrupolar splittings beyond 60 °C. It is worth mentioning here that the solvent loss in a heat-cool cycle was less than 1% of the dry wood mass. In *L* direction, at the lower temperature cooling steps

showed slightly lower quadrupolar splitting. The splitting change couldn't be attributed to the minor solvent loss, as that would have increased the splitting. However, the lowering in the splitting could be due to the reduction in the orientational order upon cooling the specimen from the rubbery phase. However, the broad low temperature lines caused higher fitting errors, making the subtle differences in splitting inconclusive.

Figure 5-5 also indicates that the two transverse grain orientations (*R* and *T*) generally exhibited identical splitting over the experimental temperature range. Note the low temperature divergence, which is ascribed to broad lines causing poor curve fitting. Moreover within experimental variations the transverse splittings equaled half the longitudinal splitting, again consistent with a uniaxial phase symmetry that was retained at all temperatures. Furthermore, the *L* grain splitting vs. temperature curves (both in heating and cooling) exhibited a change in slope (downturn) near 40 °C perhaps due to increased mobility of the polymer matrix with temperature increase. The mobility increase was also reflected in the spin-spin relaxation time (T_2), plotted as a function of temperature in Figure 5-6.

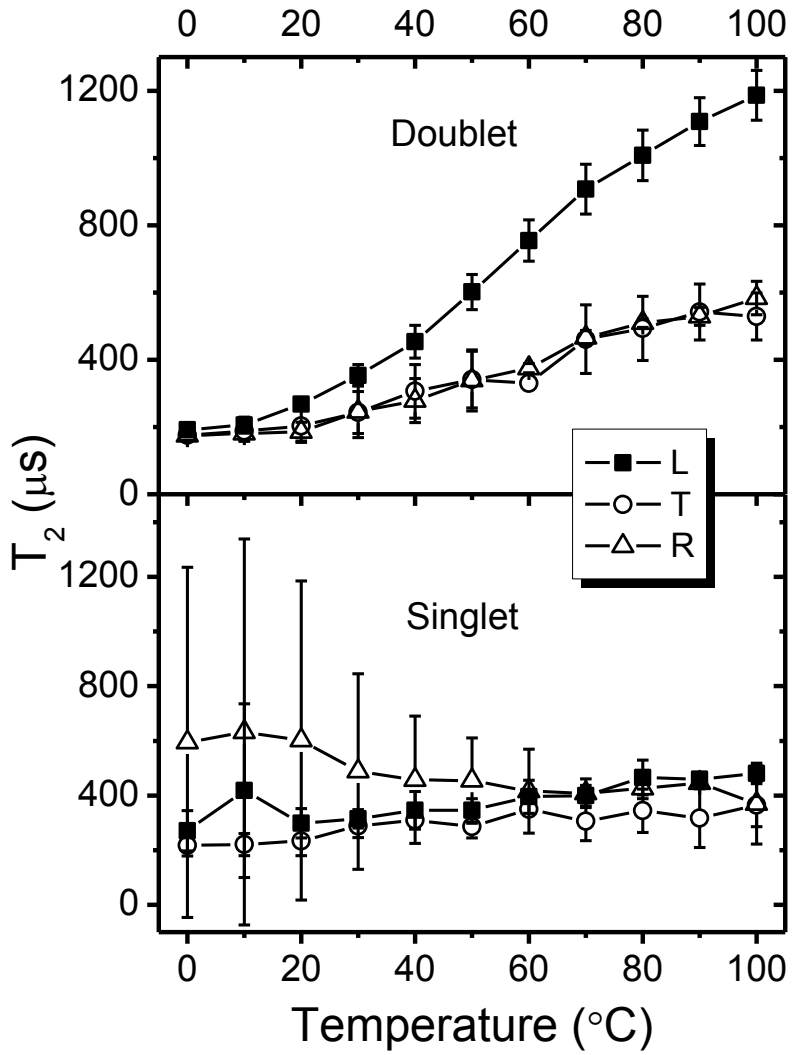

Figure 5-6 Average T_2 relaxation time as a function of temperature for doublet (top) and singlet (bottom) along the three grain directions. Error bars indicate ±1 standard deviation (n=3).

Doublet and singlet widths were used to calculate the spin-spin relaxation time, $T_2 = (\pi \times \text{width})^{-1}$. In the oriented phase (doublet) with *L* along B_0, a nonlinear increase in T_2 was recorded between 40 and 60 °C. This temperature correlates reasonably well with the "quasi-static (100s relaxation time)" T_g for ethylene glycol-plasticized yellow-polar, 71-77 ˚C (Chowdhury and Frazier, 2011b). Thus, T_2 directly reflects this segmental relaxation of the oriented phase. Moreover this change in T_2 correlates to the

$\Delta\nu_Q$ downturn near 40 °C seen in Figure 5-5. The T_2 increase for the transverse grain directions was much smaller, and the nature of the increase (linear vs. non-linear) was not clear. The wood grain dependence of the probe T_2 (longitudinal vs. transverse) could reflect differences in the segmental dynamics between parallel and perpendicular directions of wood polymer chains. However further study is required on this matter. The singlet T_2 for all grain directions was similar, but its temperature dependence was obscured by the fitting errors that dominated at lower temperatures.

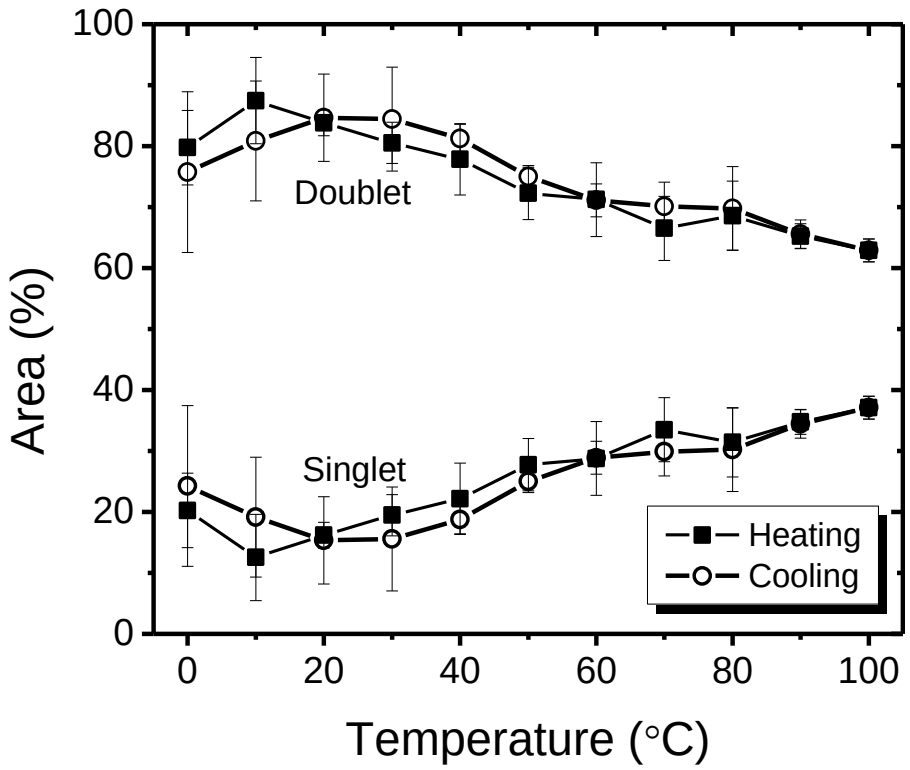

Figure 5-7 Average (n=3) proportion of doublet and singlet area as a function of temperature. Specimens heated from 0 to 100 °C followed by cooling in 10 °C increments. Error bars indicate ±1 standard deviation.

Figure 5-7 shows the proportions of the isotropic and oriented phases at each temperature. Above 40 ˚C where fits were more reliable, increasing temperature slightly

decreases the proportion of the doublet while the singlet increases. Note that these relative proportions were thermally reversible. This might suggest the isotropic and oriented phases substantially differ in thermal expansion, where the greater expansion of the isotropic phase causes probe redistribution at the expense of the oriented phase. If the oriented phase did experience a substantial loss of the probe, then we might expect the splitting to increase, while we observed a mild opposite trend (Figure 5-5). For instance in perfluorosulfonate ionomers (Nafion®), the probe content strongly correlates to the degree of swelling and the observed splitting is higher at lower probe concentrations (Li *et al.*, 2009). In the present case, perhaps the increasing thermal motions in the oriented phase overpower the effects of probe redistribution such that the overall orientation is reduced. The interpretation of probe redistribution is consistent with the singlet signal arising from the CML where the cellulose concentration is quite low and lignin concentration is high (~85%) (Fergus and Goring, 1970). In contrast, cellulose comprises more than 80% of the S2 layer (doublet) (Fergus and Goring, 1970; Fengel and Wegener, 1984). Thermal expansion of the S2 layer should be restricted by the "undulating cellulose aggregate structure" and that cellulose fibrils undergo further aggregation when heated under plasticized conditions (Salmén, 2007; Salmén and Burgert, 2009). Since the CML is primarily amorphous, its thermal expansion is expected to be greater than the S2 layer; and on a unit volume basis the CML has a greater swelling capacity than the S2 layer. Considering the relative lignin content in these two morphological domains, S2 contains ~ 77% and the CML contains ~19% of the total lignin of hardwood tissue (Fergus and Goring, 1970). These distributions correlate well with the relative proportions of oriented (doublet) and isotropic (singlet)

phases (at 40 °C, doublet: 77%, singlet: 22%). Under this scenario, the thermal redistribution of the probe is controlled by the segmental relaxation of amorphous chains in the S2 layer and the CML, a reversible process that is consistent with the thermal reversibility of signal proportions shown in Figure 5-7. Again, we anticipate predictions for optimal biomass processing in a variety of liquid media that are amenable to this NMR technique.

In this work, DMF was also studied; compared to ethylene glycol, DMF is a much more powerful wood swelling agent (Sadoh, 1981; Chowdhury and Frazier, 2011a).

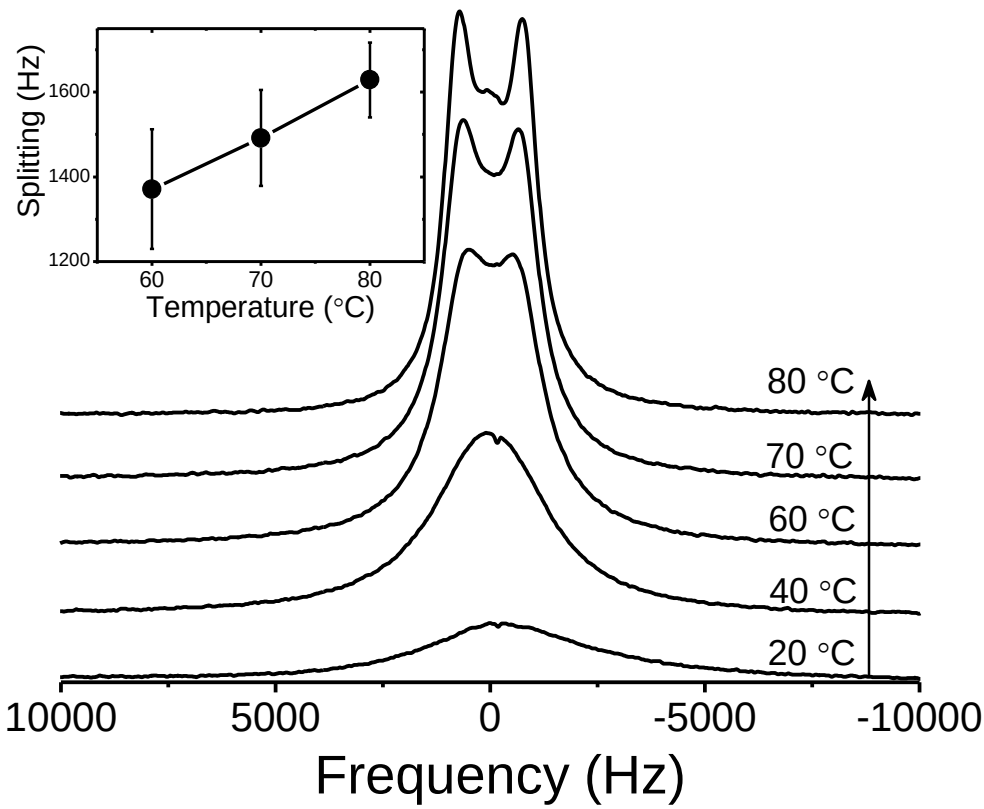

Figure 5-8 Deuterium NMR spectra of 25% DMF-d1 in yellow-poplar at different temperatures. *L* is parallel to B_0. Inset shows average (n=3) quadrupolar spitting at the three highest temperature steps. Error bar: ±1 standard deviation.

Figure 5-8 shows isothermal ^{2}H spectra of DMF-d1 in yellow-poplar wood versus temperature. At lower temperatures (below 60 °C) a broad single peak was observed. With increasing temperature a doublet emerged and a singlet was visually discernible only at 80 °C. Compared with ethylene glycol, peak overlap was much greater in DMF, and so peak fitting and splitting estimation became less reliable. Nevertheless the spectra and the splitting values depict a clear trend of increased splitting on raising temperature, in contrast to the effects observed in ethylene glycol. This observation was surprising because it indicates that DMF experiences an increase in the local ordering as the temperature is increased. As mentioned, DMF is a better wood swelling agent than ethylene glycol. In either case the parallel organization of cellulose fibrils is believed to severely limit swelling in the longitudinal direction. However, the greater swelling power of DMF will substantially alter the competing effects of probe redistribution (increased splitting) and increased segmental relaxation (reduced splitting). Given that DMF is a more powerful swelling agent perhaps the effects of probe redistribution outweighs the effects of segmental relaxation such that an overall increase in splitting is observed with DMF. With ethylene glycol the reversibly changing proportions of isotropic and anisotropic signal are consistent with probe redistribution. As temperature increases, the greater thermal expansion of the CML might cause probe to transfer out of the S2 layer and into the CML. The splitting is expected to change under competing effects, increased splitting due to S2-probe loss and decreased splitting due to increased wood polymer motion. Under the postulated scenario, the lower swelling power of ethylene glycol results in the domination of polymer motion effects; splitting decreases with temp. Whereas under the greater swelling power of

DMF, probe redistribution dominates; the S2 layer loses probe and this effect dominates such that an overall splitting increase is observed. A study with isolated secondary cell wall material might provide further insight regarding the solvent redistribution and associated local orientation change. Additionally, advanced multiple-quantum NMR experiments (Saalwachter, 2007) to eliminate the singlet (isotropic) response may improve clarity by exclusively monitoring the change in the doublet with temperature.

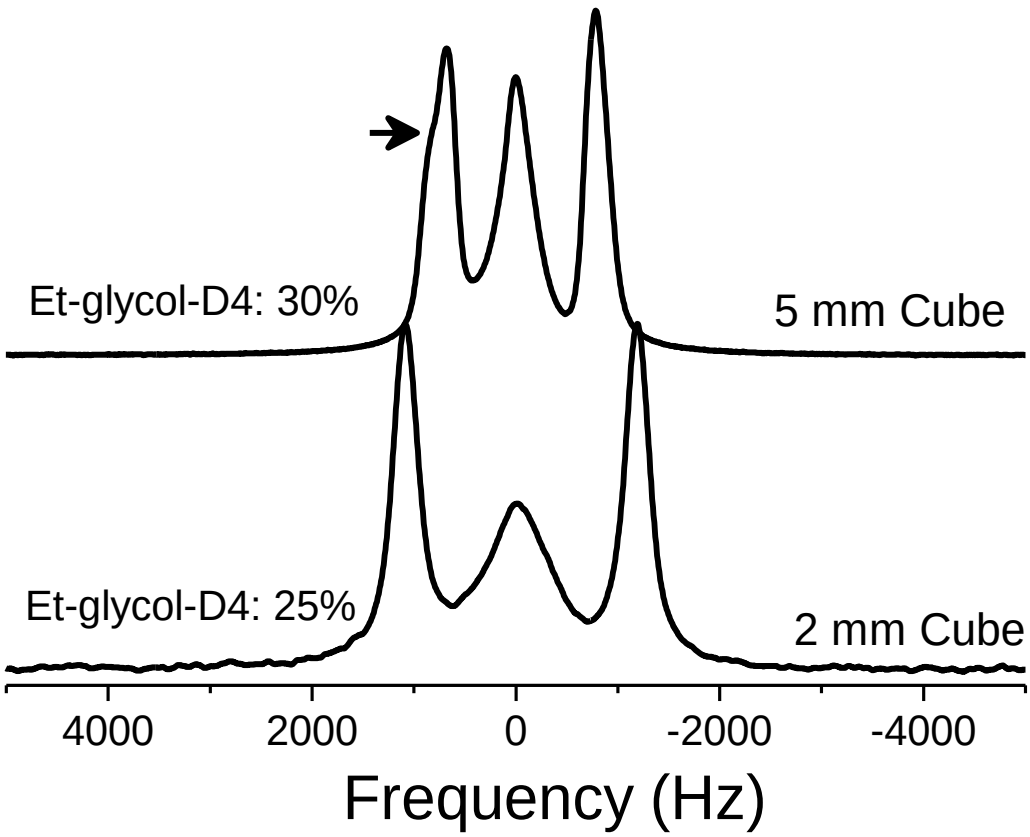

Figure 5-9 Effect of specimen size and solvent content on ^{2}H spectra of ethylene glycol-d4 in yellow-poplar wood. Solvent content for 5 mm cube was 30%, for 2 mm cube was 25%. Spectra were collected at 100 °C, while the *L* direction was parallel to B_0. The arrow denotes the additional shoulder observed in 5 mm specimens, due to within-specimen orientational variability.

Effects of solvent content and specimen size are demonstrated in Figure 5-9. The 2 mm specimen had a 5% lower solvent content, and this caused increased

quadrupolar splitting (500 Hz). This inverse relationship of solvent content and splitting reflects the degree of swelling, where at reduced swelling the matrix imposes greater bias on probe motions (Li *et al.*, 2009; Hou *et al.*, 2010). Furthermore, with higher solvent content the singlet intensity increased with narrower linewidth, whereas the doublet linewidth did not change.

In addition to the solvent content effect, Figure 5-9 also demonstrates the specimen size effects. The 5 mm specimen showed an additional shoulder in the spectrum (denoted by the arrow) suggesting an additional domain with slightly different orientational order, which was not present in 2 mm specimens. Moreover, the linewidth-to-splitting ratio was higher in the 5 mm specimens, suggesting a higher material heterogeneity (inhomogeneous broadening). The 5 mm specimens contained both early and late wood, which have significantly different morphologies. The late wood cellulose microfibril angle is significantly lower than it is in the early wood fibril angle (Jang, 1998; Salmén, 2007), i.e., cellulose microfibrils bear lower angle with the fiber axis. Additionally, the density of the late wood is significantly higher than the early wood density. These differences cause significantly different orientational order in the amorphous polymer domains in early and late wood.

5.5. Summary

This study demonstrates the application of ^{2}H NMR quadrupolar couplings in analyzing cell wall polymer morphology in intact wood tissue using two different deuterated probe molecules (protic alcohol: ethylene glycol-d4 and tertiary amide: DMF-d1). This technique is experimentally relatively simple and very powerful in investigating

sub-micron polymer domains. Deuterium spectra revealed features of two different amorphous domains within the wood cell wall: a highly oriented phase in the S2 layer and an isotropic domain postulated to be in the CML. Using ethylene glycol-d4 as a probe, it was demonstrated that the oriented amorphous phase was uniaxial, i.e., only one major symmetry axis along the fiber direction (transverse directions indistinguishable). Additionally, between 40 and 60 °C a segmental relaxation in the oriented domain was observed, which was manifested in the non-linear increase in the T_2 relaxation time. ^{2}H NMR should provide an efficient tool to bring novel insights into deconstructive strategies specific to the oriented and unoriented matrices inside the wood cell wall. In addition to the polymer mobility/relaxation information, probable solvent redistribution between S2 and CML was identified. Significantly different solvent-lignocellulose interactions were observed for ethylene glycol and DMF. This holds great potential in understanding solvents and temperature dynamics inside the cell wall layers, which is very important in lignocellulose pulping, fractionation and other biomass deconstruction strategies.

5.6. Acknowledgement

Authors sincerely thank Jianbo Huo for his help in acquiring self-diffusion coefficient data during this work.

5.7. References

Åkerholm, M. and L. Salmén, 2001. Interactions between wood polymers studied by dynamic FT-IR spectroscopy, *Polymer*, 42(3), 963-969.

Åkerholm, M. and L. Salmén, 2003. The oriented structure of lignin and its viscoelastic properties studied by static and dynamic FT-IR spectroscopy, *Holzforschung*, 57(5), 459-465.

Atalla, R. H. and U. P. Agarwal, 1985a. Raman microprobe evidence for lignin orientation in the cell-walls of native woody tissue, *Science*, 227(4687), 636-638.

Burnell, E. E. and C. A. De Lange, 2003: NMR of ordered liquids. Kluwer Academic Publishers,Dordrecht ; Boston

Callaghan, P. T. and E. T. Samulski, 2003. Biaxial deformation of a polymer network measured via deuteron quadrupolar interactions, *Macromolecules*, 36(3), 724-735.

Chowdhury, S. and C. E. Frazier, 2011a. Chapter 3: Compressive-torsion DMA of wood in organic media *in* Advancing characterization techniques for structure-property determination of in-situ lignocelluloses, Macromolecules and Interefaces Institute and Department of Wood Science and Forest Products, Virginia Polytechnic Institute and State University, Blacksburg, VA,

Chowdhury, S. and C. E. Frazier, 2011b. Chapter 4: Time-temperature equivalence and fragility of organic solvent plasticized wood *in* Advancing characterization techniques for structure-property determination of in-situ lignocelluloses, Macromolecules and Interefaces Institute and Department of Wood Science and Forest Products, Virginia Polytechnic Institute and State University, Blacksburg, VA,

Deloche, B. and E. T. Samulski, 1981. Short-range nematic-like orientational order in strained elastomers - a deuterium magnetic-resonance study, *Macromolecules*, 14(3), 575-581.

Fahlén, J. and L. Salmén, 2005a. Pore and matrix distribution in the fiber wall revealed by atomic force microscopy and image analysis, *Biomacromolecules*, 6(1), 433-438.

Fahlén, J. and L. Salmén, 2005b. Ultrastructural changes in a holocellulose pulp revealed by enzymes, thermoporosimetry and atomic force microscopy, *Holzforschung*, 59(6), 589-597.

Fengel, D. and G. Wegener, 1984: Wood : chemistry, ultrastructure, reactions. W. de Gruyter,Berlin ; New York

Fergus, B. J. and D. A. I. Goring, 1970. Distribution of lignin in birchwood as determined by ultraviolet microscopy, *Holzforschung*, 24(4), 118-124.

Hofstetter, K., B. Hinterstoisser and L. Salmen, 2006. Moisture uptake in native cellulose - the roles of different hydrogen bonds: a dynamic FT-IR study using Deuterium exchange, *Cellulose*, 13(2), 131-145.

Hou, J., J. Li and L. A. Madsen, 2010. Anisotropy and Transport in Poly(arylene ether sulfone) Hydrophilic-Hydrophobic Block Copolymers, *Macromolecules (Washington, DC, U. S.)*, 43(1), 347-353.

Jang, H. F., 1998. Measurement of fibril angle in wood fibres with polarization confocal microscopy, *Journal of Pulp and Paper Science*, 24(7), 224-230.

Klemm, D., B. Philipp, T. Heinze, U. Heinze and W. Wagenknecht, 1998: Comprehensive cellulose chemistry. Volume I. Wiley-VCH,Weinheim; New York,43-82.

Lawoko, M., G. Henriksson and G. Gellerstedt, 2005. Structural Differences between the Lignin-Carbohydrate Complexes Present in Wood and in Chemical Pulps, *Biomacromolecules*, 6(6), 3467-3473.

Levitt, M. H., 2008: Spin dynamics : basics of nuclear magnetic resonance. John Wiley & Sons,Chichester, England ; Hoboken, NJ

Li, J., R. Martin-Sampedro, C. Pedrazzi and G. Gellerstedt, 2011a. Fractionation and characterization of lignin-carbohydrate complexes (LCCs) from eucalyptus fibers, *Holzforschung*, 65(1), 43-50.

Li, J., J. K. Park, R. B. Moore and L. A. Madsen, 2011b. Linear coupling of alignment with transport in a polymer electrolyte membrane, *Nature Materials (Published online: June 19, 2011)*

Li, J., K. G. Wilmsmeyer and L. A. Madsen, 2008. Hydrophilic channel alignment modes in perfluorosulfonate ionomers: Implications for proton transport, *Macromolecules*, 41(13), 4555-4557.

Li, J., K. G. Wilmsmeyer and L. A. Madsen, 2009. Anisotropic Diffusion and Morphology in Perfluorosulfonate Ionomers Investigated by NMR, *Macromolecules*, 42(1), 255-262.

Loo, L. S., R. E. Cohen and K. K. Gleason, 2000. Deuterium nuclear magnetic resonance of deuterium oxide in nylon 6 under active uniaxial deformation, *Polymer*, 41(21), 7699-7704.

MacGregor, R. P., H. Peemoeller, M. H. Schneider and A. R. Sharp, 1983. Anisotropic diffusion of water in wood, *J. Appl. Polym. Sci.: Appl. Polym. Symp.*, 37(Proc. Cellul. Conf., 9th, 1982, Part 2), 901-909.

Maki-Arvela, P., I. Anugwom, P. Virtanen, R. Sjoholm and J. P. Mikkola, 2010. Dissolution of lignocellulosic materials and its constituents using ionic liquids-A review, *Industrial Crops and Products*, 32(3), 175-201.

Olsson, A.-M., I. Bjurhager, L. Gerber, B. Sundberg and L. Salmén, 2011. Ultra-structural organisation of cell wall polymers in normal and tension wood of aspen revealed by polarisation FTIR microspectroscopy, *Planta*1-10.

Page, D. H., F. El-Hosseiny, M. L. Bidmade and R. Binet, 1976. Birefringence and the chemical composition of wood pulp fibers, *Applied Polymer Symposium*, 28923-929.

Park, J. K., J. Li, G. M. Divoux, L. A. Madsen and R. B. Moore, 2011. Oriented Morphology and Anisotropic Transport in Uniaxially Stretched Perfluorosulfonate Ionomer Membranes, *Macromolecules*, 44(14), 5701-5710.

Ruel, K. and J.-P. Joseleau, 2005. Deposition of hemicelluloses and lignins during secondary wood cell wall assembly., The hemicelluloses workshop 2005. , University of Canterbury, Christchurch, 103–113,

Saalwachter, K., 2007. Proton multiple-quantum NMR for the study of chain dynamics and structural constraints in polymeric soft materials, *Progress in Nuclear Magnetic Resonance Spectroscopy*, 51(1), 1-35.

Sadoh, T., 1981. Viscoelastic Properties of Wood in Swelling Systems, *Wood Science and Technology*, 15(1), 57-66.

Sadoh, T. and E. Yamaguchi, 1968. Swelling of wood in amines and the rigidity of wood swollen with amines, *Bulletin of the Kyoto University Forests*, 40276-283.

Salmén, L., 2007. The mechanical deformation of wood—relation to ultrastructure., The comprised wood workshop 2007. , University of Canterbury, Christchurch, 143-157,

Salmén, L. and I. Burgert, 2009. Cell wall features with regard to mechanical performance. A review: COST action E35 2004-2008: wood machining - micromechanics and fracture, *Holzforschung*, 63(2), 121-129.

Sjöström, E., 1993: Wood chemistry : fundamentals and applications. Academic Press,San Diego,51.

Sjöström, E. and R. Alén, 1999: Analytical methods in wood chemistry, pulping, and papermaking. Springer,Berlin; New York

Stevanic, J. S. and L. Salmén, 2009. Orientation of the wood polymers in the cell wall of spruce wood fibres, *Holzforschung*, 63(5), 497-503.

Tanner, J. E., 1970. Use of the stimulated echo in NMR diffusion studies, *Journal of Chemical Physics*, 52(5), 2523-2526.

Chapter 6 Probing hydroxymethyl resorcinol-wood interactions through compressive-torsion DMA and rheo-IR spectroscopy

Sudip Chowdhury and Charles E. Frazier
Macromolecular Science & Engineering, Wood Science & Forest Products
Virginia Tech, Blacksburg VA 24061, U.S.A.

6.1. Abstract

Hydroxymethyl resorcinol (HMR) is a powerful wood-adhesion promoter. However the fundamental wood-HMR interactions are still unresolved. This study utilized compressive-torsion DMA under solvent plasticization and rheo-infrared spectroscopy to elucidate some important aspects of wood-HMR interactions. Compressive torsion DMA revealed that HMR significantly altered the relaxation behavior of wood amorphous phase. Both short-range configurational motions and long-range entanglements were modified. Curiously, the detection of HMR effects in compressive-torsion DMA was highly plasticizer dependent. For instance, the effects on amorphous phase crosslink density were prominent in water, whereas the effects on the short-range motions (glassy response) were clearly observed while specimens were plasticized in DMF. Rheo-IR spectroscopy indicated that HMR altered the molecular level stress-distribution mechanism in wood cell wall; cellulose experienced less load in HMR treated wood, indicating perhaps a higher participation of amorphous domain in load bearing.

6.2. Introduction

Sustainable utilization of bio-resource demands production of highly durable wood composites for its multi-billion dollar industry in North America. Several approaches have been utilized to enhance wood-composite durability including chemical modification of wood and adhesives. Hydroxymethyl resorcinol (HMR) is one such wood adhesion promoter which generated great interests among wood-science community since its discovery by Vick et al. (1995). As an aqueous alkaline solution, HMR is applied as a primer on bonding surface and this treatment dramatically improves bond durability of several wood species and adhesives. Since 1995 multiple studies have demonstrated the HMR efficacy in different systems such as, preservative treated wood bonded with epoxy (Vick *et al.*, 1995; Vick *et al.*, 1996), wax-treated wood bonded with melamine formaldehyde and polyvinyl acetate (Kurt *et al.*, 2008), composite with phenolic adhesive and yellow cedar wood (Okkonen and Vick, 1998), composite with moisture cure polyurethanes (Vick and Okkonen, 2000; Christiansen *et al.*, 2001; Lopez-Suevos and Richter, 2009) and wood-fiber reinforced vinyl ester materials (Lopez-Anido *et al.*, 2000).

Although the HMR efficacy is well established and over last decade many significant findings have improved our understanding of HMR-wood interactions, the fundamental mechanism behind this durability enhancement is still unclear. Vick et al. (1998) suggested that the efficacy of HMR depends strongly on its molecular weight distribution. An ensemble of methylolated monomers, dimers, and higher molecular weight oligomers and polymers are required, indicating the need for HMR to penetrate cell wall. Subsequently cell wall penetration and resulting reduction in swelling was

demonstrated by Son and Gardner (2004b). Son and Gardner (2005) studied the thermomechanical behavior of HMR treated Maple wood veneers using dynamic mechanical analysis (DMA) and claimed a plasticization of lignin with HMR, resulting in a reduction of glass-transition temperature (Tg). However, it must be noted that at the specified solvent content in this study (~7-15%), the lignin Tg should be well above 150 °C (Back and Salmén, 1982), therefore, it seems unlikely that the observed relaxation in this study could be from lignin relaxation. Employing isothermal stress-relaxation of HMR treated yellow-poplar Sun and Frazier (2005) reported that HMR increased the intermolecular cooperativity and characteristic relaxation time of wood-amorphous domain, thereby stiffening the wood, perhaps by physical or chemical crosslinking.

As evident from the previous section, the HMR durability enhancement mechanism is still unresolved which probably has hindered its industrial application or perhaps the development of similar wood-adhesion promoters. In an effort to shed light on HMR-wood interactions, two powerful techniques were employed in this study. Effects of HMR on wood-amorphous domain is effectively studied using recently developed parallel-plate compressive torsion DMA (Chowdhury *et al.*, 2010). Subsequently, infrared spectroscopy coupled with mechanical loading (rheo-IR)was used to investigate the effects of HMR treatment on micromechanical interactions between the cell wall polymers (Salmén and Bergstrom, 2009).

6.3. Experimental

6.3.1. Materials

All specimens were acquired from a single piece of southern yellow-pine (*Pinus spp.)* sapwood lumber (100×100×450 mm) with 2 to 4 growth rings per centimeter. Cylindrical (8 mm dia. 6 mm thick) DMA specimens were machined using a “plug-cutter.” Cylindrical specimens were tested in parallel-plate compressive-torsion using a TA instruments AR 2000 rheometer such that the cylinder axis (thickness direction, radial grain direction) was parallel to the torsional axis and the cylinder ends (tangential surfaces) were in contact with the parallel-plates; torsional slippage was prevented with a compressive clamping force (specified below) exerted by the parallel-plates. Rheo-IR specimens (25 mm× 25 mm ×40 μm: length × width × thickness) were microtomed from water saturated early wood. Specimens were cut in the tangential plane with fiber direction parallel to the length. Four different plasticizing solvents were used: distilled water, N, N-dimethylformamide (DMF, >99.8%), N-methyl-2-pyrrolidone (NMP, 99.5%) and ethylene glycol (99.8%).

6.3.2. HMR treatment

Hydroxymethyl resorcinol (HMR) solution was prepared following the method described by Vick et al. (1995); an aqueous alkaline mixture (pH: 8.4) of resorcinol and formaldehyde was allowed to react for 4 h and then impregnated in southern yellow-pine (SYP) specimens using a vacuum-pressure treatment (5 mm Hg for 45 min, followed by atmospheric pressure for 15 min). After impregnation, specimens were dried at ambient condition for 12 h, and separated into two sample groupings: partially cured

specimens, where no further thermal treatment was imposed; cured specimens, where an additional heat treatment (150 °C, 1 h) was imposed to prevent any changes that might occur in subsequent analysis. A separate set of specimens were treated with aqueous NaOH solution (pH 8.4), dried and heated as for the "cured" specimens and considered as control for the cured specimens. The control for partially-cured specimens was not treated in any way. Thereafter, all specimens were vacuum-dried (0.04-0.1 mm Hg, 24 h, ambient temperature) and stored in a desiccator (anhydrous P_2O_5 and N_2) for at least 48 h prior to analysis.

6.3.3. Methods

Compressive-torsion DMA

Compressive-torsion DMA was conducted following the protocol of Chowdhury et al.(2010). Specimens were saturated with plasticizer using a vacuum-pressure treatment (5 mm Hg for 1 h, followed by atmospheric pressure for at least 24 h). Partially cured specimens were tested with water and DMF as plasticizers, while the cured specimens were tested with DMF, NMP and ethylene glycol as plasticizers. Solvent submersion was conducted such that the bottom plate was surrounded by a stainless steel cup that maintained specimen immersion during analysis. All tests were performed under anhydrous N_2 gas; liquid N_2 was used to control temperature. Compressive clamping was achieved with a 20 N static normal force, representing approximately 1.5% and 14% of the wet compression strength respectively parallel and perpendicular to grain (Green *et al.*, 1999). Specimens were subjected to a sequential heat/cool treatment as follows: 1) heat to maximum temperature (3°C/min, 5 Hz); hold

20 min, 2) cool to minimum temperature, (3 °C/min, 5 Hz). All tests were conducted in stress-control with stress settings very near but not greater than the linear viscoelastic response limits. Temperature ranges were chosen to avoid plasticizer freezing and to minimize excessive evaporation (Water: 5 – 95 °C, DMF: -10 – 80 °C, NMP: -30 – 130 °C and ethylene glycol: 0 – 120 °C). When organic solvents are used as plasticizers, precaution is required to avoid solvent/air mixtures near the solvent flash point; the oven chamber should never be opened at elevated temperatures.

FTIR measurements

Fourier transform infrared (FTIR) spectra were recorded on a Thermo Nicolet 8700 spectrometer in transmission mode. A liquid nitrogen cooled mercury-cadmium-telluride detector was used and the IR radiation was polarized with a wire-grid polarizer aligned parallel (0°) to the tensile loading direction. The 40 µm thick SYP specimens were mounted between parallel jaws of a polymer stretcher (PM-100, Manning Applied Technology, Troy, ID, USA) with fiber direction parallel to the tensile loading direction. The polymer stretcher was equipped with a micrometer to apply exact strain and a load transducer to observe the resulting load. The strain was calculated with original clamping length ($\varepsilon = \Delta l / L$) and the stress was calculated on the basis of the specimen's initial dimension. A ~1 N preload force was applied to the specimen. The stretcher with the specimen was placed in the spectrometer sample compartment under dry air purge for 30 minutes before measurements. Thereafter the strain was increased with ~0.5% steps until the specimen ruptured. At each strain level a 1 minute time period was imposed prior to spectra collection (4 cm^{-1} resolution, 16 scans). Spectra were

processed using Omnic® 7.3 (Thermo Nicolet Corp.). The spectra were baseline corrected by setting the absorbance equal to zero at 3700, 1800, 1544 and 780 cm^{-1} ; normalization was achieved by setting the 1058 cm^{-1} absorbance intensity equal to 1. Three specimens were tested for each sample group and average spectra were reported.

6.4. Results and discussion

The effects of HMR treatment on wood was investigated using solvent submersion parallel-plate compressive-torsion DMA. Consequently these observations probed the impact that HMR had on the wood glass/rubber transition that occurs under solvent submersion. Depending upon the solvent, the corresponding glass transition temperature (Tg) ranges from 45 – 100 ˚C (Salmén, 1984; Chowdhury *et al.*, 2010). Figure 6-1 demonstrates the effects of partial HMR cure in southern yellow-pine (SYP) specimens saturated in water; 1st heating and 1st cooling DMA scans are shown.

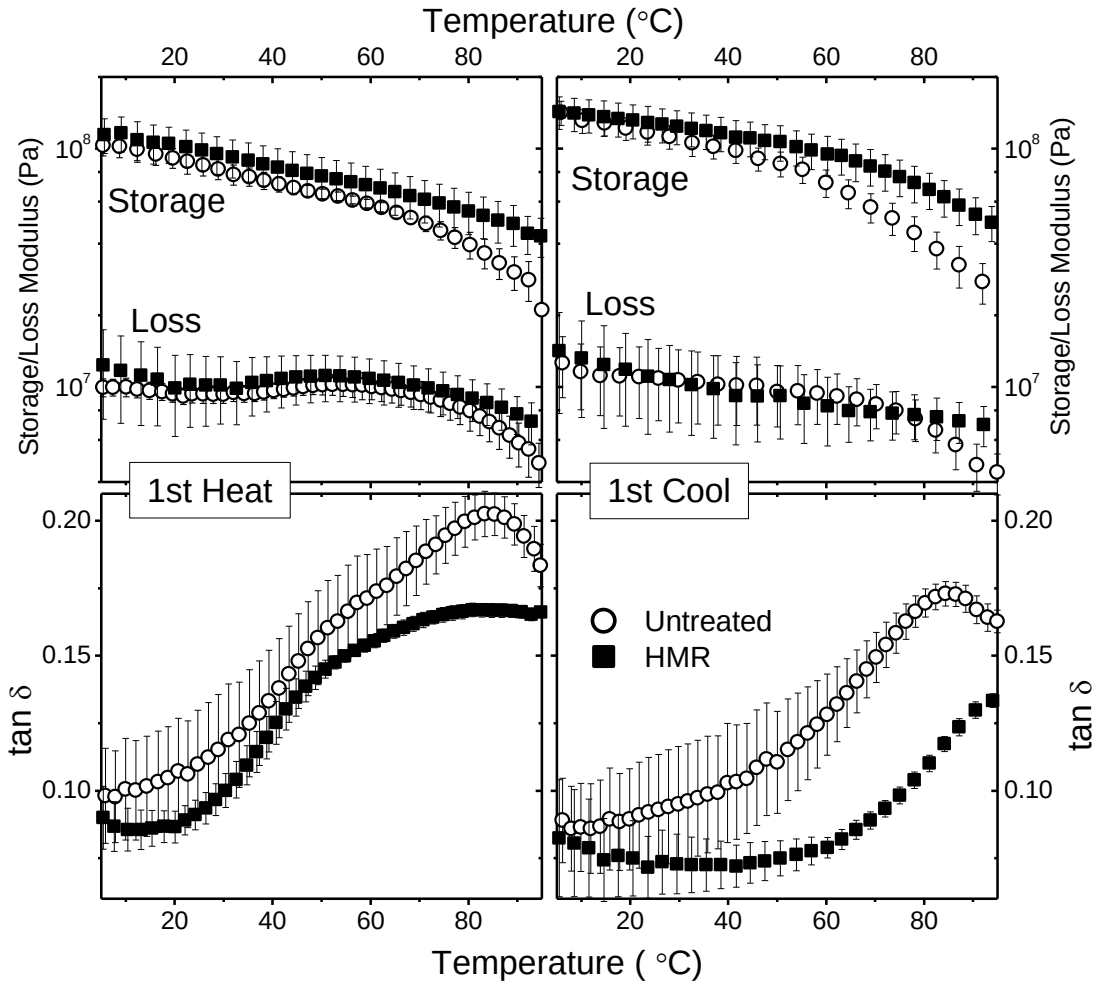

Figure 6-1 Effects of partially-cured HMR on dynamic mechanical response of water saturated SYP. Average 1st heating and 1st cooling scans are shown which were separated by a 20 min isothermal condition at the maximum temperature. Error bars represents ±1 standard deviation (n=3).

Considering the first heat, it is seen that partially cured HMR caused a minor stiffness increase that is most apparent at the high temperature rubbery region. Minor changes in the loss modulus occurred such that the tan δ response was dramatically altered; damping breadth was increased while the intensity was reduced. While tan δ changes were significant, it was not clear if the Tg (defined as temperature of the tan δ

maximum) was actually changed. However the stiffness increase near the rubbery region implies some degree of matrix crosslinking. HMR effects became clearer in the first cool, which occurred after a 20 min heating period at the maximum temperature (95 ˚C). The first cool demonstrates that additional HMR cure occurred such that the rubbery stiffness was increased, and the Tg was increased but with a tan δ intensity reduction.

The specimen conditions in Figure 6-1 are somewhat analogous to those occurring in the standard adhesion test commonly referred to as the delamination test (ASTM D2559). The delamination test is perhaps the greatest hurdle towards certification of structural wood adhesives; it imposes two cycles of the following treatment: vacuum/pressure water impregnation, 65 ˚C drying (21.5 h), 100 ˚C steaming (90 min). In this context the first heat in Figure 6-1 is analogous to delamination test conditions prior to and including the steam treatment; whereas the first cool resembles the delamination specimen after the HMR curing that would occur during steaming. Cooling that occurs as steaming is terminated.

Table 6-1 Summary of solvent plasticized SYP wood glass transition temperatures (Tg: temp at tan δ max) as a function of partially cured HMR treatment. Average (n =3) values are reported with ±1 standard deviation in parenthesis.

Treatment	Solvent	1st Heat Tg	1st Cool Tg
Untreated SYP	Water	84 (1)	86 (0.3)
	DMF	44 (3)	27 (0.5)
SYP + Partially-cured HMR	Water	No peak or > 95 °C	No peak or > 95 °C
	DMF	41 (1.3)	30 (1.5)

Effects of partially cured HMR on lignocellulose mobility were further investigated under DMF-plasticized conditions Figure 6-2.

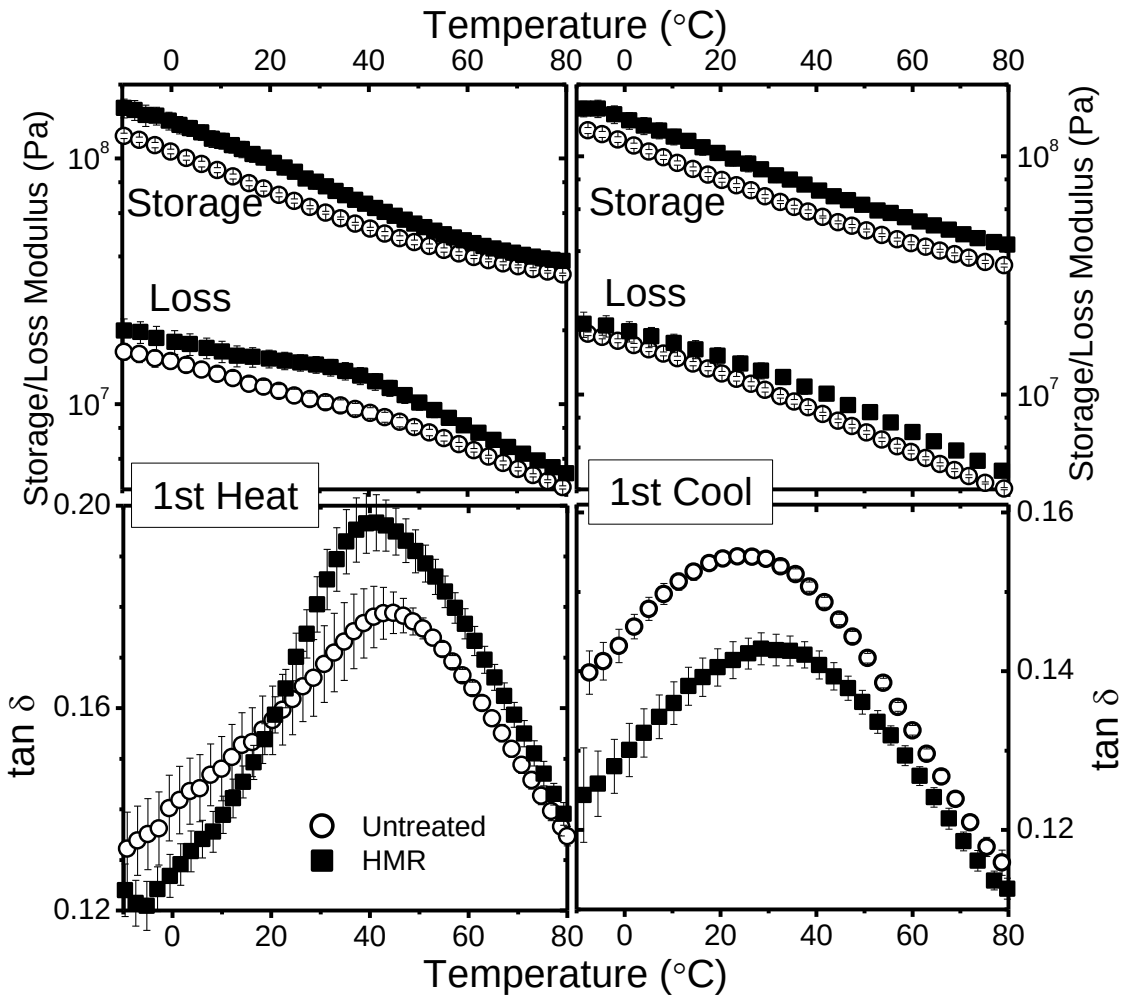

Figure 6-2 Effects of partially cured HMR on dynamic mechanical response of DMF-plasticized southern yellow-pine. Average 1st heat and 1st cool are shown. Error bars represent ±1 standard deviation (n=3). Note: variable tan δ scale.

DMF is an extremely powerful wood-swelling agent (volumetric swelling > 26%) and mobilizes lignocellulosic polymers differently than other organic solvents (Chowdhury and Frazier, 2011a, b). In 1st heat, the partially cured HMR treatment increased the storage modulus that is most prominent in the glassy region. The loss

modulus was also increased, such that the tan δ response was significantly altered; the relaxation breadth was decreased with significant increase in the damping intensity. The lignin Tg was slightly reduced with HMR treatment. These observations implicate the existence of HMR monomers or oligomers in the wood-amorphous domain, causing a plasticization to the lignin relaxation, thereby enhancing the damping intensity and slightly reducing the lignin Tg. In 1st cool (after 20 min heating at 80 ˚C) additional curing was evident such that the stiffness increased across the whole temperature range, and the lignin Tg was increased (~ 3 °C, Table 6-1) with significant reduction in damping intensity.

Interestingly water and DMF probed HMR-lignocellulose interactions differently. Recall that in water the effect of partially cured HMR was more prominent in the rubbery region (Figure 6-1, 1st heat). Conversely, DMF revealed the changes in the glassy region (Figure 6-2, 1st heat). This suggests that DMF and water probed the HMR effects on different molecular motion regimes.

Figure 6-3 and Table 6-2 reports DMA response of SYP treated with HMR and cured at 150 °C for 1 h. As the control, wood was treated with aqueous NaOH solution of exactly same pH as the HMR solution, and then heat treated similarly. DMA scans were performed in ethylene glycol, NMP and DMF. HMR has demonstrated efficacy in hot-press wood-adhesive composites and cured HMR analysis should simulate the wood-HMR interactions in such systems.

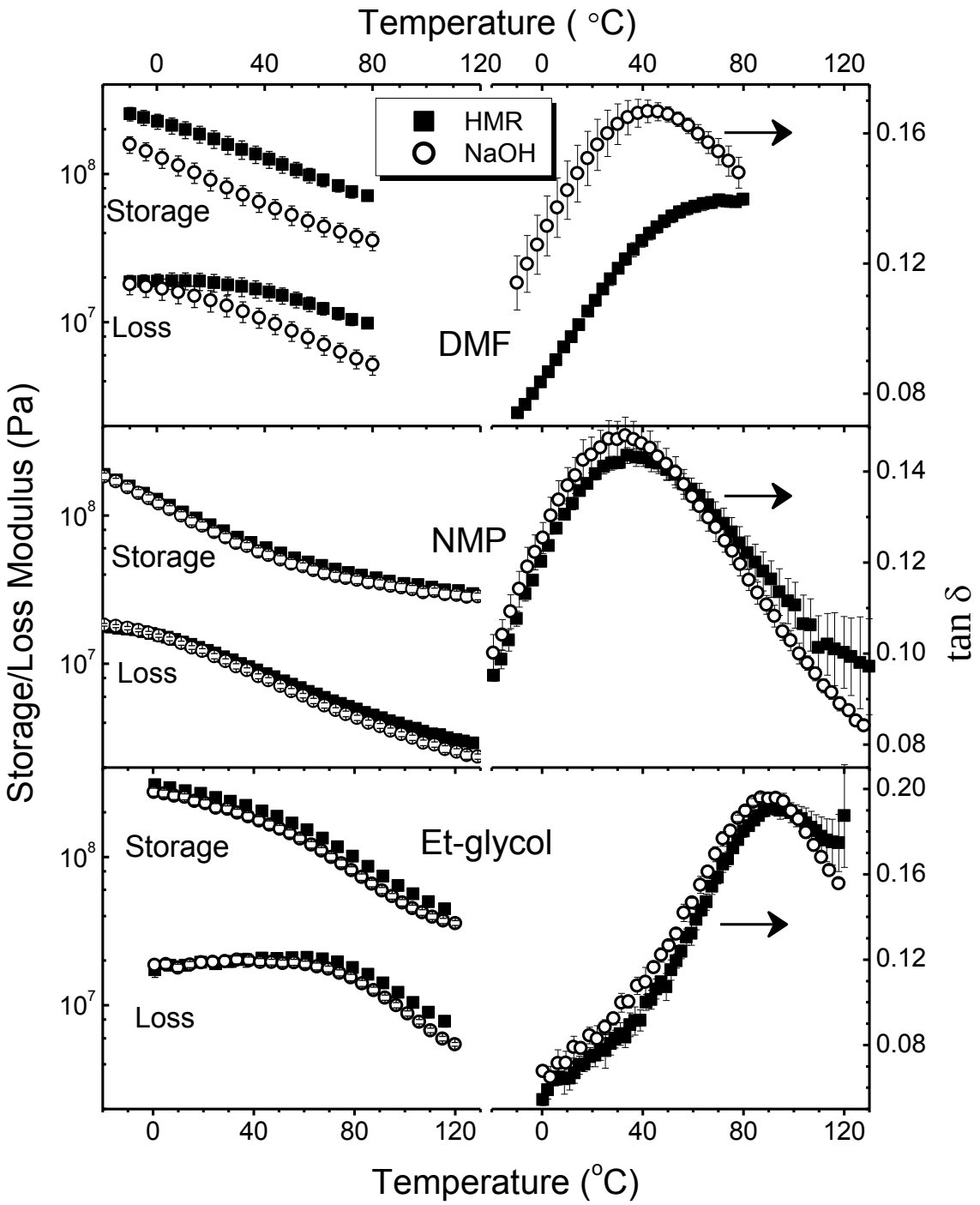

Figure 6-3 Comparison of hydroxymethyl resorcinol (HMR) and aqueous NaOH treatments on the dynamic mechanical properties of solvent plasticized southern yellow-pine wood. Average (n = 3) cooling scans are presented, which were preceded by 1st heating scan and 15 min thermal conditioning at the maximum temperature. Error bars represent ±1 standard deviation. Note: identical moduli scale, variable tan δ scale.

Table 6-2 Effects of cured HMR on the lignin glass-transition temperature of solvent plasticized SYP. Aqueous NaOH (pH: 8.4) treated wood was used as control. Average (n=3) 1st heat and 1st cool Tgs are reported with ± standard deviations in the parenthesis. Note: The 1st heat Tg for NMP plasticized specimens were missing due to experimental problem.

Treatment	Solvent	1st Heat Tg	1st Cool Tg
NaOH + 150 °C, 1 h heat	Ethylene glycol	90 (2)	92 (4)
	DMF	53 (2)	46 (2)
	NMP	48 (5)	34 (2)
HMR + 150 °C, 1 h heat	Ethylene glycol	101 (1)	93 (3)
	DMF	70 (2)	> 80 °C
	NMP	--	38 (2)

In ethylene glycol, the 1st heat lignin Tg increased (~ 10 °C) with HMR treatment, however, in the 1st cool this increase was not evident (Table 6-2). The storage modulus was slightly increased, especially in the rubbery region, implicating increase in the crosslink density. In addition to the major transition HMR treated specimens indicated another high temperature transition. This high temperature relaxation only appeared in ethylene glycol and its origin is yet unknown and needs further investigation. In NMP, small increase in the lignin Tg (~ 2 °C) was observed with HMR treatment, no discernable change in the moduli was observed. Intriguing results were obtained for DMF plasticized specimens. Significant increase in the stiffness was observed. More curiously, the lignin Tg was dramatically increased with HMR treatment. In the 1st heat, ~17 °C Tg increase was recorded. In the 1st cool the tan δ peak could not be seen, either due to Tg > 80 °C, or extreme broadening of the peak due to very little softening.

This huge Tg increase or diminished softening clearly indicates that the lignocellulose mobility was significantly restricted by HMR. However, more interesting was that detection of this effect was highly solvent dependent. DMF and NMP are both tertiary amides with very similar wood-swelling power (Chowdhury and Frazier, 2011a). Nevertheless, it is evident that the mechanism of lignocellulose mobilization is very different in DMF as compared to NMP and also ethylene glycol.

Compressive torsion DMA indicated significant changes in the in-situ lignocellulose mobility with HMR treatment. However, it was not clear which polymer was altered or how the micromechanical interactions between cell wall polymers had changed. Cell wall is a complex composite of semi-crystalline cellulose embedded in the amorphous matrix of hemicelluloses and lignin (Salmén and Burgert, 2009). The mechanical response of wood depends on its component polymers and interactions between them. Vibrational spectroscopy (Raman and infrared) coupled with mechanical stimulus has been successfully used to gain valuable insights regarding the interactions and mechanisms of load transfer between cell wall polymers (Gierlinger *et al.*, 2006; Salmén and Bergstrom, 2009). When loaded along the fiber, the crystalline cellulose bears most of the load. In the IR spectra significant shift in the characteristic cellulose bands take place, indicating celluloses role in load bearing. Specifically the cellulose band at 1160 cm^{-1}, related to the antisymmetric C-O-C vibration of the skeletal bond of glucose ring, has been found to be a reliable measure of cellulose deformation and molecular level stress distribution in wood (Hinterstoisser *et al.*, 2003; Salmén and Bergstrom, 2009).

Figure 6-4 demonstrates the IR absorbance spectra for 40 µm thick untreated and partially cured HMR treated SYP wood. Note that no heat treatment was involved in partially cured HMR treatment. Additionally, all IR experiments were conducted under dry condition.

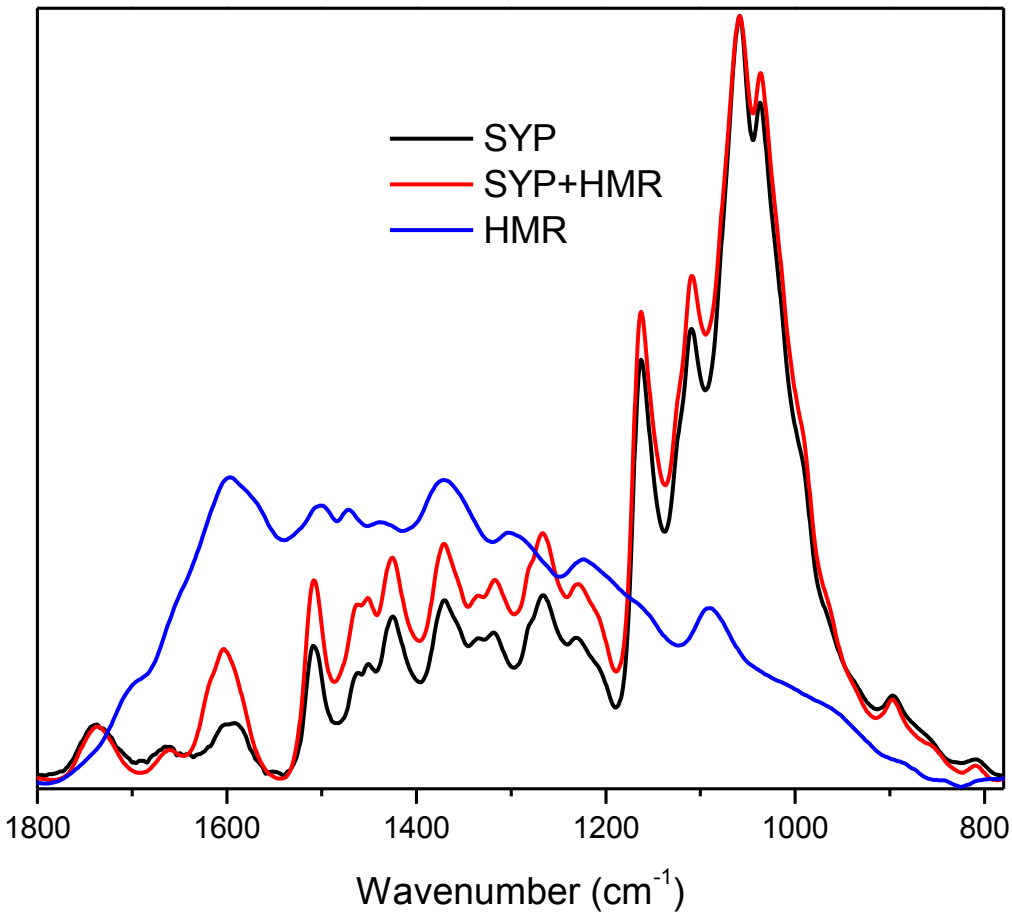

Figure 6-4 Average (n=3) infrared absorption of untreated and partially-cured HMR treated southern yellow-pine wood. Spectra were baseline corrected at 1800, 1546 and 780 cm^{-1}, normalized (0,1) at 1058 cm^{-1} and averaged. Also included is the spectra for neat HMR.

It is evident from the spectra that HMR treatment did not induce any significant peak shift in the wood's fingerprint region (1800 – 750 cm^{-1}). The intensity change in the HMR treated wood spectra was due to the presence of HMR in the system. This indicates that perhaps HMR did not chemically react with in-situ lignocelluloses.

Figure 6-5 reports the average stress-strain plot for partially-cured HMR treated and untreated SYP sections, while stretched along the fiber direction during the IR measurements.

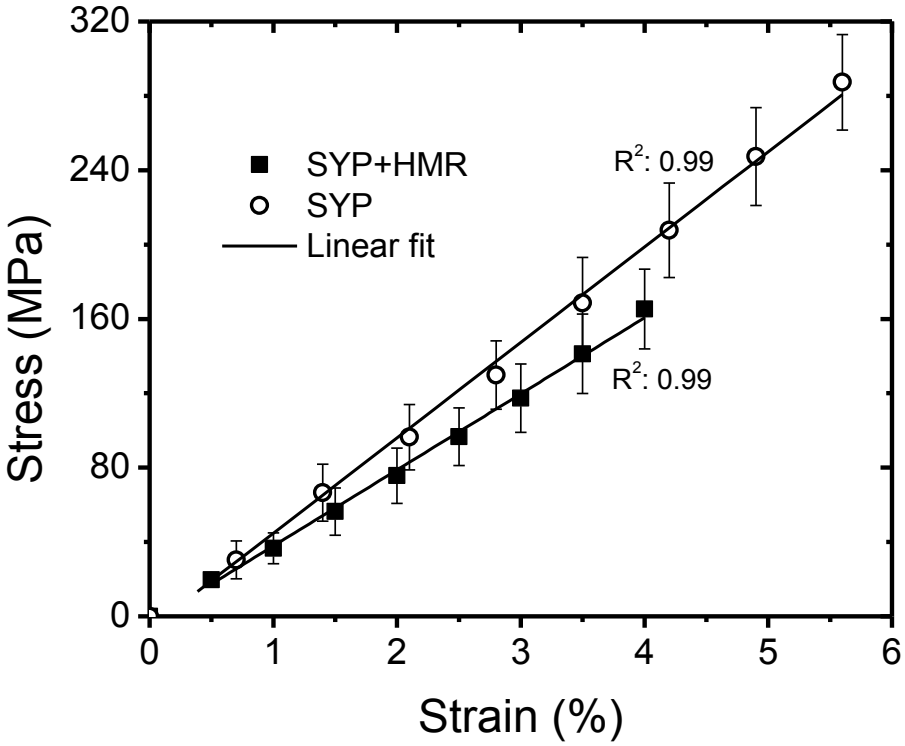

Figure 6-5 Average (n=3) stress-strain plots for partially-cured HMR treated and untreated southern yellow-pine wood section (40 µm thick). Strain calculated on the basis of initial length between the clamps, stress calculated on the basis of specimen dimension. Linear fit to the average plot is also included. Error bars represent ±1 standard deviation.

Both sample demonstrated elastic response until ruptured at the maximum strain (data not shown). The average maximum stress/strain was lower for the HMR treated specimens (160 MPa and 4%), as compared to the untreated SYP (260 MPa, 5.6%). A marginally lower slope for HMR treated specimens indicated slightly lower stiffness, perhaps due to the presence of unpolymerized HMR monomers and oligomers which may have increased the toughness of the system.

Tensile loading along the fiber direction induced significant shifts of cellulose bands towards the lower wavenumber. Figure 6-6 demonstrates the peak shift for absorption band at 1160 cm^{-1} corresponding to the C-O-C vibration in a partially-cured HMR treated SYP wood section. Significant shift in the peak maxima was recorded for both untreated and treated specimens, upon tensile loading. This demonstrates the extension of the C-O-C bond length causing a lower frequency vibration (Wool, 1981; Salmén and Bergstrom, 2009).

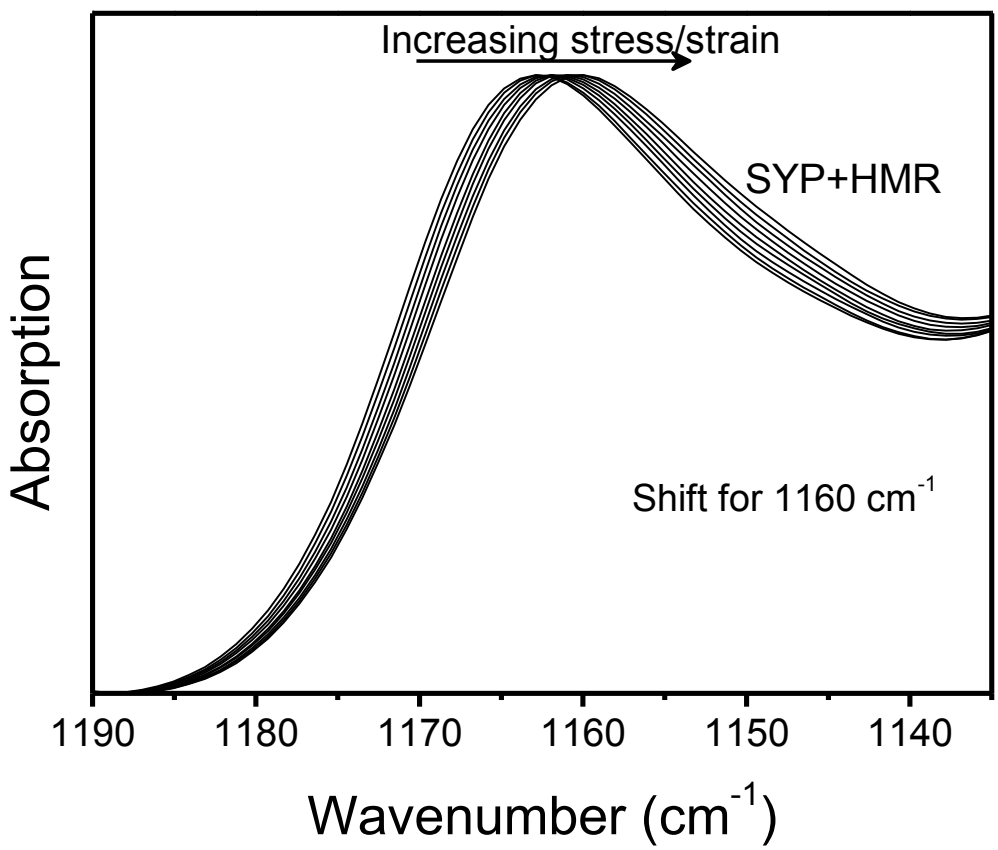

Figure 6-6 Absorption spectra of C-O-C antisymmetric vibration peak of cellulose at 1160 cm^{-1} as a function of stress/strain for partially-cured HMR treated southern yellow-pine wood. With increasing stress the peak shifted to lower wavenumber.

Average (n=3) shift in the 1160 cm^{-1} peak as a function of strain is shown in Figure 6-7 along with linear fit.

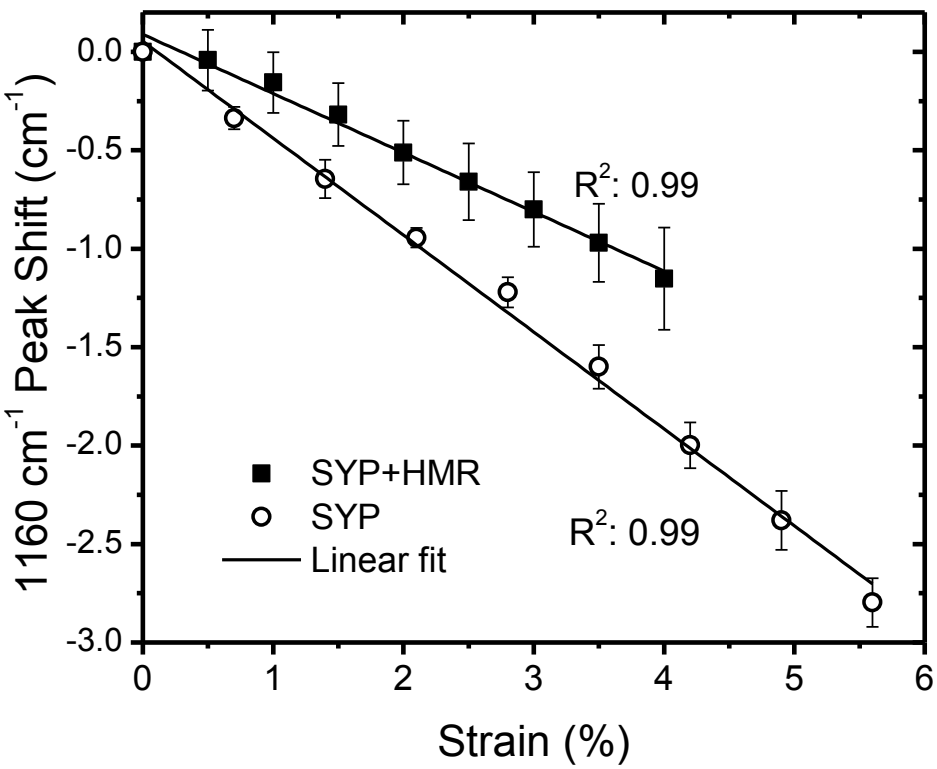

Figure 6-7 Average (n=3) of the C-O-C peak at 1160 cm^{-1} as a function of tensile strain for partially-cured HMR treated and untreated southern yellow-pine wood. Linear fits to the data were also included. Error bars represents ±1 standard deviation.

The peak shift was linear as a function strain. This trend is in accordance with previous IR and Raman studies on the effects of mechanical loading on *Picea abies* (Gierlinger *et al.*, 2006; Salmén and Bergstrom, 2009). Interesting difference was observed between HMR treated and untreated wood. The slope of peak shift as a function of strain in untreated SYP was significantly higher as compared to the HMR treated wood. As mentioned before, the peak shift towards the lower wavenumber is directly proportional to the increase in the covalent bond length and a measure of the load experienced by that specific bond. Lower slope in the HMR treated wood indicates

that that the C-O-C bond (and the glucose ring) was less strained as compared to the untreated wood. This suggests that cellulose chains were bearing less load, with perhaps more load experienced by the amorphous phase. Therefore, the stress transfer mechanism between amorphous and crystalline phase in wood is modified with HMR treatment. Perhaps the mobility of cellulose chain was also restricted by the modified amorphous domain. However, the lignin and hemicellulose peaks did not show any stress/strain effects, similar to the findings from previous studies where characteristic lignin, xylan and glucomannan peaks did not shift as a function of tensile loading (Gierlinger *et al.*, 2006; Salmén and Bergstrom, 2009). In cell wall wood-polymers form a very interactive composite and it is difficult to exclude molecular straining of amorphous polymers during macroscopic loading. However, no shift of the characteristic peaks during mechanical loading suggest that either the bonds responsible for characteristic peaks do not significantly involve in stress transfer, or perhaps the stress is instantaneously transferred from the amorphous polymers to the rigid cellulose and no stress effect could be seen on lignin and hemicelluloses.

It is evident from the compressive-torsion DMA and IR spectroscopy that HMR penetrates the cell wall and significantly alters wood ultrastructure, which is in accordance to previous reports (Son and Gardner, 2004b; Sun and Frazier, 2005). Simple impregnation of dilute HMR solution altered both short range configurational motions and long range entanglements (effective cross-link density) within the wood-amorphous domain. However in compressive-torsion DMA the detection of HMR effect was highly plasticizer dependent. Water and DMF revealed information of different molecular motions. The solvent effect was highly significant in cured HMR treated

wood. HMR effect was marginal when wood was plasticized with ethylene glycol and NMP, and it was dramatic when tested in DMF. This demonstrates the fundamental differences in the interactions of lignocelluloses with different solvents, as suggested before (Chowdhury and Frazier, 2011a, b). It is reasonable to postulate that the HMR efficacy is closely related to the changes in the crosslink density as well as modification of the short-range configurational motions. The increased crosslink density should reduce the wood swelling, thereby stabilizing the bondline from swelling stress, which is indicated before (Son and Gardner, 2004b; Sun and Frazier, 2005). Modification in the short-range configurational motions must also impact the energy dissipation. Partially-cured HMR treated wood showed higher damping (higher loss modulus and tan δ intensity) when investigated in DMF. This indicates that the enhanced localized or short-range mobility in HMR treated wood is efficient in energy dissipation and can further contribute to the enhanced bondline stability. Although long range mobility restriction due to HMR treatment is evident, formation of covalent bonds between HMR and lignocelluloses seemed unlikely from the IR spectra. Therefore, it seems reasonable to support the hypothesis of HMR forming an interpenetrating network inside the wood amorphous phase and physically restricting the mobility (Sun and Frazier, 2005; Gardner *et al.*, 2006). Novel information regarding the stress transfer mechanism in HMR treated wood was revealed using IR spectroscopy coupled with tensile loading. HMR changed the fundamental micromechanical interactions between crystalline and amorphous phase; cellulose experienced lower degree of loading in HMR treated wood. However, no stress induced changes in the amorphous phase spectral responses were observed. Nevertheless, from the changes in the cellulose loading it can be implied that

perhaps the interpenetrating network of HMR caused a more uniform load distribution between the crystalline and amorphous domain, which could relate to the formation of a mechanically stable and highly durable wood-adhesive bondline.

6.5. Summary

This study reveals some important aspects of HMR-lignocellulose interactions using compressive-torsion DMA and IR spectroscopy coupled with tensile loading. Solvent submersion compressive-torsion DMA revealed that the HMR treatment significantly alters the mobility of amorphous domain; both short-range configurational motions and long-range entanglements were modified, enhancing the energy dissipation and contribute to the previously reported swelling reduction, respectively. The detection of HMR effects were plasticizer dependent. For instance, while in water HMR effects on long-range entanglements were more prominent, whereas in DMF changes in the short-range localized motions were probed. This demonstrated the fundamental differences in the lignocellulose mobility in different solvents and perhaps different wood-polymeric regimes can be probed using different plasticizers. IR spectroscopy coupled with mechanical loading showed great potential in analyzing effects of chemical or any other relevant treatments on the micromechanical interactions between in-situ wood-polymers. HMR treatment changed fundamental stress distribution mechanism within wood cell wall. Summarily, the efficacy of HMR treatment closely relate to the fundamental polymer mobility change and the stress distribution inside the wood cell wall causing a more stable wood-adhesive bondline. Compressive-torsion DMA and IR spectroscopy coupled with mechanical stimulus shows potential in

advancing the lignocellulose rheology to better understand chemical treatments relevant to biomass deconstruction or durable wood-composite manufacturing.

6.6. References

Back, E. L. and L. Salmén, 1982. Glass transitions of wood components hold implications for molding and pulping processes, *Tappi*, 65(7), 107-110.

Chowdhury, S., J. Fabiyi and C. E. Frazier, 2010. Advancing the dynamic mechanical analysis of biomass: comparison of tensile-torsion and compressive-torsion wood DMA, *Holzforschung*, 64(6), 747-756.

Chowdhury, S. and C. E. Frazier, 2011a. Chapter 3: Compressive-torsion DMA of wood in organic media *in* Advancing characterization techniques for structure-property determination of in-situ lignocelluloses, Macromolecules and Interefaces Institute and Department of Wood Science and Forest Products, Virginia Polytechnic Institute and State University, Blacksburg, VA,

Chowdhury, S. and C. E. Frazier, 2011b. Chapter 4: Time-temperature equivalence and fragility of organic solvent plasticized wood *in* Advancing characterization techniques for structure-property determination of in-situ lignocelluloses, Macromolecules and Interefaces Institute and Department of Wood Science and Forest Products, Virginia Polytechnic Institute and State University, Blacksburg, VA,

Christiansen, A. W., C. B. Vick and E. A. Okkonen, 2001. Enhanced durability of one-part polyurethane bonds to wood due to the use of HMR primer, *Wood Adhesives 2000, [International Symposium], 7th, S. Lake Tahoe, NV, United States, June 22-23, 2000*489-494.

Gardner, D. J., C. E. Frazier and A. W. Christiansen, 2006. Characteristics of the wood adhesion bonding mechanism using hydroxymethyl resorcinol, 93-97, Forest Products Society.

Gierlinger, N., M. Schwanninger, A. Reinecke and I. Burgert, 2006. Molecular changes during tensile deformation of single wood fibers followed by Raman microscopy, *Biomacromolecules*, 7(7), 2077-2081.

Green, D. W., J. E. Winandy and D. E. Kretschmann. 1999: Mechanical properties of wood. *Wood handbook, wood as an engineering material.*, Madison, WI, USA: Forest Products Society, 1-45.

Hinterstoisser, B., M. Åkerholm and L. Salmén, 2003. Load Distribution in Native Cellulose, *Biomacromolecules*, 4(5), 1232-1237.

Kurt, R., A. Krause, H. Militz and C. Mai, 2008. Hydroxymethylated resorcinol (HMR) priming agent for improved bondability of wax-treated wood, *Holz Roh- Werkst.*, 66(5), 333-338.

Lopez-Anido, R., D. J. Gardner and J. L. Hensley, 2000. Adhesive bonding of eastern hemlock glulam panels with E-glass/vinyl ester reinforcement, *Forest Products Journal*, 50(11/12), 43-47.

Lopez-Suevos, F. and K. Richter, 2009. Hydroxymethylated resorcinol (HMR) and novolak-based HMR (n-HMR) primers to enhance bond durability of Eucalyptus globulus glulams, *Journal of Adhesion Science and Technology*, 23(15), 1925-1937.

Okkonen, E. A. and C. B. Vick, 1998. Bond-ability of salvaged yellow-cedar with phenol-resorcinol adhesive and hydroxymethylated resorcinol coupling agent, *Forest Products Journal*, 48(11-12), 81-85.

Salmén, L., 1984. Viscoelastic properties of in situ lignin under water-saturated conditions, *Journal of Materials Science*, 19(9), 3090-3096.

Salmén, L. and E. Bergstrom, 2009. Cellulose structural arrangement in relation to spectral changes in tensile loading FTIR, *Cellulose*, 16(6), 975-982.

Salmén, L. and I. Burgert, 2009. Cell wall features with regard to mechanical performance. A review: COST action E35 2004-2008: wood machining - micromechanics and fracture, *Holzforschung*, 63(2), 121-129.

Son, J. and D. J. Gardner, 2004b. Dimensional stability measurements of thin wood veneers using the Wilhelmy plate technique, *Wood and Fiber Science*, 36(1), 98-106.

Son, J., W. T. Y. Tze and D. J. Gardner, 2005. Thermal behavior of hydroxymethylated resorcinol (HMR)-treated maple veneer, *Wood and Fiber Science*, 37(2), 220-231.

Sun, N. and C. E. Frazier, 2005. Probing the hydroxymethylated resorcinol coupling mechanism with stress relaxation, *Wood and Fiber Science*, 37(4), 673-681.

Vick, C. B., A. W. Christiansen and E. A. Okkonen, 1998. Reactivity of hydroxymethylated resorcinol coupling agent as it affects durability of epoxy bonds to Douglas-fir, *Wood and Fiber Science*, 30(3), 312-322.

Vick, C. B., R. L. Geimer and J. E. Wood, 1996. Flakeboards from recycled CCA-treated southern pine lumber, *Forest Products Journal*, 46(11-12), 89-91.

Vick, C. B. and E. A. Okkonen, 2000. Durability of one-part polyurethane bonds to wood improved by HMR coupling agent, *Forest Products Journal*, 50(10), 69-75.

Vick, C. B., K. Richter, B. H. River and A. R. Fried, Jr., 1995. Hydroxymethylated resorcinol coupling agent for enhanced durability of bisphenol-A epoxy bonds to Sitka spruce, *Wood and Fiber Science*, 27(1), 2-12.

Wool, R. P., 1981. Measurements of infrared frequency shifts in stressed polymers, *J. Polym. Sci., Polym. Phys. Ed.*, 19(3), 449-457.

Chapter 7 Effects of hydroxymethyl resorcinol treatment on lignocellulose mobility – A creep TTS study

(Short study)

Sudip Chowdhury and Charles E. Frazier
Macromolecular Science & Engineering, Wood Science & Forest Products
Virginia Tech, Blacksburg VA 24061, U.S.A.

7.1. Abstract

Wood-hydroxymethyl resorcinol (HMR) interactions were studied thought creep mode time/temperature superposition (TTS) using parallel-plate compressive torsion analysis. Isothermal creep profiles shifted smoothly to produce smooth creep-compliance master curves and shift factor plots. HMR increased creep-compliance of wood. However, no effects were observed in the shift factor plot. Application of Kohlrausch-Williams-Watts (KWW) equation to the master curves revealed that the characteristic retardation time of wood amorphous domain was significantly increased with HMR treatment, suggesting a resistance in the mobility in the wood amorphous domain.

7.2. Introduction

Application of dilute hydroxymethyl resorcinol (HMR) solution as a primer significantly improves wood-adhesive bond durability (Vick *et al.*, 1995; Okkonen and Vick, 1998; Kurt *et al.*, 2008; Lopez-Suevos and Richter, 2009). As described in Chapter

6, the molecular mechanism underlying HMR efficacy is not fully understood till date. Fundamental changes in wood-polymer mobility as a function of HMR treatment has been investigated using dynamic and static mechanical analysis (Son *et al.*, 2005; Sun and Frazier, 2005). For instance, Sun and Frazier (2005) studied HMR effects on dry *Liriodendron tulipifera* using isothermal stress-relaxation and subsequent application of Kohlrausch-Williams-Watts equation (KWW). The study showed that HMR penetrates the cell wall and increases the cooperativity between non-bonded polymer segments. They speculated formation of crosslinks within the wood cell wall.

A new protocol for compressive-torsion DMA under solvent submersion has been established by Chowdhury et al. (2010) that is useful in analyzing thermomechanical responses of lignocelluloses (Chowdhury and Frazier, 2011a, b, c; Horvath *et al.*, 2011). This study utilizes the abovementioned technique in isothermal creep mode to improve the understanding of the changes in the polymeric behavior with HMR treatment.

7.3. Experimental

7.3.1. Materials

Specimens were acquired from a single piece of southern yellow-pine (*Pinus spp.)* sapwood lumber (100×100×450 mm) with 2 to 4 growth rings per centimeter. Cylindrical (8 mm dia. 6 mm thick) DMA specimens were machined using a “plug-cutter.” Cylindrical specimens were tested in parallel-plate compressive-torsion using TA instruments AR 2000 rheometer such that the cylinder axis (thickness direction, radial grain direction) was parallel to the torsional axis and the cylinder ends (tangential grain) were in contact with the parallel-plates; torsional slippage was prevented with a

compressive clamping force exerted by the parallel-plates (specified below). Ethylene glycol (99.8%) was used as the plasticizer during solvent submersion compressive torsion DMA.

7.3.2. Methods

Standard HMR solution was prepared with 4 h reaction time (Vick *et al.*, 1995). Southern yellow-pine (SYP) discs were vacuum-pressure impregnated with HMR solution to achieve complete saturation (5 mm Hg for 45 min, followed by atm. pressure for 15 min). After impregnation specimens were dried at ambient condition for 12 h and subsequently thermally treated (150 °C, 1 h) to prevent any changes that might occur in subsequent analysis.. A separate set of specimens were treated with aqueous NaOH solution (pH 8.4), dried and thermally treated as for the HMR treated specimens and considered as control. These specimens were then stored in a desiccator (anhydrous P_2O_5 and N_2) for a minimum of 48 h prior to analysis.

Compressive-torsion DMA was conducted following the protocol set by Chowdhury et al. (2010). Specimens were saturated with ethylene glycol using a vacuum-pressure treatment (5 mm Hg for 1 h, followed by atmospheric pressure for at least 24 h). Solvent submersion was conducted such that the bottom plate was surrounded by a stainless steel cup that maintained specimen immersion during analysis. All tests were performed under anhydrous N_2 gas; liquid N_2 was used to control temperature. Compressive clamping was achieved with a 20 N static normal force, representing approximately 1.5% and 14% of the wet compression strength parallel and perpendicular to grain respectively (Green *et al.*, 1999).

All experiments were carried out within the linear viscoelastic response (LVR) limit of solvent plasticized wood. Ethylene glycol plasticized specimens were subjected to a sequential heat/cool/heat as follows: 1) heat to 120 °C(3 °C/min, 5 Hz); hold 20 min, 2) cool to 0 °C, (3 °C/min, 5 Hz), 3) Isothermal creep loading (5 min, 6 – 15 KPa depending upon the LVR limit), 4) Rapid heat (~6-13 °C/min) to next temperature step (10 °C increment), creep recovery (10 min, no load), 5) Repeat steps 3 and 4 over the experimental temperature range (0 – 120 °C). Note, the data from step 3 to 5 were used for creep TTS. Temperature ramp data from step 1 and 2 were discussed in Chapter 6.

Data analysis

Time/temperature-superposition (TTS) master curves were constructed by shifting isothermal compliance vs. time curves along the time axis. The reference temperature was selected as 60 °C. The amount of shifting along the log-time scale was plotted against the corresponding temperatures to form the shift factor plot.

Creep-compliance master curves were fitted with Kohlrausch-William-Watts (KWW) stretched exponential equation (Kohlrausch, 1854; Williams and Watts, 1970a; Plazek and Ngai, 1991).

$$J_t = J_u + (J_r - J_u) \times \left[1 - exp\left(-\left(\frac{t}{\tau}\right)^{1-n}\right)\right] \qquad \text{Equation 7.1}$$

Where, J_t, J_u and J_r are the time dependent compliance, unrelaxed or glassy compliance (t→0) and relaxed or rubbery compliance (t→∞), respectively. The τ is the characteristic retardation time and *n* is the coupling parameter. Least-square fitting to the master curves was performed using OriginPro® version 8.0.63 (OriginLab,

Northampton, MA, U.S.A.). Estimated parameters from each master curves were then averaged.

7.4. Results and Discussion

Creep mode time temperature superposition was used to analyze effects of HMR treatment on the polymer mobility within the wood amorphous phase. Figure 7-1 represents creep-compliance master curves for HMR and aqueous NaOH treated specimens, along with corresponding shift factor plots.

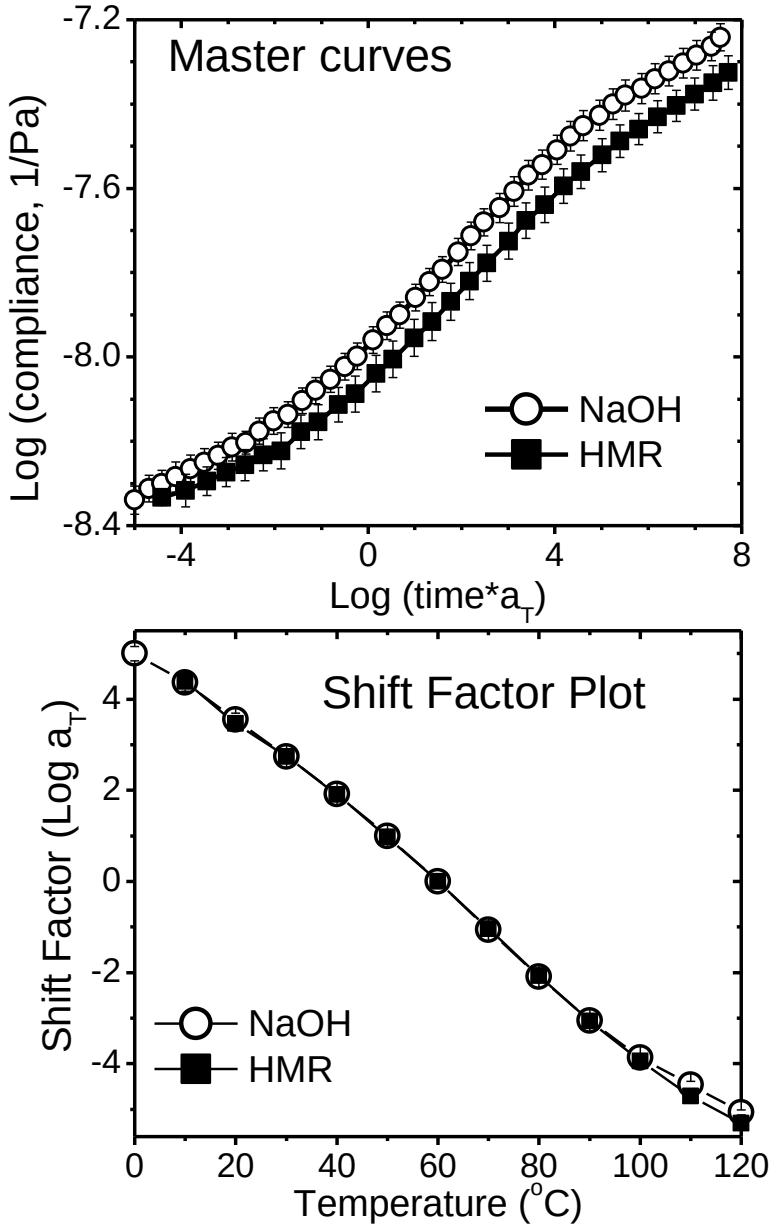

Figure 7-1 Average (n = 3) creep-compliance master curves (Top) and average shift factor plots (Bottom) for HMR and NaOH treated southern yellow-pine wood. Compressive torsion thermomechanical analysis was performed while specimens were immersed in ethylene glycol. Error bars represent ±1 standard deviation.

Smooth creep-compliance master curves were obtained, along with continuous evolution of shift factor vs. temperature plot. This satisfies the empirical validity criteria for time temperature superposition (Ferry, 1980). HMR treatment clearly reduced wood compliance in comparison to the NaOH treated specimens. The difference in the compliance was more significant in the longer time zone (rubbery region). Reduction in compliance due to HMR treatment is consistent with our previous study, where the storage modulus of HMR treated SYP was found to be slightly higher than NaOH treated specimens (Chowdhury and Frazier, 2011c). However, the shift factors were not affected by HMR treatment. Arrhenius (linear) behavior was evident at temperature below (~ 50 °C) and a non-linear relaxation zone followed at higher temperature.

Creep TTS data were further explored by fitting Kohlrausch-Williams-Watts (KWW) stretched exponential function as demonstrated in Figure 7-2.

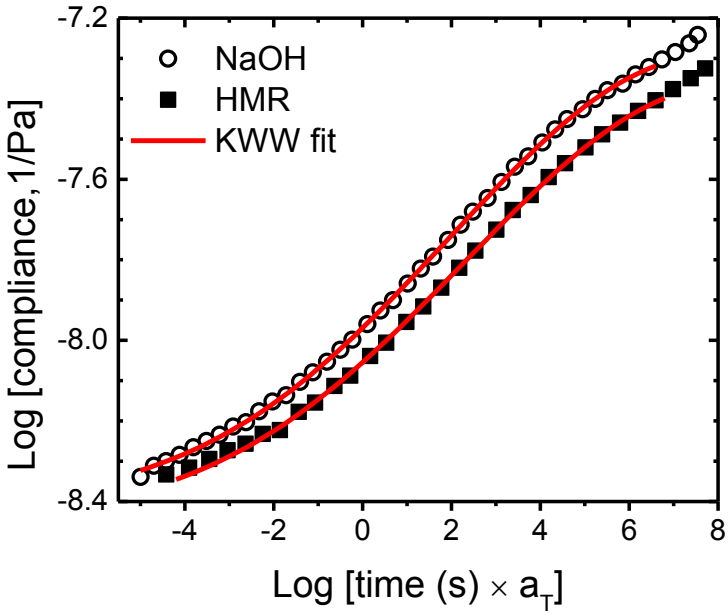

Figure 7-2 Average (n=3) creep compliance master curves for HMR and NaOH treated SYP. Average (n=3) KWW fits are shown as solid lines.

KWW stretched exponential function fit the master curves very well (R^2>0.99). Note that at the longest time boundary of the experiment, the sign of a second transition was visible. This region was excluded from the KWW fit, as this KWW is best suited to describe single polymeric transition.

Figure 7-3 reports the average retardation time (τ) and coupling parameter (n) for HMR and NaOH treated wood.

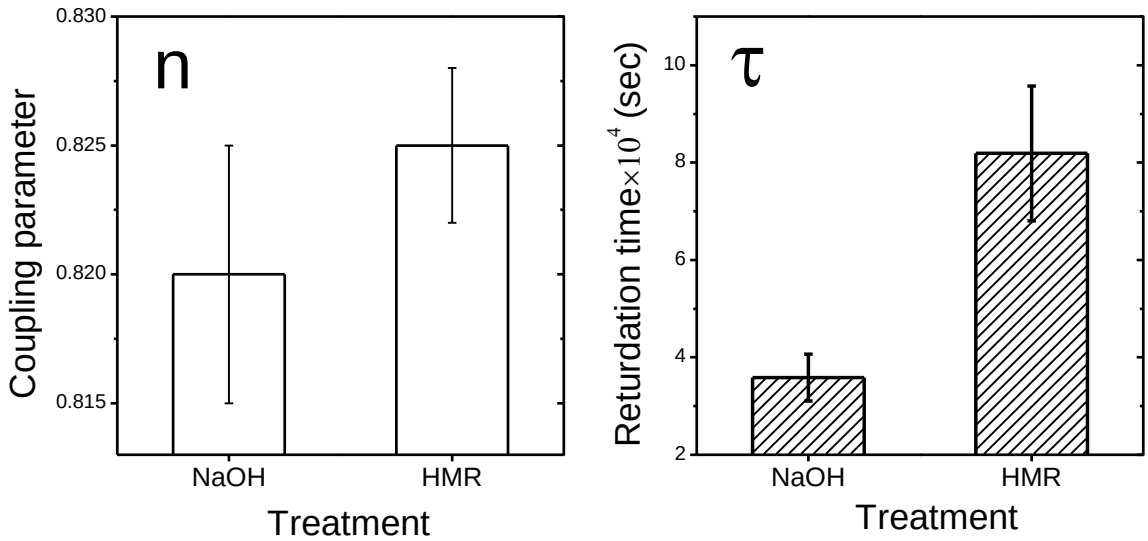

Figure 7-3 Average (n = 3) coupling parameters (n) and retardation time (τ) obtained from Kohlrausch-Williams-Watts equation for HMR and NaOH treated southern yellow-pine wood. Compressive torsion thermomechanical analysis was performed while specimens were saturated with ethylene glycol. Error bars represent ±1 standard deviation.

KWW fit showed that the coupling parameter, indicative of the intermolecular cooperativity, was not significantly different for HMR and NaOH treated wood (p-value: 0.2). This indicates that the intermolecular cooperativity between non-bonded neighboring polymers was not significantly altered by HMR treatment. The coupling parameters obtained were very high (> 0.8), indicating a high intermolecular cooperativity within the amorphous wood-polymers. Similar high coupling or

intermolecular cooperativity was reported by Laborie et al. (2004) in ethylene glycol plasticized softwood (*Picea abies*) and hardwood (*Liriodendron tulipifera*).

The retardation time, indicative of the characteristic time scale for polymeric motions, was significantly higher with HMR treatment ($p = 0.005$). This implies that the resistance to the creep mobility was increased due to the HMR treatment, which is consistent with the previous finding of Sun and Frazier, where an increase in the resistance towards the stress relaxation was reported for HMR treated wood (Sun and Frazier, 2005).

7.5. Summary

The effects of Hydroxymethyl resorcinol (HMR) treatment on creep response of ethylene glycol plasticized southern yellow-pine were investigated using compressive-torsion thermomechanical analysis. Smooth creep-compliance master curves were obtained, along with continuous evolution of shift factor vs. temperature plots for both HMR and NaOH treated specimens. Creep-compliance was reduced with HMR treatment. However, no differences in the shift factors were observed. Master curves were further investigated by fitting the KWW equation and intermolecular coupling and characteristic retardation times were determined. Although intermolecular coupling was not significantly different between treatments, the retardation time was significantly higher in HMR treated wood. This suggests that the creep mobility was restricted by HMR treatment, perhaps by the formation of an interpenetrating network within the wood amorphous phase.

7.6. References

Chowdhury, S., J. Fabiyi and C. E. Frazier, 2010. Advancing the dynamic mechanical analysis of biomass: comparison of tensile-torsion and compressive-torsion wood DMA, *Holzforschung*, 64(6), 747-756.

Chowdhury, S. and C. E. Frazier, 2011a. Chapter 3: Compressive-torsion DMA of wood in organic media *in* Advancing characterization techniques for structure-property determination of in-situ lignocelluloses, Macromolecules and Interefaces Institute and Department of Wood Science and Forest Products, Virginia Polytechnic Institute and State University, Blacksburg, VA,

Chowdhury, S. and C. E. Frazier, 2011b. Chapter 4: Time-temperature equivalence and fragility of organic solvent plasticized wood *in* Advancing characterization techniques for structure-property determination of in-situ lignocelluloses, Macromolecules and Interefaces Institute and Department of Wood Science and Forest Products, Virginia Polytechnic Institute and State University, Blacksburg, VA,

Chowdhury, S. and C. E. Frazier, 2011c. Chapter 6: Probing hydroxymethyl resorcinol-wood interactions through compressive-torsion DMA and rheo-IR spectroscopy *in* Advancing characterization techniques for structure-property determination of in-situ lignocelluloses, Macromolecules and Interefaces Institute and Department of Wood Science and Forest Products, Virginia Polytechnic Institute and State University, Blacksburg, VA,

Ferry, J. D., 1980: Viscoelastic properties of polymers. Wiley,New York

Green, D. W., J. E. Winandy and D. E. Kretschmann. 1999: Mechanical properties of wood. *Wood handbook, wood as an engineering material.*, Madison, WI, USA: Forest Products Society, 1-45.

Horvath, B., P. Peralta, C. Frazier and I. Peszlen, 2011. Thermal softening of transgenic aspen, *Bioresources*, 6(2), 2125-2134.

Kohlrausch, R., 1854. Theorie des elektrischen Rückstandes in der Leidner Flasche, *Pogg. Ann. Phys.*, 9156-82, 179-214.

Kurt, R., A. Krause, H. Militz and C. Mai, 2008. Hydroxymethylated resorcinol (HMR) priming agent for improved bondability of wax-treated wood, *Holz Roh- Werkst.*, 66(5), 333-338.

Laborie, M.-P. G., L. Salmén and C. E. Frazier, 2004. Cooperativity analysis of the in situ lignin glass transition, *Holzforschung*, 58(2), 129-133.

Lopez-Suevos, F. and K. Richter, 2009. Hydroxymethylated resorcinol (HMR) and novolak-based HMR (n-HMR) primers to enhance bond durability of Eucalyptus globulus glulams, *Journal of Adhesion Science and Technology*, 23(15), 1925-1937.

Okkonen, E. A. and C. B. Vick, 1998. Bond-ability of salvaged yellow-cedar with phenol-resorcinol adhesive and hydroxymethylated resorcinol coupling agent, *Forest Products Journal*, 48(11-12), 81-85.

Plazek, D. J. and K. L. Ngai, 1991. Correlation of Polymer Segmental Chain Dynamics with Temperature-Dependent Time-Scale Shifts, *Macromolecules*, 24(5), 1222-1224.

Son, J., W. T. Y. Tze and D. J. Gardner, 2005. Thermal behavior of hydroxymethylated resorcinol (HMR)-treated maple veneer, *Wood and Fiber Science*, 37(2), 220-231.

Sun, N. and C. E. Frazier, 2005. Probing the hydroxymethylated resorcinol coupling mechanism with stress relaxation, *Wood and Fiber Science*, 37(4), 673-681.

Vick, C. B., K. Richter, B. H. River and A. R. Fried, Jr., 1995. Hydroxymethylated resorcinol coupling agent for enhanced durability of bisphenol-A epoxy bonds to Sitka spruce, *Wood and Fiber Science*, 27(1), 2-12.

Williams, G. and D. C. Watts, 1970a. Non-symmetrical dielectric relaxation behavior arising from a simple empirical decay function, *Transactions of the Faraday Society*, 6680-85.

Chapter 8 Probing impacts of hydroxymethyl resorcinol on lignocellulose morphology using ^{2}H NMR

(Short study)

Sudip Chowdhury, Louis A. Madsen, and Charles E. Frazier
Departments of Wood Science and Chemistry, and
Macromolecules and Interfaces Institute
Virginia Tech, Blacksburg, VA 24061

8.1. Abstract

Deuterium quadrupolar NMR was used to investigate the effects of hydroxymethyl resorcinol (HMR) on the morphology of wood-amorphous domain. 2H spectroscopy of partially deuterated probe molecules doped in wood revealed that HMR significantly altered the cell wall morphology. The wood-polymer mobility was reduced with HMR treatment, which was evident in increased quadrupolar splitting. This indicates that HMR forms a network within the wood amorphous phase.

8.2. Introduction

Deuterium nuclear magnetic resonance (^{2}H NMR), more specifically the ^{2}H quadrupolar interaction is widely employed to study the orientation and phase dynamics of liquid crystals and synthetic polymers (Deloche and Samulski, 1981; Burnell and De Lange, 2003; Callaghan and Samulski, 2003; Li *et al.*, 2009). In Chapter 5 of this dissertation we have demonstrated the efficacy of this method in understanding the in-situ morphology of wood-polymers (Chowdhury *et al.*, 2011). In this chapter ^{2}H NMR is

being used to investigate the effects of hydroxymethyl resorcinol (HMR) treatment on morphology of in-situ wood polymers.

8.3. Experimental

8.3.1. Materials

All specimens were machined from a single piece of commercial yellow-poplar (*Liriodendron tulipifera*) sapwood lumber (30×5×5 cm); density was not measured but on average the diffuse-porous cross-section exhibited two growth rings per centimeter. Specimens dimension was 2×2×16 mm, with the longest dimension along the fiber direction. The probe solvent used was N,N-dimethylformamide-d1 ($DCON(CH_3)_2$), obtained from Cambridge Isotopes Laboratories, Inc (Andover, MA) with minimum purity of 99%.

8.3.2. Sample preparation

Standard HMR solution was prepared with 4 h reaction time (Vick *et al.*, 1995). Dry yellow-poplar specimens were vacuum-pressure impregnated with HMR solution to achieve complete saturation (5 mm Hg for 45 min, followed by atm. pressure for 15 min). Thereafter specimens were dried at ambient condition for 12 h and subsequently thermally treated (150 °C, 1 h) to prevent any changes that might occur in subsequent analysis. Another set of specimens was only heat treated and considered as control. Specimens were then stored in a desiccator (anhydrous P_2O_5 and N_2) for at least 48 h.

After noting the dry weight, specimens were saturated with DMF-d1 using room temperature vacuum/pressure treatment: specimens soaked in an excess of DMF-d1; vacuum applied (10 – 12 mm Hg, 30 min) followed by atmospheric pressure (15 min).

From this saturated condition the specimen solvent content was reduced via controlled evaporation using a rotary evaporator (10 mm Hg). The final specimen solvent content was targeted at 25% of dry wood weight. The solvent content variation was within 1% in a sample group. After reaching the required solvent content and before NMR analyses, specimens were wrapped with Teflon tape and allowed to equilibrate for a minimum of 24 h at 4 °C in a 15 × 45 mm (OD × L) Teflon-capped glass vial.

8.3.3. Temperature dependence of orientational order

Experiments were performed on Varian Unity spectrometer at 9.39 T magnetic field (B^0). A 5 mm multinuclear probe was used. Specimens were placed in a standard 5 mm NMR glass tube and the head space above the specimen was occupied using a 5 mm diameter Kel-F® plug (Wilmad-LabGlass, Vineland, NJ). Acquisition parameters were: acquisition time = 0.3 s, relaxation delay = 0.02 s, pulse time = 25 μs (π/2 pulse: 28 μs), spectral width = 25 KHz, and number of scans = 6000. Temperatures were increased (-10 to 80 °C) with 10 °C increments, followed by a 10 °C stepwise cooling to the minimum temperature. At each temperature, specimens were equilibrated for 10 min before collecting spectra. Three specimens were tested for each treatment.

All spectra were exponentially apodized (10 – 20 Hz) and phase and baseline corrected. The high temperature spectrum (at 80 °C), which showed best peak resolution, was used to establish the number of peaks to be fitted across the temperature range. Only spectra at 60 to 80 °C showed clear doublets and were used for splitting calculation. All spectra were fitted with one Lorentzian doublet and a

Lorentzian singlet. The distance between the doublet peaks (in Hz) was recorded as the quadrupolar splitting.

8.4. Results and Discussion

Figure 8-1 reports isothermal ^{2}H spectra of 25% DMF-d1 in untreated (no HMR treatment, only heat at 150 °C, 1 h) and HMR treated yellow-poplar wood at different temperatures.

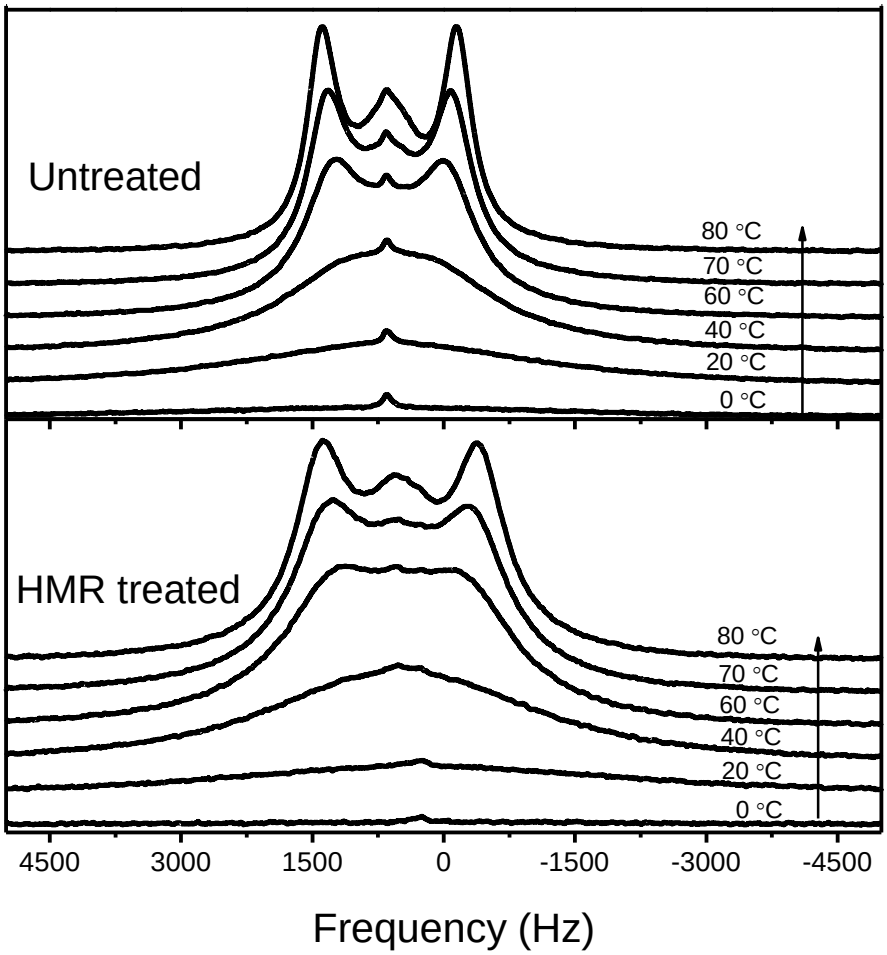

Figure 8-1 Deuterium NMR spectra of 25% DMF-d1 in untreated (Top) and HMR treated (Bottom) yellow-poplar at different temperatures. Specimens were heated from low to high temperatures with 10 °C increments, isothermal ^{2}H NMR spectra were collected at each temperature after 10 min equilibration. Longitudinal grain was parallel to the static magnetic field.

In the untreated specimen the low temperature spectra (below 60 °C) had a broad peak and a hint of relatively sharper singlet. A doublet emerged with increasing temperature and the singlet was clearly visible. The doublet signifies an oriented phase and the singlet denotes an isotropic polymer phase. In our previous paper we have argued that the oriented phase observed in the ^{2}H spectra originate from the major cell wall layer in the xylem tissue (the S2 layer) and the singlet originates from the unoriented compound middle lamella (CML: middle lamella+ primary wall) (Chowdhury *et al.*, 2011) . In the HMR treated specimens the ^{2}H spectra were much broader than the untreated specimen and only spectra recorded beyond 60 °C showed a discernable doublet and a singlet. The increased breadth suggests slower probe mobility (shorter T_2), signifying stronger probe-matrix interactions in HMR treated wood. Both sample types showed high degrees of peak overlaps (especially below 60 °C), which caused the estimation of spectral parameters less reliable. Nevertheless, spectra beyond 60 °C, where the doublet and singlet were identifiable, were used to determine quadrupolar splittings.

Figure 8-2 demonstrates the average quadrupolar splitting of untreated and HMR treated SYP specimens as a function of temperature.

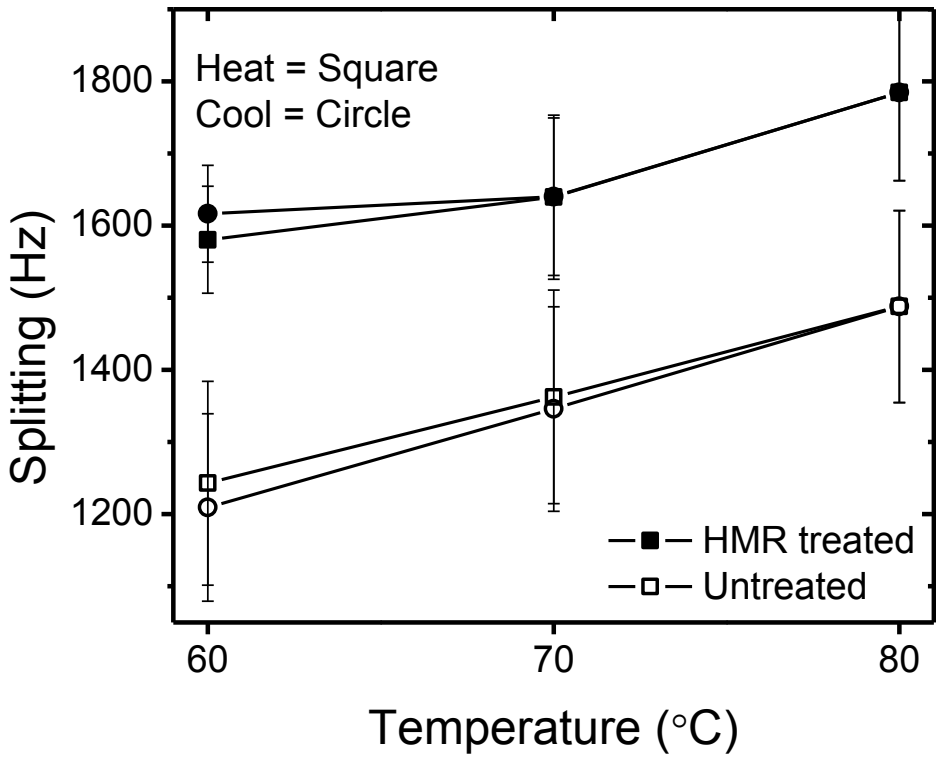

Figure 8-2 Average (n=3) quadrupolar splitting as a function of temperature for 25% DMF-d1 in untreated and HMR treated yellow poplar. Splittings were calculated while heating the specimens, also while cooling. Longitudinal grain direction was parallel to the static magnetic field. Error bars indicate ±1 standard deviation.

The quadrupolar splitting increased as the temperature was raised. This was similar to our previous report, where local orientation of the DMF increased with temperature (Chowdhury *et al.*, 2011). However, this observation was surprising, generally the quadrupolar splitting decreases with increasing temperature (Li *et al.*, 2009; Chowdhury *et al.*, 2011). Increased temperature causes higher thermal energy which stimulates greater configurational changes in the matrix polymers such that the average degree of matrix orientation is reduced, and less bias is exerted upon the probe (Callaghan and Samulski, 2003). Therefore, the ensemble average orientational order (S) reduces, resulting in a lower splitting with increasing temperature (Li *et al.*, 2009). However splitting-temperature trend was opposite For DMF-d1 in wood; DMF

experienced an increased local ordering as the temperature was increased. Chowdhury et al. explained this phenomena with a mechanism of probe redistribution within the cell wall (Chowdhury *et al.*, 2011). As temperature increases, the greater thermal expansion of the CML (being completely amorphous CML expands more than the highly fibril-reinforced S2 layer) might cause probe molecules to transfer out of the S2 layer and into the CML. This loss of probe in the oriented S2 layer resulted in the splitting increase (Chowdhury *et al.*, 2011).

HMR effect was also evident on the quadrupolar splitting values, where the spitting was higher with HMR treatment. This indicates that HMR penetrated the cell wall and significantly modified the amorphous phase. Previous studies have reported that increasing the crosslinking within the polymer matrix increases the quadrupolar splitting (Dubault *et al.*, 1984). Higher splitting in HMR treated wood suggests that higher bias was applied by the matrix on probe molecules. This was caused by less swelling of the matrix at a specific temperature (and solvent content) with HMR treatment, suggesting a restriction in the matrix mobility. A reduction in the matrix configurational mobility induced by crosslinking is also expected to increase the quadrupolar splitting.

8.5. Summary

Deuterium NMR quadrupolar coupling was used to investigate the effects of hydroxymethyl resorcinol (HMR) on wood amorphous phase. HMR significantly altered the wood-amorphous domain. HMR treatment increased the quadrupolar spitting,

indicating restricted polymer mobility possibly due to the formation of crosslinks in the oriented amorphous phase.

8.6. References

Burnell, E. E. and C. A. De Lange, 2003: NMR of ordered liquids. Kluwer Academic Publishers,Dordrecht ; Boston

Callaghan, P. T. and E. T. Samulski, 2003. Biaxial deformation of a polymer network measured via deuteron quadrupolar interactions, *Macromolecules*, 36(3), 724-735.

Chowdhury, S., L. A. Madsen and C. E. Frazier, 2011. Chapter 5: Probing Alignment and Phase Behavior in Intact Wood Cell Walls Using 2H NMR Spectroscopy *in* Advancing characterization techniques for structure-property determination of in-situ lignocelluloses, Macromolecules and Interefaces Institute and Department of Wood Science and Forest Products, Virginia Polytechnic Institute and State University, Blacksburg, VA,

Deloche, B. and E. T. Samulski, 1981. Short-range nematic-like orientational order in strained elastomers - a deuterium magnetic-resonance study, *Macromolecules*, 14(3), 575-581.

Dubault, A., B. Deloche and J. Herz, 1984. Effect of crosslinking density on the orientational order generated in strained networks - a deuterium magnetic-resonance study, *Polymer*, 25(10), 1405-1410.

Li, J., K. G. Wilmsmeyer and L. A. Madsen, 2009. Anisotropic Diffusion and Morphology in Perfluorosulfonate Ionomers Investigated by NMR, *Macromolecules*, 42(1), 255-262.

Vick, C. B., K. Richter, B. H. River and A. R. Fried, Jr., 1995. Hydroxymethylated resorcinol coupling agent for enhanced durability of bisphenol-A epoxy bonds to Sitka spruce, *Wood and Fiber Science*, 27(1), 2-12.

Chapter 9 Conclusions

This study utilized several polymer characterization techniques to advance the structure-property determination of in-situ lignocelluloses. In Chapter 2 of this work a parallel-plate compressive-torsion DMA technique is developed to analyze solvent plasticized biomass with or without any mechanical integrity. The benefits and limitations of this technique are demonstrated by comparing it with a more traditional tensile-torsion DMA. While the compressive-torsion DMA has a more complicated stress-mode, it provides distinct benefits in analyzing extremely small and/or “difficult to clamp” specimens because of simplified specimen clamping. The lignin glass/rubber transition of plasticized lignocelluloses is effectively probed as a function of solvent and grain orientation by compressive-torsion DMA.

Chapter 3 utilizes the parallel-plate compressive-torsion DMA to analyze viscoelasticity of yellow-poplar (*Liriodendron tulipifera*) while immersed in four different organic solvents: two aprotic tertiary amides (DMF and NMP) and two protic alcohols (ethylene glycol and glycerol). A detailed mapping of linear viscoelastic response (LVR) region as a function of solvent, grain orientation and temperature indicates that the wood LVR responses are extremely complex and require careful and constant attention if operation within the LVR is critical. As expected, plasticizers significantly alter wood viscoelasticity; lignin glass/rubber transition temperature (Tg) is lower in DMF and NMP as compared to ethylene glycol, and lignin Tg is highest in glycerol. In addition to the solvents, wood grain orientation also affects the lignin relaxation. Grain effect is most prominent in glycerol, the weakest plasticizer, where each grain orientation differs with

respect to the Tg and storage modulus. In more powerful plasticizers (DMF, NMP and ethylene glycol) varied grain dependency is observed.

Chapter 4 further advances the solvent-plasticized wood rheology through time/ temperature superposition (TTS). The storage modulus shifts smoothly in all four aforementioned solvents. However the thermorheological complexity of plasticized wood is observed in the form of shift failures in the loss component (loss modulus and tan δ) master curves. Solvent and grain direction are found to significantly influence the severity of the shift failure. It is argued that the classic TTS validity criteria are somewhat arbitrary and even in a severely thermorheologically complex material TTS can provide valuable insights into the relaxation behavior. Plasticized lignocellulose fails to satisfy the TTS validity, however it seems probable that loss component shift failures are useful in understanding the complexities of lignocellulose structure and properties.

Vogel-Fulcher-Tamman-Hess equation is used to determine the Tg at relaxation time = 100s (Tg_0), for wood in four different solvents. The WLF model is applied to the shift factor plots over a temperature range of Tg_0+40 to 120 K. However it is argued that the WLF model is not well suited to plasticized lignocellulose since the breadth of the relaxation window can vary dramatically in different solvents. Instead the fragility analysis of cooperative segmental motions offers a more robust approach to analyze segmental relaxation and intermolecular cooperativity near lignocellulose Tg. This treatment should offer practical utility in developing useful correlations for biomass processing and for probing the effects of chemical, thermomechanical, or genetic manipulations.

Chapter 5 introduces the deuterium quadrupolar NMR in analyzing the lignocellulose morphology in an intact wood cell wall. ^{2}H NMR spectroscopy of small deuterated probe molecules doped in yellow-poplar (*Liriodendron tulipifera*) shows two distinct amorphous polymer domains: a highly oriented phase in the S2 layer of the secondary cell wall and an isotropic phase postulated to occur in the compound middle lamella (CML). ^{2}H NMR offers a unique path to independently investigate the sub-micron scale morphology and phase dynamics of CML and S2 in an intact tissue. This technique shows promise in providing novel insights into the deconstructive strategies specific to the oriented and unoriented domains. Using ethylene glycol-d4 as a probe, this study shows that the highly oriented amorphous phase (matrix orientational order ~ 1) is uniaxial, i.e. it has only one major symmetry axis along the fiber direction (transverse directions are indistinguishable). The oriented polymer matrix exhibits glass-transition with increasing temperature (40 to 60 °C), which is manifested in the non-linear increase in the T_2 relaxation time. This suggests that ^{2}H NMR can provide a localized probe to investigate segmental relaxation in sub-micron scale lignocellulose domains. This study also shows that the interactions of lignocellulose with ethylene glycol and DMF are significantly different. It is inferred that a probable temperature induced solvent redistribution occurs between the S2 and the CML phase. ^{2}H NMR shows great potentials in understanding the correlations between biomass processing and morphological changes, and also in providing novel perspectives on lignocellulose ultrastructure.

In Chapter 6, effects of a powerful wood-adhesion promoter (hydroxymethyl resorcinol, HMR) on lignocellulose mobility and morphology are investigated using

parallel-plate compressive-torsion DMA and rheo-infrared spectroscopy. Solvent submersion compressive-torsion DMA shows that the HMR treatment significantly alters the mobility of amorphous domain. Both short-range configurational motions and long-range entanglements are modified, which should influence the energy dissipation and solvent induced swelling of wood. Curiously, the study shows that the detection of the HMR effect is solvent dependent. For instance, water-plasticized wood reveals increase in the crosslink density (long range motional regime), whereas DMF plasticized wood shows changes in the short-range configurational motion regime. This finding demonstrates the fundamental differences in the lignocellulose mobility in different solvents and reveals the value in using different plasticizers in probing different wood-polymeric regimes.

IR spectroscopy coupled with mechanical loading (rheo-IR) shows great potential in analyzing effects of chemical and other relevant treatments on the micromechanical interactions between in-situ wood-polymers. The contribution of a specific bond in load bearing can be identified by observing the shift of any characteristic peak as a function of stress/strain. Rheo-IR spectroscopy shows that the HMR treatment modifies the stress distribution mechanism within wood cell wall. In a HMR treated specimen, rigid cellulose microfibrils bear less load than an untreated system.

Further investigation of the HMR effects is done using creep TTS of solvent plasticized wood (Chapter 7). HMR treatment reduces the creep-compliance of wood. However, no change is observed in the shift factor plot. Subsequent application of Kohlrausch-Williams-Watts (KWW) equation to the compliance master curves reveals that the characteristic retardation time of wood-amorphous region is significantly

increased with HMR treatment, indicating reduced polymer mobility. This conclusion is supported by the subsequent ^{2}H NMR study of HMR treated wood (Chapter 8). Using DMF-d1 as the probe molecule, this study demonstrates that the quadrupolar splitting is higher in HMR treated wood than untreated specimens, thereby suggesting increased crosslinking and resulting restriction in the swelling of the wood amorphous phase This finding corroborates with the increased crosslink density observed using DMA and possibly with the change in the stress-distribution mechanism observed with rheo-IR. Since no evident chemical change is observed in the IR spectra, it is reasonable to believe that the mobility restriction in the amorphous domain is due to the formation of an interpenetrating network of HMR within the cell wall.

Overall, this dissertation developed/optimized multiple polymer characterization techniques to analyze lignocelluloses in an intact cell wall. These methods hold high promise in explaining fundamental questions regarding biomass processing and the ultrastructure of lignocellulosic cell wall. This research should initiate stimulating studies towards correlating fundamental lignocellulose relaxation and morphology to various biomass processing pathways.

Appendix A Determination of 100 s glass transition temperature (Tg_0)

The glass transition with 100 s relaxation time was considered as the quasi-static glass transition temperature (Tg_0), calculated as follows (Plazek and Ngai, 1991; Saiter *et al.*, 2010).

Step 1

Isothermal frequency scans (1-100 Hz, 7-10 data points/decade) at different temperatures were used to construct tan δ vs. temperature profiles for each discrete frequency. High frequency responses (generally beyond 40 Hz) did not produce clear tan δ maxima, therefore not used for Tg detection. The resulting tan δ curves had a temperature resolution of 10 °C. A 6th order polynomial was fitted to tan δ curves so as to clearly identify the Tg (temperature at tan δ max) with 1 °C resolution. Figure A.1 shows the raw tan δ vs. temperature data along with the polynomial fit.

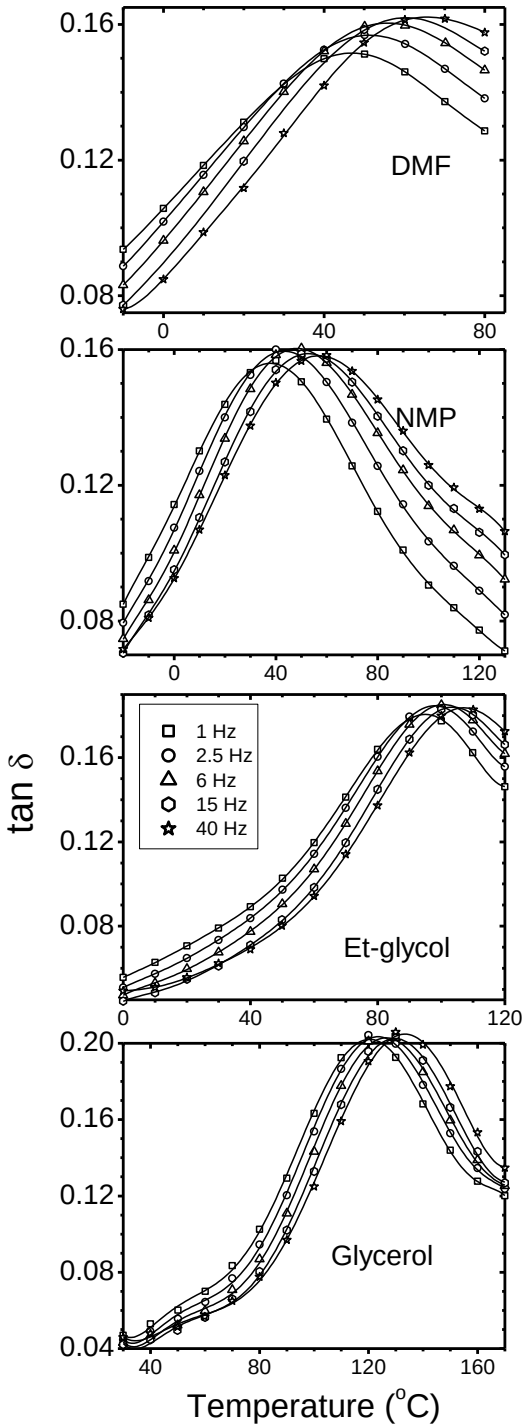

Figure A-1 Tan δ vs. temperature at different frequencies, overlaid with 6th order polynomial fits for yellow poplar RT specimens in all solvents. Note: variable temperature and tan δ axes.

Step 2

For each frequency (*f*) the relaxation time at Tg (τ_{Tg}) was calculated as, $\tau_{Tg} = 1/2\pi f$. Next, τ_{Tg} vs. Tg was plotted, and was fitted to the Vogel-Fulcher-Tamman-Hess (VFTH) equation (Eq. A.1) to obtain VFTH parameters ($\tau_0, B\ and\ T_0$) (Vogel, 1921; Fulcher, 1925; Tammann, 1926).

$$\tau = \tau_0 \exp\left(\frac{B}{T - T_0}\right) \qquad \text{Equation A.1}$$

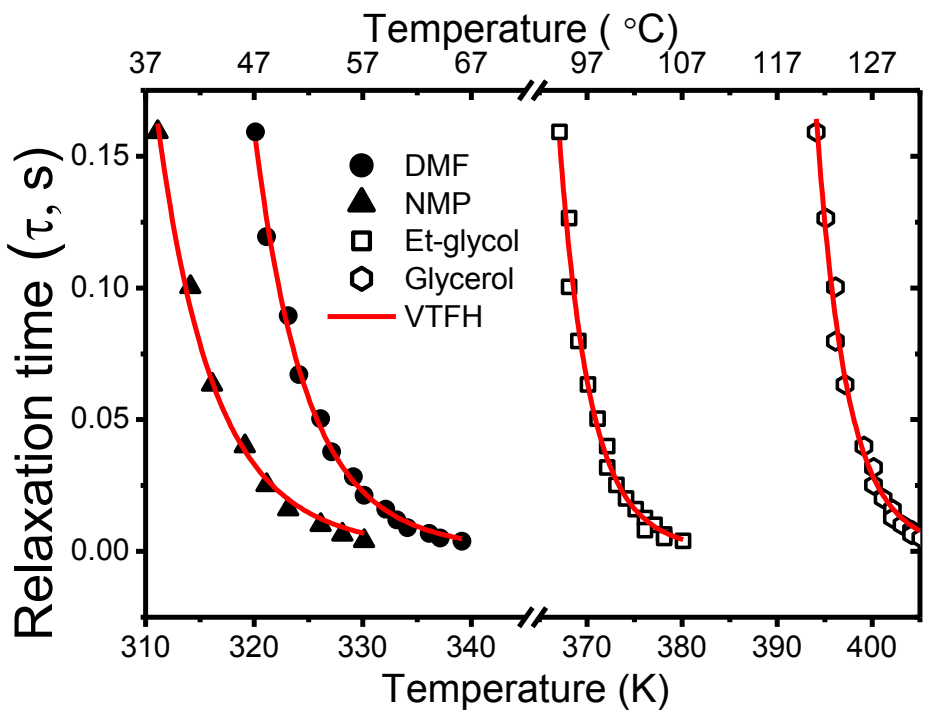

Figure A-2 Relaxation time vs. temperature plots for yellow-poplar RT specimens in all four solvents. The fitted VTFH equation is overlaid.

Obtained VTFH parameters for each sample is summarized in Table A.1

Table A-1 Vogel-Fulcher-Tamman-Hess (VTFH) parameters obtained from least square fit of relaxation time vs. temperature plot for yellow-poplar wood. Mean (n=3) data presented, standard deviations in the parenthesis.

Solvent	Grain	τ_0	B	T_v, K
DMF	RT	6.45E-11	2470	218
		(6E-11)	(985)	(25)
	TR	2.51E-11	2743	200
		(4E-11)	(591)	(13)
	XL	5.01E-12	3686	181
		(8E-12)	(818)	(16)
NMP	RT	2.95E-12	4613	150
		(5E-12)	(1486)	(33)
	TR	2.18E-12	5759	101
		(3E-12)	(751)	(2)
	XL	9.15E-12	3385	174
		(9E-12)	(726)	(18)
Et-glycol	RT	1.27E-12	2170	283
		(1E-12)	(73)	(7)
	TR	4.05E-13	2644	268
		(3E-13)	(972)	(26)
	XL	2.38E-13	2244	279
		(2E-13)	(104)	(5)
Glycerol	RT	2.80E-13	2333	308
		(4E-14)	(107)	(3)
	TR	2.09E-13	2618	291
		(1E-13)	(312)	(15)
	XL	1.39E-13	2355	295
		(7E-14)	(124)	(5)

Step 3

The 100 s relaxation time glass transition temperature (Tg_0) was then estimated from the rearranged VTFH equation, as in equation A.2.

$$T_{g_0}(\tau = 100s) = T_0 + \frac{B}{\ln(100) - \ln \tau_0}$$ Equation A.2

References

Fulcher, G. S., 1925. Analysis of recent measurements of the viscosity of glasses, *Journal of the American Ceramic Society*, 8339-355.

Plazek, D. J. and K. L. Ngai, 1991. Correlation of Polymer Segmental Chain Dynamics with Temperature-Dependent Time-Scale Shifts, *Macromolecules*, 24(5), 1222-1224.

Saiter, J. M., L. Dobircau, R. Saiah, P. A. Sreekumar, A. Galandon, R. Gattin, N. Leblanc and R. Adhikari, 2010. Relaxation map of a 100% green thermoplastic film. Glass transition and fragility, *Phys. B (Amsterdam, Neth.)*, 405(3), 900-905.

Tammann, G., 1926. Die abhangigkeit der viskositat von der temperature bei unterkuhlten flussigkeiten, *Zeitschrift für anorganische und allgemeine Chemie (1950)*, 156245-257.

Vogel, H., 1921. The law of relation between the viscosity of liquids and the temperature, *Physik Z*, 22645-646.

Appendix B Thermomechanical Analysis (TMA) of plasticized wood

Dimensional changes of plasticized yellow-poplar wood (*Liriodendron tulipifera*) as a function of temperature were measured using a TMA 2940 (TA Instrument). Disc specimens (8 mm dia, 4 mm thick) were saturated with solvents using vacuum-pressure treatment (5 mm Hg for 1 h followed by 24 h atmospheric pressure) at room temperature. Dimensional changes as a function of temperature were measured while specimens were immersed in excess of solvents. Experimental parameters were: 1. First heat: heat to maximum temperature (2 °C/min); 2. Rapid cool to minimum temperature (~ 5 to 15 °C/min; using liquid nitrogen); 3. Second heat: heat to maximum temperature (2 °C/min). Following figures show the percent dimensional changes from the initial dimension (dimension at the beginning of each step) as a function of temperature.

Dimension change of yellow-poplar in ethylene glycol

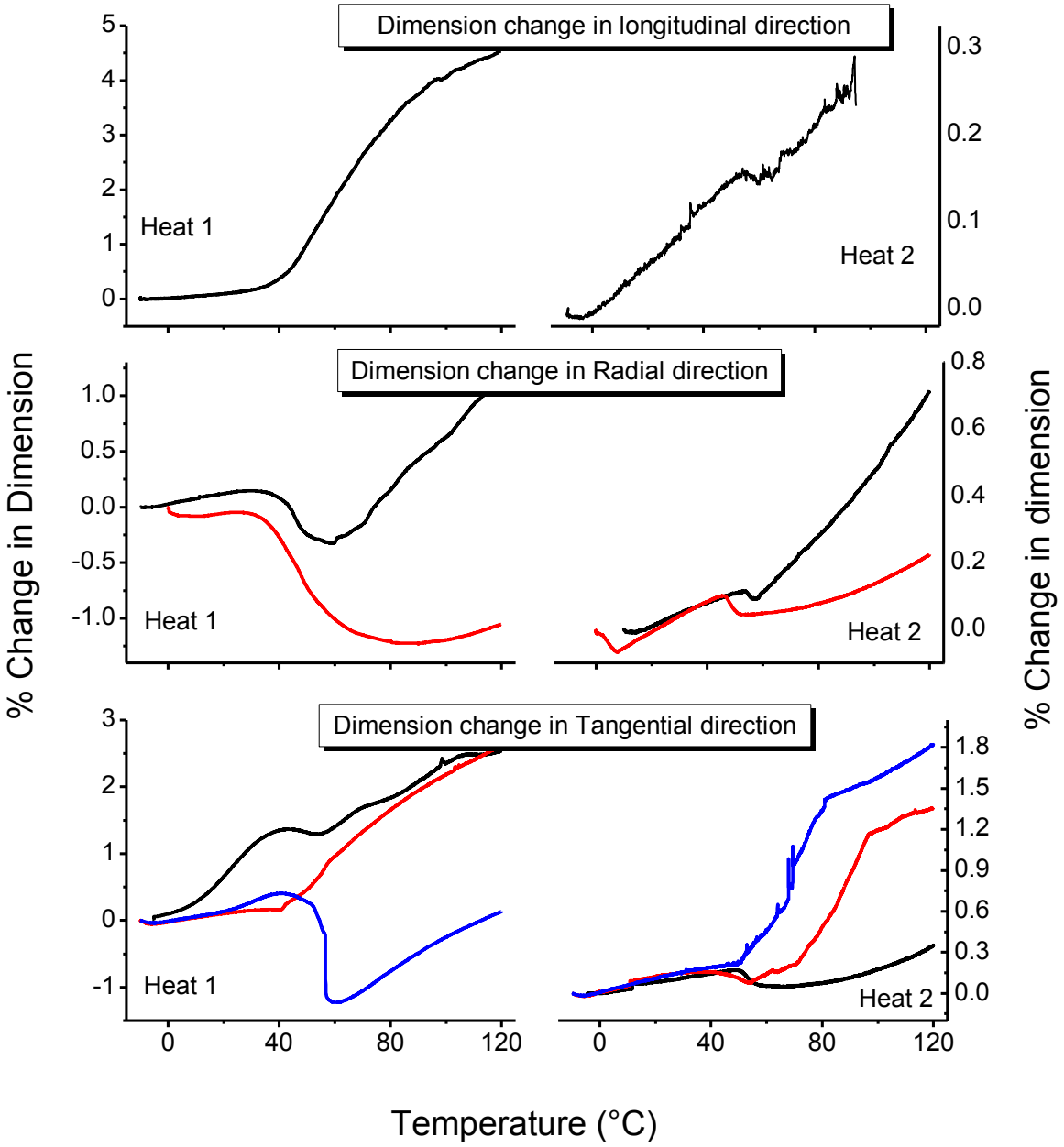

Figure B-1 Percent dimensional change from the initial dimension of ethylene glycol plasticized yellow-poplar as a function of temperature. Dimensional changes in three different grain orientations are shown for first heat and second heat.

Dimension change of yellow-poplar in DMF

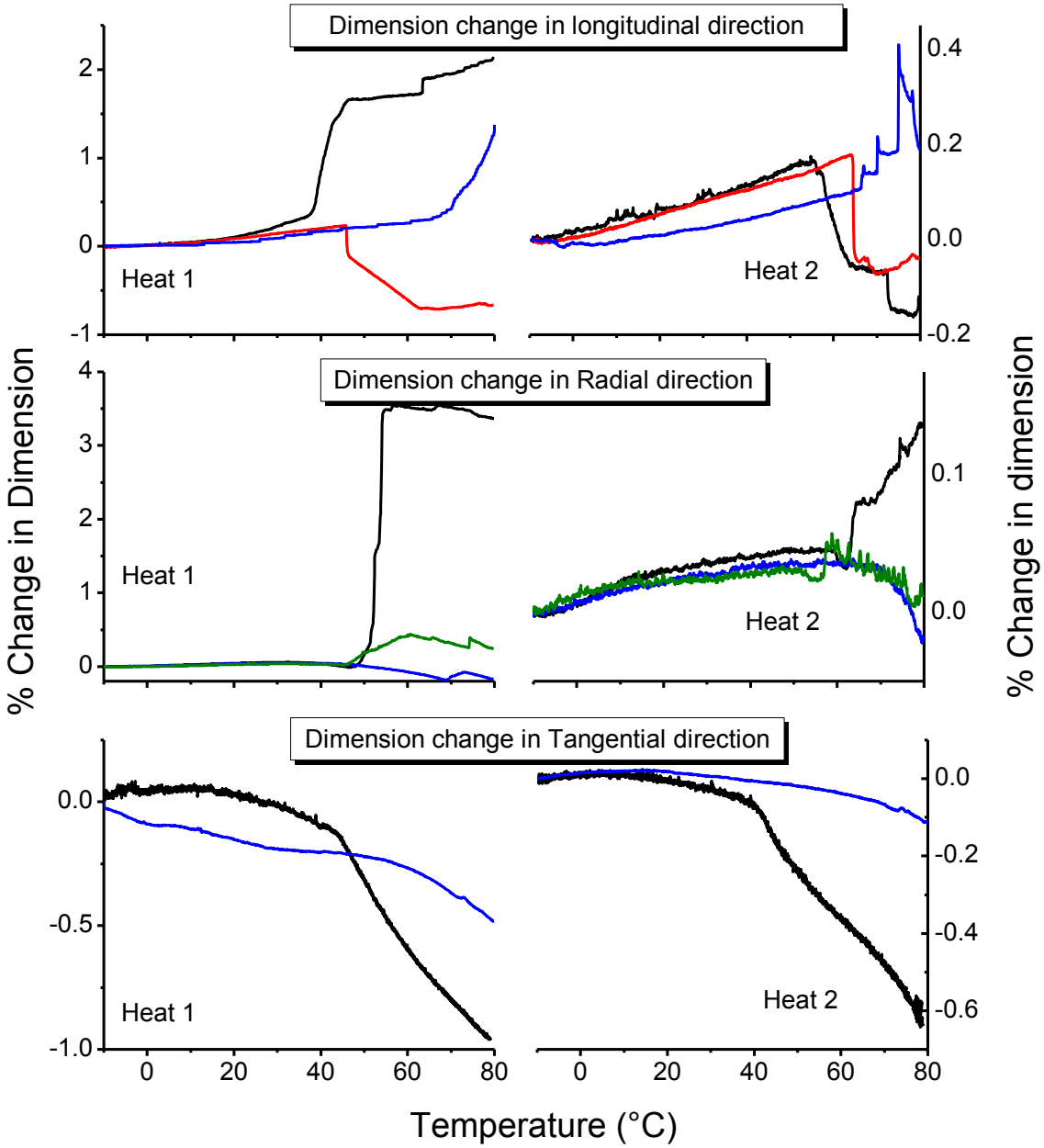

Figure B-2 Dimensional change of DMF plasticized yellow-poplar as a function of temperature. Dimensional changes in three different grain orientations are shown for first heat and second heat.

Dimension change of yellow-poplar in water

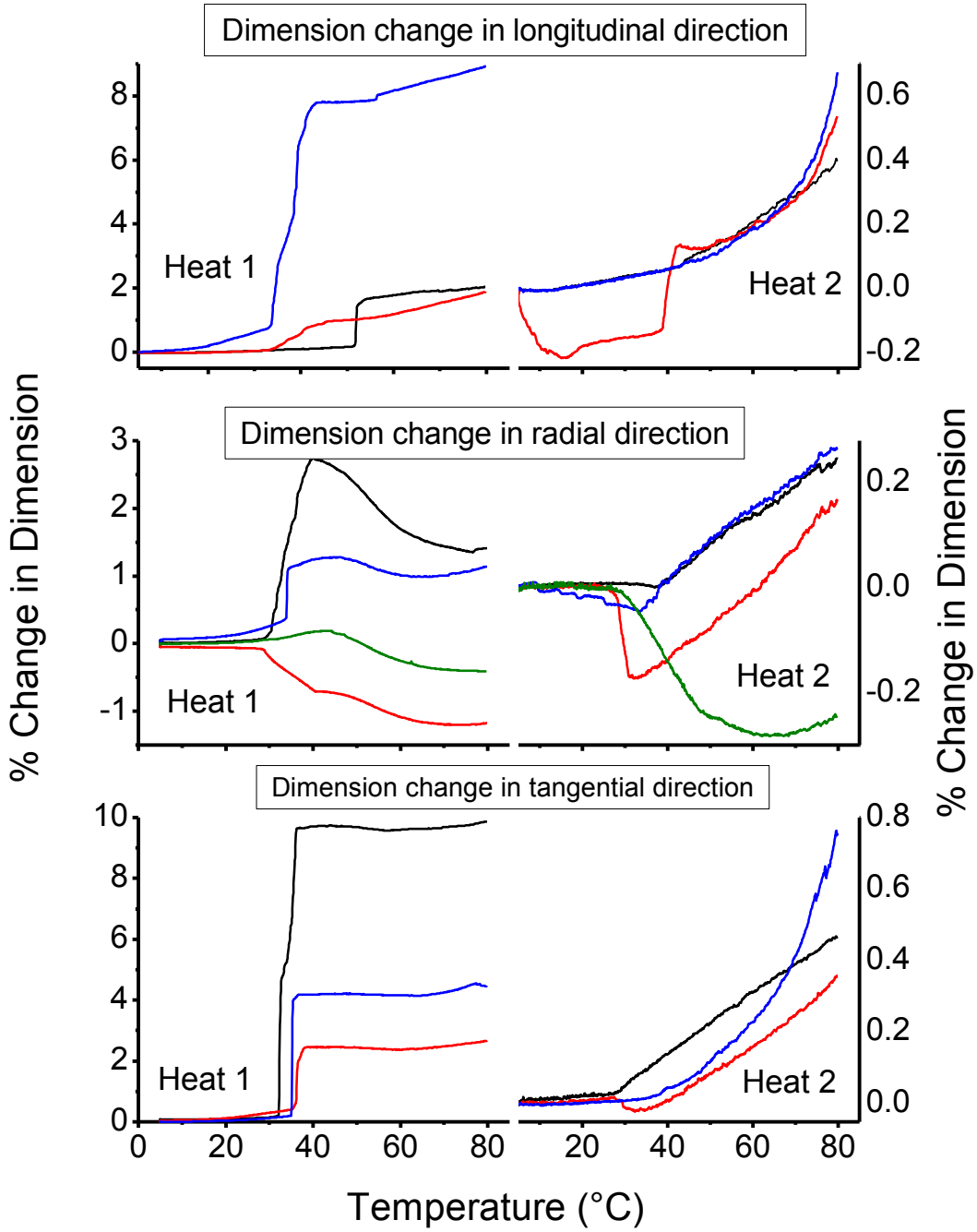

Figure B-3 Dimensional change of water plasticized yellow-poplar as a function of temperature. Dimensional changes in three different grain orientations are shown for first heat and second heat.